Development of an anti-invasive therapeutic strategy for paediatric high grade glioma

Julia Veronica Cockle

Submitted in accordance with the requirements for the degree of
Doctor of Philosophy

The University of Leeds
School of Medicine
January 2016

The candidate confirms that the work submitted is her own, except where work which has formed part of jointly authored publications has been included. The contribution of the candidate and the other authors to this work has been explicitly indicated below. The candidate confirms that appropriate credit has been given within the thesis where reference has been made to the work of others.

Details of work contained within this thesis based upon publications

Chapter 1

Cockle JV, Picton S, Melcher A. Future Clinical Potential of Oncolytic Virotherapy for Pediatric CNS tumors. *CNS Oncology* 2013 2 (4), 1-4.

This editorial review was written by JV Cockle and the manuscript was reviewed by all co-authors.

Chapter 3

Cockle JV, Picton S, Levesley J, Ilett E, Carcaboso AM, Steel L, Short S, Melcher A, Lawler S, Brüning-Richardson A. Cell migration in paediatric glioma; characterisation and potential therapeutic targeting. *British Journal of Cancer* 2015 112, 693-703.

All assays in this publication were planned and carried out by JV Cockle with supervision from E Ilett, A Melcher, S Lawler and A Brüning-Richardson. The manuscript was written by JV Cockle and reviewed by all co-authors.

Preface

Acknowledgements

I would like to thank my supervisors Professor Alan Melcher, Dr Elizabeth Ilett, Dr Anke Brüning-Richardson and Dr Susan Picton for all their laboratory support and advice during my PhD. I would also like to express my ongoing gratitude to Dr Anke Brüning-Richardson and Dr Susan Picton for their mentorship and guidance over the past three years.

I would also like to thank Professor Susan Short, Professor Peter Selby, Professor Richard Vile, Dr Ewan Morrison and Dr Sean Lawler for their added contributions. Additionally, I am very grateful to Jill Thompson and Timothy Kottke for carrying out the *in vivo* experiments under chapter 6, Dr Azam Ismail for his neuropathology advice and Dr Angel M Carcaboso for his input with the diffuse intrinsic pontine glioma experiments. Furthermore, I would like to thank all members of lab 6, especially Dr Harry King for his help with data analysis, Dr Jane Levesley for her expert paediatric scientific advice and Ailsa Rose for her help with the *in vivo* experiment analysis.

This project was kindly funded by Yorkshire Cancer Research, to whom I am incredibly grateful for the opportunity.

Karen J Scott, there is too much to thank you for; however, you know you are a great friend and I will always cherish that. I would also like to thank my parents and sister for their incredible support throughout my PhD and especially during the writing of this thesis.

Finally, I would like to dedicate the work within this thesis to my late nonna, Maria Elena, whose support, love and encouragement has been at the heart of all my achievements to date.

Abstract

Paediatric high grade glioma (pHGG) and diffuse intrinsic pontine glioma (DIPG) are highly aggressive brain tumours. Their invasive phenotype contributes to their limited therapeutic response and novel treatments that block brain tumour invasion are needed. Here, two novel anti-invasive therapeutic strategies are evaluated: glycogen synthase kinase-3 (GSK-3) inhibitors and oncolytic viruses (OVs).

Small molecule GSK-3 inhibitors, lithium chloride (LiCl) and the indirubin derivative 6-bromoindirubin-oxime (BIO), reduced migration and invasion of pHGG cell lines (SF188 and KNS42) and one patient-derived DIPG cell line (HSJD-DIPG-007) in 2D and 3D *in vitro* assays. Following drug treatment, pHGG cells demonstrated loss of polarity and altered morphology as seen by live cell imaging and cytoskeletal rearrangement of actin fibres and focal adhesions as seen by immunofluorescence.

OVs (herpes simplex virus (HSV), reovirus and vaccinia virus (VV)) were able to inhibit the migration and invasion of pHGG and DIPG cell lines. Oncolytic HSV was the most interesting candidate, as anti-migratory and anti-invasive effects did not appear to be a consequence of cytotoxicity or altered proliferation. Oncolytic HSV altered pHGG cytoskeletal dynamics, stabilising microtubules through the accumulation of post-translational tubulin modifications, as evaluated by Western blotting and immunofluorescent labelling. Furthermore, oncolytic HSV treatment of pHGG cell lines inhibited GSK-3β activity and prevented the localised clustering of adenomatous polyposis coli to the leading edge of the cell. These observations are highly novel and begin to document the molecular mechanisms by which oncolytic HSV may inhibit pHGG migration and invasion.

In conclusion, this study is the first to demonstrate that it is possible to target migration and invasion of pHGG and DIPG *in vitro* using either small molecule GSK-3 inhibitors or OVs, such as HSV. These agents warrant

further *in vivo* pre-clinical investigation as potential anti-invasive therapeutics and have the potential to improve outcomes of these devastating childhood diseases.

Table of Contents

List of Figures

List of Tables

Abbreviations

2D	Two-dimensional
3D	Three-dimensional
ACVR1	Activin A receptor type 1
ANOVA	Analysis of variance
APC	Adenomatous polyposis coli
APCs	Antigen-presenting cells
Arf6	Adenosine diphosphate ribosylation factor 6
ATP	Adenosine triphosphate
ATRX	Alpha thalassemia/mental retardation syndrome X
BBB	Blood brain barrier
BIA	6-bromoindirubin acetoxime
BIO	6-bromoindirubin-oxime
BL/6	Black 6
BRAF	Rapidly accelerated fibrosarcoma kinase B
BSA	Bovine serum albumin
CAF	Cancer-associated fibroblasts
Cas	Crk-associated substrate
CCL	Chemokine (C-C motif) ligand
CCR	Chemokine (C-C motif) receptor
CD	Cluster of differentiation
Cdc42	Cell division control protein 42
CDKN2	Cyclin-dependent kinase 2
CEV	Cell-associated enveloped virus
CLASP	Cytoplasmic linker-associated protein
CLIP-170	Cytoplasmic linker protein 170
cm	Centimetre
CMFDA	5-chloromethylfluorescein diacetate
CNS	Central nervous system
CO_2	Carbon dioxide
CXCL	Chemokine (C-X-C motif) ligand
CXCR	Chemokine (C-X-C motif) receptor
DAMPs	Danger-associated molecular pattern signals

DAPI	4’,6-Diamidine-2’-phenylindole dihydrochloride
DCs	Dendritic cells
ddH_2O	Double distilled water
DIPG	Diffuse intrinsic pontine glioma
DKFZ	Deutsches Krebsforschungszentrum
DMEM	Dulbecco’s Modified Eagles’ medium
DMSO	Dimethyl sulfoxide
DNA	Deoxyribonucleic acid
DOCK3	Dedicator of cytokinesis 3
DPX	Distyrene plasticizer xylene
DTT	Dithiothreitol
EB	End binding protein
E-Cadherin	Epithelial-cadherin
ECM	Extracellular matrix
EEV	Extracellular enveloped virus
EGF	Epidermal growth factor
EGFR	Epidermal growth factor receptor
ELISA	Enzyme-linked immunosorbent assay
EMT	Epithelial-mesenchymal transition
EORTC	European Organisation for Research and Treatment of Cancer
FACS	Fluorescence-activated cell sorting
FAK	Focal adhesion kinase
FGF	Fibroblast growth factor
FGFR1	Fibroblast growth factor receptor 1
FGFR2III	Fibroblast growth factor receptor isoform 2
g	Grams
G	Gravitational force
GFP	Green fluorescent protein
GM-CSF	Granulocyte macrophage colony stimulating factor
GSK-3	Glycogen synthase kinase-3
GTP	Guanosine triphosphate
GTPases	Guanosine triphosphatases
h	Hour

H	Histone
H&E	Haematoxylin and eosin
HGF	Hepatocyte growth factor
HGG	High grade glioma
HI-FCS	Heat-inactivated foetal calf serum
HMGB-1	High mobility group box 1 protein
HRP	Horseradish peroxidase
HSV	Herpes simplex virus
HVEM	Herpesvirus entry mediator
ICP	Infected cell protein
IDH	Isocitrate dehydrogenase
IF	Immunofluorescence
IFN	Interferon
IGF-1R	Insulin-like growth factor 1 receptor
IgG	Immunoglobulin G
IL	Interleukin
IMPase	Inositol monophosphatase
IMV	Intracellular mature virus
ICP	Infected cell protein
ISVPs	Infectious subvirion particles
i.v.	Intravenous
JAM-A	Junctional adhesion molecule A
kb	Kilobyte
kDa	Kilodalton
LFA-1	Lymphocyte function-associated antigen 1
LGG	Low grade glioma
LICAP	Leeds Institute of Cancer and Pathology
LiCl	Lithium chloride
Lis1	Lissencephaly protein
Luc	Luciferase
M	Molar
mm	Millimetre
mM	Millimolar
MAMs	Microtubule-associated motors

MAPs	Microtubule-associated proteins
MDSCs	Myeloid-derived suppressor cells
MET	Mesenchymal-epithelial transition
Mg^{2+}	Magnesium
MGMT	O(6)-methylguanine-DNA methyltransferase
MHC	Major histocompatibility complex
MI	Migration index
min	Minutes
ml	Millilitre
mM	Millimolar
MMP	Matrix metalloproteinase
MPIs	Synthetic matrix metalloproteinases inhibitors
mRNA	Messenger ribonucleic acid
MTD	Maximum tolerated dose
MTOC	Microtubule organising centre
MTT	3-(4,5-dimethylthiazol-2-yl)-2,5-diphenyltetrazolium bromide
NaCl	Sodium chloride
NaOH	Sodium hydroxide
N-cadherin	Neural-cadherin
NDV	Newcastle disease virus
NF1	Neurofibromatosis 1
NF-κB	Nuclear factor-kappa B
ng	Nanogram
NK	Natural killer
nm	Nanomolar
NOD.SCID	Nonobese diabetic severe combined immunodeficiency
OV	Oncolytic virus
p	Probability
PAMPs	Pathogen-associated molecular patterns
PBS	Phosphate buffered saline
PBST	Phosphate buffered saline and tween
PCV	Prednisolone, lomustine and vincristine
PDGF	Platelet-derived growth factor

PDGFRA	Platelet-derived growth factor receptor alpha
PD-L	Programmed cell death ligand
PFA	Paraformaldehyde
pfu	Plaque forming unit
pH	Potential hydrogen
pHGG	Paediatric high grade glioma
PKR	Protein kinase R
RANTES	Regulated on Activation, Normal T cell Expressed and Secreted
Ras	Rat sarcoma viral oncogene homolog
Rb	Retinoblastoma
Reo	reovirus
RFP	Red fluorescent protein
Rho	Rat sarcoma (Ras) homolog
RhoG	Rat sarcoma (Ras) homology growth-related
RhoGAP	Rho GTPase-activating proteins
RIPA	Radioimmunoprecipitation assay
RNA	Ribonucleic acid
ROS	Reactive oxygen species
rpm	Revolution per minute
RT	Radiotherapy
SAE	Severe adverse event
SCID	Severe combined immunodeficiency
SDS	Sodium dodecyl sulphate
SDS-PAGE	Sodium dodecyl sulphate polyacrylamide gel electrophoresis
SEM	Standard error of the mean
Ser9	Serine 9
Ser21	Serine 21
siRNA	Small interfering ribonucleic acid
SVV	Seneca valley virus
TAAs	Tumour-associated antigens
TBST	Tris-Buffered saline and tween
TGF-β	Transforming growth factor beta

tk	Thymidine kinase
TP53	Tumour protein p53
T-regs	Regulatory T cells
TSM	Tumour stem medium
Tyr216	Tyrosine 216
Tyr279	Tyrosine 279
UK	United Kingdom
uPA	Urokinase-type plasminogen activator
uPAR	Urokinase-type plasminogen activator receptor
USA	United States of America
v	Volt
VV	Vaccinia virus
VEGF	Vascular endothelial growth factor
WHO	World Health Organisation
WST-1	Water soluble tetrazolium-1
Zeb	Zing finger E-box binding homeobox
+TIPs	Plus-end-tracking proteins
°C	Degrees Celsius
µg	Microgram
µl	Microlitre
µm	Micrometre
µM	Micromolar

Chapter 1: Introduction

1.1 Paediatric central nervous system tumours

Central nervous system (CNS) tumours are the most common solid tumours of childhood (1), accounting for a significant proportion of paediatric cancer morbidity and mortality (2). Paediatric CNS tumours have an incidence of 5.1 cases per 100,000 children, with peaks seen at three to seven years of age (1,3). Whereas the majority of tumours result from sporadic mutations, genetic cancer predisposition syndromes account for a small percentage of cases (4). Overall, the five-year survival for paediatric CNS tumours is around 73 % (1); however, this statistic represents an extremely heterogeneous group of tumours (Table 1) with prognosis based on histology, staging, patient age at diagnosis, disease location and specific tumour biology (5).

Tumour type	% of all brain tumours	Most common site	5-year survival (%)
Low grade glioma	30 - 50 %	Cerebral hemispheres	90 - 100 % (resectable) 75 - 90 % (unresectable)
Medulloblastoma	20 - 25 %	Cerebellar vermis	80 - 85 % (average risk) 40 - 70 % (high risk)
Ependymoma	10 %	Fourth ventricle	50 - 75 %
High grade glioma	8 - 12 %	Cerebral hemispheres	15 - 35 %
Diffuse intrinsic pontine glioma	3 - 9 %	Brainstem	0 - 5 %
Craniopharyngioma	6 - 9 %	Suprasellar midline	80 - 95 %
Germ cell tumours	3 %	Pineal (male) Suprasellar (female)	>90 %
Atypical teratoid rhabdoid tumours	1 - 2 %	Cerebellar hemispheres	0 - 33 %

Table 1: Summary of the distribution, location and five-year survival of the most common CNS tumours of childhood
Adapted from (5-11).

Paediatric CNS tumours are challenging to treat; complete surgical resections are limited by the safety of operating within critical brain locations, radiotherapy can significantly damage the fragile developing brain and several tumours respond poorly to current available chemotherapeutics (6). Over the last decade, surgical advancements have helped improve the safety and feasibility of resections (4,12), radiotherapy has advanced through the use of conformal techniques and proton therapy (6,13,14) and chemotherapy protocols and delivery methods have been optimised (3,6,15). Improved understanding of tumourigenesis and molecular pathways has led to the development of biologically targeted therapeutics, which are currently being explored in early phase trials (16-19). However, in spite of this, survival statistics over the past two decades have not considerably improved and there still remains a group of tumours associated with poor prognosis (20). Of these, paediatric high grade glioma (pHGG) and diffuse intrinsic pontine glioma (DIPG) represent a significant treatment challenge and novel therapeutic strategies for these tumours are clearly needed.

1.2 Paediatric high grade glioma and diffuse intrinsic pontine glioma

1.2.1 Histopathology and classification

For the purpose of clinical studies, glioblastoma, anaplastic astrocytoma, anaplastic oligodendroglioma, gliomatosis cerebri, and DIPG comprise the group of tumours collectively referred to as high grade gliomas (HGGs) (21). pHGGs are tumours of the glial cell lineage (comprised of astrocytes, oligodendrocytes and microglia) which are non-neuronal cells that play a role in supporting and protecting neurons within the CNS (22). The World Health Organisation (WHO) uses a histological grading system to classify brain tumours on a scale of grade I (most benign) to IV (most aggressive) (23). Low grade gliomas (LGGs) are grade I and II tumours, whereas HGGs encompass grade III and IV tumours (23). Grade III tumours (anaplastic astrocytoma, anaplastic oligodendroglioma and anaplastic oligoastrocytoma) are diffusely infiltrative with distinct nuclear atypia, increased cellularity and marked mitotic activity (19,23,24). Grade IV tumours (glioblastoma and

gliosarcoma) are classified by the presence of prominent microvascular proliferation and necrosis, in addition to the features described for grade III tumours (19,23,24). DIPGs are classified as WHO grade II-IV tumours; however, grade II tumours have the same clinical behavior as aggressive HGGs and are not considered benign (21,25,26).

1.2.2 Epidemiology, clinical presentation and management

Approximately 0.8 per 100,000 children (age<19) develop pHGG per year (1). Overall, incidence increases with age (1), with infratentorial (brainstem and cerebellar) tumours seen more commonly within the paediatric population and supratentorial (cerebral hemisphere and midline structure) tumours developing in adolescent and adult patients (27-29). Although prognosis of HGG is poor, with most studies showing five-year survival ranging between 15-35 %, age is a significant prognostic factor, with children under the age of three years having noticeably better outcomes (29,30). HGGs in childhood typically arise after a short clinical history, with *de novo* (primary) tumours. Secondary tumours from malignant transformation of LGGs are particularly rare in the paediatric compared to the adult population (7 versus 50 %) (29,31,32). The standard treatment approach for non-brainstem pHGG is maximal surgical resection, radiotherapy and chemotherapy. Adjuvant chemotherapy has been shown to improve survival compared to radiotherapy and surgery alone (33); however, no significant difference in outcome has been seen between different chemotherapy schedules (prednisolone, lomustine and vincristine (PCV), “8-drugs-in-1-day” regimen or temozolomide) (34,35) and temozolomide is widely adopted as the standard of care treatment due to improved tolerability (29).

Brainstem gliomas account for 10 % of pHGGs and 75-80 % of brainstem tumours are classified as DIPGs (26,29). DIPG is mainly a disease of mid childhood (peak age at diagnosis six- to eight-years-old) and over 50 % of children present with the classic triad of cranial nerve deficits, long tract and cerebellar signs (36). DIPG is a major cause of brain-related death in childhood, with over 90 % of children dying within two years of diagnosis

(36-38). Brainstem glioma and DIPG can not be treated surgically, due to tumour location. Standard treatment for DIPG includes six weeks of radiotherapy to stabilise disease progression and improve neurological function; however, effect on overall survival is minimal (36). Unfortunately, no chemotherapeutics to date have improved the outcome of DIPG in any prospective clinical trial (39).

1.2.3 Molecular biology and genetic alterations

Over the past decade, exome and whole genome sequencing alongside molecular and clinical data gathered from clinical trials, has helped shape understanding of the biology of pHGG and DIPG. It has now become clear that pHGGs are both biologically and clinically distinct from adult HGGs and that novel therapeutic strategies should be evaluated using paediatric pre-clinical models where possible, rather than simply extrapolating data from adult-based models (29). Whereas mutations in the isocitrate dehydrogenase (IDH)-1 gene are a hallmark aberration in the adult disease, this is rarely documented in paediatric tumours (21,40). Additionally, pHGGs typically have fewer deoxyribonucleic acid (DNA) copy number changes than histologically similar adult tumours and are characteristically associated with 1q gain (29,41).

Two significant key genomic differences appear to define the paediatric disease. Firstly, platelet-derived growth factor receptor alpha (PDGFRA) is a predominant target of focal amplification, whereas in adult HGG, epidermal growth factor receptor (EGFR) is the common target (29,41,42). Secondly, novel oncogenic driver mutations in histone (H) 3.1 (at position K27), H3.3 (at position K27 and G34) and in the activin A receptor type 1 (ACVR1) appear to be unique to pHGG and DIPG (39,43-47). Several groups have attempted to use genetic profiling to molecularly classify HGG (42,43,48,49). Table two summarises six epigenetically distinct subgroups of glioblastoma, based on genome-wide methylation profiling by the German cancer research centre (Deutsches Krebsforschungszentrum; DKFZ), which classifies tumours based on methylation, age at onset, tumour location, oncogenic

drivers, gene expression and survival (39,43). Such molecular stratification may be useful for future clinical trial design, allowing a more rational approach for patient selection of novel targeted biological agents (39).

	K27	G34	IDH	RTK-1	Mesenchymal	PXA-like
Gene expression	Proneural	Mixed	Proneural	Proneural	Mesenchymal	?
Principle location in the brain	Midline structures and spinal cord	Cerebral hemispheres	Frontal and parietal lobe	Cerebral hemispheres	Cerebral hemispheres	Cerebral hemispheres
Main oncogenic drivers	• H3.3 or 3.1 • K27 mutation • TP53 mutation • ATRX mutation • FGFR1 mutation (thalamus) • ACVR1 mutation (pons) • PDGFRA amplification	• H3.3 • G34 mutation • TP53 mutation • ATRX mutation	• IDH1&2 mutation • TP53 mutation • ATRX mutation	• PDGFRA amplification • TP53 mutation • CDKN2A & CDKN2B deletion • EGFR amplification	• NF1 mutation • TP53 mutation • CDKN2A & CDKN2B deletion • EGFR amplification • PDGFRA amplification	• BRAF V600E mutation • CDKN2A deletion
Age group	Young children	Young children, adolescents, young adults	Adolescents and young adults	Young children, adolescents, young adults	Adolescents and young adults	Young children
Estimated median survival	6 months	1 year	>2 years	1 year	1 year	>4 years

Table 2: A summary of the six epigenetically distinct subgroups of glioblastoma, based on genome-wide methylation profiling by the German cancer research centre (DKFZ)
Taken and adapted from (39). H (histone), TP53 (tumour protein p53), ATRX (alpha thalassemia/mental retardation syndrome X), FGFR1 (fibroblast growth factor receptor 1), ACVR1 (activin A receptor type 1), PDGFRA (platelet-derived growth factor receptor alpha), IDH (isocitrate dehydrogenase), CDKN2 (cyclin-dependent kinase 2), EGFR (epidermal growth factor receptor), NF1 (neurofibromatosis 1), BRAF (rapidly accelerated fibrosarcoma kinase B).

1.2.4 Summary of the unique challenges for researchers studying pHGG and DIPG

Development of an effective treatment for HGG is viewed to be a huge challenge. Firstly, HGGs represent an extremely heterogenous group of tumours and even within individual tumours, there can be subpopulations of cells with epigenetic and genetic variation (43,50). Such intra-tumoural heterogeneity may contribute to the development of tumour progression and

treatment failure through the development of resistant subpopulations of cells that harbor mutations, allowing continuous self renewal and proliferation (43). Secondly, brain tumours, as a whole, represent a unique treatment challenge to the field of oncology, as systemically delivered therapeutics need to cross the blood brain barrier (BBB), a highly organised structural unit critical for CNS homeostasis and the prevention of entry of biological toxins (51). Although the presence of a brain tumour itself can destabilise areas of the BBB (51,52), drug penetration of the BBB must be considered when testing novel therapeutics. Several technologies that allow either transient BBB disruption in order to aid local drug delivery (51,53,54) or novel administration routes, such as convection enhanced delivery to bypass blood-CNS barriers (55,56), are under investigation and offer promise of improved brain-drug delivery.

pHGG and DIPG are relatively rare diseases (1) and this has implications for recruitment and design of feasible clinical trials. Large international collaborative efforts are required in order to effectively test new therapies in a timely manner, which are expensive and difficult to facilitate. Challenges to research include limited numbers of immortalised pHGG cell lines (there are currently none for DIPG) with only some key genetic aberrations present. Only recently have pHGG and DIPG neurosphere cultures been developed (29). Biological material for DIPG research is particularly rare as tumour diagnosis is based upon the presence of characteristic imaging alongside typical clinical presentation and, as such, biopsy is not often clinically indicated. Over the last decade, there has been a consensus for collecting biological material for DIPG. Initially tissue was taken at autopsy; however, new consensus guidelines now support conducting a biopsy upfront at diagnosis in order to enhance the understanding of the molecular biology of the disease and to develop pre-clinical models for new agent testing (57-60).

Compared to adult HGG, there is a lack of robust *in vivo* models of pHGG and DIPG for drug testing. Over the past few years, orthotopic xenotransplantation of pHGG or DIPG cells (collected at autopsy, biopsy or surgery, in the case of pHGG) into the cerebrum/pons has been successfully

used as a pre-clinical tool (29,61-63). Research is currently focused to create genetically engineered models of DIPG/pHGG (29,61,64) and the development of orthotopic syngeneic mouse models is critical for pre-clinical testing of novel treatment approaches, such as immunotherapy.

1.3 Migration and invasion of glioma cells

1.3.1 Background

A hallmark characteristic of glioma cells and, indeed, of cancer, is their ability to invade and diffusely infiltrate normal brain tissue (24,65,66). Thus, these tumours inevitably recur, as by the time of surgical resection, tumour cells have invaded into the surrounding brain, preventing their complete removal (65). Approximately 95 % of malignant gliomas will recur within two to three cm of the resection cavity; however, recurrence has been documented several centimeters away from the original tumour site, as well as in the contralateral cerebral hemisphere (67-70), highlighting the ability of glioma cells to migrate across significant distances. Despite such infiltrative and invasive behaviour, HGGs hardly ever metastasise outside of the brain, illustrating that invasion is likely to be governed by interactions between tumour cells and the brain environment (71). HGG cells are known to migrate in specific patterns, following the orientation of white matter tracts, capillaries and unmyelinated axons (24,72,73). Interestingly, this pattern of migration is similar to the pattern followed by glial progenitors during normal brain development (73,74). The next section will evaluate mechanisms underlying both the migration and invasion of cancer cells and the key agents involved in regulating these processes.

1.3.2 Cell migration

Cell migration is the directed movement of cells from one location to another (75,76). This process is critical for many physiological and pathological processes in biology and is a prerequisite for invasion (75,76). Individual tumour cells demonstrate different modes of migration, which are mainly amoeboid or mesenchymal (77). The mode of migration adopted by the cell

is influenced by tumour type, as well as factors within the tumour microenvironment such as chemokine and growth factor gradients and proteolysis (77). In amoeboid migration, cells are more rounded and are able to squeeze through gaps in the extracellular matrix (ECM). This type of migration is referred to as ‘pathfinding’ migration. Typically, cells moving with amoeboid morphology move at high speeds (approximately 4 μm min^{-1}) (77). Conversely, the mesenchymal mode is characterised by elongated cell morphology and relies on proteolytic degradation of the ECM to form a path for migrating cells (77,78). Hence, this type of migration is known as ‘path generating’. Cells moving with mesenchymal morphology demonstrate relatively low speeds of migration (approximately 0.1-1 μm min^{-1}) (77). Glioma cells mainly adopt the mesenchymal pattern of migration (71); however, cancer cells can interconvert between the different modes of migrations depending on microenvironmental cues (77,79). Such plasticity may allow tumour cells to adapt their mode of migration to the surrounding microenvironment, promoting tumour aggression (80). Additionally, these switches contribute to drug resistance of tumours and highlight one of the key challenges involved in trying to pharmacologically target cancer cell movement (81,82).

In addition to the two types of migration, tumour cells can also move in groups, demonstrating multicellular patterns of migration. The cells may move collectively in clusters or sheets (collective migration), where cells held together by cell-cell junctions move through the ECM (77,83). In this mode of migration, the front line of elongated leader cells, made up of either tumour and/or stromal cells, form tracks via proteolysis which facilitate a pathway for movement of sheets of cuboidal-shaped cells (77). Collectively migrating cells do not retract their cellular tails in order to propel themselves forward but exert a pulling force on neighbouring cells that are connected by cell-cell junctions (84). Alternatively, cells may migrate via streaming, where individual cells not held together by cell-cell junctions follow each other down tracks formed by ECM degradation (77,85).

1.3.3 Mechanisms of cell migration

In order for a cell to move, it needs to be able to adapt and alter its shape. This process is made possible by the presence of the cell cytoskeleton, which is composed of actin microfilaments, microtubules and intermediate filaments (86). To start the process of movement, the cell becomes polarised, generating a front-rear axis that allows the cell to have a leading protrusive front and a trailing edge (87,88). Polarisation appears to be initiated by the small guanosine triphosphatases (GTPases), including cell division control protein 42 (Cdc42), Rac, and Rat sarcoma homolog (Rho), which play a role in cytoskeletal re-organisation, as well as controlling direction sensing for the cell (87,89). The leading edge of the cell protrudes into a broad flat lamellipodium and long thin filopodium composed of actin filaments, whose polymerisation controlled by Rac and Cdc42, allows movement (90,91). Microtubules are also believed to play a role in generating protrusive activity and influence the rearrangement and dynamics of actin (92). The actin cytoskeleton, forming the front and rear protrusions, is attached to the ECM at focal adhesions via integrin receptors, anchoring the cell to its substrate and allowing a traction force when actomyosin contracts. During this process, the rear focal adhesions detach from the ECM, thus allowing retraction of the trailing edge, progressing the cell forwards (71,90) (Figure 1). In summary, the mechanism of cell migration involves the coordinated repetition of an ordered sequence of events, involving cell protrusion, adhesion, contraction and retraction (93) based on an interplay between the actin filament, microtubules and focal adhesions.

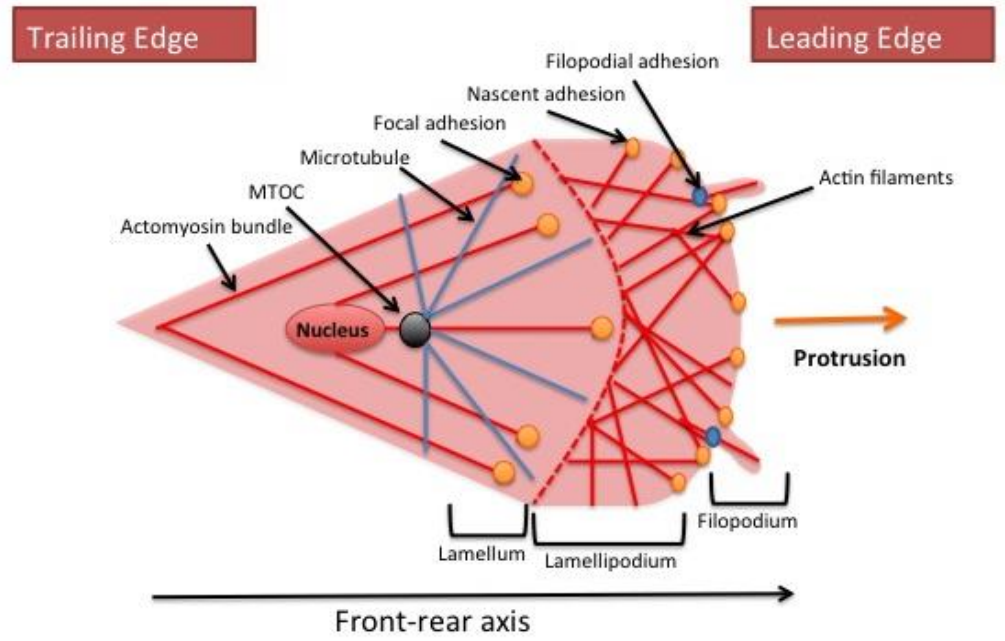

Figure 1: Structure of a migrating cell
Polarisation generates a front-rear axis and results in a leading and trailing edge. The leading edge protrudes as filopodia and lamellipodia. Adhesions form in the filopodia (filopodial adhesion) and lamellipodia (nascent adhesion). Adhesion maturation to focal adhesions occurs in the lamellum. Actin forms bundles and cross-bridges into filaments. Microtubules assemble as arrays initiating from the microtubule organising centre (MTOC). Adapted from (87,90,92,94).

1.3.4 Microtubules in cell migration

Microtubules are polymers of α- and β- tubulin dimers that bind to form stiff cylindrical hollow tubes that play a critical role in cell migration, cell polarity, cell division and neuronal differentiation (93,95,96). Microtubules assemble as arrays initiating from microtubule organising centres (MTOCs), with the main MTOC associated with the centrosome in the majority of cell types (93). In most cells, the MTOC is localised in front of the nucleus, in the direction of cell migration (93,97,98). Microtubule polymers have molecular polarity, with a minus end anchored at the MTOC and a dynamic plus end which reaches into the cytoplasm and cell periphery (95). The plus end functions by a process called dynamic instability, which involves catastrophes (depolymerisation/shrinkage) and rescues (polymerisation/growth), allowing microtubules to search, explore and

interact with cellular organelles and target sites (93,95,99,100). Microtubule-associated motors (MAMs) and microtubule-associated proteins (MAPs) are critical for microtubule functioning (93,95). MAMs, such as dyneins and kinesins, allow transport of vesicles, organelles, cytoskeletal components, proteins and messenger ribonucleic acid (mRNA) along microtubule tracks (93,96), whereas MAPs play a role in stabilising or destabilising microtubules during dynamic instability.

Plus-end-tracking proteins (+TIPs) (including cytoplasmic linker protein 170 (CLIP-170), cytoplasmic linker-associated protein (CLASP), end binding protein (EB)-1 and -3, adenomatous polyposis coli (APC), dynein, dynactin and lissencephaly protein (Lis1)) (101,102) are a sub-group of MAPs that specifically bind to growing microtubule ends and play a key role in regulating microtubule interactions and dynamics (93,103,104). EB1 and -3 are a type of +TIPs with a function in promoting persistent growth of microtubules (93,105). The EBs can recruit +TIP stabilising factors, such as APC, which clusters at microtubule plus ends and act to limit the frequency of catastrophes, stabilise microtubules, promote microtubule growth and encourage cell migration (93,106,107). APC also plays an essential role in regulating the polarity of migrating cells (93,108,109). In this process, glycogen synthase kinase-3 (GSK-3)-β is inactivated by Cdc42 at the leading edge of the cell. Inactivation of GSK-3β suppresses the phosphorylation of APC and, in this unphosphorylated form, APC is able to cluster and bind to the plus ends of microtubules promoting directional cell protrusion. This localisation of inactive GSK-3β, resulting in spatially restricted APC clustering to plus ends of microtubules, is critical to the establishment of cell polarity (110).

Whilst the majority of microtubules undergo dynamic instability and demonstrate short half-lives (five to ten minutes (min)), a subgroup of microtubules do not undergo this process and subsequently have much longer half-lives (more than one hour (h)) (100,111). These ‘stable’ microtubules accumulate post-translational modifications, such as acetylation, detyrosination, glutamylation and glycylation and are more

resistant to microtubule depolymerisation agents (93). Stable microtubules may be found in the protrusions of migrating cells, polarising cells and differentiated cells (93,100). The post-translational modification of tubulin can act to alter microtubule dynamics. For example, tubulin detyrosination can inhibit both +TIP protein recruitment and depolymerising motors, resulting in subpopulations of microtubules resistant to disassembly (112). Additionally, post-translational tubulin modifications can enhance the interaction of specific motor proteins with microtubule tracks, allowing for preferential transportation of intracellular organelles, vesicles or proteins and can support the formation of stable directed tracks from the centrosome to the leading edge in migrating cells, that facilitate directional trafficking within the cell (93,100,113,114).

1.3.5 Invasion

Where migration is the directed movement of cells from one location to another, invasion represents a separate, highly dynamic process, involving regulation of cell-cell adhesion, proteolysis of the ECM and cell migration (75,84). This process allows cells to move through the ECM into neighbouring tissues. Cells relying on amoeboid migration do not invade in a classical sense, as they do not rely on proteolysis of the ECM. Invasion is a hallmark feature of cancer pathogenesis and is a key event in metastasis (66).

The ECM of the brain is a dynamic environment with several roles. It can provide a pool of growth factors and matrix proteins to help regulate cellular functions during normal and pathological remodelling processes and it can also act to provide structural support within the brain (82,115,116). The ECM of the brain consists mainly of hyaluronic acid, except around blood vessels and the pial surface, where the basal lamina consists of type IV and V collagen and other fibrous proteins (24,115). Proteases are known to be involved in remodelling the ECM in order to allow a passage for cells to migrate and, additionally, generate a favourable environment for tumour growth (24). Glioblastoma cells are able to express and release specific proteases that are able to degrade the surrounding ECM, thus facilitating

tumour invasion (82). Three groups of proteases have been linked to this process (115): serine proteases (including urokinase-type plasminogen activator (uPA) and its membrane-bound receptor (uPAR), which induce the degradation of fibronectin and laminin) (117), cysteine proteases (including Cathepsin B which degrades laminins and collagen) (118) and matrix metalloproteinases (MMPs) (in particular, MMP2 and -9, which are linked as promoters of glioblastoma invasion) (119). Specific inhibitors act to control protease activity and an imbalance of the levels of their expression may also contribute to glioma invasion (82).

Integrins are adhesion molecules that play a key role in cell migration and invasion by communicating signals between the ECM and the intracellular environment (16,65). The integrin receptor is a transmembrane glycoprotein constructed of an α- and β- subunit that connects to the focal adhesion kinase (FAK)/Src family protein tyrosine kinase/Crk-associated substrate (Cas) signalling network. This activates GTPase proteins to control cytoskeletal modifications necessary for cell movement (71). 18 α- and eight β- subunits exist, resulting in the development of a range of integrin receptors made up of different α/β integrin pairs, each capable of interacting with different ECM proteins (65,82). In glioblastoma, pro-migratory ECM proteins are upregulated and increased expression of corresponding integrin receptors to these proteins have been documented in glioblastoma tumour specimens (82). Importantly, integrin αvβ3 and αvβ5, which allow communication between the ECM and endothelial cells during angiogenesis and play a role in invasion by acting as adhesive receptors, have been shown to be expressed at high levels in glioblastoma tumour samples (65,82,120). These specific integrins have been linked to glioblastoma tumour progression as they are associated with an increase in expression in higher grade tumours (82,121,122). Finally, integrins appear to be critical for glioblastoma invasion. This was demonstrated *in vitro* by antibody blockade of integrin receptors resulting in reduced adhesion, motility and invasion of glioblastoma cells (82,123,124).

In order to invade, tumour cells must alter their attachment to other cells, as well as to the ECM. Changes in the levels of adhesion molecules play a key

role in this process (66). One such molecule that plays an important role in tumour invasion is epithelial-cadherin (E-cadherin), a transmembrane glycoprotein that mediates cell-cell adhesion and helps to assemble epithelial cell sheets (66,125). Expression of E-cadherin appears to inversely correlate with the ability of tumours to invade and metastasise, with reduced levels of E-cadherin associated with a more invasive tumour phenotype (66). Epithelial cells can undergo changes in cell-cell adhesion and can transform to acquire a more invasive phenotype through a developmental regulatory programme called epithelial-mesenchymal transition (EMT) (66). During EMT, loss of function mutations in cadherins, proteolytic cleavage of cadherins and upregulation of cytokines that alter cell-cell adhesion occur (126). This is also accompanied by the *de novo* expression of vimentin (126,127). Overall, these changes allow cells to acquire a much more invasive phenotype (126,127). EMT is controlled by a set of transcription factors, including Slug, Snail, Twist and Zing finger E-box binding homeobox (Zeb)-1 and -2, which are able to alter cell morphology (from polygonal to spindly/fibroblastic), increase expression of ECM proteases and increase resistance to apoptosis, all of which favour tumour motility and invasiveness (66).

EMT is a reversible process and tumour cells are capable of undergoing mesenchymal-epithelial transition (MET) (66). This plasticity appears to play an important role in cancer metastasis, as colonies of cancer cells that have metastasised to distant tissue are able to revert to their original epithelial phenotype, which may be histologically more similar to that of the primary tumour and may assist integration into distant tissue/organs (66,128).

Finally, the surrounding tumour stroma, consisting of angiogenic vascular cells, infiltrating immune cells and cancer-associated fibroblasts (CAF), also plays a role in promoting cancer progression and can adapt to facilitate tumour invasion (129,130). CAF are able to secrete effector molecules which promote invasion (130). Examples of such effector molecules include secretion of transforming growth factor beta (TGF-β), which can activate EMT, and hepatocyte growth factor (HGF), capable of stimulating invasion and proliferation (130-134). Stromal mesenchymal cells secrete cytokines,

such as Regulated on Activation, Normal T Expressed and Secreted (RANTES), which are involved in facilitating tumour cell invasion (66,135). Immune cells, such as mast cells and macrophages, resident in the stroma, can also support cancer cell invasion by secreting ECM-degrading enzymes, including MMPs or cysteine and serine proteases in response to cytokine signalling from tumours (66,130,136). Macrophages secrete growth factors such as epidermal growth factor (EGF), which facilitate chemotaxis and invasion of tumour cells into the surrounding tissues and blood vessels (130,137). Additionally, stromal macrophages may play a role in inhibiting the expression of known metastasis suppressor genes (130,138-140). Taken together, it is clear to see that the tumour microenvironment is a key regulator of cancer cell invasion and must be considered when designing potential anti-invasive cancer therapies.

1.4 Therapeutic targeting of cancer migration and invasion

An effective therapeutic strategy for the treatment of HGG must target the process of tumour infiltration into normal surrounding brain tissue. Improved understanding of the molecular mechanisms underpinning cell migration and invasion have resulted in the development of biologically targeted anti-invasive therapies. This next section will review such approaches for the management of both adult and paediatric HGG.

1.4.1 Integrin targeting

Cilengitide is a peptidomimetic designed to function as a selective antagonist of αvβ3 and αvβ5 integrins (141,142) and is thought to play a role in disrupting angiogenesis, invasion and tumour cell growth (142). Pre-clinical *in vitro* and *in vivo* studies have demonstrated that cilengitide has anti-glioma activity, both alone (143,144) and in combination with temozolomide and radiotherapy (145,146). Phase I/II clinical trials of cilengitide for adult HGG, both as a single agent or in combination with temozolomide/radiotherapy, have shown modest proof of concept anti-

tumour activity, with preferential benefit for patients with O(6)-methylguanine-DNA methyltransferase (MGMT)-methylated tumours (142,147-153). However, rather disappointingly, a phase III randomised study of cilengtide combined with temozolomide chemoradiotherapy in adult patients with a new diagnosis of MGMT promoter-positive glioblastoma (CENTRIC European Organisation for Research and Treatment of Cancer (EORTC) study), failed to reach its primary end point, showing no difference in survival with the addition of cilengitide to temozolomide/radiotherapy in this patient cohort (154). Single agent cilengitide has been evaluated separately for paediatric patients with refractory HGG in a phase II study but, again, demonstrated no treatment effect. Despite the negative results observed in trials of cilengitide therapy, there may still be a role for other integrin antagonists as a treatment for HGG and further pre-clinical research is required (82).

1.4.2 FAK/Src inhibition

The FAK/Src tyrosine kinase signalling network plays a critical role in regulating cell migration (71). FAK is activated by integrins to recruit Src signalling proteins that are involved in the regulation of actin and focal adhesions to promote cell migration (71). Expression of FAK is elevated in glioma and has been shown to promote migration and infiltration (155,156). Liu *et al.* have shown that a novel dual tyrosine kinase inhibitor, TAE226, capable of inhibiting FAK and insulin-like growth factor 1 receptor (IGF-1R), reduced invasion of glioma cells by at least 50 % compared to controls in an *in vitro* matrigel invasion assay and significantly increased survival in an intracranial xenograft model, highlighting its clinical potential (157). Src family kinase-specific pharmacological inhibitors have also been developed and have been shown to inhibit invasion of adult glioma cells *in vitro* (158). Dasatinib is a potent Src inhibitor and has been evaluated clinically for use in several solid tumours (159). Currently, there is interest in developing dasatinib in early phase trials for adult glioma and paediatric DIPG (160-164). Dasatinib has been shown to reduce proliferation and invasion of DIPG cell lines (164). Interestingly, dasatinib has been shown to block

bevacizumab-induced glioma invasion, highlighting the potential for evaluation of combination anti-invasion and anti-angiogenesis therapy (165).

1.4.3 Protease inhibitors

Proteases are capable of degrading the ECM, thus creating a path allowing cancer cells to migrate. MMPs can be inhibited either by the overexpression of their tissue inhibitors or by the use of synthetic MMP inhibitors (MPIs). MPIs have been shown to reduce glioma invasion in two-dimensional (2D) and three-dimensional (3D) *in vitro* models. The MPI AG3340 promoted survival and profoundly inhibited glioma growth and invasion in treated mice compared to controls (166,167) and the MPIs marimastat and barmistat have also been shown to block glioma invasion in 3D *in vitro* culture systems (166). Disappointingly, the overall results of clinical trials of MPIs have not shown therapeutic benefits in a range of human cancers (including glioma) and have been associated with unacceptable toxicity in patients (168-170). Marimastat failed to improve survival in a phase III randomised, double-blind, placebo-controlled trial in patients with glioblastoma who had undergone surgery and radiotherapy (170). Pre-clinical studies have also focused on evaluating inhibition of the cysteine protease, cathepsin B and the serine proteases, uPA and its receptor, uPAR. *In vitro* studies have demonstrated that blockade or reduction in expression of these proteases can inhibit HGG cell adhesion, invasion and migration, suggesting their potential for clinical evaluation (115,171-174).

1.4.4 Cytoskeleton targeting

It is unsurprising that many cancer chemotherapies have been developed to target elements of the cell cytoskeleton. Microtubule targeting agents play a key role in the treatment of many solid tumours, including CNS malignancies and mainly act by deregulating microtubule dynamics, which results in mitotic arrest (175). Microtubule-targeting drugs can act either as destabilising agents (such as vinca alkaloids and colchicine-site binders), which inhibit microtubule polymerisation or can be classified as stabilising agents (for example, taxol and docetaxel), capable of enhancing microtubule polymerisation (175). Alongside their effects on mitosis and cell proliferation,

both destabilising agents and stabilising agents are able to reduce glioma cell invasion in an *in vitro* system (176,177). Most of the microtubule-targeting drugs available on the market act by binding to different sites on tubulin molecules (175). Newer agents are under development for different targets, including motor proteins (for example, AZD4877 is currently under development due to its role as a potent inhibitor of the mitotic spindle kinesin, Eg5) (178-180), MAPs such as the tau protein (181) or mitotic centromere-associated proteins (175,182).

Other approaches targeting the cytoskeleton have been evaluated. Small molecule inhibitors that target actin dynamics, such as cytochalasin, phalloidin and jasplakinolide have been assessed *in vitro* and demonstrate anti-migratory activity (183-185). Myosin II is a molecular motor that facilitates glioma invasion by generating the compressive force to squeeze cells through small intercellular spaces and pre-clinical 3D tissue models of invasion have shown that myosin II inhibition can block glioma invasion (186). Despite such clinical potential, it must be taken into account that actin and myosin are critical to normal cell motility and intracellular transportation and, thus, targeting these key molecules in humans could be associated with unreasonable toxicity (186). For this reason, small molecule actin/myosin inhibitors have not undergone translation for cancer treatments (184,186).

Finally, research has also focused on targeting upstream proteins involved in cytoskeleton signalling pathways (184). Rho family small GTPases are signalling molecules that play a role in multiple cellular pathways controlling cell proliferation, survival and invasion (187). Ras homology growth-related (RhoG) is overexpressed in human glioblastoma tissue and appears to mediate glioblastoma cell invasion (187). Small interfering ribonucleic acid (siRNA) depletion of RhoG has been shown to reduce glioblastoma cell invasion in an *ex vivo* brain slice assay (187). Unlike actin/myosin, RhoG appears to play a restricted role in normal cells (187,188) and, therefore, drugs developed to specifically inhibit RhoG may have a role as an effective anti-invasive glioma therapy (187).

1.4.5 Targeting EMT

During the process of EMT, cancer cells develop a more invasive phenotype and are able to disseminate to distant metastatic sites (66). Targeting this process could have a significant impact on patient outcome, as localised organ-contained tumours are associated with improved prognosis and are more amenable to different modes of cancer treatment, including surgery and radiotherapy (189). EMT may be pharmacologically targeted using one of four strategies (189). The first approach entails blocking signals from the tumour microenvironment that facilitate the onset of EMT. This involves blocking cytokine or growth factor signalling pathways (for example, TGF or EGF induction of EMT) or using small molecules to block cell surface receptors activated by such signals (189). A second approach is to block intracellular signal transduction pathways that induce EMT. This could involve molecular targeting of transcription factors such as Snail, Slug, Zeb and Twist, critical to EMT induction, or blocking of other upstream signal transducers (189). Thirdly, selective pharmacological targeting of cancer cells expressing mesenchymal marker proteins such as vimentin or neural-Cadherin (N-Cadherin) could reduce the presence of cancer cells possessing an invasive phenotype (189-191). Finally, formation of metastatic colonies may be preventable by blocking MET and blocking growth factors, such as fibroblast growth factor receptor isoform FGFR2IIIc, which conveys an epithelial phenotype on cancer cells, may be a therapeutic strategy to prevent MET (189,192). Although these different approaches are currently being investigated in several cancer models, including glioma, successful clinical translation will involve consideration of a personalised stage-specific approach. For example, targeting of EMT induction will have a limited role in patients with advanced metastatic disease (189). Additionally, EMT-targeted therapies must be evaluated with caution, as the delivery of therapies inhibiting the mesenchymal state could also enhance the speed of epithelialisation of metastatic deposits, worsening patient outcome (189).

1.5 GSK-3 inhibition

1.5.1 GSK-3: structure and activity

GSK-3 is a serine/threonine protein kinase with two main isoforms: GSK-3α and GSK-3β (193). A third splice variant of GSK-3β (GSK-3β2) has recently been identified (194). GSK-3α and GSK-3β are encoded by two distinct genes, mapped at 19q13.2 (GSK-3α) and 3q13.3 (GSK-3β) (195). Both isoforms share approximately 85 % identity, 98 % of which is in the catalytic domain (196). Despite such similarity, both isoforms appear to play different roles within the cell. For example, GSK-3β knock-out mice are non-viable, with late embryonic toxicity attributed to liver degeneration (197), whereas GSK-3α knock-out mice are viable but have metabolic and neuro-developmental sequelae (198,199). GSK-3 was originally noted to have an important role in glycogen metabolism; however, it is now clear that GSK-3 isoforms are involved in multiple cellular signalling pathways and play a part in orchestrating cell division, cell death, cell survival, DNA damage response, cell migration, neuronal development and neuronal functioning (196). Given such diversity in function, it is unsurprising that GSK-3 is implicated in the pathogenesis of several diseases, including cancer, metabolic disorders (diabetes, heart disease) neurological disorders (Alzheimer's, Parkinson's) immune dysfunction and psychiatric disease (193,195,196,200,201).

The GSK-3 family of kinases are able to phosphorylate over 40 proteins and 12 transcription factors (201). Both GSK-3α and GSK-3β preferentially phosphorylate substrates that have already been 'primed' by phosphorylation following activity of other kinases (201). Activity of GSK-3 itself is controlled by post-translational phosphorylation. Phosphorylation of GSK-3β at serine nine (Ser9) is inhibitory and at tyrosine 216 (Tyr216) is activating (196). For GSK-3α, phosphorylation of serine 21 (Ser21) is inhibitory and tyrosine 279 (Tyr279) is activating (196). When GSK-3β is phosphorylated at Ser9, this acts as a pseudosubstrate, preventing other substrates entering the kinase catalytic site. Conversely, when Tyr216

remains unphosphorylated, this blocks entry to the catalytic site, a process which is reversed by Tyr216 phosphorylation (196). GSK-3β activity is also modulated by its interaction with other proteins in complex formations (202). Axin and presenilin are examples of such proteins and play a role in controlling the specific function of GSK-3β within the cell.

1.5.2 GSK-3 in tumourigenesis

The role of GSK-3 in cancer development is unclear and it may be that there is a fine balance between GSK-3 acting as a tumour suppressor or a tumour promoter (201). Increased GSK-3β levels have been observed in ovarian, thyroid, colon, liver, glioma and pancreatic cancers; however, non-melanoma skin cancers are associated with reduced GSK-3β expression (195,203-207). One well-described role for GSK-3 in inhibiting cancer development is its involvement as a regulator in Wnt/β-catenin signalling. When Wnt signals are absent, β-catenin forms a complex with axin, APC and GSK-3. Active GSK-3 phosphorylates β-catenin, which targets β-catenin for ubiquitylation and proteolytic destruction. In the presence of Wnt signals, GSK-3 is inactivated and, thus, β-catenin accumulates, moves to the nucleus and increases transcription of proto-oncogenes, such as *c-MYC* and *cyclin-D1*, as well as genes involved in cell migration and invasion, such as *MMP7* (195). The fact that GSK-3 can suppress the Wnt/β-catenin pathway and reduce β-catenin, suggests that GSK-3 may have a role as a tumour suppressor (201). Additional evidence supporting the role of GSK-3 as a tumour suppressor includes the ability of GSK-3β to promote *p53*-induced apoptosis (195,208,209) and the observation that GSK-3 inhibition promotes EMT and cell invasion (201,210).

GSK-3 may also function to promote tumourigenesis. GSK-3β knockdown in pancreatic cancer cell lines arrested proliferation, increased apoptosis and significantly decreased vascular endothelial growth factor (VEGF) (211). When modelled *in vivo*, the authors showed that GSK-3β knockdown inhibited tumour growth and angiogenesis, highlighting the possible role of GSK-3β in tumour development and the potential therapeutic benefits of

GSK-3β inhibitors (211). GSK-3β has also been shown to promote ovarian cancer proliferation both *in vitro* and *in vivo (212)*. Hence, the role of GSK-3 as a tumour promoter or suppressor appears to be cancer-type-dependent.

1.5.3 The role of GSK-3 in cell migration

GSK-3 has a multi-faceted role in controlling cell migration and can influence the dynamics of the actin cytoskeleton, microtubule remodelling and cell-ECM adhesions (213). The Rho family of GTPases (including Rho, Rac and adenosine diphosphate ribosylation factor 6; Arf6) regulate actin cytoskeleton organisation and dynamics and contribute to lamellipodia formation at the front of the cell (213,214). GSK-3 appears to inhibit p190 Rho GTPase-activating proteins (RhoGAP) which, in turn, can activate Rho in fibroblasts, triggering downstream effectors that result in actin polymerisation (213,215). Additionally, GSK-3 can function as an upstream regulator of Rac and Arf6, again promoting actin polymerisation and lamellipodia formation in the migrating cell (213,216,217). As described in section 1.3.4, GSK-3 also plays a role in determination of cell polarity. The localised inactivation of GSK-3 results in APC clustering at the plus end of microtubules at the leading edge of cells, controlling the direction of movement (110). GSK-3 can also influence MAPs, MAMs and proteins of the MTOC (213). For example, GSK-3 phosphorylation can facilitate the release of intracellular cargo from kinesin motors in neurons (213,218). The MAP CLASP can act to stabilise microtubules and GSK-3 may indirectly target CLASP by affecting association with intermediate binding proteins in order to inhibit microtubule stabilisation (213,219,220). Paxillin is a docking protein that plays a key role in focal adhesions by recruiting signalling molecules into the complex (221). Phosphorylation of paxillin appears to be mediated in part by GSK-3 and plays an important role in formation of adhesions, cell spreading and cytoskeletal rearrangement (213,222). Finally, GSK-3 has been shown to inhibit FAK catalytic activity and this control of FAK activity is critical for adhesion dynamics during cell spreading and migration (213,223).

1.5.4 GSK-3 inhibitors

It is unsurprising that there is substantial interest in developing pharmacological inhibitors of GSK-3. As highlighted above, GSK-3 has a broad range of substrates and plays a role in the pathogenesis of a wide range of diseases. To date, more than 50 GSK-3 inhibitors have been described (201). GSK-3 inhibitors act by either: i) competing with adenosine triphosphate (ATP) or metal-binding sites (i.e. magnesium) essential for catalytic reactions; ii) modulating the inhibitory or activating phosphorylation sites of the kinase; or iii) inhibiting the formation of protein complexes that are critical for binding substrates (196).

Lithium was one of the first GSK-3 inhibitors to be described and is a non-specific inhibitor of GSK-3 (IC_{50} ~2 mM), acting both directly (as a competitive inhibitor of Mg^{2+}) and indirectly (by increasing the inhibitory phosphorylation of GSK-3) (224). Lithium is also able to target inositol monophosphatase (IMPase), phosphomonoesterases, phosphoglucomutase and the arrestin-2/Akt complex (225). Despite such a wide range of targets, there is evidence to demonstrate that lithium effectively targets GSK-3, as lithium increases intracellular β-catenin levels, activates glycogen synthase and reduces the phosphorylation of tau in neurons (225-228). There is a wealth of clinical experience of using lithium as a mood stabilising agent for the treatment of bipolar disease; however, more recently, lithium has been evaluated in patients with neurodegenerative diseases, such as Alzheimer's disease and motor neuron disease (226,229-231), as well as patients with cancer (232-234). It is well documented that lithium has a narrow therapeutic index, with safe effective therapy achieved at concentrations between 0.5-1.5 mM (226). Above 1.5 mM, lithium is often toxic *in vivo*, mainly secondary to nephrotoxicity (226,235,236).

Indirubins are bis-indole isomers of indigo, collected from natural sources, including plants, molluscs, bacteria and mammalian urine (237). Indirubins have been identified as the active ingredient of the Chinese medicine Danggui Longhui Wan, which has been shown in clinical trials to have anti-

leukaemic activity (238-240). In 2001, Leclerc *et al*. showed that indirubins are powerful inhibitors of GSK-3 (IC_{50} 5-50 nM) and cyclin-dependent kinases (IC_{50} 50-100 nM) (241), rendering them promising anti-cancer agents. 6-bromoindirubin-oxime (BIO) is an indirubin derivative that has been shown to be a selective inhibitor of GSK-3β both *in vitro* and *in vivo* and can activate Wnt signalling, thus stabilising β-catenin (242,243). There has been interest in the pharmacological development of indirubins, in particular for Alzheimer's disease, as inhibition of GSK-3 may be able to prevent the hyperphosphorylation of tau proteins, which are pathological for the disease (243,244). Investigation of indirubins for cancer treatment is mainly in the pre-clinical phase (245,246).

In the last decade, novel GSK-3 inhibitors have been developed and are beginning to make their way into the clinic (196,226). One such example is AZD1080, an orally bioavailable brain-permeable selective GSK-3 inhibitor, that has been used in a phase-I study of healthy volunteers to determine its pharmacologic profile (247). This trial demonstrated that AZD1080 could target GSK-3 activity in humans, as prolonged suppression of glycogen synthase activity was recorded in blood cells (247). Although there is concern that GSK-3 inhibitors may be tumourigenic through their ability to increase β-catenin levels and transcription of proto-oncogenes, current evidence suggests otherwise (195). Mice treated with GSK-3 inhibitors do not appear to have increased incidence of cancers (201) and patients who received lithium therapy for treatment of mental illness do not have elevated prevalence of cancer (248). Finally, Gould *et al*. have shown that mice predisposed to cancer development by the activation of Wnt signalling pathways do not demonstrate a significant increase in the number of tumours developed when treated with 60 days of lithium therapy (249). Despite such encouraging observations, this concern should be addressed for each GSK-3 inhibitor undergoing clinical development (196).

1.5.5 Potential of GSK-3 inhibitors in the treatment of glioma

Studies have demonstrated that GSK-3 plays a central pathological role in the development and maintenance of HGG. Miyashita *et al.* found higher expression of GSK-3β and phosphorylated GSK-3β^{y216} (active form) in adult glioblastoma, compared to non-neoplastic brain tissue (207). The authors also showed that inhibition of GSK-3β with the inhibitor AR-A014418 suppressed the viability and proliferation of glioma cells and induced apoptosis by activating retinoblastoma (Rb)-mediated pathways (207). Interestingly, AR-A014418 significantly sensitised glioma cells to chemotherapy and radiotherapy (207). Aguilar-Morante *et al*. also showed that the GSK-3β inhibitor, TDZD-8, induced apoptosis and decreased proliferation of mouse glioma cells *in vitro* and significantly improved survival in an orthotopic mouse model (250). Kotliarova *et al*. have also demonstrated that GSK-3 inhibition can arrest cell proliferation and induce both intrinsic and extrinsic apoptosis pathways in glioma, which may be mediated by *c-MYC* (251). In this study, GSK-3 inhibition was also able to inhibit pro-survival signals by causing a reduction in intracellular nuclear factor-kappa B (NF-κB) activity (251).

Work by Nowicki *et al*. demonstrated the effects of GSK-3 inhibition on adult glioma migration and invasion. The authors showed that inhibition of GSK-3 with lithium blocked invasion of adult glioma cells in spheroid, wound-healing and brain slice assays (236). Subsequent studies also showed that indirubins (including BIO) reduced invasion of adult glioma cells *in vitro* and *in vivo* and improved survival in a mouse intracranial xenograft model. Furthermore, indirubins were also able to block migration of blood vessel endothelial cells and reduce angiogenesis in tumour models (246).

1.5.6 Summary

Invasiveness is a key feature of HGG cells and significantly contributes to the dismal prognosis for this disease. Compared to the adult disease, very little is known about the migratory and invasive characteristics of pHGG cells and the effects of GSK-3 inhibitors on paediatric gliomas are unknown.

Although the efficacy of a number of anti-invasive therapeutics for adult and paediatric glioma have been demonstrated in pre-clinical and limited clinical studies, further work is needed to develop novel anti-invasive therapeutic approaches that work in synergy with chemotherapeutics and target the numerous biological pathways involved in glioma pathogenesis.

1.6 Oncolytic virotherapy for high grade glioma

1.6.1 Introduction

Oncolytic virotherapy, which uses viruses to selectively infect and destroy cancer cells (252), offers a novel treatment approach for poor prognosis paediatric CNS tumours, including pHGG and DIPG. While there is extensive literature on oncolytic virotherapy for adult brain malignancies such as glioblastoma, work on paediatric CNS tumours is only just beginning to gather momentum. This section of the introduction will summarise the biological characteristics of several oncolytic viruses (OVs) that have the potential for development as anti-cancer agents for poor prognosis children's brain tumours and will evaluate the pre-clinical and clinical evidence for the use of oncolytic virotherapy for HGGs.

1.6.2 Oncolytic viruses as anti-cancer agents: direct and immune mediated mechanisms of cancer cell death

OVs selectively infect and lyse cancer cells, while sparing normal tissue (252,253). Once a virus has entered a cell, it aims to take advantage of cellular resources in order to replicate and synthesise new viruses (252). To allow sufficient time to adequately replicate, viruses inhibit cellular death pathways, ensuring that cell death can only occur once all valuable cellular resources have been maximally exploited (252). Cells have evolved to have mechanisms in place in order to limit viral replication and infection. In normal cells, detection of viral infection via the identification of viral pathogen-associated molecular patterns (PAMPs), including viral capsids, DNA, ribonucleic acid (RNA) and protein products, initiates signals promoting the production of pro-inflammatory cytokines, including type-I interferons (IFN)

(254). These activate downstream anti-viral signalling pathways, including upregulation of protein kinase R (PKR), a cell cycle regulator that is capable of inhibiting cell protein synthesis and initiating apoptosis (254-256). Together, this intracellular anti-virus response promotes the death of virus-infected cells, preventing further virus replication (254). Cancer cells are more susceptible to killing by viruses (254). IFN signalling and PKR activity may be downregulated, hence limiting viral clearance through the suppression of protein synthesis and induction of apoptosis (254). Thus, within cancer cells, OVs are able to make use of abnormal signalling pathways in order to block apoptosis, allowing more time for successful virus replication (254). Following successful replication, OVs induce host cell death and this may be achieved by one of several mechanisms, including apoptosis, necrosis, pyroptosis and autophagy (252,254).

There has recently been a shift in the oncolytic virotherapy paradigm to suggest that OVs may also generate tumour cell killing through the induction of potent innate and adaptive anti-tumour immune responses (257,258). Following infection with an OV, cancer cells respond by releasing cytokines (in particular type-I IFN), PAMPs, danger-associated molecular pattern signals (DAMPs) (including heat shock proteins, calreticulin, ATP, uric acid and high mobility group box 1 protein (HMGB-1)) and reactive oxygen species (ROS) (254). DAMPs, PAMPs and type-I IFN can generate the innate immune response, through recruitment of natural killer (NK) cells, which can kill virus-infected tumour cells (253,254). ROS, cytokines, PAMPS and DAMPs may also activate antigen-presenting cells (APCs), which take up and present viral- and tumour-associated antigens (TAAs) released from infected cancer cells (254). APCs present viral antigens and TAAs to $CD8^+$ T cells and $CD4^+$ T helper cells. The $CD8^+$ T cells can then mature into cytotoxic effector cells and accumulate at sites of tumour growth, killing cancer cells upon antigen recognition, as part of an adaptive anti-tumour immune response (253,254).

Tumours have evolved multiple strategies in order to avoid immune system detection and subsequent destruction by T cell-mediated attack (259).

Tumour-derived soluble mediators and cytokines can disrupt the function of dendritic cells (DCs), which play a key role in tumour antigen presentation to B and T cells (259-264). Altered activity of tumour-expressed chemokines can suppress T cell movement and recruitment into tumours (259,265,266). Immunosuppressive leukocyte populations such as regulatory T cells (T-regs) and myeloid-derived suppressor cells (MDSCs) are recruited and expanded within cancers (259,267,268). Furthermore, the tumour microenvironment is rich with soluble mediators, such as TGF-β, interleukin (IL)-10, prostaglandin E_2, histamine, hydrogen peroxide and adenosine which can inhibit cytotoxic T cell function and, finally, tumours express surface proteins such as programmed cell death ligand (PD-L)-1 and PD-L2 which can further suppress T cell function (259,269,270).

OVs can be exploited for their ability to enhance the immunogenicity of the tumour microenvironment (253). OV-induced cancer cell death enhances the availability of TAAs for uptake by DCs (253). This is achieved in the context of danger signals, such as inflammatory cytokines, DAMPs and PAMPs released by cancer cells following OV infection (253,254). In consequence, DC activation is enhanced, increasing tumour antigen presentation in an appropriate costimulatory context to the adaptive immune system (253). This, in turn, increases the activation of cytotoxic $CD8^+$ T cells, enhancing the anti-tumour immune response (253,259). Additionally, OVs are capable of altering the balance of cytokine production within tumours, which can enhance T cell responses and inhibit tumour-derived immunosuppressive properties (253). For example, reovirus treatment has been shown to reduce tumour secretion of the immunosuppressive cytokine IL-10 (253). Reovirus treatment can also increase IL-8 and RANTES secretion, both of which are involved in DC, monocyte and neutrophil recruitment to tumours, as well as IL-6, which acts to inhibit the immunosuppressive function of T-regs (253). Finally, IFN-γ is a critical anti-viral mediator secreted by $CD4^+$, $CD8^+$ and NK cells and is central to the elimination of viruses by the immune system (271,272). Alongside its ability to traffic specific immune cells to sites of inflammation, enhance NK cell activity and stimulate macrophages, IFN-γ can also upregulate cell surface expression of class I major

histocompatibility complex (MHC) in response to intracellular viral infection (271). This increases the potential for cytotoxic T cell recognition of foreign viral peptides and subsequent destruction of virus-infected cells (271). In the context of oncolytic virotherapy, this upregulation of MHC class I on virus-infected cancer cells promotes the induction of cell-mediated immunity which results in tumour cell killing.

1.6.3 Oncolytic virus selectivity and replication

Viruses have specific cellular tropisms that determine the tissues that they will naturally selectively infect (252). It has been observed that many wild-type viruses are able to preferentially infect cancer cells over normal cells and this may be secondary to aberrations in cancer cell signalling, surface molecules and stress responses that viruses are able to exploit to gain cell entry (66,254). There are several well-described mechanisms that OVs can employ in order to selectively target tumour cells (273). These may be achieved naturally or through viral engineering. DNA viruses (excluding poxviruses) and retroviruses can be made tumour selective by inserting tumour specific promoters into their genome that regulate the expression of certain genes that are essential for virus replication (273). Translational targeting may also be employed, which takes advantage of defective IFN signalling in cancer cells (273). Viruses can be modified to disable proteins that suppress IFN signalling so that in normal host cells, replication is aborted (273). When such a modified virus enters a cancer host cell with defective IFN signalling, IFN-mediated translational shutdown is prevented and the viral infection progresses (273). Viruses can also be modified to disable proteins that prevent apoptosis, hindering their replication in normal cells. However, when such virus enters a cancer cell, which may naturally possess mutations preventing its ability to undergo apoptosis, the virus can replicate and, again, infection progresses (273). Finally, viruses may gain entry into cancer cells by targeting cell surface receptors expressed either more abundantly or exclusively by cancer cells (254,273). Some OVs may

have a natural tropism for such receptors; however, viruses can also be engineered in order to target receptors specific to cancer cells (254).

1.6.4 Virus structure and replication cycle

Viruses are made up of two basic components. An inner core of nucleic acid is surrounded by an outer protein capsid, which functions to protect the genome from digestion by nucleases and plays a role in attachment of the virus to host cells (274). Some viruses may have an additional layer of cover, called an envelope, which consists of a lipid bilayer interjected by glycosylated proteins (274). A fully assembled infectious virus is referred to as a virion (274). Viruses can undergo a replication cycle. The virion must first attach to a target cell receptor via proteins on its outer surface; an enveloped virus enters the cell via fusion at the plasma membrane, whereas a non-enveloped virus will enter by physical permeation of the host membrane and particle translocation (273,275). Once the virus has entered the cell, it is uncoated to reveal its genome, which then must be replicated and transcribed (273,275). Genome replication may occur in the cytoplasm or nucleus of the host cell and the location is specific for each individual virus (273). The virus can then express and translate genes encoding either non-structural (expressed early) or structural proteins (expressed late). Non-structural proteins serve to amplify the viral genome, overcome cell death mechanisms to allow time for viral replication and enhance the expression of structural proteins required for virus re-assembly (273). Replicated viral genomes are then packaged in capsids and progeny virus exit the cell via routing pathways, ready to infect and replicate in neighbouring cells (273,275).

The following section highlights the individual structure, biology and mechanism of cancer cell tropism for three OVs: herpes simplex virus (HSV), vaccinia virus (VV) and reovirus, which were the subjects of investigation in this research project.

1.6.5 Herpes simplex virus

HSV-1 is a member of the alphaherpesvirus subfamily of herpesvirus (276). The virus consists of an inner core of double-stranded DNA (152 kb), encoding approximately 74 genes (276,277). The HSV-1 genome is protected by an icosahedral capsid, which is surrounded by a tegument composed of viral proteins (276,278). Finally, an outer envelope of glycoproteins, that play a critical role in regulating HSV-1 entry into host cells, completes the virus structure (276). In order to replicate, HSV-1 must bind to entry receptors on the host cell via glycoproteins; although seven glycoproteins are implicated in this process, only glycoprotein D, B, H and L are critical for function (276). Host cell receptors for HSV entry include nectin-1/nectin-2 and herpesvirus entry mediator (HVEM) (276). Once bound, the virion can gain entry into the host cells by either pH-independent fusion with the host plasma membrane or by endocytosis (276). Subsequent DNA synthesis and nucleocapsid assembly occur in the host cell nucleus, causing it to re-organise and increase in size, whereas virion processing and maturation occur in the cytoplasm (278). The virus DNA does not integrate into the host cell DNA (279). Following viral replication, host cells die as viral particles lyse the cell in order to spread to infect neighbouring cells (279).

Approximately 30 kb of the HSV-1 genome codes for non-essential genes and this property can be exploited for the purpose of oncolytic virotherapy, as these genes can be deleted and/or replaced to reduce pathogenesis and enhance selective tumour infection (254,279). One such example is the oncolytic HSV1716 (SEPREHVIR), modified to contain a deletion of the *infected cell protein* (*ICP*) *34.5* neurovirulence gene, which is critical for HSV-1 infection of neurons and plays a role in antagonising the type-I IFN/PKR protective response (254,279). Overall, deletion of *ICP34.5* enhances cancer cell selectivity and improves safety by preventing virus infection of neurons (254,279). A range of oncolytic HSV strains have been engineered to enhance selectivity and reduce virulence of HSV-1 (280-284). Additionally, oncolytic HSVs have been modified to contain genes such as granulocyte macrophage colony stimulating factor (GM-CSF) that act to enhance systemic anti-tumour immune responses (254,280). Talimogene

laherparepvec (*ICP34.5* deletion, *US11* deletion, GM-CSF insertion) is one such example, which has recently been approved by the United States Food and Drug Administration (285) and has been shown to have therapeutic benefit against melanoma in a phase III trial (280).

1.6.6 Vaccinia virus

VV is a member of the poxvirus family and characteristically has large ovoid or brick shape virions (286). Like HSV-1, it is a double-stranded DNA virus (approximately 190 kb) and is able to host large transgene insertions (254,287). Vaccinia forms two distinct infectious virion particles. The first, entitled intracellular mature virus (IMV), is surrounded by a single membrane and remains inside a cell until cell lysis (286). The second consists of an IMV surrounded by an additional cell membrane and exits the cell prior to cell death (286). On exit, if this virion is maintained on the cell surface, it is referred to as a cell-associated enveloped virus (CEV) (286). Following release from the cell surface, it is termed an extracellular enveloped virus (EEV) (286). IMVs and EEVs play different roles in the viral life cycle and are functionally, structurally and antigenically different. For replication, VV sheds its membrane in order to release naked viral core/genome into the host cell cytoplasm (286). IMVs and EEVs achieve this in different ways. For IMVs, the outer membrane may fuse with the host cell plasma membrane, allowing deposition of the viral core (286). Alternatively, IMVs enter the cell via macropinocytosis (a form of endocytosis accompanied by cell surface ruffling (288)), allowing the formation of a vesicle containing the IMV. The IMV membrane then fuses with the membrane of the vesicle, dispelling the naked core into the cytoplasm (286). Once in the cytoplasm, the naked core is transported on microtubules to the perinuclear regions of the cell, where they are uncoated to allow viral DNA transcription and replication (286). Progeny virions are then assembled as IMVs within virus factories in the cytoplasm (286). Some IMVs are wrapped by a double membrane and transported to the cell surface, where they fuse with the host plasma membrane and reside as CEVs (286). These may be disseminated as EEVs

or they may develop a polymerised actin tail that propels them to neighbouring cells, encouraging local virus spread (286).

VV replication appears to be dependent on activated EGFR/Ras pathway signalling in the host cell (289). This may explain why VV has a natural tropism to cancer cells, which are known to possess upregulated Ras signalling (254). Although VV is naturally selective of cancer cells, the virus has been attenuated for safety by disrupting the *thymidine kinase* (*tk*) gene, which expresses an enzyme essential for viral DNA synthesis (254,278,289). The oncolytic VV JX-594 also expresses GM-CSF under the control of a synthetic promoter; GM-CSF is an immunostimulatory cytokine which is able to enhance tumour kill via activation of the immune system (289). Another clinical VV, GL-ONC1, is a replication competent OV that has been engineered to contain disrupted *tk*, *F14.5L* and haemagglutin genes, conferring tumour selectivity and limiting virulence in normal tissue (290-292). Haemagglutin is a glycoprotein that plays a key role in binding to host cell receptors to initiate virus infection (293). The *F14.5L* gene encodes an intracellular mature virus envelope protein that mediates cell adhesion and can be disrupted to reduce virulence, again enhancing safety (294).

1.6.7 Reovirus

Reovirus is a member of the Reoviridae family (295). The reovirus genome consists of ten segments of double-stranded RNA (23 kb), enclosed by two concentric icosahedral protein capsids, which are non-enveloped (254,295). In order to gain entry into host cells, reovirus attaches via interactions with cell surface glycans and junctional adhesion molecule A (JAM-A) (296,297). β-1 integrin mediates internalisation of the virus via endocytosis, subsequently activating Src kinases (296,298,299). The virus then localises and traverses through endosomes, where it is partially uncoated and disassembled by cysteine cathepsin proteases resulting in the formation of infectious subvirion particles (ISVPs) (296). ISVPs then penetrate the endosome membrane, releasing the transcriptionally active viral core into

the cytoplasm, where proteins are translated and new capsids are formed, prior to virion release (296).

Three reovirus serotypes have been isolated but it is the reovirus type 3 dearing strain that exhibits a natural preference for cancer cells, as it replicates in cells with activated Ras signalling (252,287). In the normal host cell, reovirus activates PKR, which, in turn, inhibits translation of viral proteins, preventing viral replication and spread (254,300). In the Ras-activated cancer cell, PKR is kept in an inactive state, allowing viral translation, replication and oncolysis to take place (254,300). The specificity of reovirus type 3 dearing strain for Ras-transformed cells, coupled with its relatively non-pathogenic nature in human subjects (301), makes it an attractive anti-cancer agent to develop. Wild type reovirus type 3 dearing strain has been developed and evaluated clinically in adults and children under the trade name of Reolysin® (302-307).

1.6.8 The effects of oncolytic viruses on cell migration

Very little is known about the effects of OVs on cancer cell invasion and migration. However, what is clear from the literature is that once a virus enters a host cell, the host cell's cytoskeleton plays a critical role in regulating the virus life cycle (308). Viruses rely on the host cell cytoskeleton for efficient transportation of capsids to the nucleus or sites of replication in the cytoplasm (308,309). Microtubules appear to form networks, which are critical for propelling and transporting viruses encased within vesicles, organelles or cytosolic complexes within the cell. Actin is essential to control the direction of such movements and also facilitates virus entry and egress from cells (308-310). Viruses, such as wild-type HSV, are able to stabilise host cell microtubules through the induction of post-translational tubulin modifications. This process may be critical for viral replication by creating a direct transport network for the virus to reach critical locations in the cell throughout its life cycle (311). Hence, an OV may be able to influence tumour cell migration, through interplay with the host cancer cell cytoskeleton. Consistent with this hypothesis, Abdullah *et al.* report that

Newcastle disease virus (NDV)-infected glioma cells have repressed motility when observed by live cell imaging (312).

It is also possible that viruses, such as HSV, may be able to influence the migration of immune cells. Pretchel *et al*. demonstrated that HSV is able to reduce the migration of DCs using a transwell assay with a chemokine gradient. The authors showed that HSV downregulates surface expression of the migration-mediating surface molecules chemokine (C-C motif) receptor (CCR)-7 and chemokine (C-X-C motif) receptor (CXCR)-4, which reduces the ability of DCs to migrate towards the corresponding chemokines, chemokine (C-C motif) ligand (CCL)-19 and chemokine (C-X-C motif) ligand (CXCL)-12 (313). This may be a mechanism that HSV uses to escape the immune system, as reducing DC migration to secondary lymphoid organs prevents antigen presentation and T cell stimulation (313). Theodoridis *et al*. have also shown that HSV can inhibit migration of DCs in 3D collagen gels. The authors suggest that this effect is a result of HSV activating lymphocyte function-associated antigen 1 (LFA-1), which functions as an adhesion molecule and increases adhesiveness of extracellular matrix proteins to DCs, consequently impairing their migration (314).

The ability of OVs to target cell migration and invasion remains an interesting concept and is explored within this thesis. If OVs have the potential to act not only as cytotoxic and immunogenic agents but also as anti-migratory agents, this would be a highly sought after therapeutic option for poor prognosis invasive tumours, such as paediatric and adult HGG.

1.7 Oncolytic virotherapy for paediatric CNS tumours

1.7.1 Pre-clinical studies

Oncolytic virotherapy research for paediatric CNS tumours is in its infancy and only a limited number of pre-clinical studies have been published in this field. It is unsurprising that the majority of studies evaluate efficacy in medulloblastoma, as this is the most common malignant brain tumour of

childhood and confers a dismal prognosis at relapse (315). Over 15 years ago, Lasner *et al.* published that the HSV variant 1716 could infect and destroy D283 medulloblastoma cells and demonstrated that intra-tumoural injection of the virus into D283 tumour-bearing mice conferred a statistically significant survival advantage when compared to controls (316). Around the same time, Pyles *et al.* also demonstrated the therapeutic potential of another modified HSV strain (3616UB) that was able to arrest growth of DAOY cell xenografts in CD17 severe combined immunodeficiency (SCID) mice (282). Finally, Freidman *et al*. have recently published that mouse xenografts of human-derived medulloblastoma cells and cancer stem cells were highly sensitive to killing by HSV G207, as well as a novel HSV IL-12 producing virus (M002) (317).

Reovirus type 3 dearing has also been investigated in medulloblastoma. Yang *et al.* have demonstrated that medulloblastoma cell lines and primary human-derived cell cultures were sensitive to infection with reovirus type 3 dearing and that intra-tumoural reovirus treatment of a mouse medulloblastoma model could significantly improve survival and inhibit development of spinal and leptomeningeal metastases (318). Other publications have also demonstrated that medulloblastoma is sensitive to killing by measles virus (319,320), myxoma virus (321) and seneca valley virus (SVV) infection (322).

A limited number of studies have focused on oncolytic virotherapy for pHGG. Friedman *et al.* have shown that a paediatric cerebellar glioblastoma xenograft, DM456, contains tumour and cancer stem cells that are more sensitive to killing by a range of modified HSVs than adult glioma xenografts (323). SVV (NTX-010) has also been tested on a range of paediatric brain tumours, including glioblastoma, medulloblastoma and ependymoma (324). Some positive response was seen to virus treatment in glioma lines; however, NTX-010 was not effective on the medulloblastoma and ependymoma lines in this study (324).

1.7.2 Clinical evidence

There are already a handful of encouraging reports in the literature that lay the foundations for the development of oncolytic virotherapy for paediatric CNS tumours. Case reports evaluating NDV MTH-68/H in paediatric patients with intracranial tumours have provided a useful insight into the feasibility, safety and efficacy of oncolytic virotherapy in this patient group. Csatary *et al.* report three paediatric patients (18 months to 12 years at diagnosis) with grade III/IV glioma at relapse who received regular intravenous (i.v.) NDV continuous maintenance therapy for several years. At time of publication, all three patients demonstrated between seven- to nine-years of survival with good quality of life, which exceeds the quoted median duration of survival of approximately 18-24 months (28,325-327). Another case report describes a 12-year-old boy with treatment-resistant grade III anaplastic astrocytoma, who received i.v. and inhaled NDV, alongside valproic acid. Although treatment initially resulted in tumour regression, the patient eventually died from progressive disease (328). Encouragingly, NDV antigen and constituents were found in tumour tissue, confirming the successful systemic delivery of the virus to the tumour and demonstrating the virus' ability to infect and replicate in paediatric human cancer cells (328). Finally, another paediatric patient with recurrent glioblastoma tolerated i.v. NDV with no major side effects in a clinical trial (329).

Oncolytic virotherapy with Reolysin®, JX-594 and NTX-010 has been evaluated by clinical trials in a limited number of paediatric patients with extra-cranial solid tumours (303,330,331). Overall, therapy was well tolerated (303,330,331). The above studies have begun to answer the questions regarding the dosing, safety and efficacy of delivering virotherapy to children. However, the next step for the field is the development and delivery of phase I trials evaluating a range of potential OVs specifically for paediatric CNS tumours. Two such trials are currently open for recruitment. The first aims to evaluate the maximum tolerated dose (MTD) and safety of delivering intra-tumoural injection of HSV1716 to paediatric patients (age 12-21) with refractory or recurrent HGG at the time of surgery (332). The second sets out to evaluate the MTD and safety of delivering i.v. Reolysin®

in combination with subcutaneous GM-CSF to paediatric patients (age 10-21) with high grade recurrent or refractory brain tumours (333).

1.8 Oncolytic virotherapy for adult glioma

Since the early 1990s, there has been a growing interest in developing oncolytic virotherapy for the treatment of glioblastoma (334). The first laboratory engineered virus, a thymidine kinase-negative mutant of HSV (dlsptk) was, in fact, evaluated in a mouse model of adult glioma (334,335). Martuza *et al.* demonstrated that HSV dlsptk had cytotoxic effects against human glioma cell lines and was able to prolong survival in nude mice with intracranial U87 glioma (335). Although promising for clinical translation, *tk* inactivation rendered the virus resistant to several anti-viral therapeutics (which rely on active *tk* to inhibit viral replication) and this loss of susceptibility to anti-viral drugs rendered these viruses unsafe for clinical use, as there would be no strategy to overcome uncontrollable viral replication within patients (336). Despite this, the study by Martuza *et al.* paved the way for the development of clinically safe oncolytic HSV, alongside a range of other OVs (335,336). To date, over 15 different OVs have been evaluated in pre-clinical studies for the treatment of adult glioma, which has led to the development of a range of early phase clinical studies for this patient group (334). Table three summarises published clinical trials to date of adult patients with HGG. Overall, clinical trials have demonstrated that oncolytic virotherapy for glioma is feasible and safe and not associated with major virus-related adverse effects (334). Although the majority of these studies are phase I, there are some encouraging observations that highlight the potential of clinical response with oncolytic virotherapy in HGG. One trial of intra-tumoural injection of reovirus reports a patient with over six-year survival (337) and a trial of HSV1716 reports three patients remaining disease free for between 15-22 months (338). Finally, in a phase I/II trial evaluating i.v. cycles of NDV-HUJ, one patient had a complete tumour response (329).

The next stage for the adult field is to improve the delivery of OVs to intracranial tumour locations. Intra-tumoural injection limits the number of opportunities for treatment, whereas systemic delivery may be fraught with problems in effectively penetrating the BBB and overcoming the potential for neutralisation of the virus by the patient's immune system before it can access the tumour target. There is clearly a fine balance between minimising destruction of administered virus by the host immune system, whilst enhancing the immune system's response to kill and ablate virus-infected cancer cells (252,253). One avenue of research is currently focused on developing cellular carriers that deliver viruses to tumours while hiding them from the neutralising effects of the immune system (252). Furthermore, viruses can be modified to express tumour antigens, so that when they are appropriately delivered to the immune system the anti-tumour immune response is enhanced (252,339,340). Finally, the potential for synergistic interactions between OVs, radiotherapy and chemotherapy for HGG must be evaluated in clinical trials, alongside the potential of combining OVs and novel immunotherapeutics such as checkpoint inhibitors, which appear to enhance therapy in *in vivo* models of glioma (341).

	Name (and study reference)	Modification	Study phase	Mode of delivery	Combination therapy	Number of patients	Toxicity
HSV	G207 (281)	*ICP34.5* deletion *UL39* disruption	I	Single intra-tumoura injection	No	21	No toxicity or SAE attributed to virus
	G207 (342)	*ICP34.5* deletion *UL39* disruption	Ib	2 intra-tumour injection (pre/post surgery)	No	6	Transient fever, delirium, and hemiparesis in one patient
	G207 (343)	*ICP34.5* deletion *UL39* disruption	I	Single intra-tumour injection 24 h prior to RT	Yes, 5 Gray RT	9	No toxicity or SAE attributed to virus
	1716 (344)	*ICP34.5* deletion	I	Single intra-tumour injection	No	9	No toxicity or SAE attributed to virus
	1716 (345)	*ICP34.5* deletion	I	Single intra-tumour injection	No	12	No toxicity or SAE attributed to virus
	1716 (338)	*ICP34.5* deletion	I	Single intra-tumour injection	No	12	No toxicity or SAE attributed to virus
Reovirus	Reolysin® (337)	Nil	I	Single intra-tumour injection	No	12	No grade III/IV SAE attributed to virus
	Reolysin® (346)	Nil	I	72 h intra-tumour infusion	No	15	One grade III SAE (convulsion) probably related to virus, no grade IV attributed to virus
Adenovirus	ONYX-015 (347)	Type 2/5 chimera *E1B* deletion	I	Single injection to resection cavity	No	24	No toxicity or SAE attributed to virus
NDV	NDV-HUJ (329)	Attenuated NDV (lentogenic)	I/II	Multiple i.v. doses	No	14	No toxicity or SAE attributed to virus

Table 3: Summary of published clinical trials for adult HGG.

SAE (severe adverse effect), RT (radiotherapy), i.v. (intravenous). Adapted from (254,334,336)

1.9 Project rationale

pHGG and DIPG are highly aggressive brain tumours associated with dismal prognosis. Their invasive phenotype contributes to their limited therapeutic response and very few studies have focused on identifying existing or novel agents that are capable of impairing the migration and invasion of these tumours. The work contained within this thesis sets out to develop novel anti-invasive therapeutic strategies for pHGG and DIPG and aims to:

1) **Characterise the migratory and invasive properties of pHGG and DIPG cells**

   The *in vitro* migratory and invasive properties of a panel of paediatric glioma cell lines will be examined using a range of 2D and 3D assays.

   Hypothesis: We hypothesise that pHGG and DIPG cell lines will demonstrate a highly migratory and invasive phenotype *in vitro.*

2) **Evaluate the effect of known GSK-3 inhibitors on the migration and invasion of paediatric glioma cells**

   The effects of small molecule GSK-3 inhibitors (lithium chloride (LiCl) and BIO) on pHGG and DIPG cell migration and invasion will be determined using 2D and 3D assays.

   Hypothesis: We hypothesise that GSK-3 inhibitors will decrease *in vitro* migration and invasion of pHGG and DIPG.

3) **Investigate the effects of a range of OVs on paediatric glioma migration and invasion**

   The effects of the OVs, HSV, reovirus and VV on the migration and invasion of pHGG and DIPG cell lines will be evaluated. Additionally, the interaction between OVs and the pHGG cytoskeleton will be investigated.

   Hypothesis: We hypothesise that OVs will interact with the cancer cell cytoskeleton and this will, in turn, reduce the migratory and invasive ability of paediatric glioma cell lines.

Chapter 2: Materials and methods

2.1 Cell lines and media

Paediatric glioma cell lines SF188 (Grade IV, glioblastoma) and KNS42 (Grade IV, glioblastoma) were obtained from Dr Chris Jones (Institute of Cancer Research, London). These cells have been comprehensively characterised in terms of genomic alterations and gene expression patterns (348). Cells were grown in Dulbecco's Modified Eagle's medium (DMEM) (Sigma-Aldrich) with 10 % heat-inactivated foetal calf serum (HI-FCS) (Labtech) and 0.5 % penicillin-streptomycin (Sigma-Aldrich). For experiments involving OVs, penicillin-streptomycin was omitted from the cell culture medium. Cell line identity was verified by serial tandem repeat profiling (Claire Taylor, in-house testing at Cancer Research UK Leeds Centre, genomics facilities). The patient autopsy-derived DIPG cell line HSJD-DIPG-007 was obtained from Dr Angel M Carcaboso (Hospital Sant Joan de Dèu Barcelona, Barcelona, Spain). Cells were cultured as neurospheres in working medium (Table 4). Murine glioma GL261-luciferase (GL261-Luc) transfected cells were obtained from Professor Richard Vile (Mayo clinic, Rochester, USA) and were grown in DMEM supplemented with 10 % HI-FCS and 1 µg/ml puromycin (Sigma-Aldrich). All cell lines were free of mycoplasma contamination (Sarah Perry, in-house testing at Leeds Institute of Cancer and Pathology (LICAP)).

	Vendor	Working concentration	Stock concentration	Volume
TSM base (see appendix 2 for constituents)				50 ml
B-27 supplement minus vitamin-A (50x) liquid	Thermo Fisher Scientific			1 ml
Recombinant human EGF	Peprotech	20 ng/ml	20 µg/ml	50 µl
Recombinant human FGF-basic	Peprotech	20 ng/ml	20 µg/ml	50 µl
Human-PDGF-AA	Peprotech	10 ng/ml	20 µg/ml	25 µl
Human-PDGF-BB	Peprotech	10 ng/ml	20 µg/ml	25 µl
Heparin solution 0.2 %	Sigma-Aldrich	2 µg/ml	2 mg/ml	50 µl

Table 4: Constituents of working medium for HSJD-DIPG-007 neurosphere culture

TSM (tumour stem medium), EGF (epidermal growth factor), FGF (fibroblast growth factor), PDGF (platelet-derived growth factor)

2.1.1 Cell culture

Cells were cultured in a Sanyo CO_2 incubator at 37 °C in a humidified atmosphere of 5 % CO_2 (in air). Cells were maintained in either 150 cm^2 or 75 cm^2 plastic tissue culture flasks (Corning). SF188, KNS42 and GL261-Luc were harvested at or near confluence by washing with phosphate buffered saline (PBS), then adding trypsin (10x solution, diluted 1:10 in Hank's Balanced Salt Solution (Sigma-Aldrich)). Cells were frozen and stored in liquid nitrogen at -196 °C in 10 % dimethyl sulfoxide (DMSO) (Sigma-Aldrich) culture medium.

HSJD-DIPG-007 cells were grown as neurospheres suspended in medium. Medium was replaced once per week or upon changing colour. Cells were passaged when growth was such that medium required changing within four

days of replacement. To passage, cell suspensions were centrifuged at 300 g for 4 min. Cell pellets were incubated for five min at 37 °C with 0.5 ml TrypLE Express Stable Trypsin Replacement Enzyme without phenol red (Thermo Fisher Scientific) and then triturated 20-30 times with a p1000 pipette (Starlab) in 1.5 ml Eppendorf tubes (Sarstedt) to disaggregate. Cells were re-suspended in 10 ml TSM in Falcon™ tubes (Corning) and centrifuged for five min at 400 g. Cell pellets were re-suspended in 5 ml of working medium and incubated overnight in 25 cm^2 plastic tissue culture flasks at 37 °C. Neurosphere suspensions were then transferred into 75 cm^2 plastic tissue culture flasks until ready for further passage. For cryopreservation, disaggregated neurospheres were re-suspended in 1 ml of Synth-a-Freeze defined cryopreservation medium (Thermo Fisher Scientific), kept at -80 °C for 24 h and then stored in liquid nitrogen at -196 °C.

For cell counts, cells were viewed/imaged with a Nikon eclipse TS100 microscope and camera and counted using an improved Neubauer haemocytometer (Weber Scientific).

2.2 Chemicals

Chemicals used were LiCl (Sigma-Aldrich), BIO (Calbiochem), sodium chloride (NaCl) (Thermo Fisher Scientific), DMSO and taxol (Selleckchem).

2.3 Viruses

Viruses used are summarised in table five.

Oncolytic virus	Strain	GFP/RFP	Modification	Stock concentration	Supplier
HSV	1716	No	Deletion *ICP34.5*	$1x10^9$ pfu/cell/ml	Virttu Biologics
HSV	1716	GFP	Deletion *ICP34.5*	$1x10^9$ pfu/cell/ml	Virttu Biologics
Reovirus	Reovirus type 3 dearing strain Reolysin®	No	Wild type virus	$5x10^9$ pfu/cell/ml	Oncolytics Biotech
VV	GLV-1h254	RFP	Contains three expression cassettes encoding turbofp635 RFP, β-galactosidase and β-glucoronidase integrated into the *F14.5L*, *J2R* and *A56R* loci of the vaccinia genome, respectively.	$2.1x10^9$ pfu/cell/ml	Genelux
VV	GLV-1h68	GFP	Contains three expression cassettes encoding Renilla luciferase-Aequorea GFP fusion protein, β-galactosidase and β-glucoronidase integrated into the *F14.5L*, *J2R* and *A56R* loci of the VV genome, respectively.	$1.74x10^9$ pfu/cell/ml	Genelux

Table 5: Summary of viruses studied
GFP (green fluorescent protein), RFP (red fluorescent protein)

2.4 Migration and invasion assays

2.4.1 Spheroid invasion assay in collagen

Spheroids were formed by placing $1x10^3$ cells per well in an ultra-low attachment round-bottom 96 well plate (Corning) and incubating for 72 h at 37 °C. The medium was removed and 100 µl of neutralised rat tail collagen 1 (BD Biosciences) was added to each well and allowed to polymerise at 37 °C for 15 min to entrap the spheroid. Collagen was neutralised with 1 M sodium hydroxide (NaOH) in 5x DMEM (Thermo Fisher Scientific). For

evaluation of the effects of GSK-3 inhibitors on invasion, the collagen was overlaid with 100 µl of cell culture medium ± GSK-3 inhibitors: LiCl at 40, 20, 10, 5 mM in NaCl or BIO at 10, 5, 1, 0.5 µM in DMSO. For investigation of the effects of OVs, the collagen was overlaid with 100 µl of cell culture medium ± $8x10^2$, $8x10^3$, $8x10^4$ or $4x10^5$ pfu/well of virus, which approximates to a nominal 0.1, 1, 10 or 50 pfu/cell. Spheroid expansion and invasion into the collagen matrix was monitored for 72 h using the EVOS cell imaging system (Thermo Fisher Scientific) at x4 magnification. Images were analysed with Volocity 3D Image Analysis software (Perkin-Elmer) and Image J (http://rsbweb.nih.gov/ij). In order to quantify invasion, two zones were defined: the *invasion zone* represents the area outside the spheroid core into which approximately 75 % of cells invaded, while the *leading edge zone* represents the total area containing any invading cells away from the core (Figure 2). This method has been previously described (349) and improved the accuracy of the analysis. For comparison of invasion between conditions, an index entitled the 'migration index (MI)' was calculated as:

$$MI = \frac{\text{area of zone} - \text{area of core}}{\text{total area}}$$

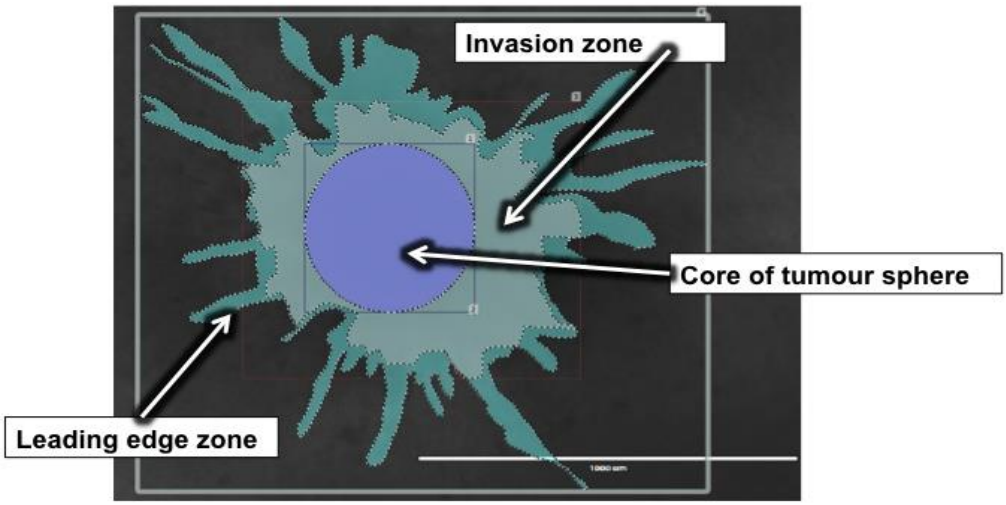

Figure 2: Invasion of cells from tumour spheroids can be represented by zones
Images of invading tumour spheroids into their surrounding collagen matrix were obtained using the EVOS cell imaging system. Volocity 3D Image Analysis software and Image J were used to define zones for quantification of tumour spheroid invasion. The invasion zone represents the area containing approximately 75 % of invading cells and the leading edge zone accounts for the whole area containing any invading cells. White scale bar represents 1000 µm.

2.4.2 Transwell migration assay

Transwell assays were performed using 8 µm pore transwell inserts (Greiner Bio-One) pre-coated with 5 µg/ml of the chemo-attractant fibronectin (Sigma-Aldrich). Cell lines were pre-treated ± 20 mM LiCl or 5 µM BIO for 1 h. $5x10^4$ cells were then placed into transwell inserts in triplicate and allowed to migrate for 4 h. Migrated cells were fixed with 1 % glutaraldehyde (Sigma-Aldrich) in PBS and visualised by staining with 0.1 µg/ml DAPI (Biotium). Migration was determined by imaging DAPI nuclear stain with the EVOS cell imaging system and quantifying the fluorescence signal for the individual transwells using Volocity 3D Image Analysis software.

2.4.3 Migration on nanofibre scaffolds

$1x10^3$ cells in 20 µl drops were suspended from the lids of petri dishes for 24 h to form aggregates in hanging drops (350). To enhance visualisation of the migrating cells and confirm migration, CellTracker™ green 5-chloromethylfluorescein diacetate (CMFDA) dye (Thermo Fisher Scientific) was added to the cell suspension according to manufacturer's instructions prior to hanging drop formation. Cell aggregates were manually transferred into wells of aligned poly-ε-caprolactone nanofibre-coated culture plates (Nanofiber solutions), which allows cell migration on a 3D scaffold stimulated by topographical cues (i.e. the surface shape and features are able to influence migration) (351). These were incubated at 37 °C with cell medium ± 20 mM LiCl or 5 µM BIO in triplicate and migration was monitored for 72 h using the EVOS cell imaging system at x4 magnification. Migration was quantified using Image J software.

2.4.4 Scratch migration assay

Cells were seeded at $1x10^5$ cells/well into 24 well plates (Corning) such that after 24 h of growth they reached 80-90 % confluence as a monolayer. After 24 h incubation at 37 °C, a line was drawn on the underside of each well across the centre with a fine marker. A gentle and slow scratch using a p200 pipette tip (Starlab) was applied across the centre of the monolayer,

perpendicular to the marker line. The well was then washed twice with culture medium to remove detached cells and replenished with fresh culture medium ± virus (HSV, reovirus or VV at 50, 10, 1, 0.1 and 0.01 pfu/cell). Migration of cells across the scratch was determined by imaging at 0 h and 24 h with the EVOS cell imaging system at x4 magnification. Migration was quantified using Image J software to determine the percentage change in the area of the scratch over the 24 h time period.

2.5 Live cell imaging

2.5.1 Live cell imaging with the Nikon Biostation IM system

10 µl of cells in 500 µl of culture medium were placed in each quarter of an Ibidi imaging dish (Nikon) and allowed to adhere for 2 h at 37 ºC. For evaluation of the effects of GSK-3 inhibitors on random cell movement/morphology, equal volumes of medium were then replaced in 2 of 4 quadrants with either 20 mM LiCl or 5 µM BIO. For evaluation of the effects of OVs, equal volumes of medium were replaced in 3 of 4 quadrants with either HSV, reovirus or VV at an approximation of 10 pfu/cell. The Ibidi dish was then cultured in the incubation/imaging chamber of the Nikon Biostation IM live cell imaging system. Cells were imaged for 24 h (GSK-3 inhibitor experiments) or 48 h (virus experiments) at 3 min intervals at 37 ºC with 5 % CO_2 in air. To evaluate effects on pHGG cell lines following GSK-3 inhibitor drug washout, 20 mM LiCl- or 5 µM BIO- treated medium was removed following 24 h of imaging, cells were gently washed with PBS and imaged in drug free culture medium for a further 24 h. The Biostation IM-associated software was used to create movies for analysis. Cell tracking, velocity and displacement analysis was performed in Image J with MTrack (www.imagescience.org/meijering/software/mtrackj/). For tracking, the nucleus of each cell was identified and tracked over the 24 h or 48 h period at 150 min intervals.

2.5.2 Live cell imaging with the IncuCyte ZOOM®

For live cell imaging of the scratch assay, 24 well plates were set up as per section 2.4.4 and placed in the IncuCyte ZOOM® (Essen BioScience) incubator at 37 ºC with 5 % CO_2 in air. Plates were imaged using the x4 microscope objective, with images of each well taken hourly. IncuCyte™ software (Essen BioScience) was used to create movies.

Imaging of HSV and VV infection within cells forming spheroids was achieved by setting up a spheroid in collagen invasion assay in a 96 well plate (see section 2.4.1). The collagen was overlaid with 100 µl of cell culture medium ± $8x10^4$ pfu/well of HSV or VV expressing GFP. The 96 well plate was placed in the IncuCyte ZOOM® incubator at 37 ºC with 5 % CO_2 in air and was imaged using the x4 microscope objective, with images of each well taken hourly for 70 h. IncuCyte™ software was used to create movies and visualise GFP expression.

2.6 Cell viability and growth assays

2.6.1 WST-1 assay

Cell viability of both monolayers and spheroid aggregates incubated with culture medium ± GSK-3 inhibitors was measured using the water soluble tetrazolium-1 (WST-1) assay (Roche). Cell viability of spheroid aggregates incubated with culture medium ± virus was also determined by WST-1 assay.

For analysis of monolayers, cells were seeded (SF188 at $2.5x10^3$ cells/well, KNS42 at $5x10^3$ cells/well in 50 µl culture medium) into flat-bottom 96 well plates (Corning) and left to adhere overnight. Cells were treated with a further 50 µl volume of culture medium ± LiCl at 40, 20, 10, 5 mM in NaCl or BIO at 10, 5, 1, 0.5 µM in DMSO. At 24, 48 and 72 h, 10 µl of WST-1 was added to each well and, after 4 h, absorbance at 450 nm was detected using a colorimetric microplate reader (Thermo Fisher Scientific). An internal control well containing BIO 10, 5, 1, 0.5 µM only (no cells) was also

evaluated and absorbance from these control wells was subtracted from the readings obtained for BIO-treated cells to account for the absorbance of the red pigmentation of the compound.

For analysis of spheroids, $1x10^3$ cells per well in 50 µl culture medium were seeded in an ultra-low attachment round bottom 96 well plate to form spheroid aggregates. Following 72 h incubation at 37 °C, cells were treated with a further 50 µl volume of culture medium ± LiCl at 40, 20, 10, 5 mM in NaCl or BIO at 10, 5, 1, 0.5 µM in DMSO. For experiments to determine the effects of OVs on spheroid aggregate viability, cells were treated with 50 µl volume of culture medium ± $8x10^2$, $8x10^3$, $8x10^4$ or $4x10^5$ pfu/well of virus. At 24 h intervals for up to 96 h, 10 µl of WST-1 was added per well and, after 4 h, absorbance at 450 nm was detected using the colorimetric microplate reader. Additionally, for GSK-3 inhibitor experiments and for virus experiments with the HSJD-DIPG-007 cell line, tumour spheroids were imaged at 0, 24, 48 and 72 h using the EVOS cell imaging system and changes in spheroid core area were calculated using Image J software to evaluate growth over time: a methodology recommended by the manufacturers of a commercially available 3D spheroid proliferation assay (352).

2.6.2 MTT assay

Cells were seeded as monolayers at $8x10^3$ cells per well in 100 µl of culture medium in flat bottom 96 well plates (Corning) and incubated at 37 ºC overnight. 100 µl of culture medium or virus dilutions (HSV, reovirus and VV at 10, 5, 2.5, 1.25, 0.625, 0.3125 and 0.156 pfu/cell) was added to each well in triplicate. At 24, 48, 72 and 96 h, 20 µl of 3-(4,5-dimethylthiazol-2-yl)-2,5-diphenyltetrazolium bromide (MTT) (Sigma-Aldrich) was added to each well and, after 4 h, incubation at 37 °C, the medium was replaced with 200 µl of DMSO. Absorbance at 550 nm was detected using a colorimetric microplate reader.

2.6.3 LIVE/DEAD® assay

Cells were seeded into 12 well plates (Corning) at 1x10^5 cells/well in 2 ml culture medium and left to adhere for a minimum of 4 h at 37°C. 100 µl of culture medium ± virus (HSV, reovirus or VV at 50, 10, 1, 0.1 and 0.01 pfu/cell) was then added to each well. At 24, 48, 72 and 96 h, cell-free culture medium was collected for analysis by enzyme-linked immunosorbent assay (ELISA). Cells were harvested into fluorescence-activated cell sorting (FACS) tubes (Corning), centrifuged at 400 g for 5 min then washed in PBS. Cell pellets were then incubated for 20 min with 1 ml of PBS containing 1 µl LIVE/DEAD® fixable dead cell stain (Thermo Fisher Scientific). For cells treated with either HSV or reovirus, a red LIVE/DEAD® cell stain was used and for cells treated with VV, a yellow LIVE/DEAD® cell stain was used to account for the RFP encoded by the VV. Following incubation, cells were washed twice in PBS and cell pellets were fixed in 300 µl of 1 % paraformaldehyde (PFA) (Sigma-Aldrich). Fixed cells were stored at 4 °C until acquisition on the FACS Attune cytometer (Thermo Fisher Scientific). Analysis was carried out using Attune Flow Cytometric software V2.1 (Thermo Fisher Scientific).

2.6.4 Ki-67 intracellular FACS assay

Cells were seeded into 12 well plates at 1x10^5 cells/well in 2 ml culture medium and left to adhere for a minimum of 4 h at 37 °C. 100 µl of culture medium ± virus (HSV or reovirus at 1 or 10 pfu/cell) was then added to each well. At 24 h, cells were harvested into FACS tubes, washed in PBS and fixed in 50 µl of 10 % PFA per tube on ice for 15 min. Cells were then washed with FACS buffer (see appendix 2) and re-suspended in 1 ml 0.3 % saponin (Sigma-Aldrich) for 15 min at room temperature to permeabilise. Cells were then washed with FACS buffer and 5 µl of Ki67 PE-Cy7 mouse anti-human antibody (BD Biosciences) was added to each tube and incubated for 30 min at room temperature, shielded from light. Cells were then washed in 2 ml of 0.1 % saponin and re-suspended in 500 µl FACS buffer. Ki67 staining was examined using the FACS Attune cytometer.

2.7 Immunofluorescence

For immunofluorescence (IF) studies, cells were grown on sterile 22 x 22 mm cover slips (Scientific laboratory supplies) in 6 well dishes (Corning) seeded at $2x10^5$ cells/well. To assess the effect of GSK-3 inhibitors on cell morphology, cells were mock-treated with culture medium (± NaCl or DMSO as negative controls) or treated with either 20 mM LiCl or 5 µM BIO and allowed to grow over a 72 h period. To assess the effects of GSK-3 inhibitors on β-catenin distribution, cells were mock-treated or treated with 20 mM LiCl or 5 µM BIO for 24 h. To investigate the effects of HSV on tubulin acetylation and detyrosination, cells were mock-treated or treated with either 10 pfu/cell HSV or 100 nM Taxol for 24 and 48 h. To evaluate the cellular location of APC, cells were mock-treated for 24 h or treated with either 10 pfu/cell HSV or 5 µM BIO. Finally, dedicator of cytokinesis 3 (DOCK3) intensity was investigated by treating cells in medium ± 10 pfu/cell HSV for 24 h.

Antibodies for IF studies are listed in table 6. For the identification of focal adhesions, a staining kit for vinculin (1:500 dilution) (Millipore) was used. Actin filament and nuclear staining was performed with rhodamine-phalloidin (1:500 dilution) (Thermo Fisher Scientific) and DAPI (1:10,000 dilution) (Thermo Fisher Scientific).

For IF studies of microtubules, acetylated tubulin, detyrosinated tubulin, APC and DOCK3, cells were fixed with ice-cold 100 % methanol (Sigma-Aldrich) for 2 min at -20 °C, followed by three washes with PBS. For IF of the actin cytoskeleton, focal adhesions and β-catenin, cells were fixed with 4 % PFA for 20 min at room temperature followed by 5 min incubation with 0.5 % Triton X-100 (Sigma-Aldrich) in PBS for permeabilisation and finally three washes with PBS. All coverslips were then blocked with 0.05 % skimmed milk (Marvel) in PBS for 5 min at room temperature. Primary antibodies were diluted (as stated in table 6) in blocking buffer (0.05% skimmed milk in PBS) and then centrifuged for 5 min at 13,000 rpm. The supernatants were removed and used for primary antibody incubation. Coverslips were incubated upside down in 200 µl of primary antibody solution in a humidified incubation chamber for 1 h and then washed three times in PBS. Coverslips

were incubated in secondary antibody solutions, containing DAPI and mounted on microslides in Fluoromount-G (SouthernBiotech). The coverslips were allowed to set overnight and imaged using the Axioplan Z imaging microscope (Zeiss). For IF studies of acetylated and detyrosinated tubulin, fluorescence intensity of each image was calculated in Image J software using a standard threshold across all images. The fluorescence intensity was then divided by the number of cells in each image to calculate the intensity of acetylated or detyrosinated tubulin per cell.

Primary antibody	Company	Working concentration of primary	Corresponding secondary antibody	Company	Working concentration of secondary
Rat anti-tubulin alpha	AbD Serotec	1:500	Donkey anti-rat IgG, Alexa Fluor® 488	Thermo Fisher Scientific	1:500
Rabbit anti-β-catenin	Sigma-Aldrich	1:500	Goat anti-rabbit IgG, Alexa Fluor® 594	Thermo Fisher Scientific	1:500
Mouse anti-acetylated tubulin	Sigma-Aldrich	1:500	Goat anti-mouse IgG, Alexa Fluor® 594	Thermo Fisher Scientific	1:500
Rabbit anti-detyrosinated alpha tubulin	Abcam	1:200	Goat anti-rabbit IgG, Alexa Fluor® 594	Thermo Fisher Scientific	1:500
Rabbit polyclonal M-APC	A kind gift to Dr Ewan Morrison from Prof Inke Näthke	1:2000	Goat anti-rabbit IgG, Alexa Fluor® 594	Thermo Fisher Scientific	1:500
Rabbit anti-DOCK3 antibody	Abcam	1:500	Goat anti-rabbit IgG, Alexa Fluor® 594	Thermo Fisher Scientific	1:500

Table 6: Primary and secondary antibodies used for immunofluorescence studies (including working concentrations used).

2.8 Western blotting

For Western blotting, cell lysates were obtained from cells grown in 25 cm^2 plastic tissue culture flasks (Corning) treated under the following conditions: to determine the effects of LiCl and BIO on GSK-3 isoform expression, cells were treated with either 20 mM LiCl, 20 mM NaCl, 5 µM BIO or DMSO at the same concentration for 24 h. To investigate the effects of HSV on GSK-3 expression and acetylated and detyrosinated tubulin expression, cells were treated ± 10 pfu/cell HSV and harvested at 24 or 48 h. Once harvested, cells were centrifuged at 400 g for 5 min with ice cold PBS and supernatants were discarded in order to obtain a dry pellet. 2 ml of ice cold radioimmunoprecipitation assay (RIPA) buffer (see appendix 2) + 25 µl/ml protease inhibitor (Sigma-Aldrich) was added to each cell pellet and left for 15 min on ice to create cell lysates.

Protein concentration of each cell lysate was determined by Bradford protein assay. Briefly, 5 µl of protein sample (diluted 1:1 with ddH_2O), or bovine serum albumin (BSA) protein standards (Sigma-Aldrich) (in serial dilution from 1.5 µg/µl to 0 µg/µl) were placed in flat-bottom 96 well Maxisorp® plates (Nunc). Protein concentration was determined using a DC™ Protein Assay kit (Bio-Rad), according to the manufacturer's instructions. Absorbance at 690 nm was detected using the colorimetric microplate reader. Protein sample concentration was evaluated using the curve derived from the BSA protein standards.

20-40 µg of protein mixed with loading buffer (see appendix 2) was loaded into wells in Tris-glycine sodium dodecyl sulphate (SDS) polyacrylamide gel (see appendix 2). A PageRuler plus pre-stained protein ladder (Thermo Fisher Scientific) was also loaded to estimate protein size. Proteins were separated by sodium dodecyl sulphate polyacrylamide gel electrophoresis (SDS-PAGE) (150 v, 3 watts per gel for approximately 60 min in a tank filled with running buffer (see appendix 2)) and transferred to nitrocellulose (Bio-Rad) (25 v over 2 h in a tank filled with transfer buffer (see appendix 2)). Once unpacked, the nitrocellulose was washed and blocked. For blots to be

treated with β-actin antibody, the nitrocellulose was rinsed for 5 min in Tris-Buffered Saline and Tween®20 (TBST) (Sigma-Aldrich) (see appendix 2) and then blocked with 3 % milk in TBST buffer overnight. For blots treated with all other antibodies, nitrocellulose was rinsed for 5 min in PBS and then blocked for 1 h with 5 % BSA diluted in PBS. The nitrocellulose was then exposed to primary antibody (see table 7) diluted with either 3 % milk in TBST for 2 h (β-actin) or 2.5 % BSA in PBS plus 0.1 % Tween®20 (PBST) overnight (all other blots). Nitrocellulose was then washed four times in either TBST (β-actin) or PBST (all other blots) and exposed for 1 h to secondary antibody (see table 7). Following four further washes with TBST or PBST, proteins were detected by the addition of SuperSignal™ West Pico Chemiluminescent substrate (Thermo Fisher Scientific) and visualised using the ChemiDoc MP imaging system (BioRad) and Image lab (BioRad) software. Protein band intensity was analysed using Image J software. The intensity of each band was normalised to the corresponding β-actin control.

Primary antibody	Company	Working concentration of primary	Corresponding secondary antibody	Company	Working concentration of secondary
Rabbit anti-β-actin	Abcam	1:2000	Polyclonal goat anti-rabbit immunoglobulin HRP	Dako	1:2000
Rabbit anti-GSK-3 β	Cell signaling technology	1:1000	Polyclonal goat anti-rabbit immunoglobulin HRP	Dako	1:2000
Rabbit anti-phospho GSK-3 β (Ser9)	Cell signaling technology	1:100	Polyclonal goat anti-rabbit immunoglobulin HRP	Dako	1:2000
Rabbit anti-GSK-3 (∝+β) (phsopho Y216+Y279)	Abcam	1:1000	Polyclonal goat anti-rabbit immunoglobulin HRP	Dako	1:2000
Mouse anti-acetylated tubulin	Sigma-Aldrich	1:5000	Goat anti-mouse IgG HRP	Thermo Fisher Scientific	1:20000
Rabbit anti-detyrosinated alpha tubulin	Abcam	1:500	Polyclonal goat anti-rabbit immunoglobulin HRP	Dako	1:2000
Mouse anti-total alpha tubulin	Genetex	1:5000	Goat anti-mouse IgG HRP	Thermo Fisher Scientific	1:20000
Rabbit anti-DOCK3 antibody	Abcam	1:600	Polyclonal goat anti-rabbit immunoglobulin HRP	Dako	1:2000

Table 7: Primary and secondary antibodies for Western blotting (including working concentrations used). HRP (horseradish peroxidase)

2.9 ELISA

Flat-bottom 96 well Maxisorp® plates were coated with 100 µl of capture antibody diluted in either PBS (VEGF) or coating buffer (IL-8) (see appendix 2) at optimised concentration (see table 8). Plates were wrapped and incubated overnight at 4 °C and then washed three times with PBST using the SkanWasher300 (Molecular Devices). Plates were then blocked with 200 µl per well of PBS + 10 % HI-FCS for 2 h at room temperature. Following three further washes with PBST, 100 µl of recombinant cytokine standards (in serial halving dilution) or sample supernatants were added to the plates in triplicate. Loaded plates were covered and left overnight at 4 °C and then washed six times with PBST. Optimised concentrations of detection antibody (table 8) diluted in block solution (PBS + 10 % HI-FCS) were added at 100 µl per well and left for 2 h at room temperature. Plates were again washed six times with PBST, before 100 µl Extravidin®-alkaline phosphatase conjugate (Sigma), diluted at 1:5000 in PBST, was added per well for 1 h. After three further washes with PBST, followed by three washes with ddH_2O, Sigmafast™ p-Nitrophenyl phosphate alkaline phosphatase substrate (Sigma) was prepared according to the manufacturer's instructions and added at 100 µl per well. Plates were kept in the dark to develop. Absorbance at 405 nm was detected using the colorimetric microplate reader. The concentration of cytokine detected in each sample was evaluated using the curve determined from the cytokine standards.

Cytokine	Coating antibody	Detection antibody	Company
IL-8	1:500	1:500	BD Biosciences
VEGF	1:180	1:180	R&D systems

Table 8: Coating and detection antibody concentrations for ELISA (including working concentrations used).

2.10 *In vivo* studies

In vivo experiments were conducted at the Department of Immunology, Mayo Clinic, Rochester, Minnesota, USA and were ethically approved by the Mayo foundation institutional animal care and use committee.

2.10.1 GL261-Luc model of migration

To establish intracranial tumours, 5 x 10^4 GL261-Luc cells in 2 µl PBS were stereotactically injected into the brains of 6-8-week-old C57 black 6 (BL/6) mice (The Jackson Laboratory) (n=8 per group). Coordinates for intracranial injection were 1 mm anterior and 2 mm lateral to the bregma. Cells were injected 2 mm deep. For one group of mice, GL261-Luc cells were premixed with HSV at 10 pfu/cell prior to intracranial injection. Four mice per group were sacrificed on day 15 of the experiment and the remainders were sacrificed on day 25 by exposure to CO_2 gas in a rising concentration. Brains were immediately harvested into 4 % PFA.

2.10.2 DIPG *in vivo* experiment

DIPG neurospheres were disaggregated with TrypLE (as described in section 2.1.1) and counted the evening before surgery, then left in culture overnight. Cells were collected immediately prior to surgery and re-suspended in either 2 µl PBS (control) or 2 µl HSV at 10 pfu/cell. To establish intracranial tumours, 5 x 10^5 disaggregated HSJD-DIPG-007 cells (pre-treated with PBS or HSV) were stereotactically injected into the brains of two groups of 4-5 week-old nonobese diabetic severe combined immunodeficiency (NOD.SCID) mice (The Jackson Laboratory) (n=6 per group (control vs. HSV-treated cells)). Location for injection was -1X, -0.8Y, 5Z from the bregma (353). Use of these coordinates targets the fourth ventricle but allows the cells to still grow and invade into the brainstem and cerebellum. Tumours were left to establish and mice were sacrificed when showing clinical signs of disease i.e. severe ataxia or >15 % weight loss.

Following death, brains were immediately harvested into 4 % PFA. Survival data was collected for analysis of treatment effects between groups.

2.10.3 Analysis of brains collected from *in vivo* studies

Brains were transferred from 4 % PFA to 70 % ethanol (Sigma-Aldrich), then sliced into coronal sections and placed in an embedding cassette (Thermo Fisher). Brains were embedded in paraffin, and then sectioned to four microns thick using a manual rotary microtome (Leica) and mounted on glass slides. Tissue sections were stained with Haematoxylin and Eosin (H&E). Briefly, tissue was dewaxed in xylene (Thermo Fisher Scientific), dehydrated in ethanol and then washed in water before incubation with Mayers haematoxylin (Atom Scientific) for 3 min. Tissue was washed in water, followed by Scott's tap water (0.2 % sodium bicarbonate, 2 % magnesium sulphate in water), then washed again with water before the addition of Eosin Y stain (Atom Scientific) for 2 min. Tissue was then washed in water, followed by ethanol and xylene before mounting with a cover slip using distyrene plasticizer xylene (DPX) (Solmedia). Nuclei were stained blue and cell cytoplasm and extracellular matrix were stained pink. Slides were analysed with the help of a consultant neuropathologist (Dr Azam Ismail, Department of Histopathology, St James's University Hospital), to identify the presence of brain tumours and their invasion/migration into the surrounding normal brain. Images were taken using the SPOT Insight camera (SPOT Imaging, Diagnostic Instruments) and SPOT software (SPOT Imaging, Diagnostic Instruments) with the Leitz DMRB (Leica) microscope at x5, x10 or x20 magnification.

2.11 Statistical analysis

Statistical analysis was carried out using Graph Pad Prism 6 (Graph Pad Software), SPSS version 21 (IBM) and Excel (Microsoft). Statistical significance between multiple groups was determined by analysis of variance (ANOVA). Statistical significance between two groups was

determined by Student's two-tailed t-test. Survival data from the DIPG *in vivo* experiment was analysed using the log rank test. p-values <0.05 were considered statistically significant.

Chapter 3: Cell migration and invasion in paediatric glioma: characterisation and potential therapeutic targeting with GSK-3 inhibitors

3.1 Introduction

pHGG and DIPG are highly aggressive tumours associated with dismal treatment outcomes (29). Both pHGG and DIPG are known to have diffuse infiltrative growth patterns and this invasive phenotype contributes to their limited therapeutic response (24,65). Despite intensive treatment, tumours inevitably recur, as by the time of surgical resection (pHGG) or localised radiotherapy (DIPG and pHGG) tumours have already invaded into the surrounding brain, preventing their complete removal/eradication (65). As a result, there is a pressing clinical need to develop novel therapeutic approaches that effectively target and reduce paediatric brain tumour migration and invasion.

One such approach may be through the use of GSK-3 inhibitors. GSK-3 is a serine/threonine protein kinase that plays a key role in orchestrating cell migration through regulating cellular structure, motility, adhesion and cytoskeleton dynamics (195,202,213). Pharmacological inhibitors of GSK-3, including LiCl and the indirubin derivative BIO, have been evaluated in pre-clinical studies of adult HGG and have been shown to be able to block both *in vitro* and *in vivo* migration and invasion (236,246). The effects of GSK-3 inhibitors on pHGG and DIPG migration and invasion are unknown and given the distinct biological and clinical phenotype of the adult and paediatric diseases (29), warrant separate investigation.

The results within this chapter report on a comprehensive analysis of cell migration and invasion of two pHGG cell lines and one rare patient-derived DIPG cell line, using a range of 2D and 3D assays. Additionally, the hypothesis that the small molecule GSK-3 inhibitors, LiCl and BIO, are capable of inhibiting the migration and invasion of pHGG and DIPG cells *in vitro,* is tested. These agents represent novel anti-invasive candidates that

may improve the clinical management of these challenging childhood tumours.

3.2 Paediatric glioma cell lines can readily form tumour spheroids

Tumour spheroids represent a useful model for examining tumour biology *in vitro* as they are three-dimensional and comprise of a surface with ready access to nutrients and oxygen and an inner hypoxic core (236). Moreover, once embedded in a matrix such as collagen, cells can migrate outward from the core and invade into the surrounding collagen matrix, representing a model of the process of tumour invasion (236). The spheroid-forming potential of four paediatric glioma cell lines (SF188 (glioblastoma), Res186 (pilocytic astrocytoma), KNS42 (glioblastoma) and UW479 (anaplastic astrocytoma), was initially investigated. However, serial tandem repeat profiling revealed concerns with the identity of two cell lines (Res186 and UW479) and consequently these cell lines were excluded from further analysis. Similar to the findings of Vinci *et al.* (354), it was noted that both SF188 and KNS42 readily formed round dense spheroids within 24 h when cultured in low adherence 96 well round-bottomed plates (Figure 3).

The patient-derived primary DIPG cell line HSJD-DIPG-007 normally grows as neurospheres suspended in culture medium. The ability of HSJD-DIPG-007 to form individual spheroids in low adherence 96 well plates was also investigated. This method offered the advantage of being able to create spheroids with the same fixed number of cells, improving uniformity of the tumour model. HSJD-DIPG-007 readily formed dense spheroids within 24 h when cultured using this method (Figure 3).

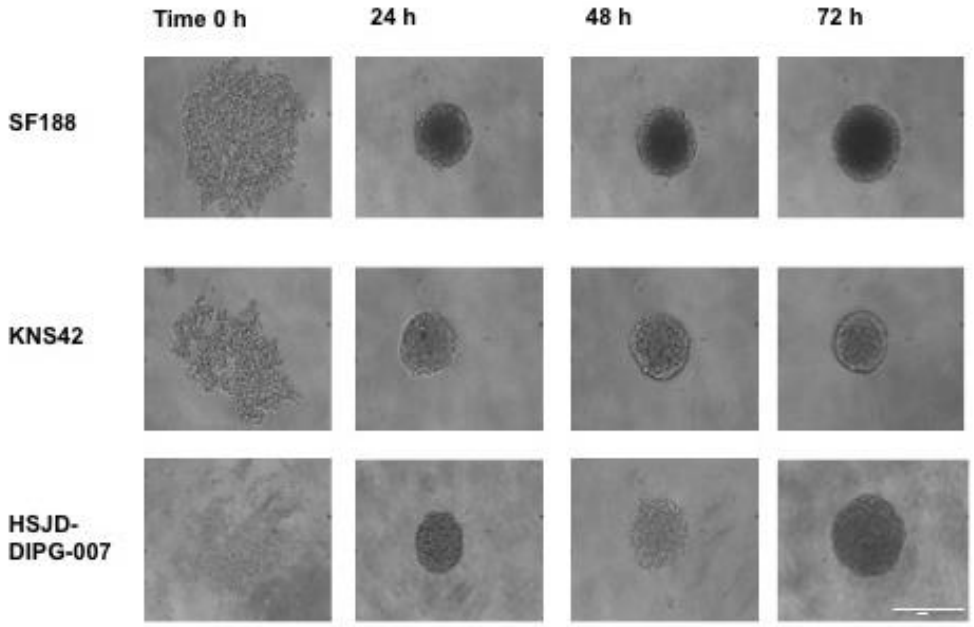

Figure 3: Paediatric glioma cell lines readily form tumour spheroids
SF188, KNS42 and HSJD-DIPG-007 were seeded into ultra-low attachment 96 well plates at $1x10^3$ cells per well and cultured for 72 h. Spheroid formation was evaluated at 24, 48 and 72 h by microscope at x10 magnification. The white scale bar represents 400 µm.

3.3 Paediatric glioma tumour spheroids display different patterns of invasion

After embedding in collagen, the invasive behavior of the paediatric glioma spheroids was monitored over 72 h using the EVOS cell imaging system. The cell lines exhibited distinct invasive characteristics and patterns. SF188 displayed a cogwheel pattern of invasion with what appeared to be long thin symmetrical protrusions branching from the central core. KNS42 and HSJD-DIPG-007 invaded by extending flattened protrusions and spreading in a sheet like manner (Figure 4A). During invasion of HSJD-DIPG-007 spheroids, the tumour core became elongated and lost definition. This was not observed for SF188 or KNS42 spheroids. The observed differences in invasive patterns were also reflected by the migration indices obtained for the leading edge for each cell; (the migration index was used as a measurement for comparison of invasion between cell lines and is described in section 2.4.1); KNS42 migrated significantly less than SF188 and HSJD-

DIPG-007 (mean±SEM: SF188 leading edge: 0.87±0.014; HSJD-DIPG-007 leading edge: 0.78±0.1; KNS42 leading edge: 0.59±0.31 p<0.001). No statistically significant difference was observed between the migration index of SF188 and HSJD-DIPG-007 (Figure 4B).

A

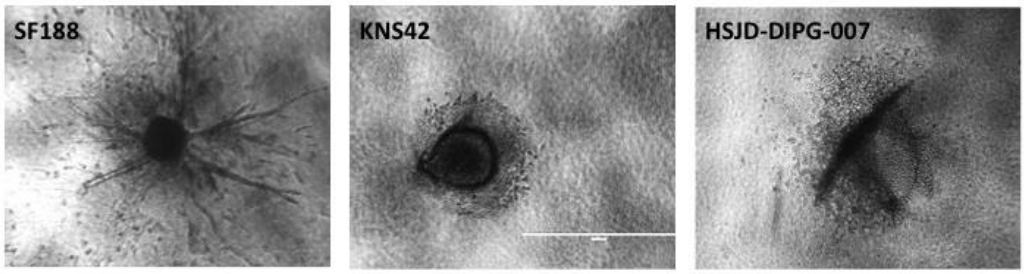

B

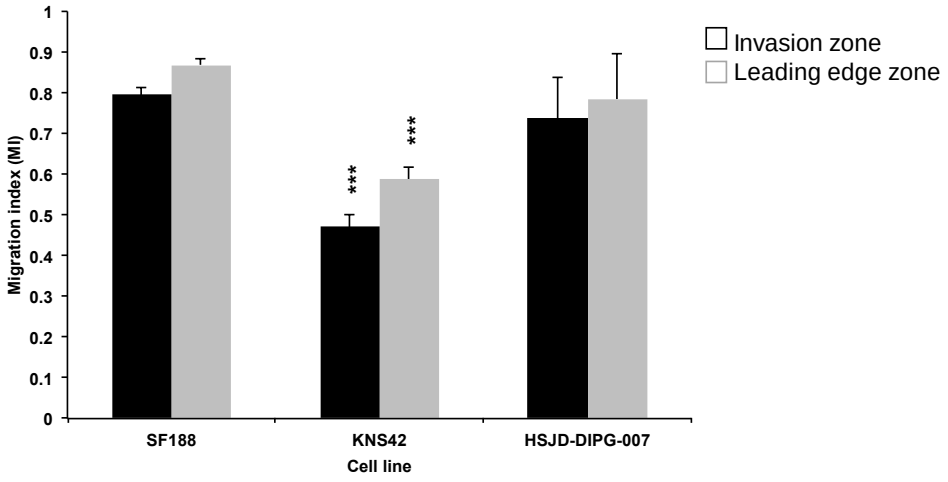

Figure 4: Tumour spheroids of paediatric glioma cell lines have different patterns of invasion
(A) SF188, KNS42 and HSJD-DIPG-007 tumour spheroids were encased in collagen and incubated in culture medium for 72 h. Images shown were taken at 72 h at a magnification of x4 and are representative of n=3 individual experiments. The white scale bar represents 1000 µm. **(B)** Images generated were analysed using Volocity 3D Image Analysis software and Image J by calculating the area of the invasion zone and the leading edge zone (as defined in section 2.4.1). A migration index (MI) for both the invasion front and leading edge ((area of zone – area of core) ÷ total area) was calculated. KNS42 invaded significantly less than SF188 and HSJD-DIPG-007. Graph shows mean±SEM of multiple repeats pooled from at least n=3 individual experiments for SF188 and KNS42 and one individual experiment with multiple internal repeats for HSJD-DIPG-007. *** p<0.001 by two-tailed t-test.

3.4 LiCl and BIO inhibit invasion of paediatric glioma tumour spheroids in a 3D assay

The small molecule GSK-3 inhibitors, LiCl and the indirubin derivative BIO, have recently been shown to block migration and invasion in adult

glioblastoma cell lines (236,246). Moreover, indirubin derivatives show therapeutic efficacy in animal glioblastoma orthotopic xenograft models and block invasion *in vivo* (246). However, whether these agents exert similar effects upon migration and invasion in pHGG and DIPG cell lines has not been previously determined.

Tumour spheroids from each cell line were embedded in collagen, overlaid with the drugs (LiCl and BIO) at varying concentrations as indicated and invasion was imaged over 72 h (Figure 5A and B). A migration index was then calculated from the images obtained for each condition as described in section 2.4.1 to compare the invasion front and leading edge zone for each treatment (Figure 6).

LiCl and BIO reduced invasion of pHGG and DIPG tumour spheroids in a concentration-dependent manner (Figure 6). After 72 h, 10 or 5 µM BIO significantly blocked invasion of both pHGG cell lines (SF188 and KNS42) (Figure 6A and B) (mean±SEM: SF188 leading edge: control 0.869±0.014, BIO 10 µM 0.292±0.069 $p<0.001$, BIO 5 µM 0.401±0.065 $p<0.001$; KNS42 leading edge: control 0.587±0.31, BIO 10 µM 0.157±0.036 $p<0.001$, BIO 5 µM 0.166±0.033 $p<0.001$). Invasion of the DIPG cell line at 72 h was significantly blocked by BIO at both 5 and 1 µM (Figure 6C) (mean±SEM HSJD-DIPG-007 leading edge: control 0.784±0.1, BIO 5 µM 0±0 $p<0.001$, BIO 1 µM 0.36 ± 0.040 $p<0.001$).

Treatment with 40 and 20 mM LiCl for 72 h also caused a statistically significant reduction of invasion for SF188 and KNS42 (for both the invasion and leading edge zone (Figure 6A and B)) (mean±SEM: SF188 leading edge: control 0.869±0.014, LiCl 40 mM 0.256±0.042 $p<0.001$, LiCl 20 mM 0.667±0.05 $p=0.005$; KNS42 leading edge: control 0.587±0.31, LiCl 40 mM 0.123±0.02 $p<0.001$, LiCl 20 mM 0.112±0.026 $p<0.001$). LiCl at 20 and 5 mM significantly reduced the invasion of HSJD-DIPG-007 following 72 h of treatment (Figure 6C) (mean±SEM HSJD-DIPG-007 leading edge: control 0.784±0.1, LiCl 20 mM 0.19±0.92 $p<0.01$, LiCl 5 mM 0.322±0.11 $p<0.05$).

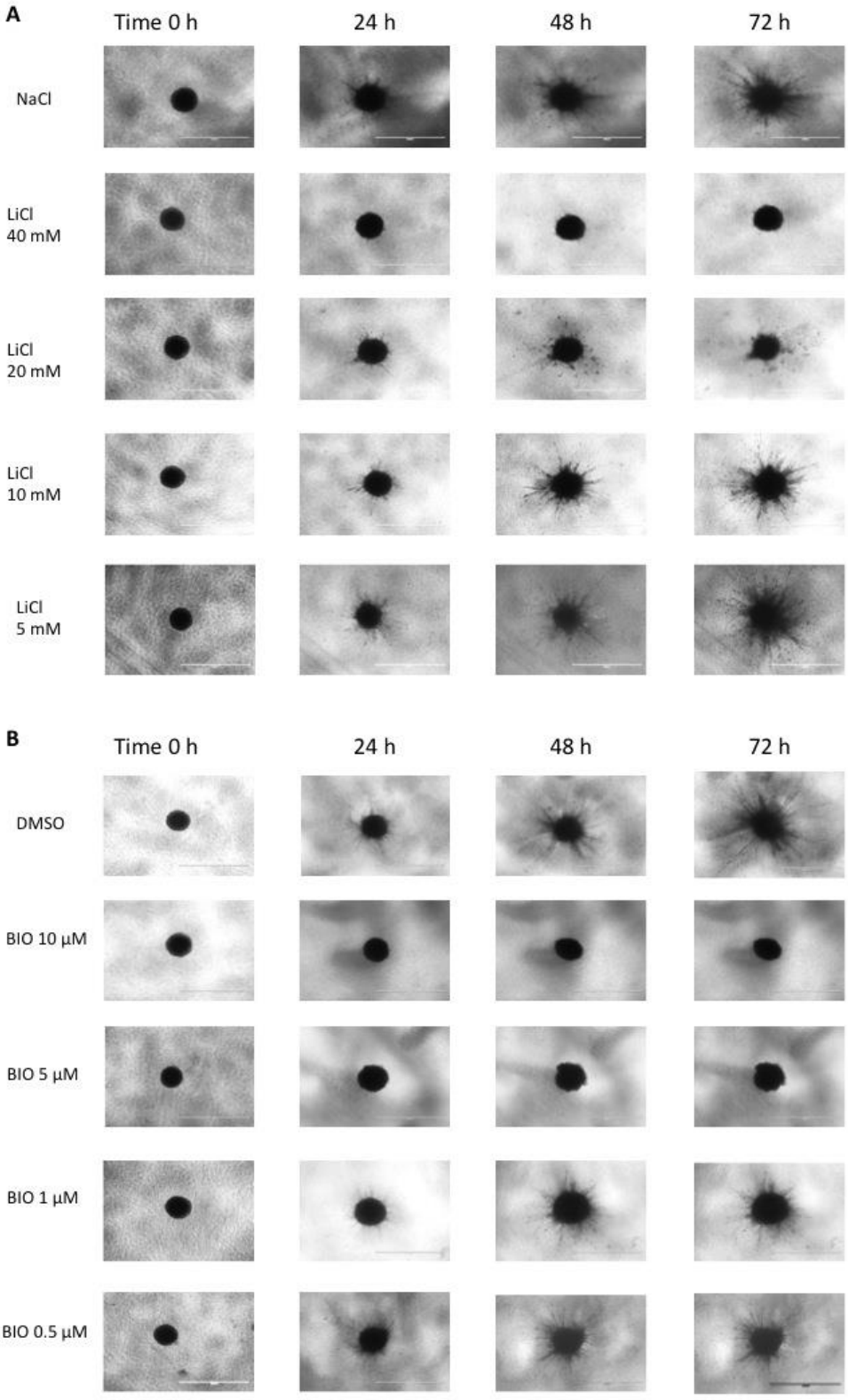

Figure 5: Inhibition of paediatric glioma tumour spheroid invasion by LiCl and BIO
Tumour spheroids (SF188) were encased in collagen and incubated in LiCl at 40, 20, 10, 5 mM in NaCl **(A)** or BIO at 10, 5, 1, 0.5 µM in DMSO **(B)** for 72 h. Tumour spheroid invasion was evaluated at 24, 48 and 72 h using the EVOS cell imaging system at x4 magnification. White scale bar represents 1000 µm. Images shown are representative of n=3 individual experiments.

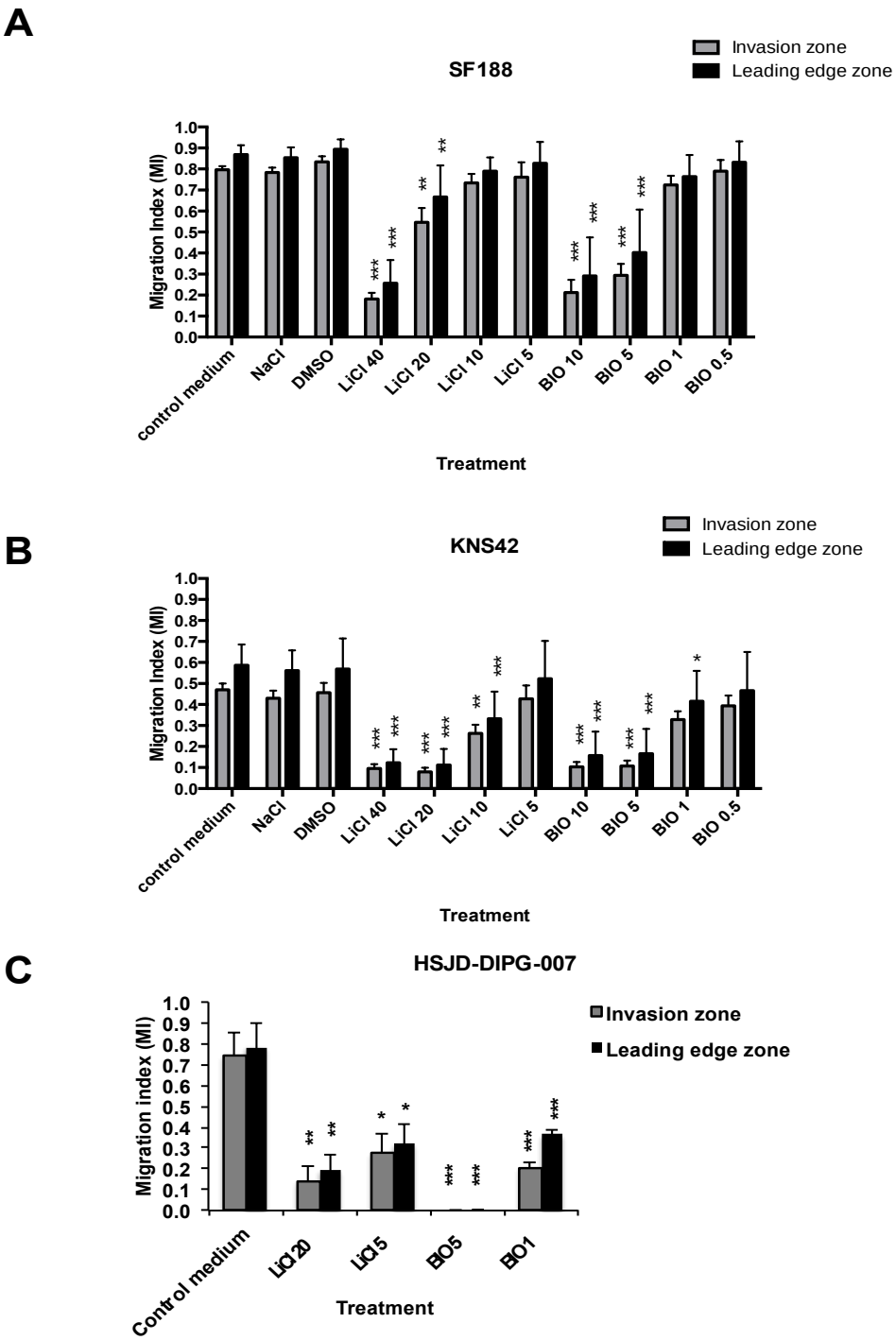

Figure 6: The effect of LiCl and BIO treatment on the migration index of tumour spheroids of paediatric glioma cell lines

SF188 **(A)**, KNS42 **(B)** and HSJD-DIPG-007 **(C)** tumour spheroids were encased in collagen and incubated in culture medium ± LiCl at 40, 20, 10, 5 mM in NaCl or BIO at 10, 5, 1, 0.5 µM in DMSO for 72 h. Tumour spheroid invasion was evaluated at 72 h using the EVOS cell imaging system. Images generated were analysed using Volocity 3D Image Analysis software or Image J by calculating the area of the invasion zone and the leading edge zone (as defined in section 2.4.1). A migration index (MI) for both the invasion zone and leading edge zone ((area of zone – area of core) ÷ total area) was calculated. Graphs show mean±SEM of multiple repeats pooled from up to n=3 individual experiments for SF188 and KNS42 and one individual experiment with multiple internal repeats for HSJD-DIPG-007 (For HSJD-DIPG-007: control n=4, LiCl 20 mM n=6, LiCl 5 mM n=5, Bio 5 and 1 µM n=8). * p<0.05, ** p<0.01, *** p<0.001 by one-way ANOVA for each cell type and treatment.

3.5 Effects of LiCl and BIO on pHGG tumour spheroid viability and growth

To confirm that the observed effects on tumour spheroid invasion after drug treatment were not due to changes in spheroid viability or growth, the effects of the two inhibitors on spheroid viability were assessed using a WST-1 assay. This assay has previously been used to determine viability of cells grown as spheroids (355). In the 3D spheroid system, both pHGG cell lines (SF188 and KNS42) displayed viability of at least 75 % or above for all treatments with LiCl and BIO (Figure 7). When normalised to the NaCl or DMSO corresponding control, it appears that the anti-invasive effects of LiCl and BIO are not accompanied by a marked loss of viability of SF188 and KNS42 cell lines when cultured as multicellular spheroids.

Additionally, an evaluation of tumour spheroid growth was made by measuring changes in the spheroid area over time for each drug treatment. Growth was only significantly reduced by 40 mM LiCl for SF188 (Figure 8). Given that a statistically significant reduction in invasion was seen with 20 mM LiCl in all cell lines with no significant reduction in tumour spheroid growth, it is unlikely that the anti-invasive effects of LiCl are attributed to non-specific inhibitory growth effects.

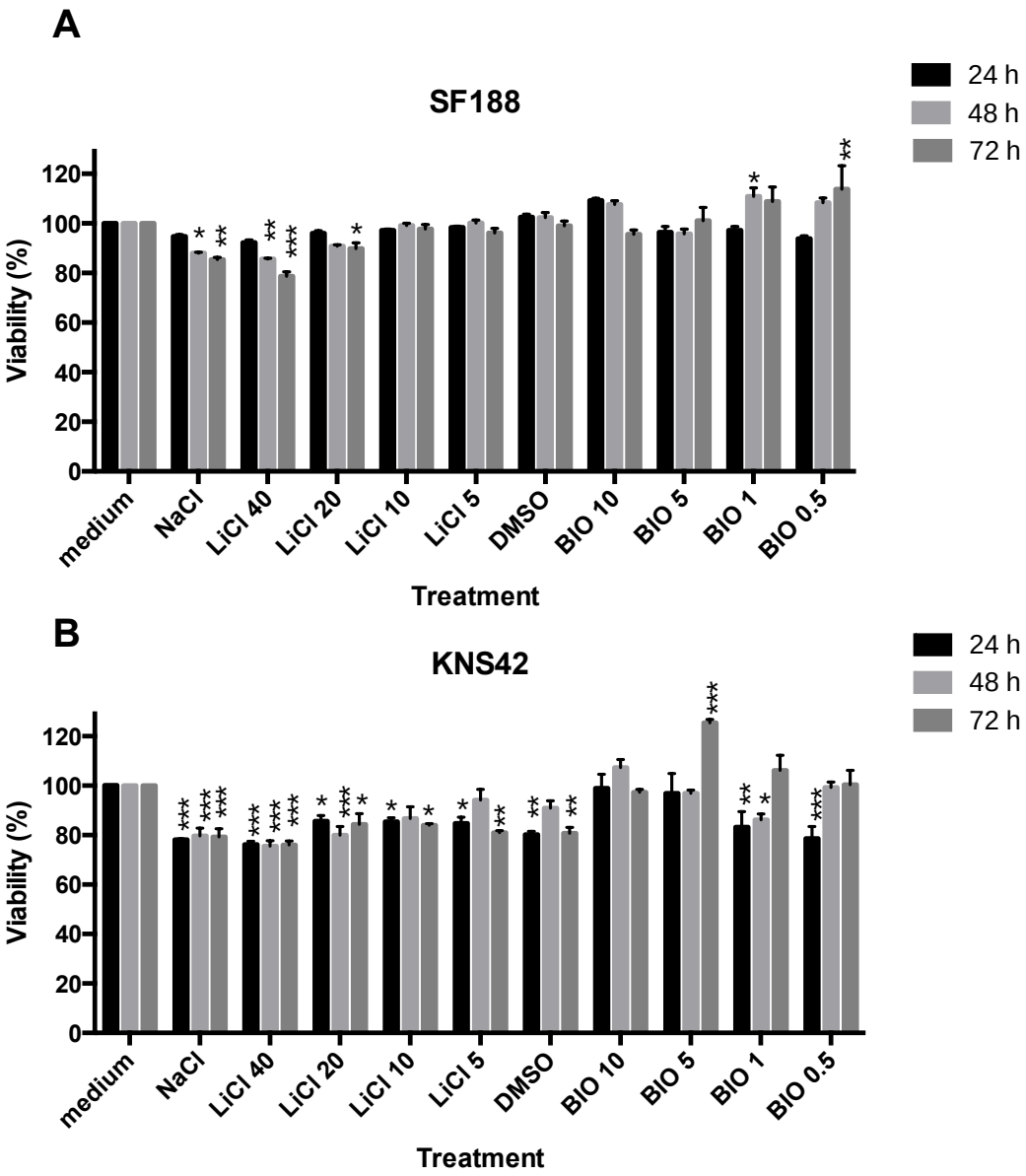

Figure 7: The effects of LiCl and BIO on pHGG tumour spheroid viability
SF188 **(A)** or KNS42 **(B)** were seeded in an ultra-low attachment 96 well plate at $1x10^3$ cells per well to form spheroid aggregates. Following 72 h incubation, cells were treated with culture medium or drugs (LiCl at 40, 20, 10, 5 mM in NaCl or BIO at 10, 5, 1, 0.5 µM in DMSO). Cell viability at 24, 48 and 72 h was determined by WST-1 assay and was expressed as a percentage of controls. Graphs show mean±SEM of one experiment performed in triplicate. *p<0.05, **p<0.01, ***p<0.001 by two-way ANOVA.

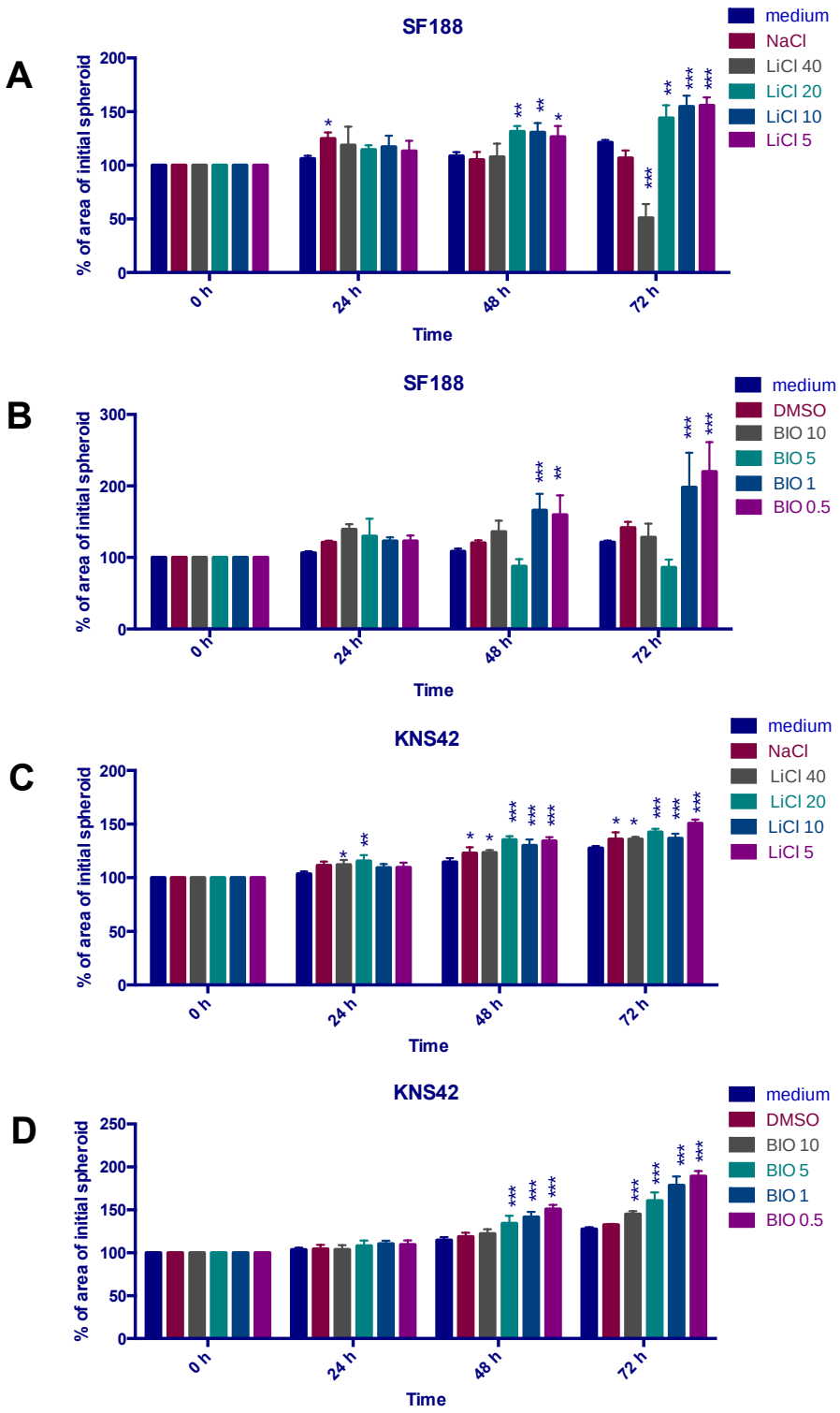

Figure 8: The effects of LiCl and BIO on pHGG tumour spheroid growth
SF188 (**A** and **B**) or KNS42 (**C** and **D**) were seeded in an ultra-low attachment 96 well plate at $1x10^3$ cells per well to form spheroid aggregates. Following 72 h incubation, cells were treated with culture medium or drugs (LiCl at 40, 20, 10, 5 mM in NaCl (**A** and **C**) or BIO at 10, 5, 1, 0.5 µM in DMSO (**B** and **D**)). Tumour spheroids were imaged at time 0, 24, 48 and 72 h following drug treatment. Growth over time ((area of spheroid at a given time point ÷ area of spheroid at time 0 h) x100) was calculated. Graphs show mean±SEM of one experiment performed in triplicate. * $p<0.05$, ** $p<0.01$, *** $p<0.001$ by two-way ANOVA.

3.6 LiCl and BIO inhibit GSK-3 in paediatric glioma cell lines

The effects of LiCl and BIO on migration and invasion has previously been investigated in adult glioma and their anti-migratory and anti-invasive activity has been attributed to their ability to inhibit GSK-3 and stabilise β-catenin (236,246). In order to confirm that LiCl and BIO target GSK-3 in pHGG, Western blot analysis of the activated and inactivated forms of GSK-3 protein following drug treatment was conducted. Based on qualitative analysis, LiCl appeared to increase Ser9 phosphorylated GSK-3β (inactivated form), although this was also accompanied by an increase in the activating phosphorylated tyrosine form of GSK-3αβ. BIO was observed to cause a decrease in the activating phosphorylated tyrosine form of GSK-3αβ, although this was also associated with a decrease in the inactivated form of GSK-3β (Figure 9). To further examine these results, β-catenin localisation and staining patterns were evaluated by IF post-drug treatment (Figure 10). GSK-3 plays an important role in Wnt/β-catenin signalling and when it is inactivated, β-catenin accumulates and is re-located to the nucleus. Conversely, active GSK-3 phosphorylates β-catenin and targets it for ubiquitylation (195). SF188 cells treated with either LiCl or BIO displayed reduced staining of β-catenin at the plasma membrane and enhanced cytoplasmic and peri-nuclear staining, demonstrating the ability of LiCl and BIO to target GSK-3. This was more marked for cells treated with BIO than LiCl (Figure 10A). For KNS42, both surface and intracellular staining of β-catenin was observed in the control; however, BIO and LiCl treatment again resulted in the increased internalisation of β-catenin into the cytoplasm, which was more pronounced for BIO treatment (Figure 10B).

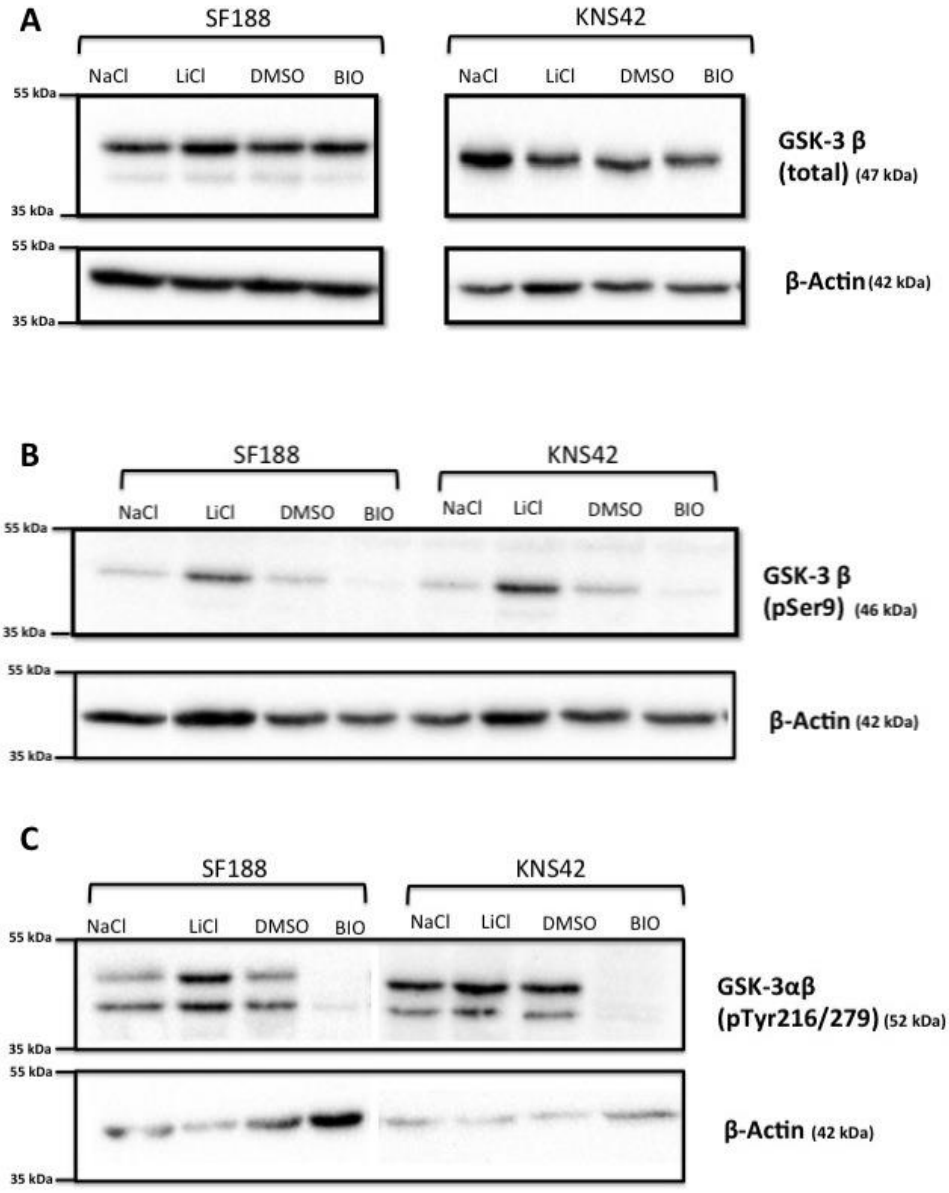

Figure 9: LiCl and BIO affect GSK-3 in paediatric glioma cell lines
pHGG cell lines SF188 and KNS42 were treated with 20 mM LiCl and 5 µM BIO. Following 24 h incubation, cell lysates were obtained. Western blotting determined the expression of GSK-3 substrates: (total GSK-3β **(A)**, Ser9 phosphorylated GSK-3β (inactivated form) **(B)** and Tyr216/279 phosphorylated GSK-3 αβ (active form) **(C)**) in LiCl and BIO treated cell lysates compared to NaCl or DMSO treated controls. All blots included a β-actin control to evaluate protein loading and transfer. A and C are representative of n=2 separate experiments. B is representative of n=3 separate experiments.

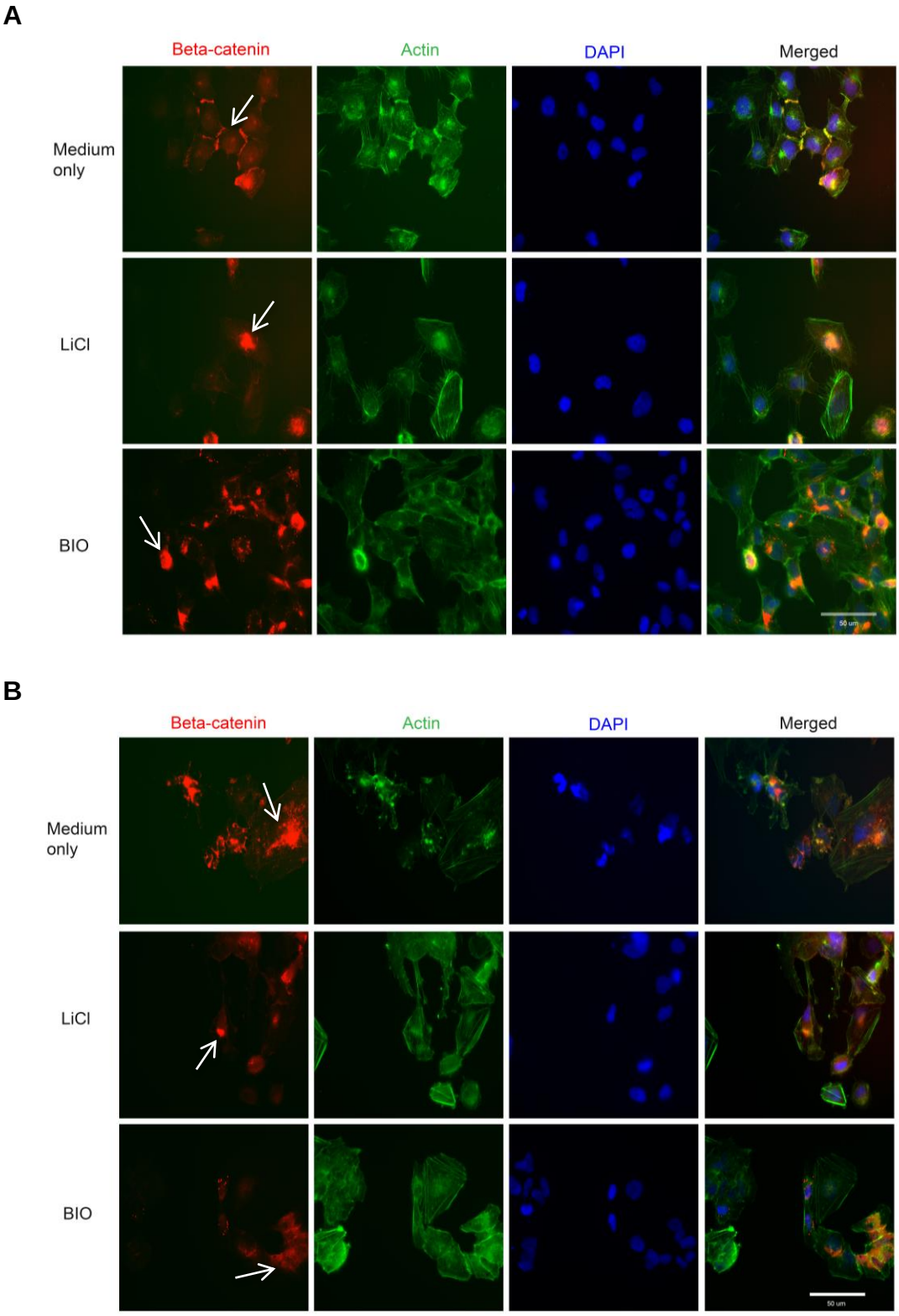

Figure 10: The effects of LiCl and BIO on β-catenin localisation
2x10^5 cells (SF188 **(A)** and KNS42 **(B)**) were grown on sterile cover slips and mock-treated with culture medium or medium containing either 20 mM LiCl or 5 µM BIO for 24 h. The effects of LiCl and BIO on β-catenin localisation were evaluated by immunofluorescent labelling. Arrows indicate β-catenin localisation. Red labeling: β-catenin, Green labeling: actin, blue labeling: DAPI staining. Magnification x63. White scale bar represents 50 µm.

3.7 Migration of pHGG cells in transwell assays is inhibited after treatment with LiCl and BIO

In order to investigate any anti-migratory effects of LiCl and BIO on SF188 and KNS42 monolayers, a 2D transwell assay was performed. As HSJD-DIPG-007 grows as neurospheres, this cell line could not be used in 2D assays.

Both pHGG cell lines SF188 and KNS42 were able to migrate through the transwell membranes, with SF188 demonstrating the most migration over four hours (data not shown). SF188 appears to be more migratory than KNS42 in both 2D and 3D assays (Figure 4, 6 and data not shown). Overall, treatment with 20 mM LiCl and 5 µM BIO in the transwell experiments resulted in a trend towards reduced cell migration in both SF188 and KNS42 (Figure 11). 5 µM BIO treatment resulted in a trend towards reduced migration in both of the pHGG cell lines and this reached statistical significance for KNS42 (Figure 11) (mean±SEM: SF188 migration (% of control): control 100±0, 5 µM BIO 84.7±0.601 p=0.103; KNS42 migration (% of control): control 100±0, 5 µM BIO 58.9±9.17 p=0.023). Treatment with 20 mM LiCl resulted in a trend towards reduced migration in both cell lines and reached statistical significance for SF188 (Figure 11) (mean±SEM SF188 migration (% of control): control 100±0, 20 mM LiCl 58.7±8.11 p=0.0014; KNS42 migration (% of control): control 100±0, 20 mM LiCl 76.7±11.1 p=0.160).

In conclusion, LiCl and BIO at concentrations of 20 mM and 5 µM, respectively, appear to have statistically significant anti-migratory effects on pHGG cells. Consequently, all subsequent migration assays and IF studies were performed on cells treated with LiCl or BIO at these concentrations. Additionally, at the same highest concentrations of NaCl or DMSO, no adverse effects on cell morphology or migration were observed, thus we carried out all subsequent experiments using growth medium (DMEM plus 10 % HI-FCS) as the control.

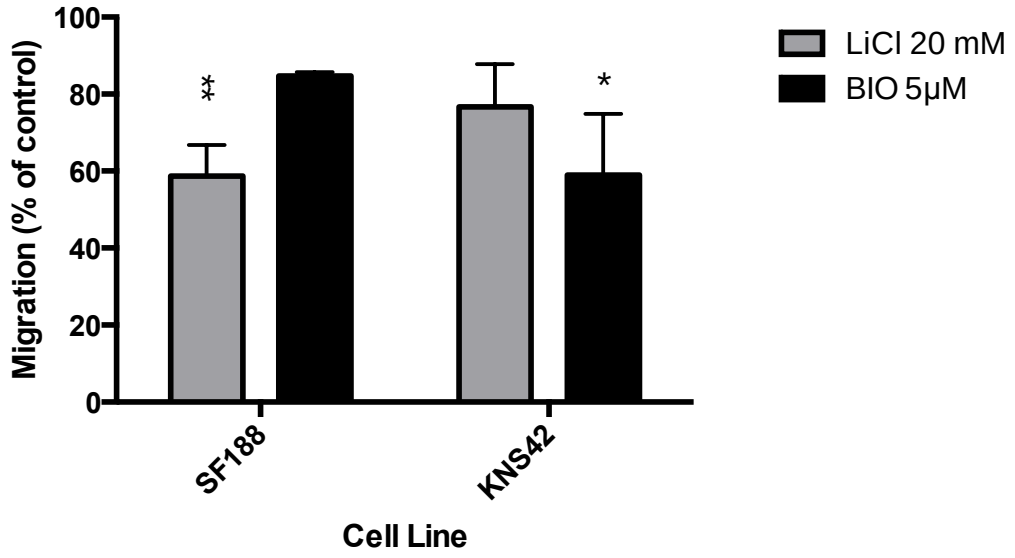

Figure 11: LiCl and BIO inhibit migration of paediatric glioma cells in a 2D Transwell assay
$5x10^4$ cells pre-treated for an hour with either culture medium, 20 mM LiCl or 5 µM BIO were placed in the upper chamber of a transwell and left to migrate for 4 h. Migrated cells were visualised by DAPI staining and photographed using the EVOS cell imaging system. Volocity 3D Image Analysis software was used to quantify the area covered by migrated cells. Graph shows mean±SEM of n=3 individual experiments. *p<0.05, **p<0.01 by one-way ANOVA for each cell type and treatment.

3.8 Effects of LiCl and BIO on pHGG monolayer cell viability

Next, the effect of LiCl and BIO treatment on the viability of cell monolayers was assessed using a WST-1 assay over a 72 h time course (Figure 12). A WST-1 assay was chosen over the MTT assay for improved accuracy. BIO is a naturally pigmented red compound and, therefore, background absorbance of BIO treatment taken up by cells had to be accounted for when interpreting the assay. This could be achieved more accurately by using the WST-1 assay as it lacks the solubilisation stage required for an MTT assay. This meant that the absorbance at each concentration of BIO could be more accurately quantified and accounted for within wells (by setting up mock control wells containing BIO only (no cell control)).

SF188 was the most sensitive cell line to both treatment effects (Figure 12). At 24 h, which most closely correlates to the time point for the transwell assay, both cell lines demonstrated greater than 80 % viability when treated with LiCl (Figure 12). SF188 was more sensitive to treatment with BIO at 24 h, with cell viability reduced to 72 % following 24 h treatment with 5 µM BIO; however, KNS42 was resistant to the effects of BIO with greater than 89 % cell viability demonstrated at 24 h across all concentrations (Figure 12).

Over 72 h, when cultured as monolayers, both pHGG cell lines exhibited increased sensitivity to LiCl and BIO treatment compared to spheroid cultures. This is unsurprising since 3D aggregates of tumour cells, including pHGG cells, have been shown to be generally more drug resistant than 2D cultures (356,357). Finally, to demonstrate that LiCl and BIO are not directly cytotoxic at concentrations of 20 mM and 5 µM, respectively, monolayers of both pHGG cell lines were imaged by time-lapse microscopy following treatment with LiCl and BIO for 24 h. After 24 h, the drugs were removed, and both pHGG cell lines demonstrated recovery and resumed their normal morphology (Figure 13).

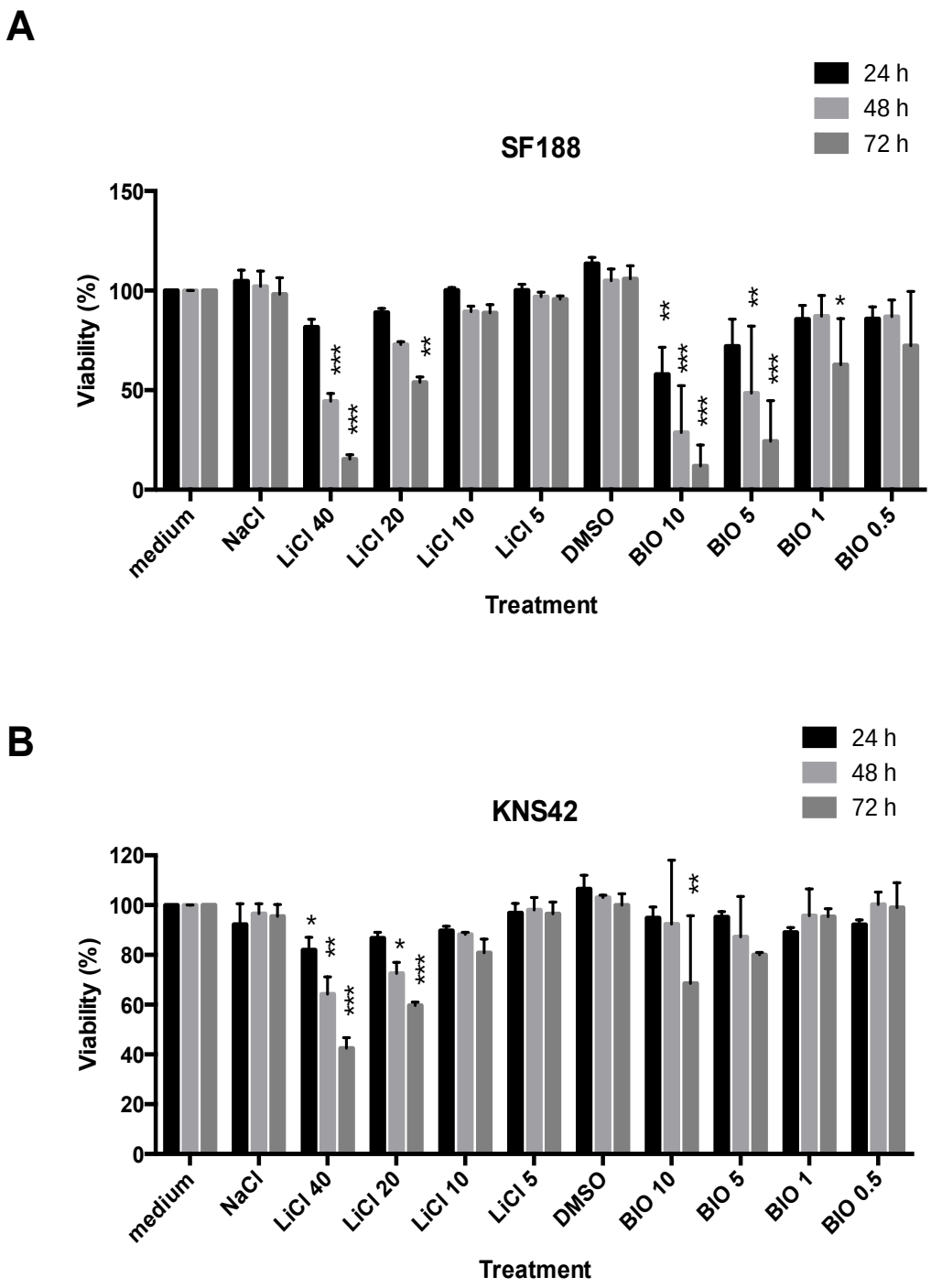

Figure 12: Effects of LiCl and BIO on pHGG monolayer cell viability
Cells were seeded (SF188 **(A)** at 2.5x10^3 cells/well, KNS42 **(B)** at 5x10^3 cells/well) in a flat-bottom 96 well plate and allowed to adhere overnight. Cells were then treated with culture medium or drugs (LiCl at 40, 20, 10, 5 mM in NaCl or BIO at 10, 5, 1, 0.5 µM in DMSO). Cell viability at 24, 48 and 72 h was determined by WST-1 assay and was expressed as a percentage of controls. Graphs show mean±SEM of n=3 individual experiments performed in triplicate. *p<0.05, **p<0.01, ***p<0.001 by two-way ANOVA.

A

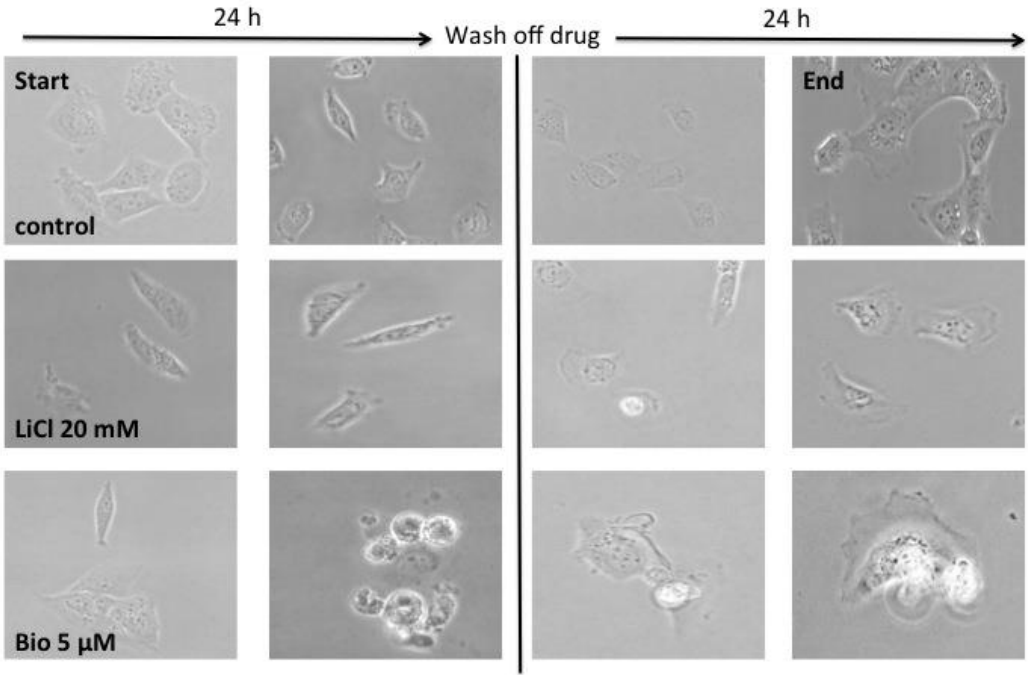

B

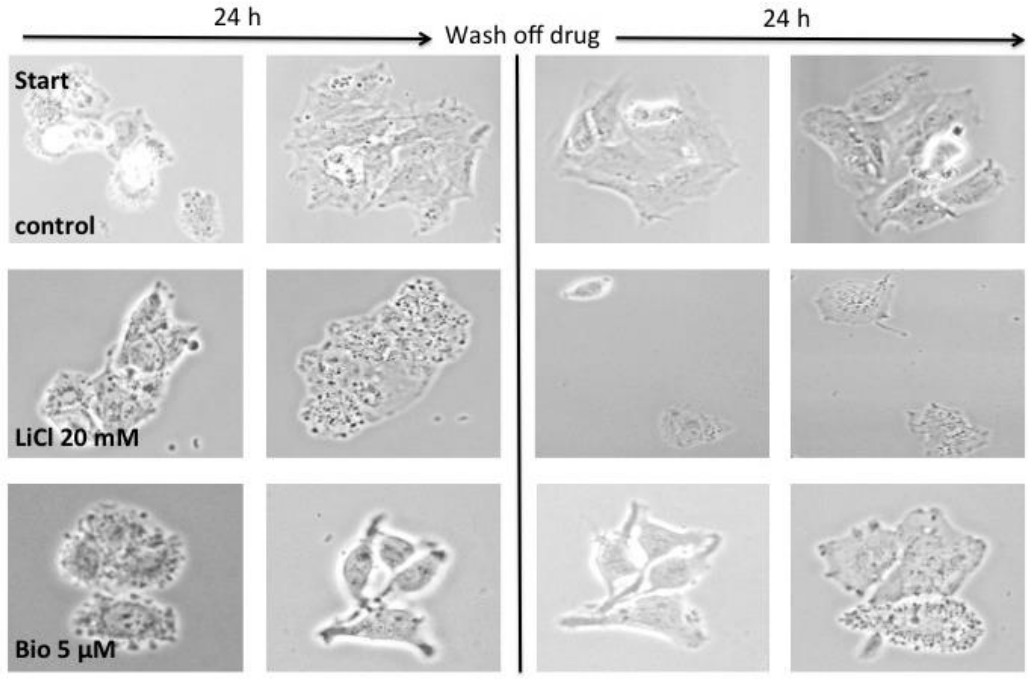

Figure 13: LiCl and BIO are not directly cytotoxic to pHGG monolayers at 24 h
pHGG cell lines SF188 **(A)** and KNS42 **(B)** were incubated with 20 mM LiCl, 5 µM BIO or culture medium and live cell imaging was performed for 24 h using the Nikon Biostation IM live cell imaging system. After 24 h, cells were washed with PBS to remove drug treatments and replenished with fresh drug-free culture medium. Cells were imaged for a further 24 h. Stills were taken from movies obtained using the Biostation IM-associated software at 0 and 24 h and 0 and 24 h post-drug removal. Magnification x40.

3.9 LiCl and BIO inhibit pHGG cell migration on a topographic nanofibre-based migration assay

A nanofibre-based assay was also used to assess the effect of GSK-3 inhibition on migration of pHGG cell lines over a 3D scaffold. This assay utilises aligned fibres of poly-ε-caprolactone to stimulate cell migration via topographic cues (351). When cells are plated on the nanofibre scaffold they adhere, elongate and move along the fibre axis (Figure 14A).

Firstly, it was noted that each pHGG cell line was able to migrate in this model system and further confirmation of the anti-migratory effect of the GSK-3 inhibitors LiCl and BIO was obtained. As seen in previous assays, SF188 was the most migratory cell line in terms of distance travelled. Perimeter indices (% increase from the spheroid perimeter to the perimeter marking the migrated cells) were calculated for each cell line. Treatment with LiCl and BIO resulted in a trend towards decreased migration index (Figure 14C) and perimeter index (Figure 14D) for both pHGG cell lines when compared to controls. However, surprisingly the effect was more marked for KNS42 when compared to SF188. LiCl and BIO resulted in a statistically significant reduction in both migration and perimeter index for KNS42 (mean±SEM: migration index: control 0.72±0.0123, LiCl 20 mM 0.337±0.061 p=<0.001, BIO 5 µM 0.327±0.0107 p=<0.001; perimeter index: control 50.6±2.50, LiCl 20 mM 20.2±5.04 p=0.0012, BIO 5 µM 20.6±3.27 p=0.0019). For SF188, LiCl and BIO resulted in a small but non-statistically significant reduction of migration index (Figure 14C) (mean±SEM migration index: control 0.911±0.001, LiCl 20 mM 0.88±0.0458 p=0.655, BIO 5 µM 0.819±0.0293 p=0.076). BIO significantly reduced the perimeter index for SF188; however, LiCl only caused a small but non-significant reduction in this index (Figure 14D) (mean±SEM perimeter index: control 79.2±1.71, LiCl 20 mM 70.6±3.55 p=0.051, BIO 5 µM 65.1±2.52 p=0.0039).

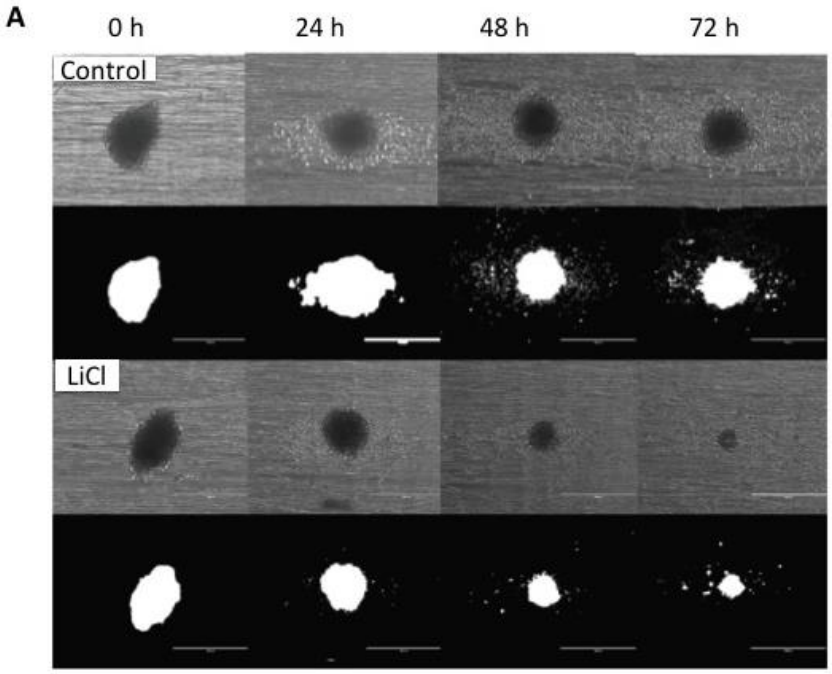
A
0 h
24 h
48 h
72 h
Control
LiCl

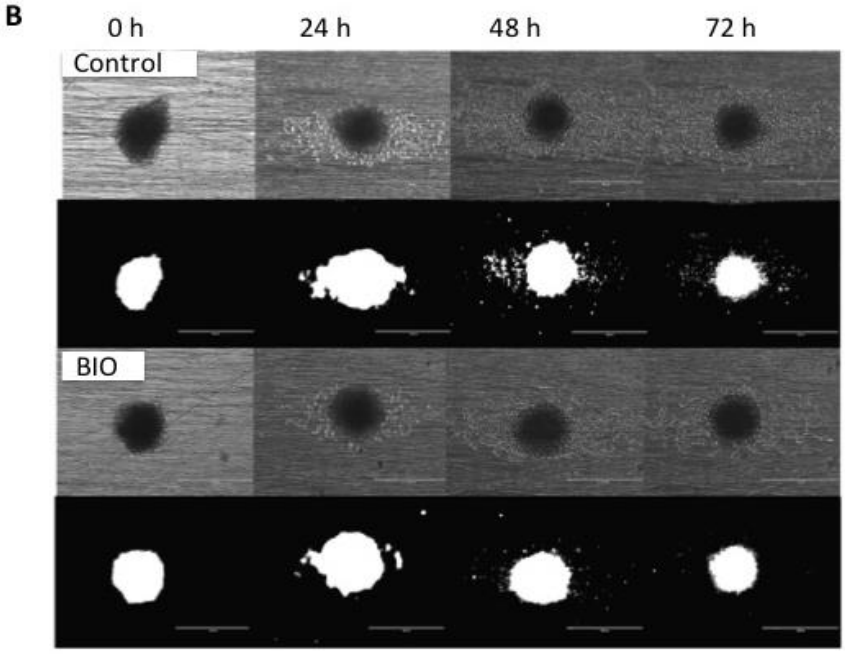
B
0 h
24 h
48 h
72 h
Control
BIO

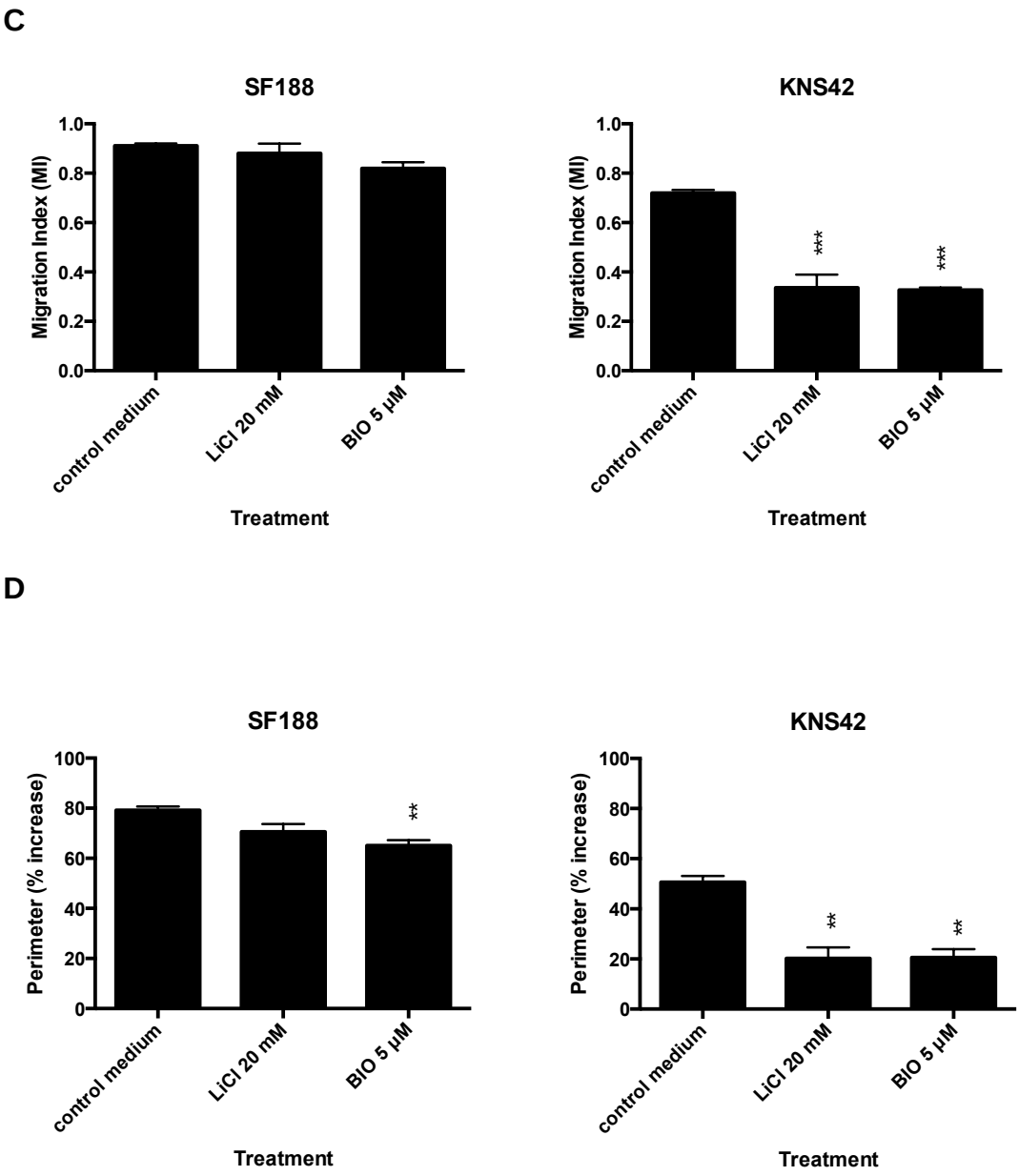

Figure 14: LiCl and BIO reduce migration of paediatric glioma cells in an aligned nanofibre 3D migration assay

Tumour cell aggregates formed from hanging drops of $1x10^3$ cells of SF188 or KNS42 were placed in wells containing aligned poly-ε-caprolactone fibres and cultured ± 20 mM LiCl or 5 µM BIO. Migration was imaged over 72 h using the EVOS cell imaging system. **(A)** Illustration of spheroids formed from cell line SF188 cultured ± 20 mM LiCl imaged over 72 h. **(B)** Illustration of spheroids formed from cell line SF188 cultured ± 5 µM BIO imaged over 72 h. Cells were labeled with CellTracker™ dye to enhance visualisation of migrating cells (black and white images in A and B). Images at x4 magnification. Scale bar represent 400 µm. **(C)** Quantification and comparison of the effects at 72 h of 20 mM LiCl and 5 µM BIO on migration index (MI) ((area of zone – area of core) ÷ total area) for both cell lines. **(D)** Quantification and comparison at 72 h of the effects of 20mM LiCl and 5 µM BIO on the perimeter index (% increase from the spheroid perimeter to the perimeter marking the migrated cells) for both cell lines. Graphs show mean±SEM of one experiment performed in quadruplicate. *p<0.05, **p<0.01, ***p<0.001 by one-way ANOVA for each cell type and treatment.

3.10 Live cell imaging of pHGG cell line migration

Given the accumulating evidence that LiCl and BIO are able to reduce the migration of SF188 and KNS42 cells, direct changes in cell morphology and motility following treatment should be observable. Thus, the effects of LiCl and BIO on individual cell morphology were investigated by live cell imaging of random cell migration. SF188 and KNS42 cells were incubated with 20 mM LiCl, 5 µM BIO or control and live cell imaging was performed over 24 h (Figure 15) (Movies 1-6).

Interestingly, both LiCl and BIO appeared to affect cell morphology with cells rounding up after treatment, blebbing and, in the case of SF188, demonstrating loss of front-rear polarity (Figure 15A) (Movies 1-6). SF188 cells treated with both LiCl and BIO appeared to lose the clear definition of their leading edge and trailing edge compared to cells mock-treated with culture medium. Individual cell tracking (Figure 15B) revealed that cells treated with either LiCl or BIO were less motile and became almost static over a 24 h time period and this difference was marked when compared to the tracking of cells treated with growth medium alone.

In terms of motility, SF188 cells were more motile and demonstrated greater velocity than KNS42 cells (mean±SEM: velocity SF188: control 0.295±0.0018 µm/min, velocity KNS42: control 0.0599±0.0048 µm/min) (Figure 15C-E). 20 mM LiCl and 5 µM BIO treatment resulted in a trend towards reduced velocity of SF188 cells (mean±SEM velocity: control 0.295±0.0018 µm/min, LiCl 20 mM 0.153±0.047 µm/min p=0.049, BIO 5 µM 0.21±0.041 µm/min p=0.247) whereas only treatment with 5 µM BIO indicated a tendancy towards reduced velocity of KNS42 cells (mean±SEM velocity: control 0.0599±0.0048 µm/min, LiCl 20 mM 0.0761±0.0063 µm/min p=0.101, BIO 5 µM 0.0501±0.041 µm/min p=0.352).

Petrie *et al.* state that directionality of a migrating cell can be defined as it's displacement divided by the total length of the path it travels (358). The authors also state that 'cells contain polarity signalling machinery that can influence directional cell motility' and that 'stability of the front-rear axis

correlates with the extent of persistent directional cell movement' (358). It is also well known that cell polarity is required to generate the front-rear axis required for random cell migration and that maintenance of such polarity is an essential part of cell migration (87). In this thesis, measurement of displacement was used to demonstrate the effect of drug treatment on cell polarity by proxy. This allowed measurement of the distance from the start point of the track of a moving cell to the point at the end of the experiment and not just the total length of distance travelled. Measuring displacement allowed illustration of whether a cell had actually moved away from its original starting point over time (a process that requires a cell to demonstrate polarity and generation of a front-rear axis), instead of just moving on the spot.

SF188 cells were able to polarize (front-rear) under normal conditions; however, treatment with 20 mM LiCl and 5 µM BIO resulted in a trend towards reduced polarity as demonstrated by a reduction in displacement, but this did not reach statistical significance (mean±SEM: displacement SF188: control 176.5±74.6 µm, LiCl 20 mM 52.5±15.3 µm p=0.259, BIO 5 µM 107.2±61.7 µm p=0.610).

A

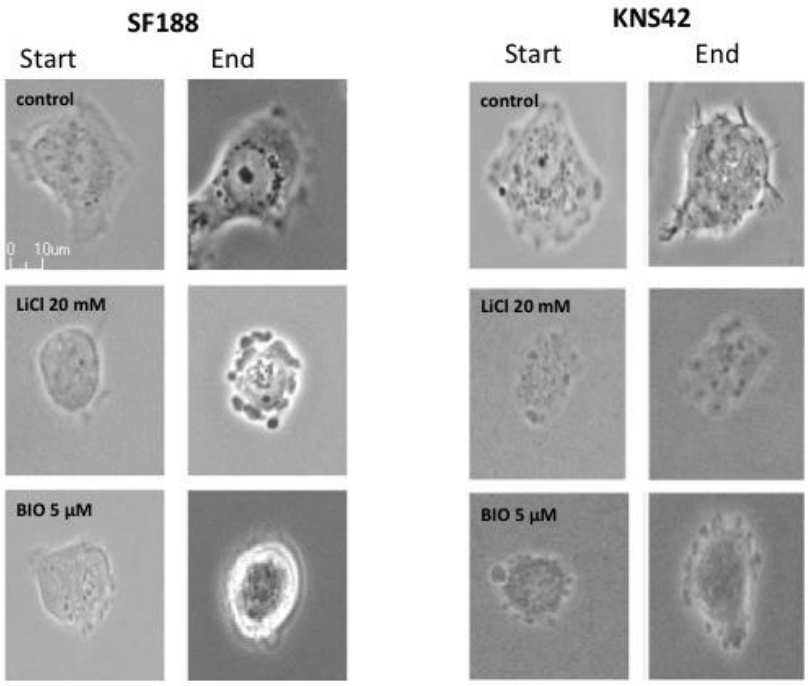
SF188
KNS42
Start
End
Start
End
control
LiCl 20 mM
BIO 5 µM
control
LiCl 20 mM
BIO 5 µM
0 10um

B

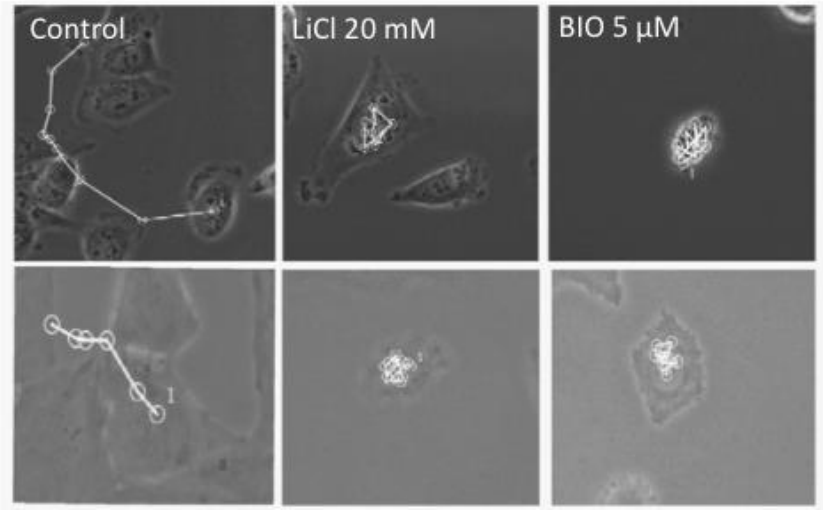
SF188
KNS42
Control
LiCl 20 mM
BIO 5 µM

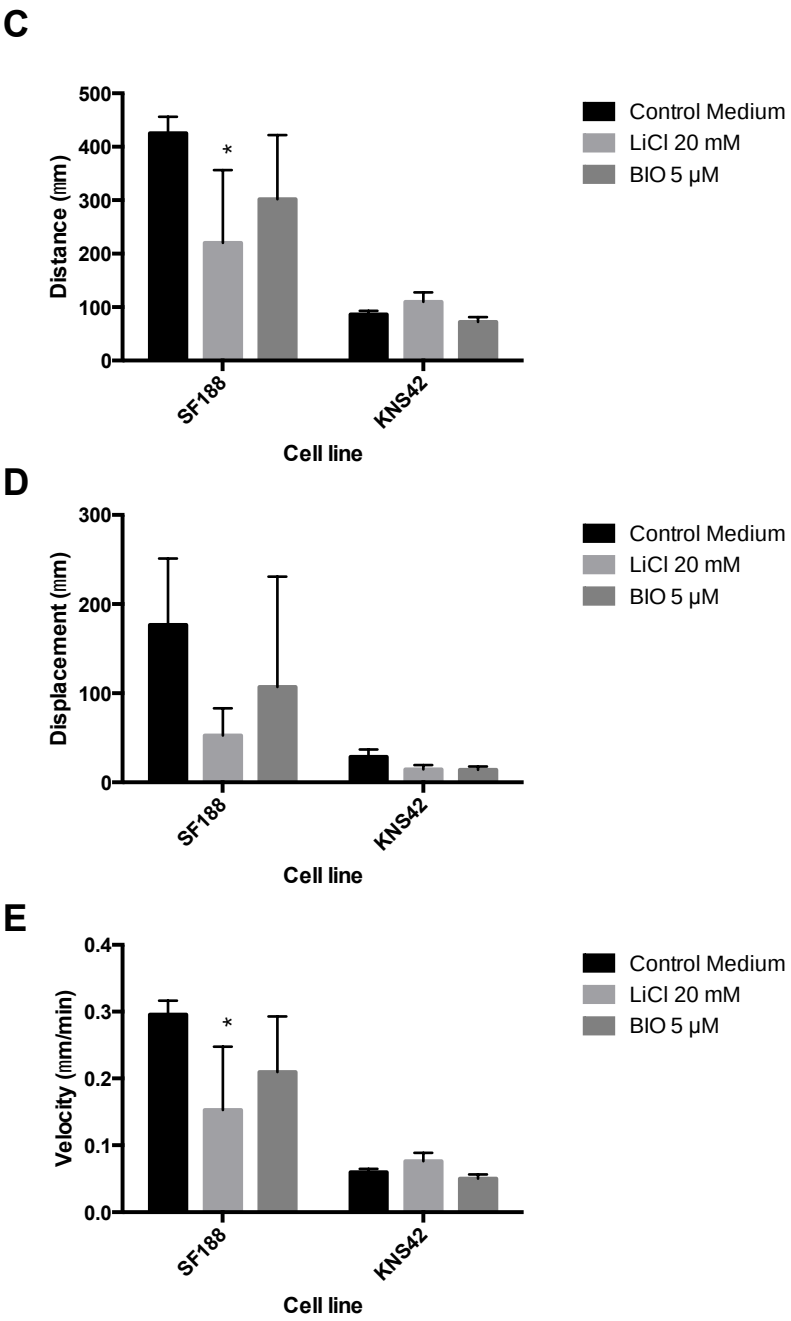

Figure 15: Live cell imaging of pHGG cell lines reveals differences in random cell migration velocity alongside changes in polarity and morphology following treatment with LiCl and BIO

Paediatric glioma cell lines SF188 and KNS42 were incubated with 20 mM LiCl, 5 µM BIO or culture medium and live cell imaging was performed for 24 h using the Nikon Biostation IM live cell imaging system. Magnification x40. Stills taken at time 0 h and 24 h from movies of SF188 and KNS42 **(A)** treated with either 20 mM LiCl, 5 µM BIO or culture medium demonstrate changes in the morphological appearance of individual cells following treatment. Tracking analysis of SF188 and KNS42 **(B)** from live cell imaging using Image J with MTrack software following treatment with 20 mM LiCl or 5 µM BIO demonstrates differences in motility between cell lines and treatments. Quantification analysis of distance **(C),** displacement **(D)** and velocity (distance/time) **(E),** from live cell imaging of both cell lines following treatment with 20 mM LiCl or 5 µM BIO was completed using Image J with MTrack. Graphs show the mean±SEM obtained from two separate experiments, with multiple fields of cells analysed for each condition. *$p<0.05$ by one-way ANOVA for each cell type and treatment.

3.11 Immunofluorescence studies reveal cytoskeletal changes in pHGG cell lines following treatment with LiCl and BIO

To investigate the effects of the GSK-3 inhibitors LiCl and BIO on the cell cytoskeleton, IF staining for microtubules and actin as well as focal adhesions were carried out on cells treated with culture medium ± drugs. Microtubules and actin, alongside intermediate filaments comprise the cytoskeleton and their interplay orchestrates cellular shape changes during migration (86). Focal adhesions reside at the end of large actin bundles and link the actin cytoskeleton to the ECM (90). Focal adhesions are highly dynamic and their constant assembly and disassembly allows the cell to generate traction forces to move forward (90).

Both cell lines were characterised by distinctive microtubule network, actin cytoskeleton and focal adhesion staining patterns. Untreated SF188 cells appeared as large cells with prominent well-defined microtubule networks spreading across the whole cell body, elaborate actin stress fibres traversing across the whole cell body and a network of multiple focal adhesions interspersed across the whole cell body (Figure 16A). After treatment with 20 mM LiCl or 5 µM BIO, the SF188 cells started to become more rounded and microtubules localised towards the cell surface. The most pronounced changes were seen in actin filament and focal adhesion distribution and, as such, at least 100 SF188 cells from each treatment condition were scored to determine the distribution of actin and focal adhesions ± drugs. Following treatment with 20 mM LiCl or 5 µM BIO, actin was no longer distributed across the whole cell body as well-defined stress fibres and staining appeared to be more diffuse throughout the cytoplasm (defined as ‘other’) (Figure 16B). Additionally, following treatment with 20 mM LiCl or 5 µM BIO, the overall presence of focal adhesions appeared to be diminished (defined as ‘diffuse’ staining) and when present, no longer appeared to be across the whole cell body as seen in control cells. Instead, LiCl and BIO treatment appeared to cause a redistribution of focal adhesions to the surface of the cell (defined as ‘cortical’ staining) (Figure 16C).

KNS42 cells appeared as medium-sized elongated cells with a prominent microtubule network and diffuse actin stress fibres traversing across the whole cell body (Figure 16D and E). Focal adhesions appeared to be associated with actin filaments in untreated cells but were less marked and had a more diffuse distribution than seen in SF188 cells (Figure 16F). After addition of the inhibitors, the cells rounded up and appeared smaller by microscopy in comparison to the untreated cells. Actin stress fibres appeared to be less pronounced and re-localised towards the cell surface (defined as 'cortical' staining) following treatment with BIO (Figure 16E). Following treatment with 20 mM LiCl, actin staining appeared to be more diffuse throughout the cytoplasm and well-defined stress fibres were less marked compared to control-treated cells. Overall, focal adhesions appeared to co-localise diffusely with the actin filaments (Figure 16F).

Figure 16: Immunofluorescence studies reveal cytoskeletal changes in two pHGG cell lines after LiCl and BIO treatment
Paediatric glioma cell lines SF188 **(A-C)** and KNS42 **(D-F)** were grown on cover slips and incubated with 20 mM LiCl, 5 µM BIO or culture medium for 72 h. The effects of LiCl and BIO on microtubules, actin and focal adhesions (by vinculin) were evaluated by IF labeling of cell lines SF188 **(A)** and KNS42 **(D)**. Green labeling: alpha-tubulin, actin or vinculin, red labeling: actin and, blue labeling: DAPI staining. Magnification x63. White scale bar represents 50 µm. At least 100 cells from each treatment condition were scored to determine changes in the distribution of the actin cytoskeleton (defined as cortical, stress fibres or other as illustrated) **(B and E)** or focal adhesion pattern (defined as cortical, diffuse or whole cell body as illustrated) **(C and F)**.

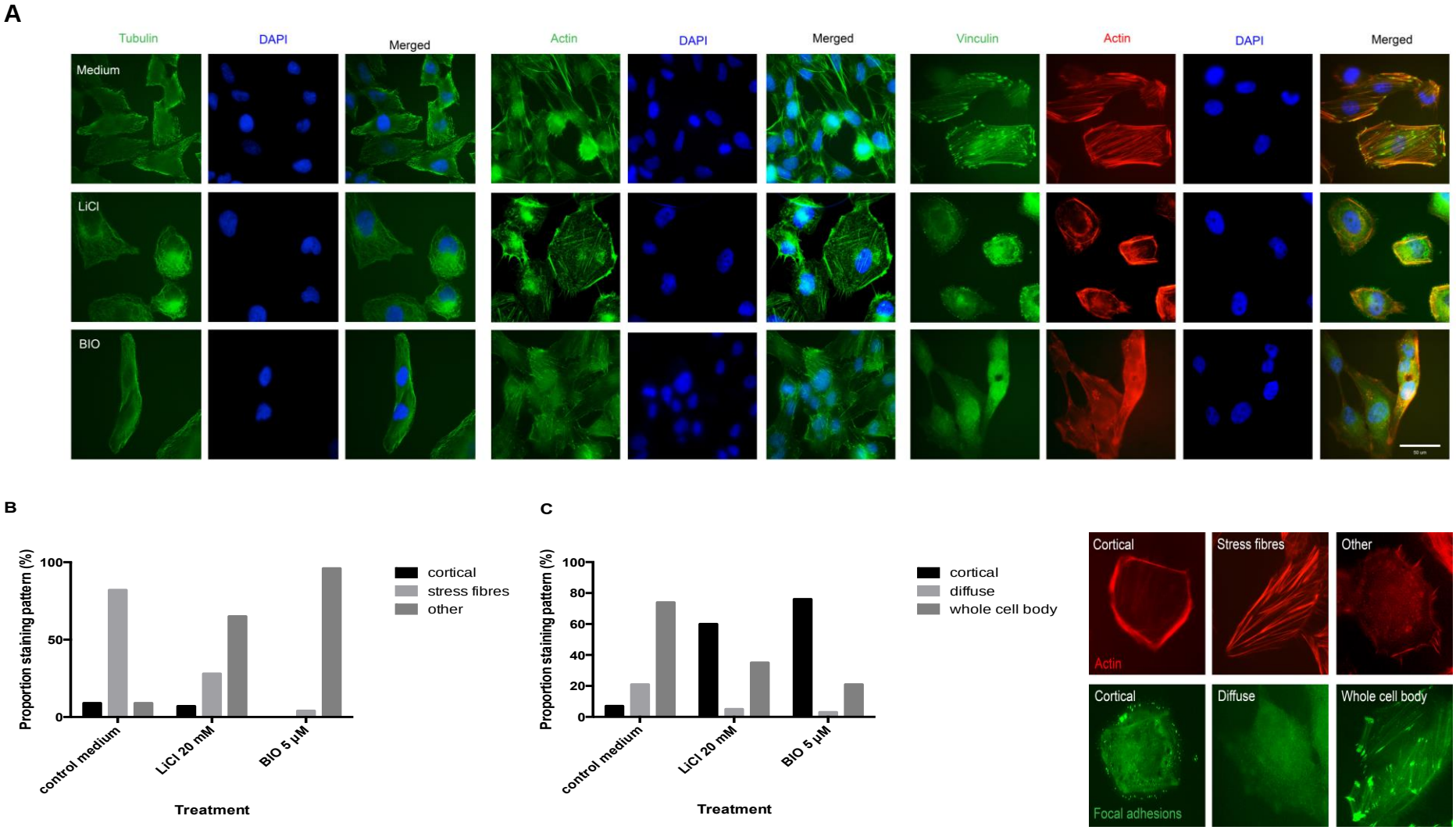
A
Tubulin
DAPI
Merged
Actin
DAPI
Merged
Vinculin
Actin
DAPI
Merged
Medium
LiCl
BIO
B
Proportion staining pattern (%)
100
50
0
control medium
LiCl 20 mM
BIO 5 µM
Treatment
cortical
stress fibres
other
C
Proportion staining pattern (%)
100
80
60
40
20
0
control medium
LiCl 20 mM
BIO 5 µM
Treatment
cortical
diffuse
whole cell body
Cortical
Actin
Stress fibres
Other
Cortical
Focal adhesions
Diffuse
Whole cell body

D

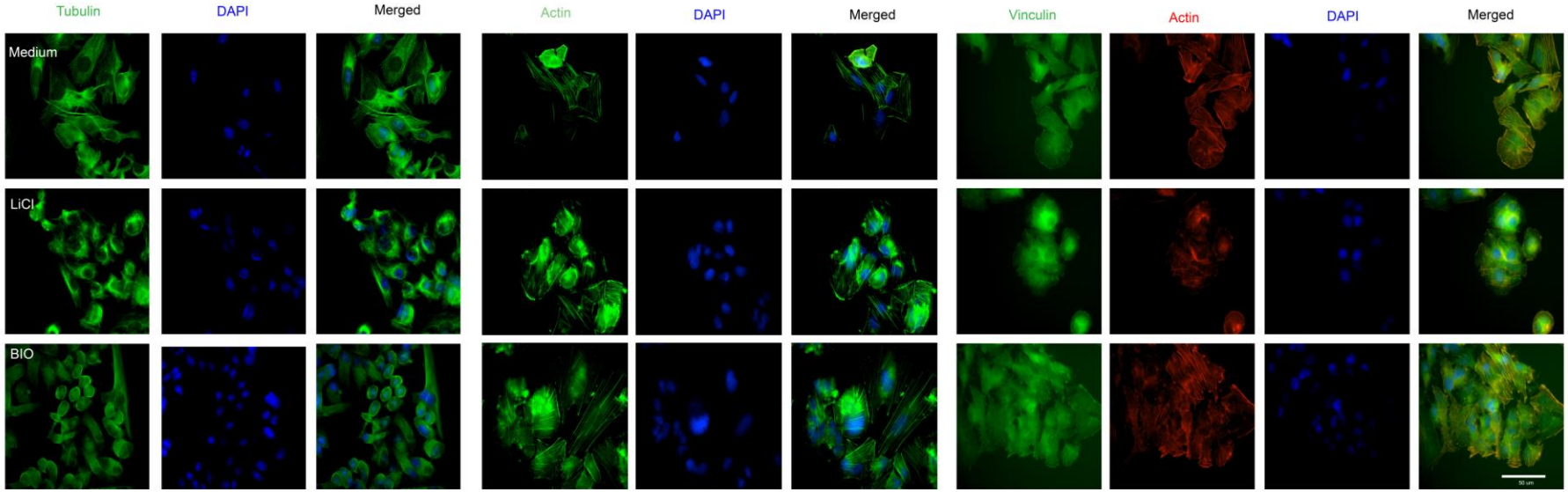
Tubulin
DAPI
Merged
Actin
DAPI
Merged
Vinculin
Actin
DAPI
Merged
Medium
LiCl
BIO

E

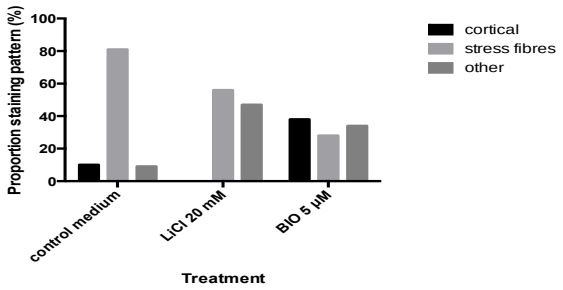
Proportion staining pattern (%)
100
80
60
40
20
0
control medium
LiCl 20 mM
BIO 5 µM
Treatment
cortical
stress fibres
other

F

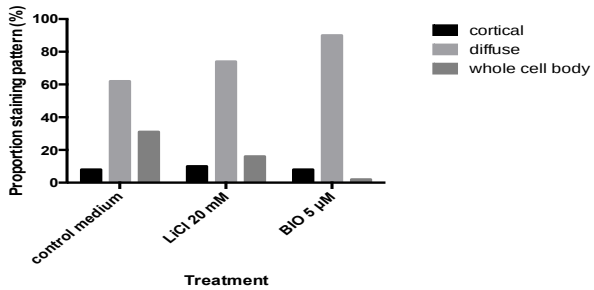
Proportion staining pattern (%)
100
80
60
40
20
0
control medium
LiCl 20 mM
BIO 5 µM
Treatment
cortical
diffuse
whole cell body

3.12 Discussion

pHGG and DIPG are devastating tumours associated with poor prognosis and despite attempts at aggressive therapy, tumours inevitably recur due to their diffuse and invasive nature. As a result, there is a need to identify and develop novel therapeutic approaches that target and block tumour invasion. In this chapter, the migratory and invasive behavior of two pHGG cell lines and one patient-derived DIPG cell line is characterised using both 2D and 3D models. The ability of paediatric glioma cell lines (SF188, KNS42 and HSJD-DIPG-007) to grow as tumour spheroids was demonstrated and these spheroids were shown to be capable of invasion through a collagen matrix. To the best of my knowledge, this is the first time that DIPG invasion has been described using a 3D model. Each cell line investigated demonstrated a unique pattern of migration and invasion and KNS42 was noted to have a significantly reduced migration index when compared to that of SF188 and HSJD-DIPG-007. The motility of individual pHGG cells was examined by live cell imaging, which indicated different speeds and migratory morphology between the two cell lines. Again KNS42 was seen to be less motile and demonstrated reduced velocity when compared to SF188 under control conditions.

In addition, the results within this chapter demonstrate, for the first time, that LiCl and BIO, which have anti-invasive effects in adult glioma cell lines (236,246), can also inhibit the migration and invasion of paediatric glioma cells in 2D (transwell) and 3D (spheroid invasion and nanofibre plate) assays. All three paediatric glioma cell lines demonstrated a statistically significant reduction in migration index when treated with either 5 µM BIO or 20 mM LiCl in the 3D spheroid invasion assay. This was not accompanied by marked loss of viability compared to appropriate controls when SF188 and KNS42 cells were cultured as multicellular spheroids. This data correlates with previously published results for these inhibitors in adult glioma models (236,246). Furthermore, LiCl and BIO treatment resulted in a tendancy towards reduced movement by tracking analysis (SF188 and KNS42) and loss of polarity (SF188) of individual pHGG cells. Cells rounded

up, demonstrated blebbing and for SF188, lost the clear definition of a leading and trailing edge when treated with either drug. Non-apoptotic plasma membrane blebbing has been implicated in cell movement, mode of migration and disruption of actin-membrane interactions (359). These observations are novel and demonstrate the specific effects of LiCl and BIO on cell morphology and motility.

Finally, the results in this chapter show that treatment of pHGG cells with 5 µM BIO or 20 mM LiCl can result in cytoskeletal rearrangements. Following treatment, prominent actin stress fibres traversing the whole cell body were lost and actin fibres appeared more diffusely distributed or re-organised to the cell surface. Focal adhesions were also re-organised and became either diffusely co-localised with actin filaments or redistributed towards the cell surface following drug treatment. Taken together, these observations offer some indication of how LiCl and BIO exert their anti-migratory and anti-invasive effects. Overall, this study is amongst the very few to have identified existing clinical and pre-clinical agents which are capable of disrupting migration and invasion in pHGG and DIPG cell lines.

Work from Dr Sean Lawler's group has previously addressed the ability of LiCl and BIO to inhibit migration and invasion of adult HGG cells. In the first of two studies, Dr Lawler's group concluded that 20 mM LiCl could potently block glioma cell migration in 3D spheroid, wound-healing and brain slice assays (236). The group's follow-on study concluded that potent GSK-3 inhibitors of the indirubin family (including 5 µM BIO) could reduce invasion of both adult glioma cells and glioma-initiating neurospheres *in vitr*o and *in vivo.* Additionally, the indirubin 6-bromoindirubin acetoxime (BIA) showed significant therapeutic efficacy in mice (246).

There are some correlations between the results presented in this chapter and those of Dr Lawler. Of note, 20 mM LiCl and 5 µM BIO appear to be the effective concentrations to significantly inhibit the invasion of both adult and pHGG cells in 3D spheroid invasion assays (236,246). Dr Lawler's group conclude that the effects of indirubins on migration appear to be more pronounced than those of LiCl, as demonstrated by a transwell assay (246).

Whilst this appears to be the case for KNS42 in a similar transwell assay in our study, 20 mM LiCl resulted in a more pronounced and significant reduction in transwell migration of SF188 compared to 5 µM BIO treatment. This observation may reflect differences in individual cell line responses to the effects of drug treatment.

The anti-migratory and anti-invasive effects of 20 mM LiCl and 5 µM BIO on paediatric glioma appear to be specific and not a consequence of cytotoxicity. The effects of the drugs on cytotoxicity can be distinguished from the effects on migration because: 1) spheroids of pHGG cell lines demonstrate a reduction in viability of only about 20 % following 72 h incubation with these drugs compared to culture medium and no marked change in viability when normalised to the NaCl or DMSO corresponding control; 2) in transwell assays, differences in migration were observed after 4 h; however, viability data obtained from monolayers at 24 h still demonstrates over 72 % viability in all cell lines following drug treatment and; 3) pHGG cells treated with either 20 mM LiCl or 5 µM BIO for 24 h demonstrate recovery and return to their normal morphology following drug washout. In keeping with these results, Dr Lawler's group also concluded that blockade of adult HGG migration with 20 mM LiCl or 5 µM BIO is not secondary to cytotoxicity and the authors demonstrated that the anti-migratory effects of both LiCl and BIO are reversible, following drug washout (236,246).

Finally, the effects of LiCl and BIO on pHGG invasion observed in our study do not appear to be related to an inhibitory effect on tumour spheroid growth. Although 40 mM LiCl appeared to significantly slow the growth of spheroids at 72 h, this effect was not noted at any other time point or with any other concentration of either drug. Surprisingly, 20 mM LiCl appeared to significantly increase the growth of pHGG spheroids over time, which is undesirable for a potential cancer treatment. Further work is required to evaluate whether the increased growth effects of 20mM LiCl on pHGG persist over a longer time period. Dr Lawler has previously shown that 20 mM LiCl slows adult glioma cell proliferation, mainly through its effect on the

cell cycle (236); however, future work is required in order to evaluate the direct effects of LiCl specifically on pHGG cell proliferation. Additionally, the effects of 20 mM LiCl in combination with other chemotherapeutics that target proliferation and growth, remain to be investigated. Future studies are also required to determine the *in vivo* effects of LiCl on pHGG tumour growth and proliferation.

One postulated mechanism for the anti-migratory effects of LiCl and BIO is through their ability to inhibit GSK-3. LiCl was one of the first GSK-3 inhibitors to be described; however, it has a wide range of molecular targets, including IMPase (224). Dr Lawler's group demonstrated that the anti-migratory effects of LiCl were not attributable to its effect on IMPase as: 1) migration could not be rescued in cells treated with LiCl by the addition of inositol (depleted following IMPase blockade) and; 2) use of a potent IMPase inhibitor had no significant effect on glioma invasion (236). By contrast, specific pharmacological GSK-3 inhibitors mimicked the dose-dependent blockade of glioma invasion observed with LiCl (236). As GSK-3 inhibition can stabilise β-catenin and target it to the nucleus via the canonical Wnt signalling pathway (195), β-catenin reporter activity was investigated in adult HGG cells following LiCl treatment at a range of concentrations. LiCl treatment increased β-catenin reporter activity and the degree of GSK-3 inhibition directly correlated with blockade of invasion (236). Dr Lawler's group also demonstrated that β-catenin knockdown could rescue the anti-migratory effects of BIO, suggesting that β-catenin stabilisation following GSK-3 inhibition may also play an important role in inhibiting glioma migration (246). Other *in vivo* studies have demonstrated contradictory findings demonstrating that β-catenin can be pro- (360,361) or anti- (362) migratory within glioma.

In our study, β-catenin localisation was studied by IF following the treatment of pHGG cells with LiCl and BIO and a marked internalisation of β-catenin to the cytoplasm and nucleus was observed following drug treatment. This observation has also been noted in adult glioma following LiCl and BIO treatment (363) and provides evidence to support the effectiveness of LiCl

and BIO as an inhibitor of GSK-3 in pHGG. Furthermore, qualitative interpretation of Western blot analysis of pHGG lines showed that LiCl treatment increased Ser9 phosphorylated GSK-3β (inactivated form), although this was also accompanied by an increase in the activating phosphorylated tyrosine form of GSK-3αβ. BIO decreased the activating tyrosine of GSK-3αβ, although this was also associated with a decrease in the inactivated form of GSK-3β. These findings were similar to the work of Dr Lawler's group, who also showed that BIO reduced Tyr^{216} phosphorylation of GSK-3β (246) while also causing a slight decrease in inhibitory Ser9 phosphorylated GSK-3β (363). Simòn et al. have demonstrated that 'GSK-3 kinase activity is not necessarily correlated with the extent of tyrosine phosphorylation' and this may be one possible explanation to why LiCl, a known inhibitor of GSK-3 (224), can cause an increase in the activating phosphorylated tyrosine form of GSK-3αβ in our system as well as increasing the inactivating form (Ser9 phosphorylated GSK-3β) (364). It appears that within cells, GSK-3 regulation is complex, involving a combination of; post-translational phosphorylation, interaction with other proteins in complexes, priming phosphorylation of the substrate and distribution within the cell (196). The results within this chapter start to provide evidence that LiCl and BIO can cause changes in the phosphorylation of GSK-3 in pHGG which can alter its activity; however, given the multiple layers of regulation of GSK-3 activity within a cell and its complex nature, additional studies are required to further prove this hypothesis.

Cell migration may be achieved by a set of component processes, which are often regulated by the same effectors, regardless of the cell type and the mode of migration. Broadly, these processes are based on polarisation, protrusion and adhesion, translocation of the cell body and retraction of the rear. They are also coordinated and integrated by extensive transient signalling networks (91). GSK-3 is thought to be a key player in the control of cell migration (202,213). GSK-3 has a role in promoting actin polymerisation and lamellipodia formation in the migrating cell (213,216,217) and is also critical for the determination of cell polarity (110). GSK-3 is also involved in

the organisation of microtubule networks (213,219,220) and plays an important role in the formation of adhesions and cell spreading (213,222). In this study, it was observed that LiCl and BIO treatment could induce changes in the microtubule cytoskeleton, actin skeleton and focal adhesion dynamics of pHGG cells. Following drug treatment, microtubules re-localised to the surface of cells, actin fibres re-localised to the cell periphery and there was a change in focal adhesion distribution with re-distribution to the cell surface and apparent loss of focal adhesion foci. Live cell imaging of random cell migration revealed that the cells appeared to be immobilised in response to either a loss of polarity and/or motility. Taken together, these observations account for the inability of pHGG cells to migrate following LiCl or BIO treatment. In conclusion, the results contained within this chapter, together with the work of Dr Lawler (236,246), suggests that GSK-3 inhibition may be one potential mechanism explaining the observed anti-migratory effects of LiCl and BIO in pHGG cells. Future studies are needed to evaluate a wide range of potent specific pharmacological inhibitors of GSK-3 in order to further prove this hypothesis and to identify drug candidates to take forward for clinical testing.

Both LiCl and BIO have potential for clinical application. LiCl has been used to treat psychiatric conditions such as bipolar disorder for many decades (365) and BIO is part of the family of indirubins, which have been identified as the active ingredient of the Chinese medicine Danggui Longhui Wan, which has anti-leukemic activity (238). Other GSK-3 inhibitors have been developed and tested in a variety of pre-clinical studies (196,226); however, current hurdles for the use of such drugs in clinical practice include optimisation of drug delivery and avoidance of toxic systemic accumulation of the drug. In particular, LiCl has a narrow therapeutic window, inducing nephrotoxicity at concentrations greater than 1.5 mM *in vivo* (236). Although data within this chapter indicates significant anti-migratory and anti-invasive effects on paediatric glioma at concentrations as low as 5 mM, alternative methods of drug delivery such as convection-enhanced delivery or local delivery with polymers may be required to attain localised high concentrations of the drug in human brain tumours (236,366) and this

requires further evaluation *in vivo* with pre-clinical models. Alternatively, development of specific novel GSK-3 inhibitors capable of crossing the BBB at concentrations associated with clinically acceptable side effect profiles will help overcome this problem. Finally, due to a lack of available mouse models of paediatric glioma invasion, the anti-migratory effects of GSK-3 inhibitors on pHGG tumours *in vivo* have not been addressed. Studies of adult glioma have shown that GSK-3 inhibitors of the indirubin family are able to reduce invasion of glioma cells *in vivo* (246) and development of a paediatric orthotopic xenograft model of migration to test novel GSK-3 inhibitors forms a major part of ongoing studies in this area (see chapter 6).

In this study, multi-cellular spheroids were used to simulate a 3D tumour. Most spheroids beyond 500 μm in size consist of a necrotic core, surrounded by an outer rim (approximately 100-300 μm thick) of viable and proliferating cells (367). Quiescent, yet intact, viable cells may also be found surrounding the necrotic core (367). Use of this model is well established in cancer biology research and emulates the organisation of an *in vivo* tumour mass (367). The use of the 96 well low adhesion plate was an extremely efficient way of making spheroids that were uniform in size. This methodology was much superior to the hanging drop method of spheroid formation (350), which resulted in the formation of spheroids that were less uniform in size and that sometimes disaggregated on transfer from petri dish lids. This was one of the main disadvantages of the nanofibre scaffold assay, which relied upon spheroids being formed by hanging drops.

When spheroids are embedded in a hydrogel matrix, cells can invade into the matrix outward from the core representing a model of the process of tumour invasion (236,368). In this study, a collagen matrix was used. Although many different matrix material are commercially available, collagen was chosen as it is well established for use in this invasion assay (75,236,369) and intra-tumoural fibrillar collagens have been shown to be an integral part of the ECM in a subset of glioblastomas (370). Collagen is also seen around blood vessels and the pial surface in the brain (24,115). One of the drawbacks of this model of spheroid invasion was that it was sometimes

difficult to fully encase each spheroid within the collagen matrix. Spheroids that were not fully encased in collagen, obstructed from view by air bubbles or that had moved and encased at the periphery of a well, had to be discounted from analysis. Additionally, quantification of the migration index was time consuming and definition of different zones could potentially be fraught by inter-observer error. Future work aims to develop computer software to quantify the number of cells migrating into pre-defined zones, which will improve both accuracy and throughput for larger scale analysis (368).

Finally, working with the DIPG primary-derived cell line HSJD-DIPG-007 was a challenge. Initially the growth of four other DIPG cell lines that were gifted by Dr Angel M Carcaboso was attempted (HSJD-DIPG-008, HSJD-DIPG-011, HSJD-DIPG-012, HSJD-DIPG-013); however, these lines failed to culture in the laboratory. Although HSJD-DIPG-007 could be cultured, the cells sometimes failed to re-form neurospheres following passage and this unpredictability made it difficult to plan experiments, bulk up large numbers of cells and perform multiple repeats. Additionally, HSJD-DIPG-007 can be differentiated to a monolayer by removing growth factors from the medium and culturing the cells in TSM plus HI-FCS; however, this alters cell phenotype and, therefore, a direct comparison between HSJD-DIPG-007 grown as neurospheres and differentiated monolayers could not be made. In this thesis, all assays evaluating HSJD-DIPG-007 were therefore conducted on cells grown as neurospheres as this method of culture was felt to be more representative of the human disease.

To conclude, the migratory and invasive behaviour of paediatric glioma cell lines has been characterised using 2D and 3D models, uncovering differences in their pattern of migration, invasion, motility and morphology. For the first time, GSK-3 inhibitors such as LiCl and BIO have been demonstrated as novel candidates for migration and invasion inhibition in pHGG and DIPG and, as such, warrant further investigation as therapeutics for this challenging group of tumours.

Chapter 4: An investigation into the effects of oncolytic viruses on paediatric glioma migration and invasion

4.1 Introduction

OVs are anti-cancer agents that are capable of selectively infecting and lysing cancer cells, while leaving normal tissue unharmed (252,253). Alongside their ability to kill infected cancer cells, OVs can also generate an anti-cancer immune response, by enhancing the immunogenicity of the tumour microenvironment and activating innate and adaptive immune responses against infected tumour cells (253). Thus, OVs have huge clinical potential for poor prognosis tumours through their ability to act as selective cytotoxic and immunogenic agents.

However, very little is known about the effects of OVs on cancer cell invasion and migration. In order for a cell to move and migrate it needs to be able to alter its shape, a process made possible by the presence of the cell cytoskeleton (86). Given that the cell cytoskeleton also plays a critical role in regulating the life cycle of infecting viruses (308-311), OVs may be able to influence cancer cell migration through their interplay with the host cancer cell cytoskeleton. If OVs have the potential to inhibit cancer cell migration, they would be a highly sought after therapeutic option for poor prognosis invasive tumours such as pHGG and DIPG.

In this chapter, the hypothesis that OVs (HSV, reovirus and VV) are capable of specifically inhibiting the migration and invasion of pHGG and DIPG cells is tested using both 2D and 3D *in vitro* models. In addition, the effects of oncolytic HSV, reovirus and VV on pHGG and DIPG cell viability, proliferation and growth are evaluated. To the best of our knowledge, this is the first time that OVs have been evaluated as potential anti-migratory and anti-invasive treatments for pHGG and DIPG and this offers a highly innovative novel therapeutic approach for these devastating childhood diseases.

4.2 Evaluation of the effects of oncolytic viruses on pHGG migration in a 2D scratch assay

The ability of three OVs (HSV, reovirus and VV) to block the migration of two pHGG cell lines (SF188 and KNS42) and one mouse glioma cell line (GL261-Luc) using a scratch assay, was evaluated. In this model, a scratch was applied to a near confluent monolayer of cells to form a cell-free zone. Cells were then treated ± virus and the migration of cells across the scratch over 24 h was evaluated using cell imaging (Figure 17). Images were quantified using Image J software to evaluate the percentage change in the area of the scratch over 24 h. The mouse glioma cell line GL261-Luc was included in the *in vitro* analysis as this cell line was to be used in the development of an *in vivo* mouse model of glioma migration.

In all three cell lines investigated, oncolytic HSV was able to significantly reduce the migration of cells across the scratch (Figure 18A, 19A and 20A). A statistically significant reduction of migration was achieved by HSV at 1 and 10 pfu/cell for SF188 (Figure 18A) (mean±SEM: percentage change of the scratch from time 0 h: control 89.4±3.4 %, HSV 1 pfu/cell 69±9.7 % $p=0.038$, HSV 10 pfu/cell 19.2±1.3 % $p<0.001$), 10 pfu/cell HSV for KNS42 (Figure 19A) (mean±SEM: percentage change of the scratch from time 0 h: control 15.9±3 %, HSV 10 pfu/cell 0.41±0.66 % $p=0.025$) and 50 pfu/cell for GL261-Luc (Figure 20A) (mean±SEM: percentage change of the scratch from time 0 h: control 59.4±5.3 %, HSV 50 pfu/cell 5.7±1.1 % $p<0.001$).

Conversely, reovirus treatment did not significantly alter cell migration over 24 h in any of the cell lines (Figure 18B, 19B, 20B), and this was particularly evident for SF188 (Figure 18B) and GL261-Luc cells (Figure 20B), where the percentage change in the area of the scratch over 24 h remained almost identical for control and reovirus treatments at all virus concentrations.

VV treatment resulted in a statistically significant reduction of migration over 24 h for SF188 and GL261-Luc in a dose-dependent manner (Figure 18C and 20C) (mean±SEM: percentage change of the scratch from time 0 h

SF188: control 89.4±3.4 %, VV 0.1 pfu/cell 50±12.2 % p=0.0014, VV 1 pfu/cell 55.3±10.8 % p=0.0048, VV 10 53.4±7.6 % p=0.0031; percentage change of the scratch from time 0 h GL261-Luc: control 59.4±5.3 %, VV 1 pfu/cell 34.7±5.2 % p=0.0246, VV 10 pfu/cell 9±1.8 % p<0.001, VV 50 pfu/cell -2.8±5.5 % p<0.001). However, when examined microscopically, VV also appeared to be exerting cytotoxic effects in all three lines in a dose-dependent manner, with cells displaying apoptotic morphology - rounding up and reducing in size by 24 h. For KNS42 and GL261-Luc (Figure 19C and 20C), the average area of the scratch increased in size by 24 h following VV treatment (KNS42 at 0.01 pfu/cell and 10 pfu/cell, GL261-Luc at 50 pfu/cell), again potentially indicating a cytotoxic effect from the virus treatment.

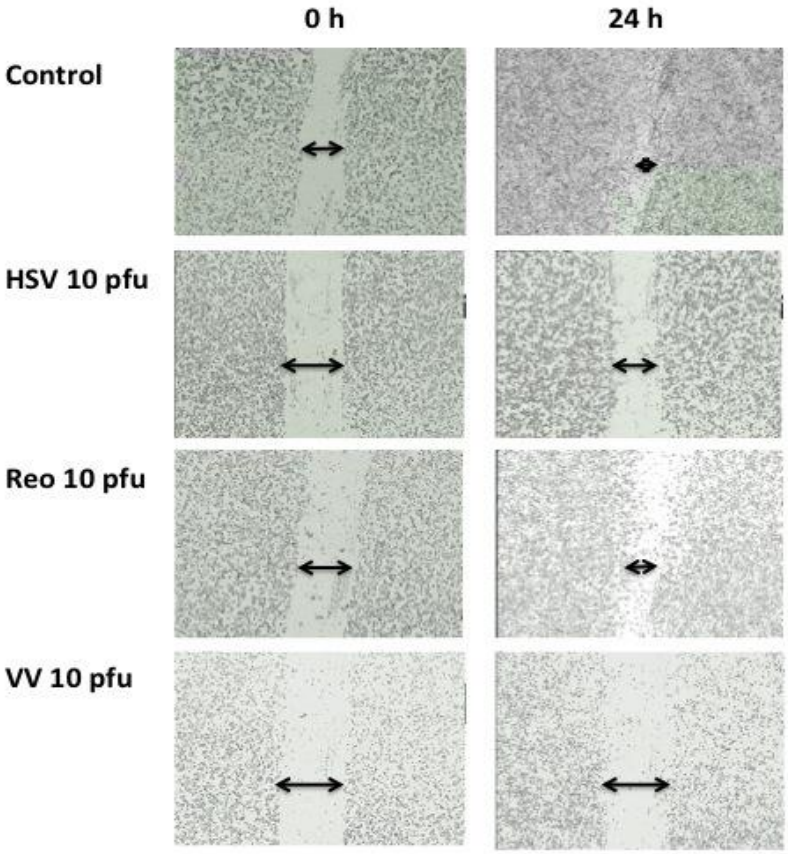

Figure 17: Illustrations of the effects of oncolytic viruses on pHGG migration over 24 h

SF188 were seeded into 24 well plates at $1x10^5$ cells/well. After 24 h, a scratch was applied across the monolayer and wells were treated ± each virus at 10 pfu/cell (HSV, reovirus (Reo) and VV). Plates were imaged at x4 magnification in the IncuCyte ZOOM® incubator. Images shown are representative stills from movies created with IncuCyte™ software at time 0 h- and 24 h-post treatment.

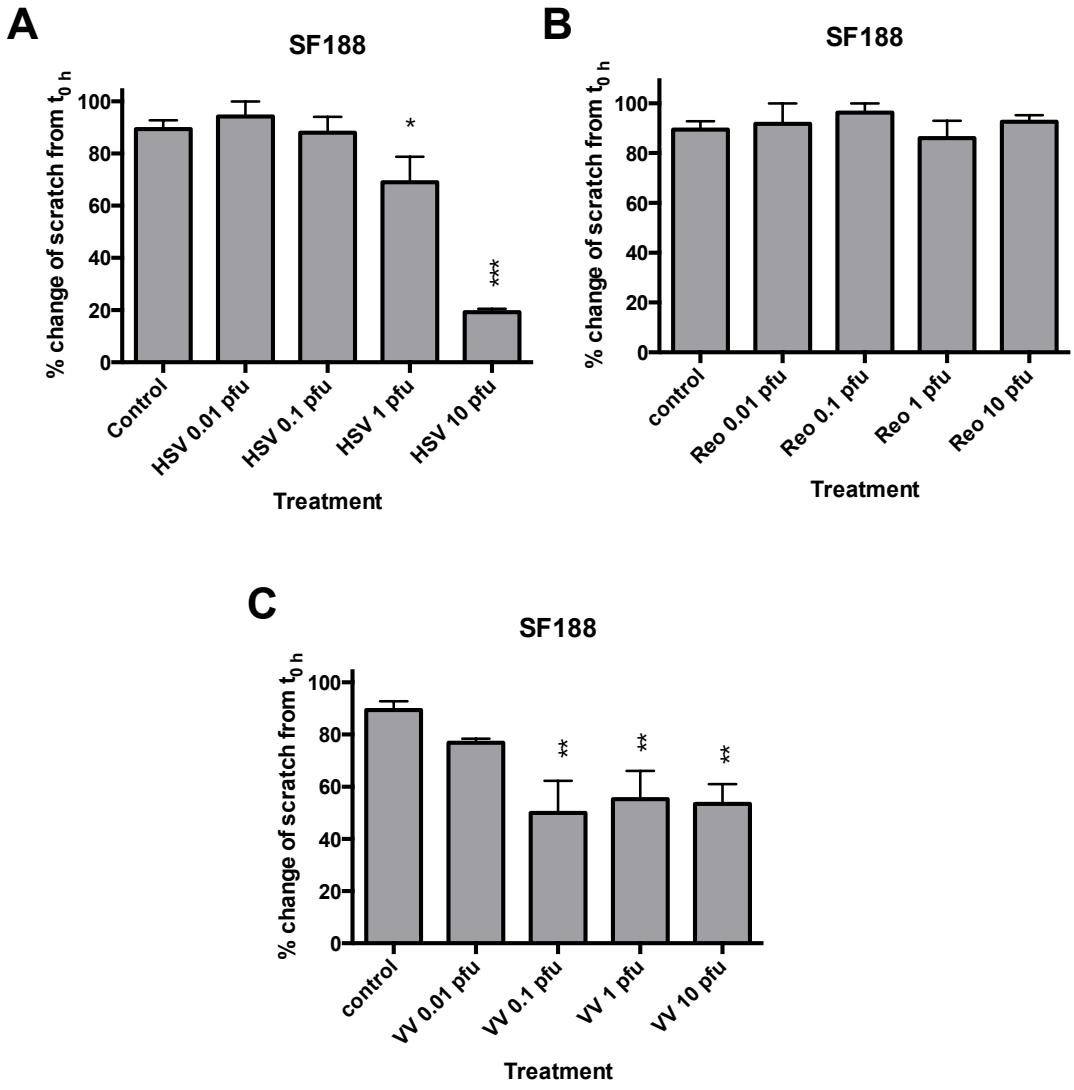

Figure 18: The effects of oncolytic viruses on SF188 migration over 24 h

SF188 were seeded into 24 well plates at $1x10^5$ cells/well. After 24 h, a scratch was applied across the monolayer and wells were treated ± each virus at 0.01, 0.1, 1 and 10 pfu/cell HSV **(A)**, reovirus (Reo) **(B)** or VV **(C)**. Plates were imaged at 0 h and 24 h using the EVOS cell imaging system at x4 magnification. Migration was quantified from images using Image J software to determine the percentage change in the area of the scratch over 24 h. Graphs show mean±SEM of n=3 individual experiments. *p<0.05, **p<0.01, ***p<0.001 by one-way ANOVA.

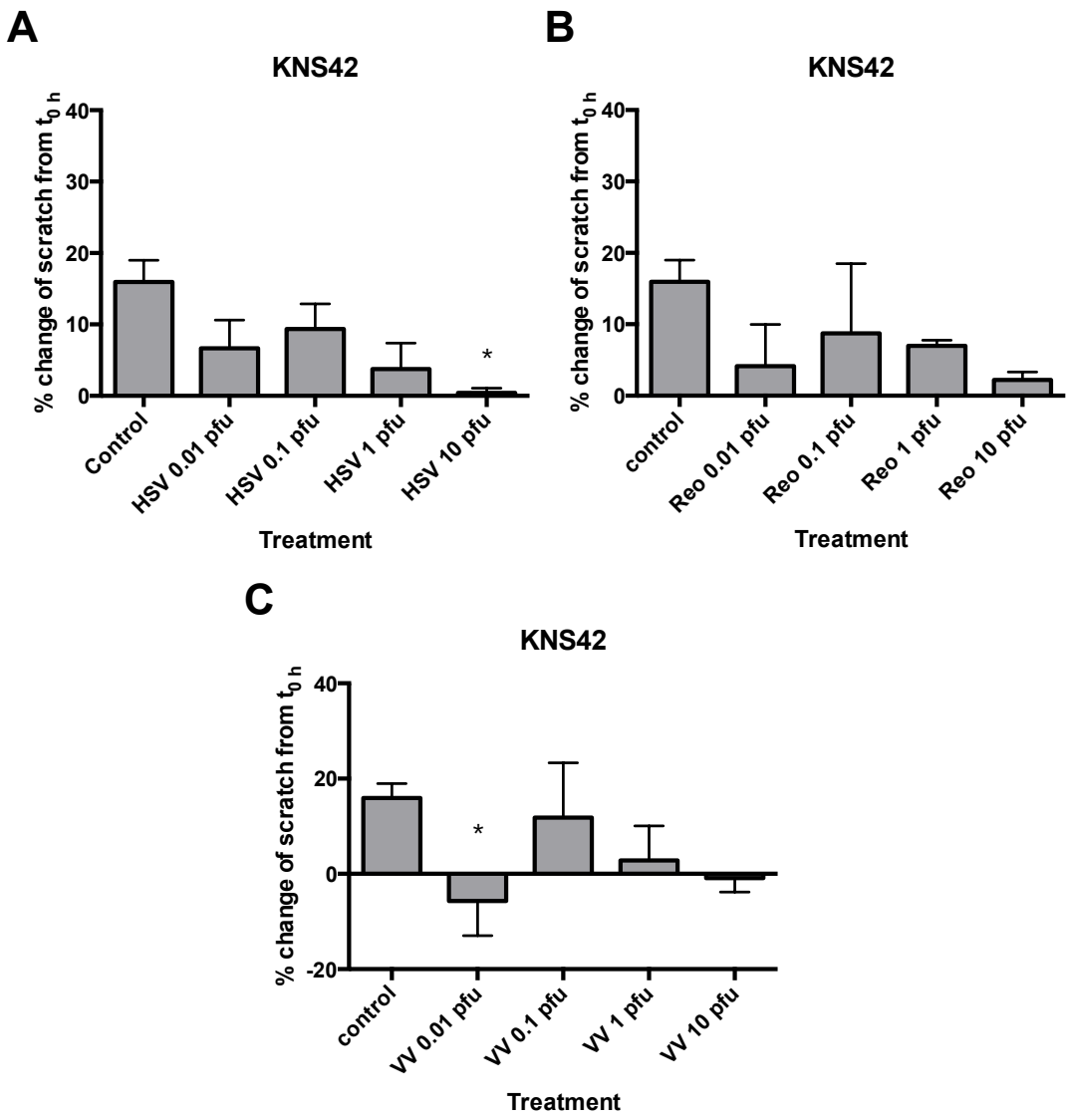

Figure 19: The effects of oncolytic viruses on KNS42 migration over 24 h

KNS42 were seeded into 24 well plates at $1x10^5$ cells/well. After 24 h, a scratch was applied across the monolayer and wells were treated ± each virus at 0.01, 0.1, 1 and 10 pfu/cell HSV **(A)**, reovirus (Reo) **(B)** or VV **(C)**. Plates were imaged at 0 h and 24 h using the EVOS cell imaging system at x4 magnification. Migration was quantified from images using Image J software to determine the percentage change in the area of the scratch over 24 h. Graphs show mean±SEM of n=3 individual experiments. *p<0.05, **p<0.01, ***p<0.001 by one-way ANOVA.

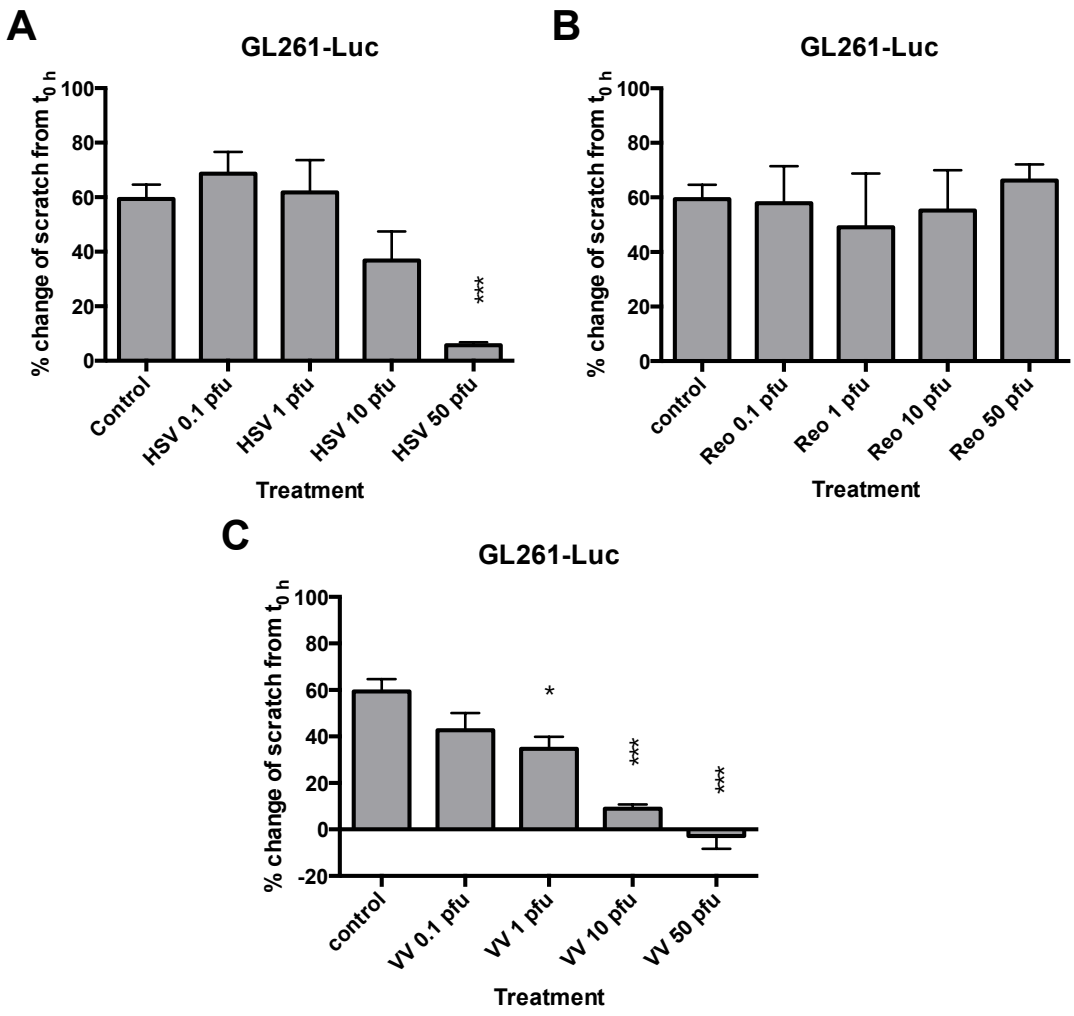

Figure 20: The effects of oncolytic viruses on GL261-Luc migration over 24 h

GL261-Luc were seeded into 24 well plates at $1x10^5$ cells/well. After 24 h, a scratch was applied across the monolayer and wells were treated ± each virus at 0.1, 1, 10 and 50 pfu/cell HSV **(A)**, reovirus (Reo) **(B)** or VV **(C)**. Plates were imaged at 0 h and 24 h using the EVOS cell imaging system at x4 magnification. Migration was quantified from images using Image J software to determine the percentage change in the area of the scratch over 24 h. Graphs show mean±SEM of n=3 individual experiments. *p<0.05, **p<0.01, ***p<0.001 by one-way ANOVA.

4.3 Evaluation of the effects of oncolytic viruses on paediatric glioma invasion

To investigate the effects of OVs on pHGG and DIPG invasion, the 3D tumour spheroid assay described previously was used (section 2.4.1 and 3.4). Tumour spheroids of each cell line (SF188, KNS42, HSJD-DIPG-007 and GL261-Luc) were encased in a collagen matrix and then overlaid with OV at varying concentration. Tumour spheroid invasion was imaged over 72 h using the EVOS cell imaging system (Figure 21).

In order to evaluate whether OV could penetrate the collagen matrix and then replicate within tumour spheroids, a GFP-expressing virus (HSV or VV) was imaged using the IncuCyte ZOOM® following co-culture with tumour spheroids encased in collagen. Within the first 24 h, the tumour spheroid began to emit green fluorescence, which increased in intensity by 70 h, indicating that the oncolytic HSV and VV were able to enter and replicate within the encased tumour spheroid (Figure 22). Reovirus entry and replication in tumour spheroids could not be evaluated by this method as the laboratory did not possess a GFP-modified virus.

The migration index was calculated for the images obtained from each virus condition (as described in section 2.4.1) and was used to evaluate the invasion front and leading edge zone for each treatment. Oncolytic HSV significantly reduced invasion of pHGG (SF188 and KNS42), DIPG (HSJD-DIPG-007) and mouse glioma (GL261-Luc) tumour spheroids by 72 h in a dose- and time-dependent manner (Figure 23A, 24A, 25A, 26A). A statistically significant reduction in both the invasion zone and leading edge zone at 72 h was observed following treatment with 10 pfu/cell HSV for SF188 and HSJD-DIPG-007 (mean±SEM: SF188 leading edge: control 0.94±0.004, HSV 10 pfu/cell 0.63±0.047 $p<0.001$; HSJD-DIPG-007 leading edge: control 0.75±0.051, HSV 10 pfu/cell 0.52±0.038 $p=0.0061$, HSV 50 pfu/cell 0.40±0.041 $p<0.001$) and by 1 pfu/cell HSV for KNS42 and GL261-Luc (mean±SEM: KNS42 leading edge: control 0.42±0.033, HSV 1 pfu/cell 0.23±0.029 $p=0.0014$, HSV 10 pfu/cell 0.20±0.05 $p<0.001$; GL261-Luc

leading edge: control 0.47±0.031, HSV 1 pfu/cell 0.28±0.035 p=0.0026, HSV 10 pfu/cell 0.18±0.044 p<0.001, HSV 50 pfu/cell 0.069±0.034 p<0.001).

Unlike the results obtained in the 2D scratch assay, reovirus was capable of significantly reducing the invasion of SF188, HSJD-DIPG-007 and GL261-Luc tumour spheroids in the 3D tumour spheroid model (Figure 23B, 25B, 26B). A statistically significant reduction in both invasion zone and leading edge zone was reached at 1 pfu/cell reovirus for SF188, HSJD-DIPG-007 and GL261-Luc (mean±SEM: SF188 leading edge: control 0.94±0.004, reovirus 1 pfu/cell 0.83±0.031 p=0.0012, reovirus 10 pfu/cell 0.67±0.040 p<0.001; HSJD-DIPG-007 leading edge: control 0.75±0.051, reovirus 1 pfu/cell 0.42±0.034 p<0.001, reovirus 10 pfu/cell 0.47±0.060 p<0.001, reovirus 50 pfu/cell 0.37±0.051 p<0.001; GL261-Luc leading edge: control 0.47±0.031, reovirus 1 pfu/cell 0.31±0.054 p=0.019, reovirus 10 pfu/cell 0.29±0.060 p=0.0075). The invasion of KNS42 tumour spheroids was not affected by reovirus treatment (Figure 24B).

Finally, VV treatment was capable of significantly reducing invasion in all four cell lines (Figure 23 C, 24C, 25C and 26C). A statistically significant reduction in both the invasion zone and leading edge zone was reached at 1 pfu/cell VV for SF188 and HSJD-DIPG-007 (mean±SEM: SF188 leading edge: control 0.94±0.004, VV 1 pfu/cell 0.9±0.007 p=0.0089, VV 10 pfu/cell 0.89±0.011 p=0.0045; HSJD-DIPG-007 leading edge: control 0.75±0.051, VV 1 pfu/cell 0.53±0.053 p=0.0105, VV 10 pfu/cell 0.51±0.037 p=0.0053, VV 50 pfu/cell 0.43±0.063 p<0.001) and 0.1 pfu/cell VV for KNS42 and GL261-Luc (mean±SEM: KNS42 leading edge: control 0.42±0.033, VV 0.1 pfu/cell 0.29±0.034 p=0.037, VV 1 pfu/cell 0.23±0.042 p<0.001, VV 10 pfu/cell 0.072±0.028 p<0.001; GL261-Luc leading edge: control 0.47±0.031, VV 0.1 pfu/cell 0.31±0.046 p=0.012, VV 1 pfu/cell 0.28±0.073 p=0.017, VV 10 pfu/cell 0.27±0.03 p<0.001).

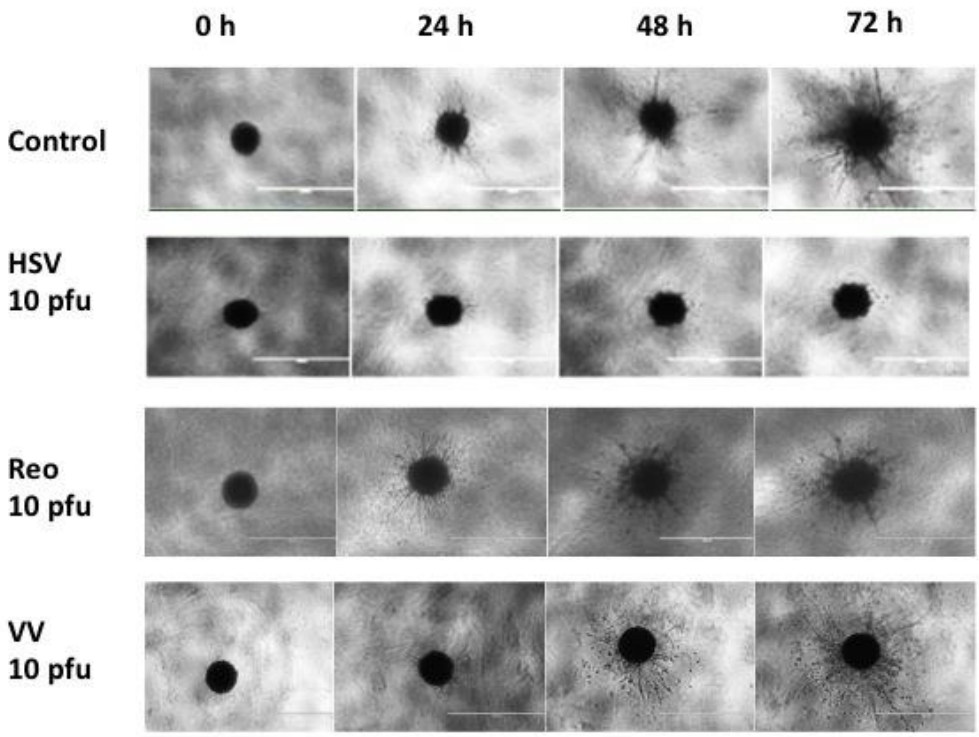

Figure 21: Inhibition of paediatric glioma tumour spheroid invasion by oncolytic viruses

Tumour spheroids (SF188) were encased in collagen and incubated ± nominal 10 pfu/cell of OV (HSV, reovirus (Reo) and VV) for 72 h. Tumour spheroid invasion was evaluated at 24, 48 and 72 h using the EVOS cell imaging system at x4 magnification. White scale bar represents 1000 μm. Images shown are representative of n=3 individual experiments.

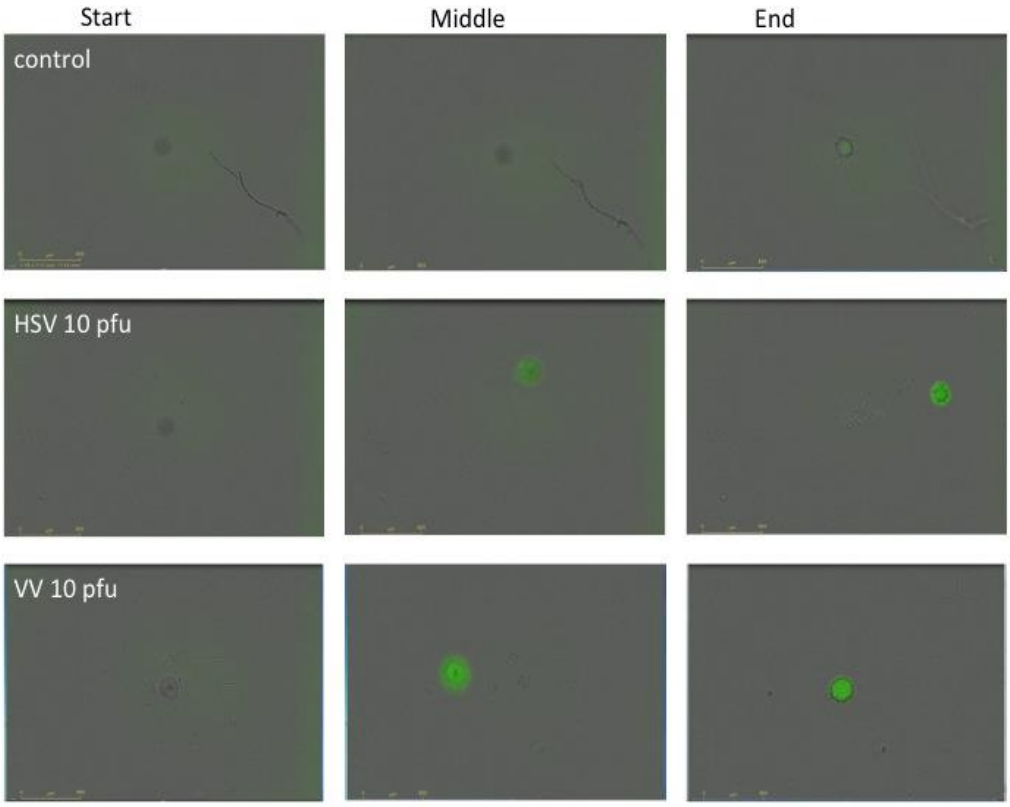

Figure 22: Oncolytic viruses can enter and replicate in pHGG tumour spheroids embedded in a collagen matrix
Tumour spheroids (SF188) were encased in collagen and incubated ± nominal 10 pfu/cell of oncolytic HSV or VV expressing GFP. Plates were imaged at x4 magnification using the IncuCyte ZOOM® incubator over 70 h. Images shown are representative stills from movies created with IncuCyte™ software which have been taken around the start, midway and end of the 70 h time period post-treatment. Yellow scale bar represents 800 µm.

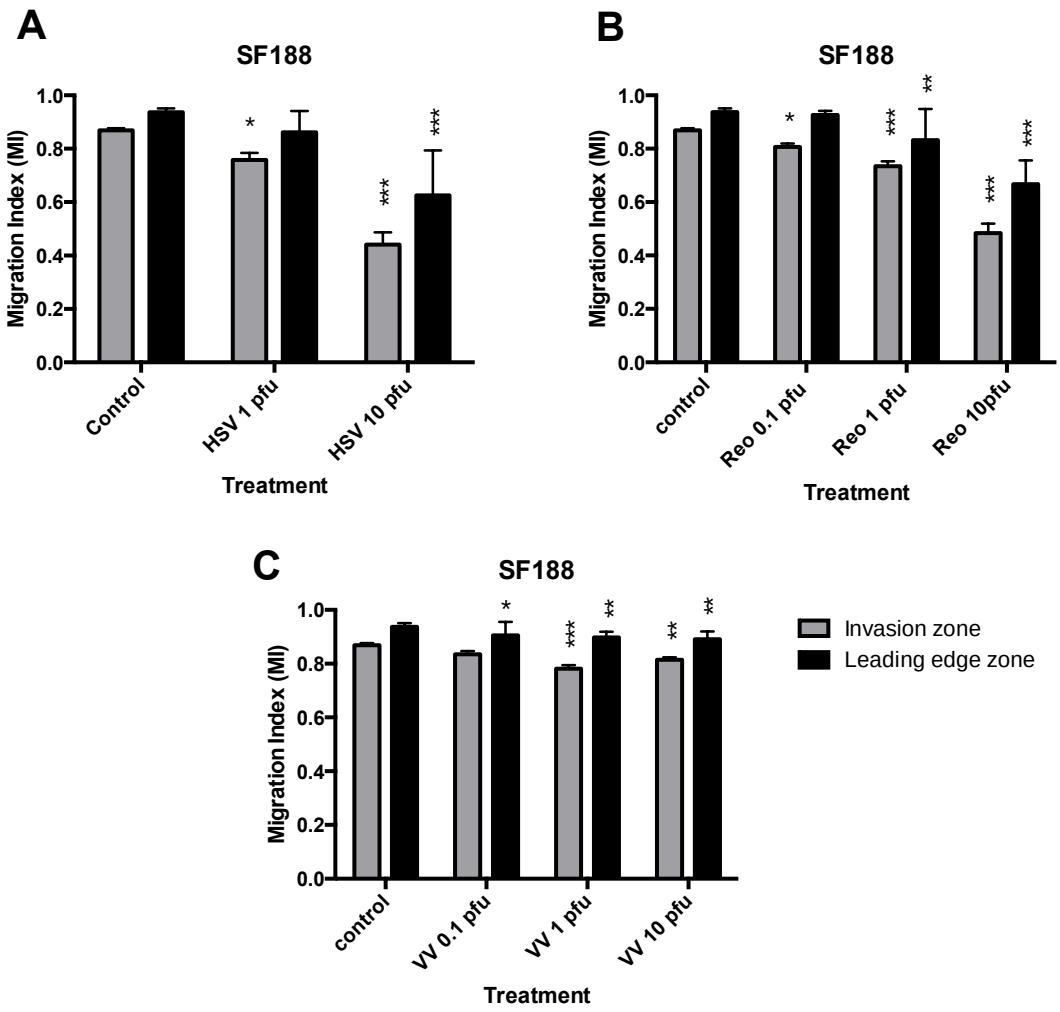

Figure 23: Analysis of the effects of oncolytic viruses on the migration index of tumour spheroids of SF188

Tumour spheroids (SF188) were encased in collagen and incubated in culture medium ± OV (HSV at nominal 1 and 10 pfu/cell **(A)**, reovirus (Reo) **(B)** and VV **(C)** at nominal 0.1, 1 and 10 pfu/cell). Invasion was evaluated at 72 h using the EVOS cell imaging system. Images generated were analysed using Image J software by calculating the area of the invasion zone and the leading edge zone (as defined in section 2.4.1). A migration index for both the invasion zone and leading edge zone ((area of zone – area of core) ÷ total area) was calculated. Graphs show mean±SEM of multiple repeats pooled from up to n=3 individual experiments. * $p<0.05$, ** $p<0.01$, *** $p<0.001$ by one-way ANOVA.

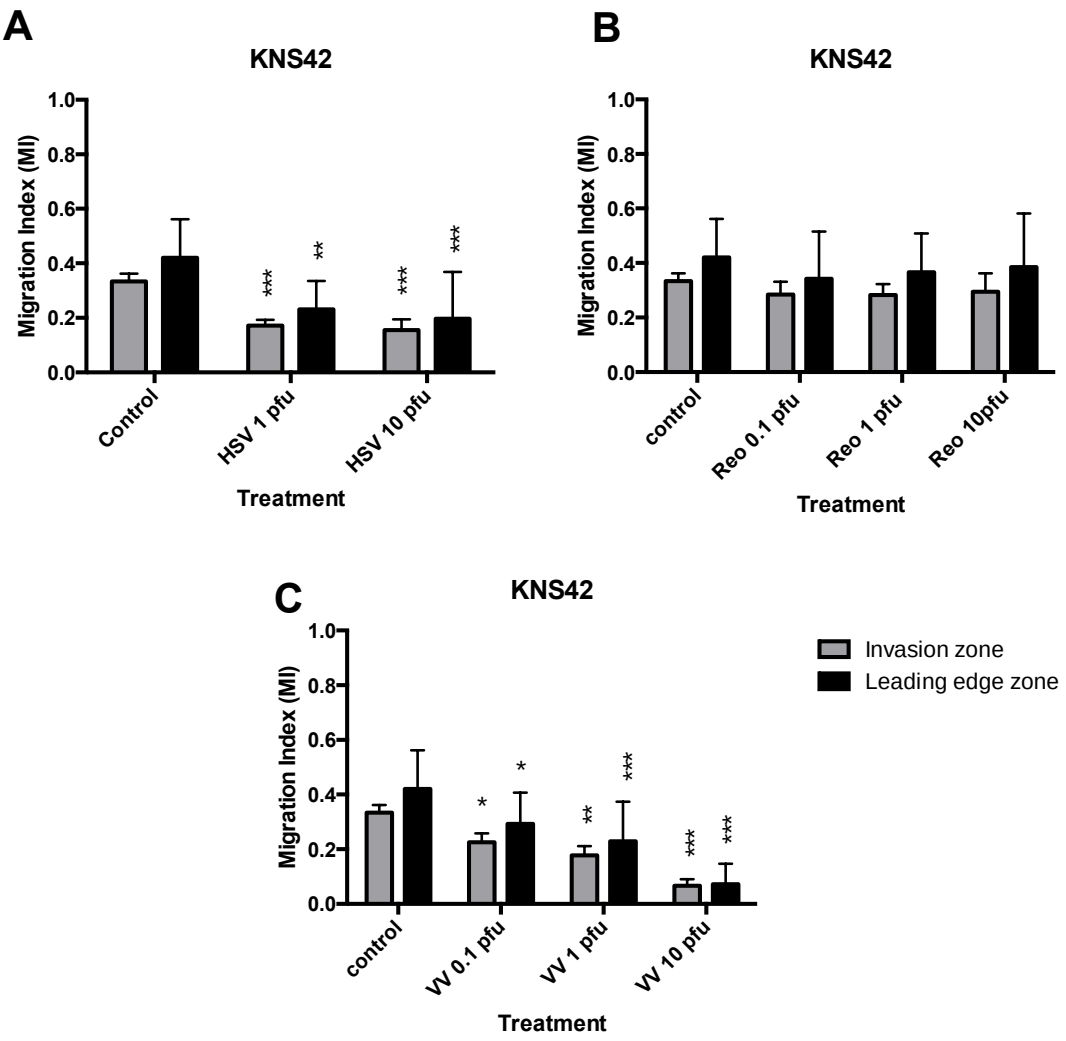

Figure 24: Analysis of the effects of oncolytic viruses on the migration index of tumour spheroids of KNS42

Tumour spheroids (KNS42) were encased in collagen and incubated in culture medium ± OV (HSV at nominal 1 and 10 pfu/cell) **(A)**, reovirus (Reo) **(B)** and VV **(C)** at nominal 0.1, 1 and 10 pfu/cell). Invasion was evaluated at 72 h using the EVOS cell imaging system. Images generated were analysed using Image J software by calculating the area of the invasion zone and the leading edge zone (as defined in section 2.4.1). A migration index for both the invasion zone and leading edge zone ((area of zone – area of core) ÷ total area) was calculated. Graphs show mean±SEM of multiple repeats pooled from up to n=3 individual experiments. * $p<0.05$, ** $p<0.01$, *** $p<0.001$ by one-way ANOVA.

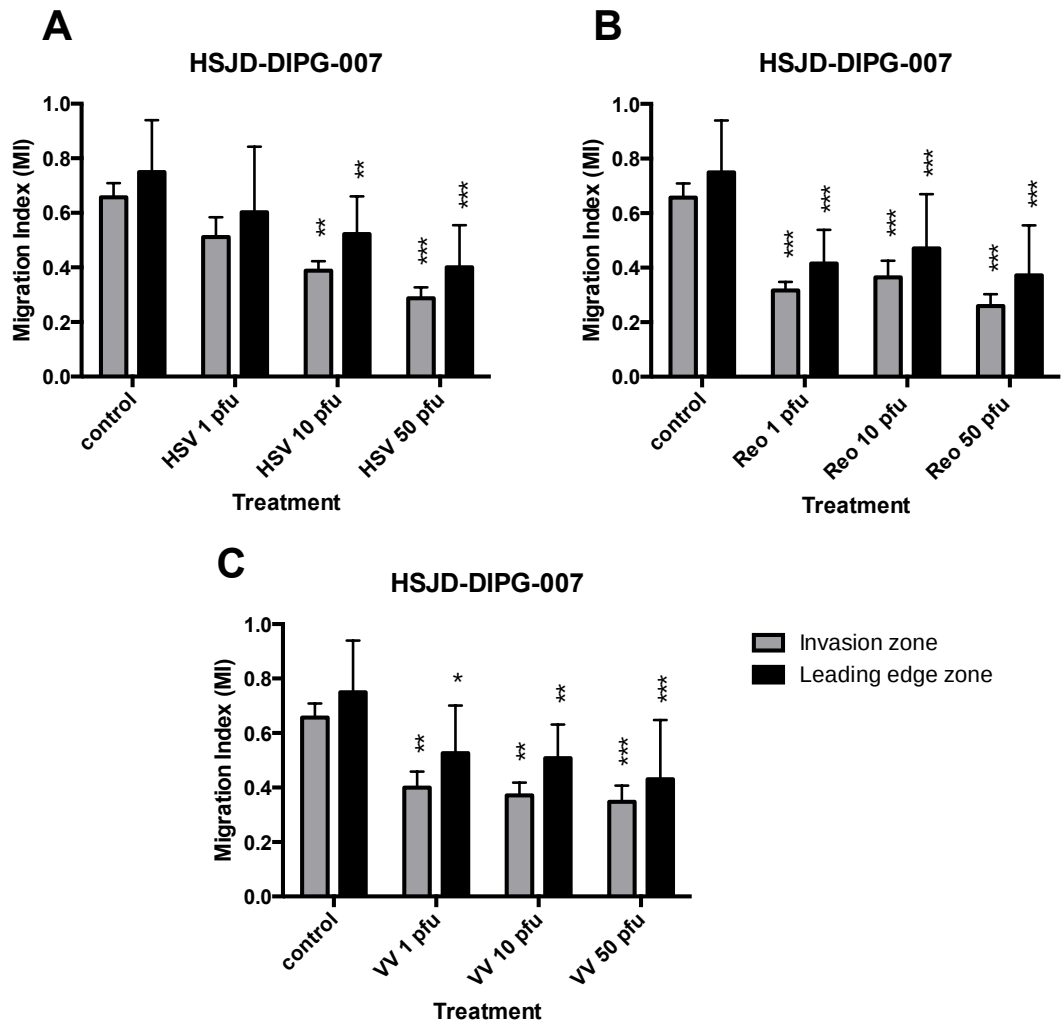

Figure 25: Analysis of the effects of oncolytic viruses on the migration index of tumour spheroids of HSJD-DIPG-007

Tumour spheroids (HSJD-DIPG-007) were encased in collagen and incubated in culture medium ± OV (HSV **(A)**, reovirus (Reo) **(B)** or VV **(C)** at nominal 1,10 and 50 pfu/cell). Invasion was evaluated at 72 h using the EVOS cell imaging system. Images generated were analysed using Image J software by calculating the area of the invasion zone and the leading edge zone (as defined in section 2.4.1). A migration index for both the invasion zone and leading edge zone ((area of zone – area of core) ÷ total area) was calculated. Graphs show mean±SEM of multiple repeats pooled from up to n=3 individual experiments. *p<0.05, ** p<0.01, *** p<0.001 by one-way ANOVA.

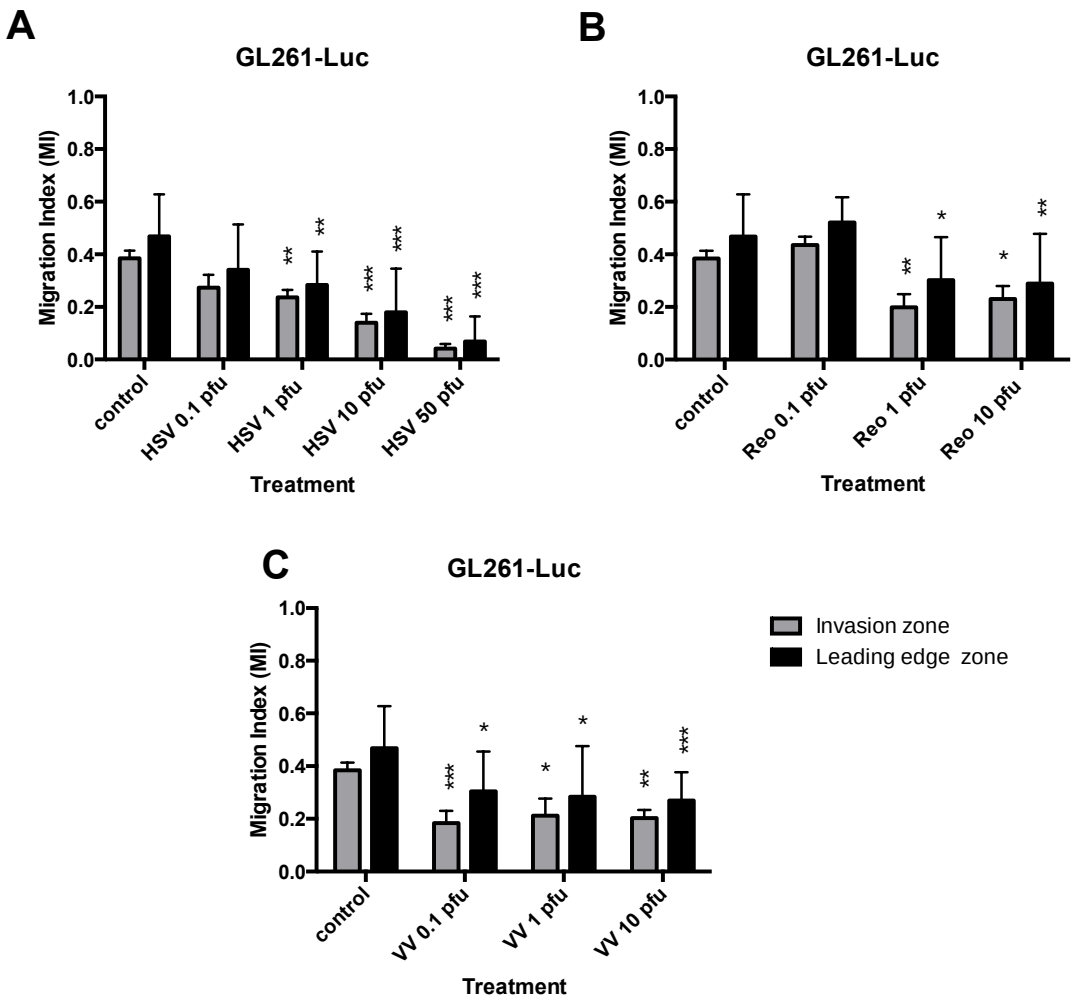

Figure 26: Analysis of the effects of oncolytic viruses on the migration index of tumour spheroids of mouse glioma

Tumour spheroids (GL261-Luc) were encased in collagen and incubated in culture medium ± OV (HSV at nominal 0.1, 1, 10 and 50 pfu/cell **(A)**, 0.1, 1 and 10 pfu/cell reovirus (Reo) **(B)** and 0.1, 1 and 10 pfu/cell VV **(C)**. Invasion was evaluated at 72 h using the EVOS cell imaging system. Images generated were analysed using Image J software by calculating the area of the invasion zone and the leading edge zone (as defined in section 2.4.1). A migration index for both the invasion zone and leading edge zone ((area of zone – area of core) ÷ total area) was calculated. Graphs show mean±SEM of multiple repeats pooled from up to n=3 individual experiments. * $p<0.05$, ** $p<0.01$, *** $p<0.001$ by one-way ANOVA.

4.4 Effects of oncolytic viruses on pHGG monolayer viability

The results described in section 4.2 and 4.3 indicate that OVs are capable of reducing the migration and invasion of pHGG and DIPG cells in 2D and 3D assays. However, to verify that the effects observed were anti-migratory and anti-invasive and not a direct consequence of cytotoxicity, the effects of OVs on pHGG and DIPG cytotoxicity and viability were also investigated.

The effects of OV (HSV, reovirus and VV) on pHGG monolayer cytotoxicity and viability were evaluated. A LIVE/DEAD® assay was used as a measure of cytotoxicity. In this assay, ethidium homodimer is taken up by dead cells with damaged plasma membranes to produce a bright fluorescence upon binding with nucleic acid, which can be quantified by FACS analysis (371). Using this assay, monolayers of SF188 appeared to be the most sensitive cell line to OV-mediated cytotoxicity (Figure 27, 28 and 29). At 24 h, which corresponds to the time point where migration was analysed by scratch assay in monolayers, HSV and reovirus exerted no significant cytotoxic effects in any of the three cell lines (SF188, KNS42 and GL261-Luc). Less than 8.1 % dead cells were detected following any HSV or reovirus treatment (Figure 27, 28 and 29). This result indicates that the effects of oncolytic HSV and reovirus on cytotoxicity at 24 h can clearly be distinguished from their effects on migration demonstrated in the scratch assay.

Over time (96 h), significant cytotoxic effects began to be observed following SF188 treatment with HSV and reovirus. SF188 was much more sensitive to the cytotoxic effects of reovirus than HSV. By 72 h and 96 h, respectively, 10 pfu/cell reovirus treatment of SF188 resulted in 68.3 % and 81 % dead cells, compared to only 16.8 % and 31.3 % following SF188 treatment by 10 pfu/cell HSV (Figure 27). KNS42 appeared to be completely resistant to the cytotoxic effects of reovirus (Figure 28B). Additionally, KNS42 demonstrated no significant cytotoxicity over 72 h of HSV treatment; however, a very small but statistically significant increase in cytotoxicity was reported at 96 h (5.3 % dead cells $p<0.001$) (Figure 28A). GL261-Luc appeared to be completely resistant to the effects of HSV and reovirus treatment over 96 h (Figure 29).

VV was notably more cytotoxic to the monolayers of all three cell lines, with significant cytotoxic effects noted by 24 h following treatment of KNS42 and GL261-Luc with 10 pfu/cell (Figure 27, 28 and 29) (KNS42: 24 % dead cells $p=0.0046$, GL261-Luc: 45 % dead cells $p=0.0092$). By 48 h, 10 pfu/cell VV treatment resulted in significant cytotoxicity in all three cell lines (SF188: 37 % dead cells $p<0.001$, KNS42: 29 % dead cells $p=0.0013$, GL261-Luc: 69 % dead cells $p<0.001$). This matched the observations made with the Nikon eclipse microscope following 24 h of VV treatment, where the cells were noted to display apoptotic morphology (rounding, blebbing and reduction in size) and lifted away from the scratch.

The effect of OVs on cell viability of SF188 and KNS42 monolayers was also determined by MTT assay (Figure 30 and 31). Both cell lines demonstrated significant changes in viability/metabolic activity in response to HSV at all viral concentrations tested (Figure 30A and 31A). SF188 was very sensitive to the effects of reovirus and demonstrated a marked and significant change in viability in a dose- and time-dependent manner (Figure 30B). Again, KNS42 was resistant to the effects of reovirus and demonstrated no change in metabolic activity over time (Figure 31B). Both cell lines demonstrated changes in metabolic activity over time when treated with VV; however, this did not reach statistical significance for KNS42 (Figure 30C and 31C). Significant changes in viability were seen for SF188 following VV treatment in both a dose- and time-dependent manner (Figure 30C).

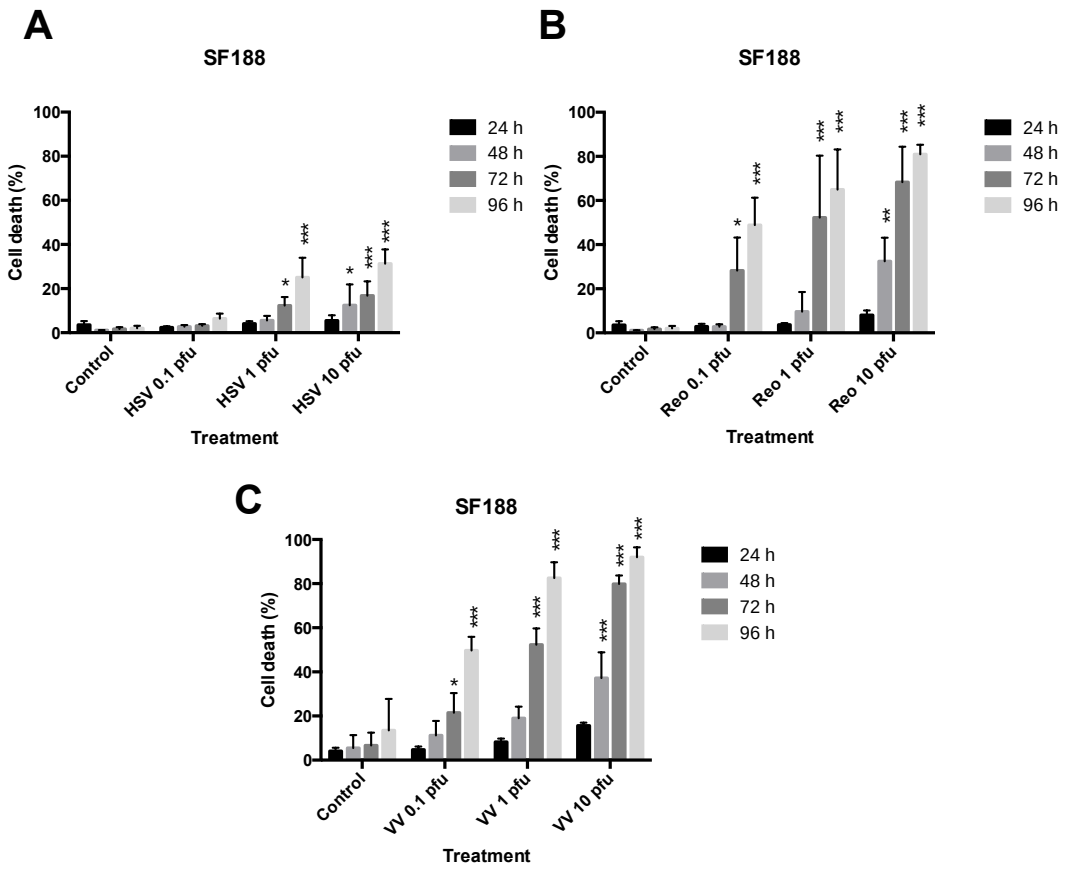

Figure 27: Effects of oncolytic viruses on SF188 monolayer cell viability

Cells (SF188) were seeded at $1x10^5$ cells/well in a 12 well plate and allowed to attach for 4 h. Cells were then incubated ± 0.1, 1 or 10 pfu/cell OV (HSV **(A)**, reovirus (Reo) **(B)** or VV **(C)**). At 24, 48, 72 or 96 h all cells were harvested, washed and incubated with LIVE/DEAD® cell stain (red for HSV/reovirus-treated cells, yellow for VV-treated cells). Cells were then fixed in 1 % PFA and the percentage of dead stained cells was determined by FACS analysis. Graphs show mean±SEM of n=3 individual experiments. * $p<0.05$, ** $p<0.01$, *** $p<0.001$ by two-way ANOVA.

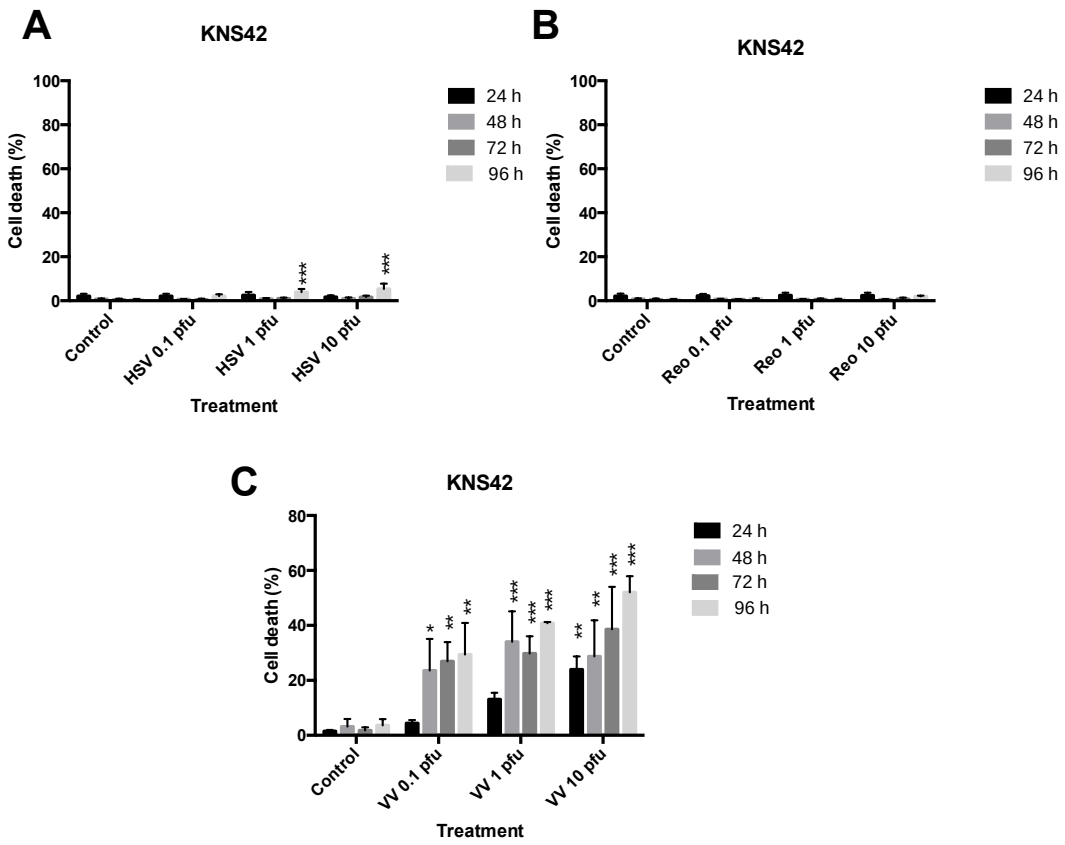

Figure 28: Effects of oncolytic viruses on KNS42 monolayer cell viability

Cells (KNS42) were seeded at $1x10^5$ cells/well in a 12 well plate and left for 4 h to adhere. Cells were then incubated ± 0.1, 1 or 10 pfu/cell OV (HSV **(A)**, reovirus (Reo) **(B)** or VV **(C)**). At 24, 48, 72 or 96 h all cells were harvested, washed and incubated with LIVE/DEAD® cell stain (red for HSV/reovirus-treated cells, yellow for VV-treated cells). Cells were then fixed in 1 % PFA and the percentage of dead stained cells was determined by FACS analysis. Graphs show mean±SEM of n=3 individual experiments. * $p<0.05$, ** $p<0.01$, *** $p<0.001$ by two-way ANOVA.

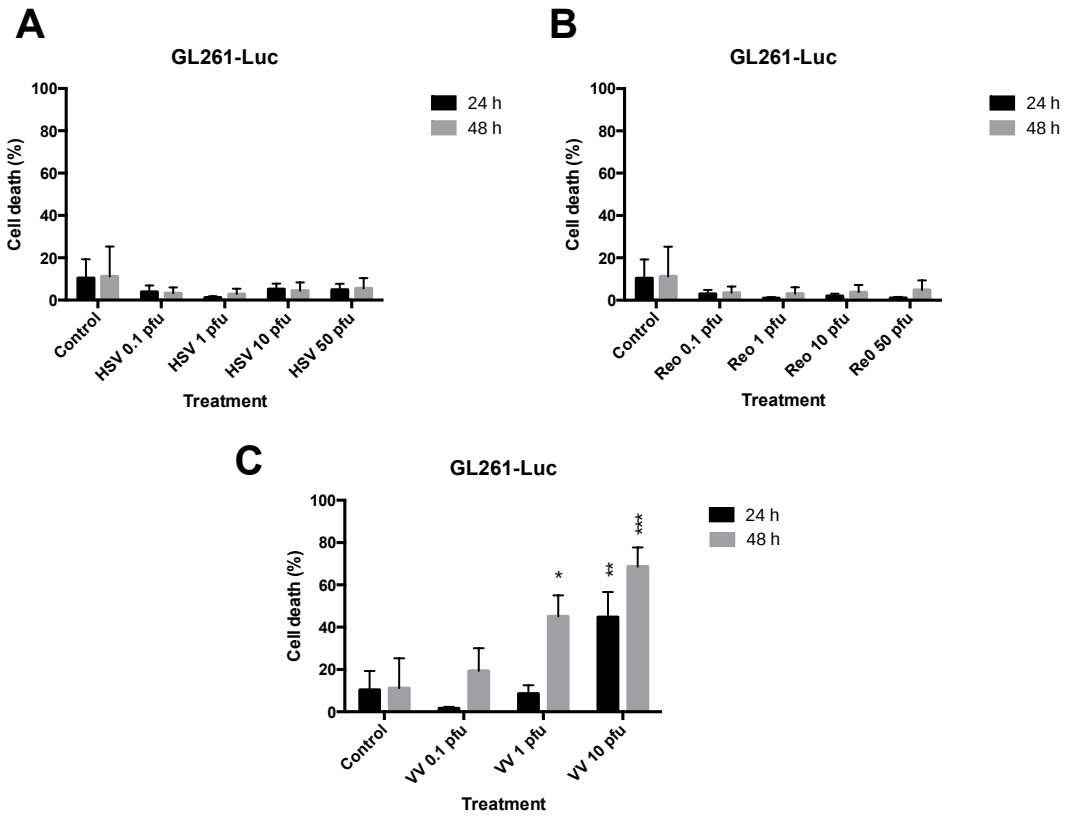

Figure 29: Effects of oncolytic viruses on GL261-Luc monolayer cell viability

Cells (GL261-Luc) were seeded at $1x10^5$ cells/well in a 12 well plate and left for 4 h to adhere. Cells were then incubated ± 0.1, 1, 10 or 50 pfu/cell OV (HSV **(A)**, reovirus (Reo) **(B)** or VV **(C)**). At 24 and 48 h all cells were harvested, washed and incubated with LIVE/DEAD® cell stain (red for HSV/reovirus-treated cells, yellow for VV-treated cells). Cells were then fixed in 1 % PFA and the percentage of dead stained cells was determined by FACS analysis. Graphs show mean±SEM of n=3 individual experiments.
* $p<0.05$, ** $p<0.01$, *** $p<0.001$ by two-way ANOVA.

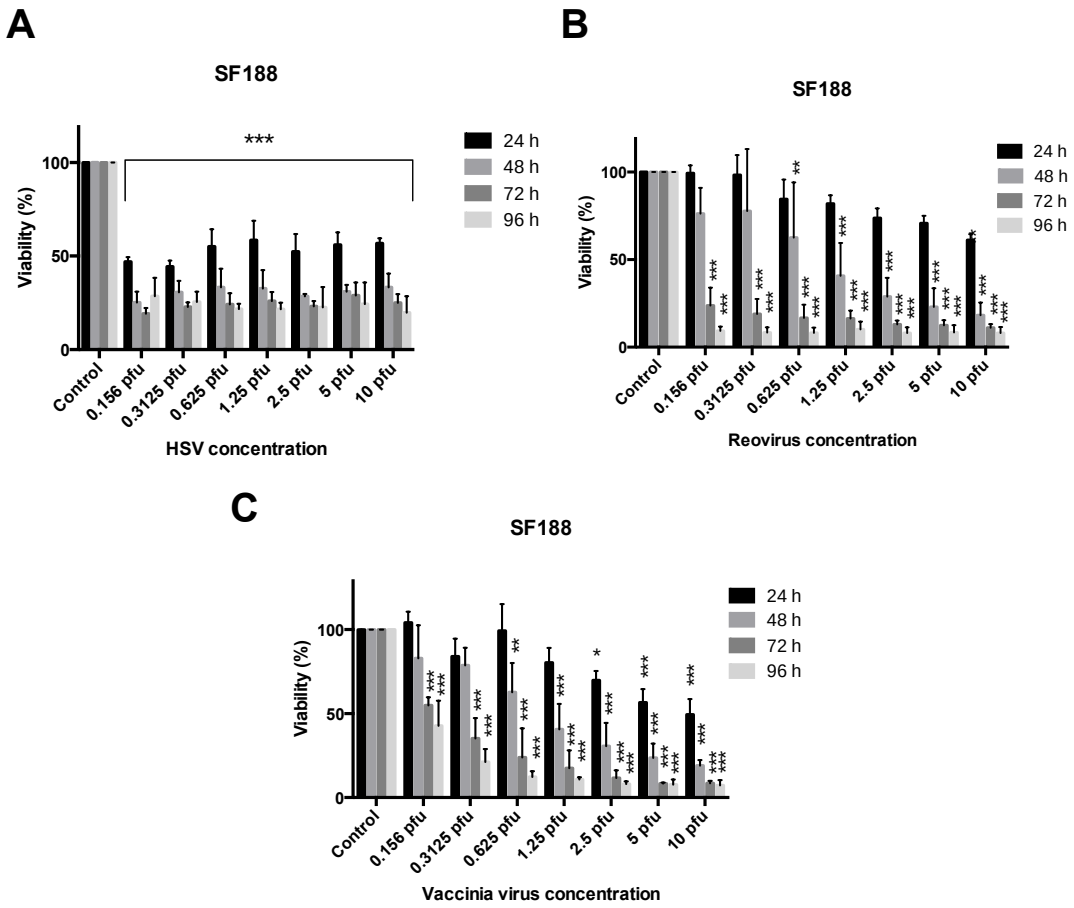

Figure 30: Cell viability of SF188 monolayers treated with oncolytic viruses

SF188 cells were seeded in triplicate in a 96 well plate at 8 x 10^3 cells/well and allowed to adhere for a minimum of 4 h. Serial dilutions of OVs (HSV **(A),** reovirus **(B)** and VV **(C)**) were added to each well. Cell viability was determined by MTT assay and was expressed as a percentage of controls. Graphs show mean±SEM of n=3 individual experiments. * $p<0.05$, ** $p<0.01$, *** $p<0.001$ by two-way ANOVA.

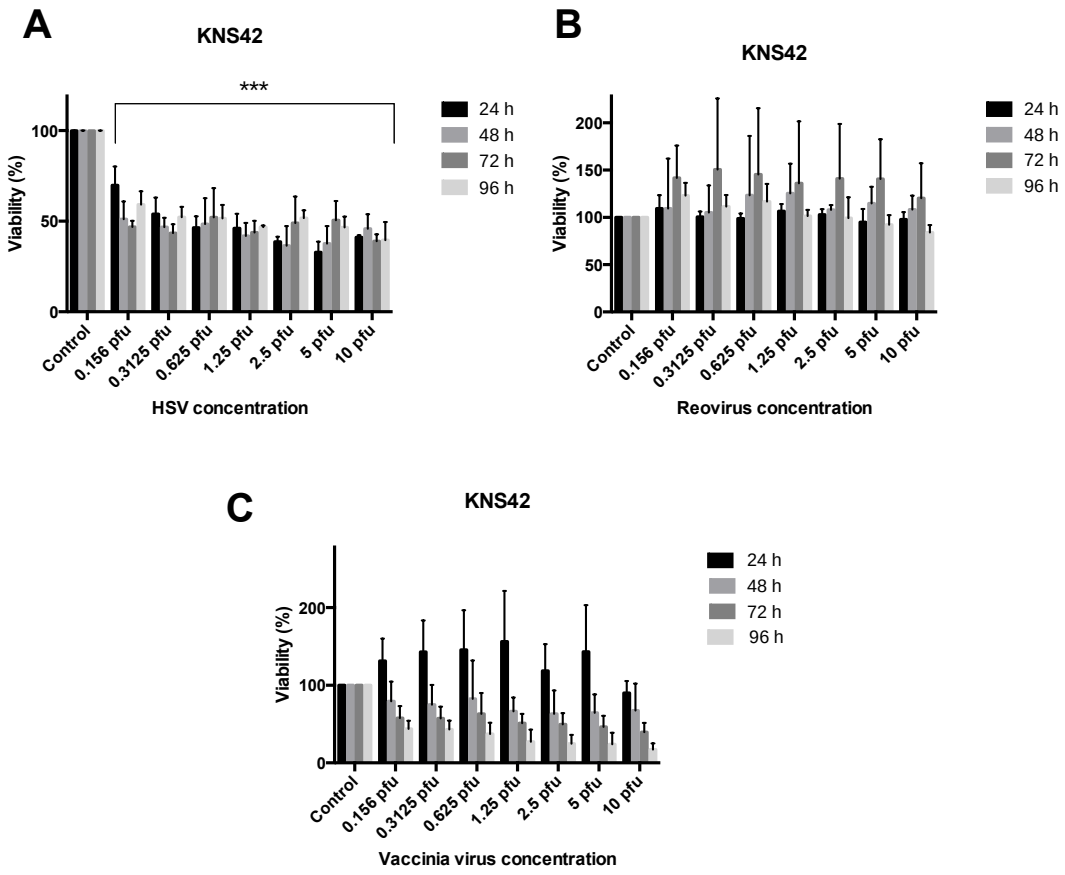

Figure 31: Cell viability of KNS42 monolayers treated with oncolytic viruses

KNS42 cells were seeded in triplicate in a 96 well plate at 8 x 10^3 cells/well and allowed to adhere for a minimum of 4 h. Serial dilutions of the OVs (HSV **(A),** reovirus **(B)** and VV **(C)**) were added to each well. Cell viability was determined by MTT assay and was expressed as a percentage of controls. Graphs show mean±SEM of n=3 individual experiments. * $p<0.05$, ** $p<0.01$, *** $p<0.001$ by two-way ANOVA.

4.5 Effects of oncolytic viruses on paediatric glioma tumour spheroid viability

Next, the effects of the OVs on tumour spheroid viability were investigated using the WST-1 assay. This assay has previously been described as a valid methodology to determine the viability of cells grown as spheroids (355). Cytotoxicity of tumour spheroids could not be accurately evaluated by LIVE/DEAD® assay as this assay requires a single cell suspension, so an estimation of viability by WST-1 assay was used as a proxy measurement. The viability of tumour spheroids was evaluated at 72 h to correlate with the anti-invasive results of the spheroid in collagen assay.

In the 3D spheroid system, both pHGG cell lines (SF188 and KNS42) displayed viability of at least 67 % at 72 h following all treatments with HSV (SF188: 82.2 % viability at 72 h following 10 pfu/cell HSV $p<0.001$; KNS42: 67.9 % viability at 72 h following 10 pfu/cell HSV $p<0.001$) (Figure 32A and 33A). Both cell lines also displayed viability of at least 68 % at 72 h following all reovirus treatment (SF188: 76.3 % viability at 72 h following 10 pfu/cell reovirus $p<0.001$; KNS42: 77 % viability at 72 h following 10 pfu/cell reovirus $p=0.043$) (Figure 32B and 33B). KNS42 was slightly more sensitive to the effects of VV than SF188, with viability reduced to 60.4 % at 72 h compared to 79.1 % at 72 h for SF188 following treatment with 10 pfu/cell (Figure 32C and 33C). Although evaluated using different assays of viability and cytotoxicity, overall, both pHGG cell lines exhibited increased sensitivity to virus treatment when cultured as monolayers compared to 3D aggregates. This is unsurprising, as 3D aggregates of tumor cells have been shown to be more drug-resistant than corresponding 2D cultures (356,357).

Figure 34 assesses the viability of HSJD-DIPG-007 spheroids treated with HSV, reovirus or VV. The data within this figure represents the average of two individual experiments and therefore statistical analysis could not be performed. HSJD-DIPG-007 spheroids demonstrated a tendency to be more sensitive to treatment with VV, compared to HSV and reovirus treatments (Figure 34). HSJD-DIPG-007 responded to treatment with HSV in a dose- and time-dependent manner, displaying viability at 72 h of 63.4 % following

10 pfu/cell HSV treatment and 53.1 % following 50 pfu/cell treatment (Figure 34A). HSJD-DIPG-007 demonstrated a tendancy to be least sensitive to reovirus-induced cytotoxicity, with viability of at least 70 % following treatment with reovirus at 0.1, 1 and 10 pfu/cell at 72 h (Figure 34B). Finally, VV treatment at 10 and 50 pfu/cell resulted in an overall trend towards reduced HSJD-DIPG-007 viability, with viability reducing to approximately 45 % following 72 h treatment (Figure 34C).

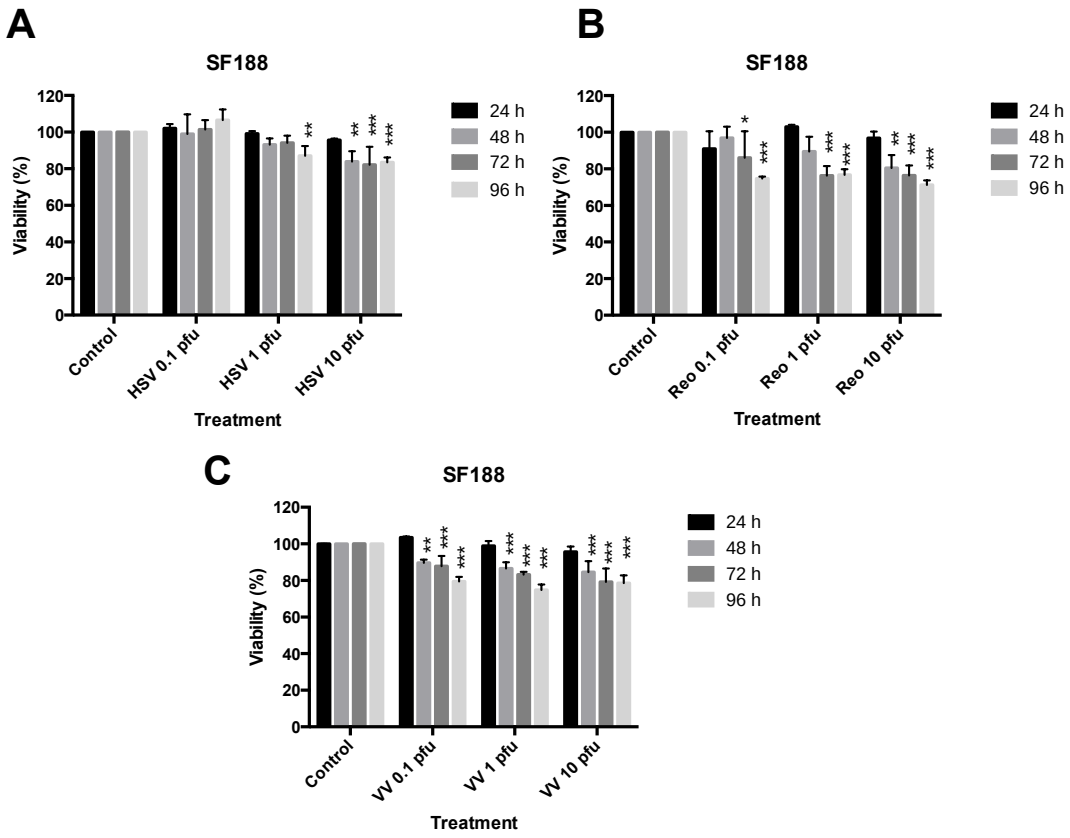

Figure 32: The effects of oncolytic viruses on SF188 tumour spheroid viability

SF188 cells at $1x10^3$ cells per well were seeded in an ultra-low attachment round-bottom 96 well plate to form spheroid aggregates. Following 72 h incubation, cells were incubated ± OV (HSV **(A)**, reovirus (Reo) **(B)** and VV **(C)**), at nominal 0.1, 1 and 10 pfu/cell. Cell viability at 24, 48, 72 and 96 h was determined by WST-1 assay and was expressed as a percentage of controls. Graphs show mean±SEM of n=3 individual experiments. * $p<0.05$, ** $p<0.01$, *** $p<0.001$ by two-way ANOVA.

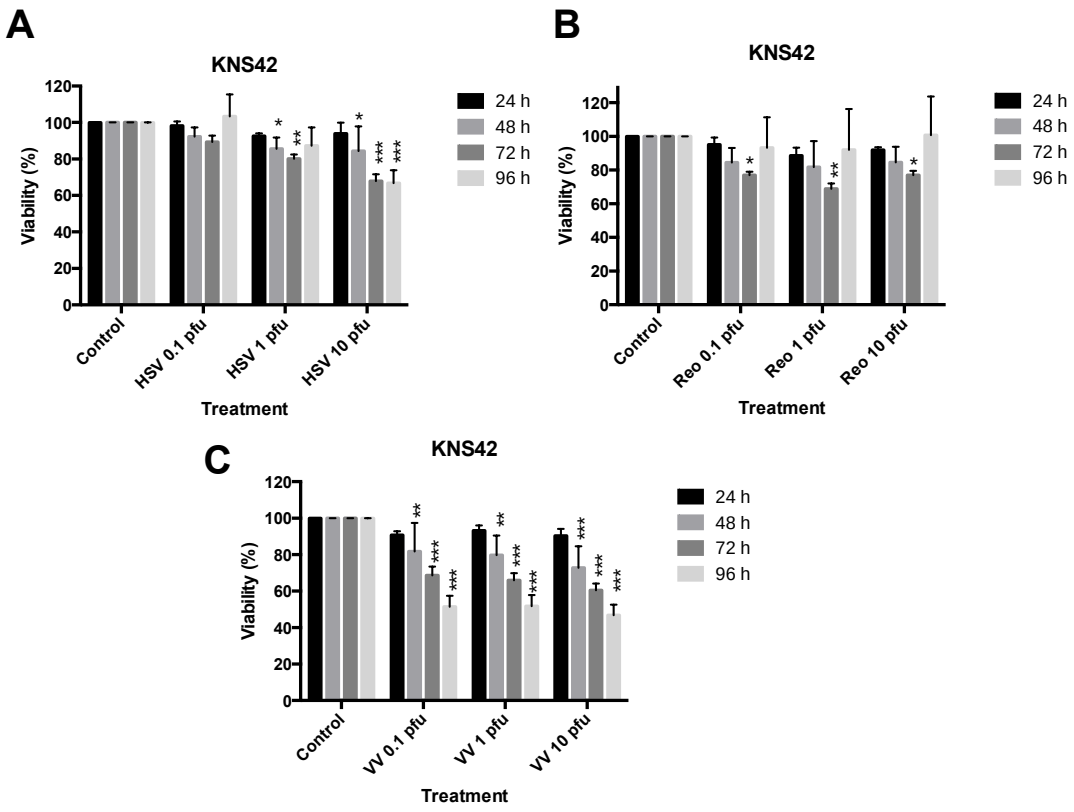

Figure 33: The effects of oncolytic viruses on KNS42 tumour spheroid viability

KNS42 cells at $1x10^3$ cells per well were seeded in an ultra-low attachment round-bottom 96 well plate to form spheroid aggregates. Following 72 h incubation, cells were incubated ± OV (HSV **(A)**, reovirus (Reo) **(B)** and VV **(C)**), at nominal 0.1, 1 and 10 pfu/cell. Cell viability at 24, 48, 72 and 96 h was determined by WST-1 assay and was expressed as a percentage of controls. Graphs show mean±SEM of n=3 individual experiments. * $p<0.05$, ** $p<0.01$, *** $p<0.001$ by two-way ANOVA.

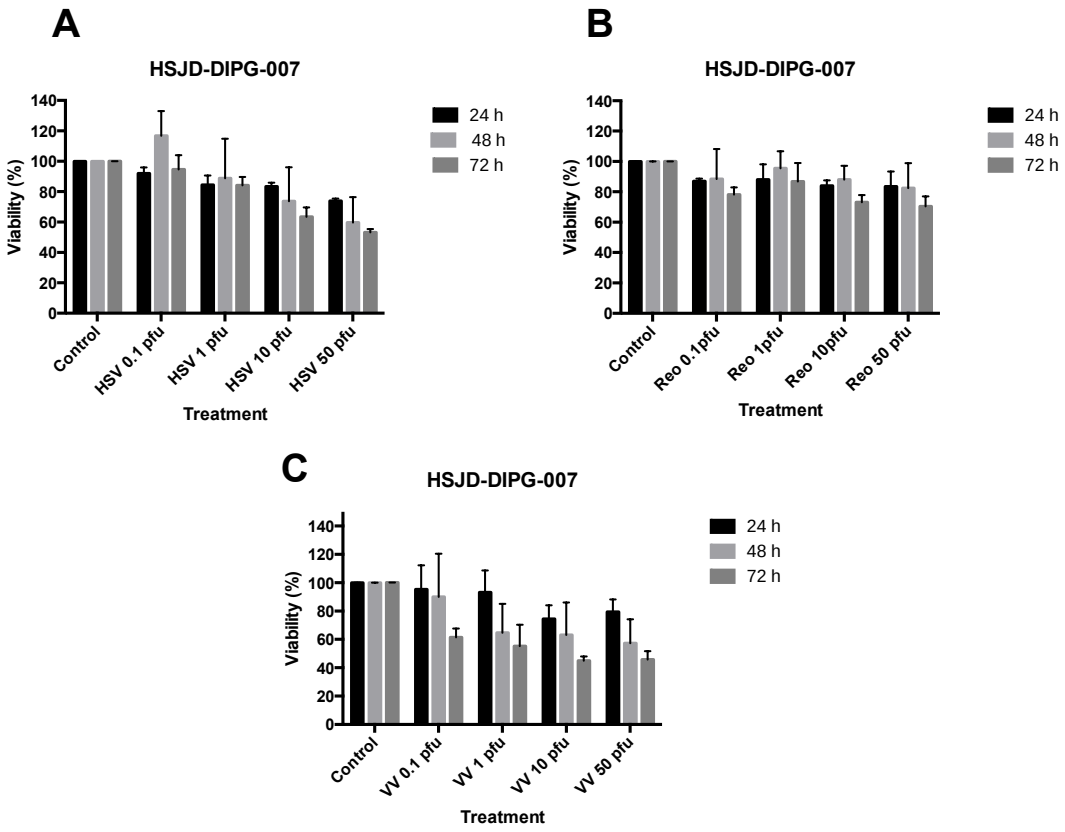

Figure 34: The effects of oncolytic viruses on HSJD-DIPG-007 tumour spheroid viability

HSJD-DIPG-007 cells at $1x10^3$ cells per well were seeded in an ultra-low attachment round-bottom 96 well plate to form spheroid aggregates. Following 72 h incubation, cells were incubated ± OV (HSV **(A)**, reovirus (Reo) **(B)** and VV **(C)**), at nominal 0.1, 1, 10 and 50 pfu/cell. Cell viability at 24, 48, 72 and 96 h was determined by WST-1 assay and was expressed as a percentage of controls. Graphs show mean±SEM of n=2 individual experiments.

4.6 Evaluation of the effects of oncolytic viruses on paediatric glioma proliferation and tumour spheroid growth

Next, the effects of oncolytic OVs on paediatric glioma proliferation and tumour spheroid growth were evaluated. This was important to confirm that the observed effects on migration and invasion following each OV treatment were not, in fact, caused by effects of the virus on proliferation and tumour growth. In order to evaluate tumour spheroid growth for pHGG and mouse glioma cell lines, changes in the area of treated tumour spheroid cores over 72 h were measured from images taken during the spheroid in collagen invasion assay. To evaluate growth over time, the area of a spheroid core at each given time point was divided by it's area at time 0 h and this fraction was expressed as a percentage. This method could not be used for HSJD-DIPG-007 tumour spheroids as during invasion into collagen, the DIPG spheroid core became elongated and lost definition, making it difficult to accurately measure (Figure 4). Thus, for HSJD-DIPG-007 tumour spheroids, changes in the area of the spheroid following virus treatment were evaluated by images taken during the WST-1 assay.

When SF188 and KNS42 were grown as tumour spheroids, none of the OV treatments resulted in a significant change in growth at any time point evaluated (Figure 35A-C and 36A-C). GL261-Luc overall demonstrated no significant change in tumour spheroid growth when treated with oncolytic HSV or VV (Figure 37A and C). Following GL261-Luc treatment with reovirus, 0.1 pfu/cell reovirus caused a small but significant increase in tumour spheroid growth; however, this was not noted at any other virus concentration or time point (Figure 37B). Both HSV and VV treatment reduced the growth of HSJD-DIPG-007 tumour spheroids at 72 h (% of area of initial spheroid: control 275 %, HSV 10 pfu/cell 183 %, HSV 50 pfu/cell 161 %; VV 10 pfu/cell 156 %, VV 50 pfu/cell 159 %) (Figure 38A and C). Reovirus treatment overall had no effect on HSJD-DIPG-007 tumour spheroid growth when compared to control-treated spheroids at any time point (Figure 38B).

A Ki67 intracellular FACS assay was used to evaluate proliferation in virus-treated pHGG monolayers. Ki67 was used as a marker of proliferation as its expression is strictly associated with cell proliferation (372). Ki67 is present throughout all active phases of the cell cycle (G(1), S, G(2), and mitosis), but is absent from resting cells (G(0)) (373). The Ki67 intracellular FACS assay could not be used for VV, as the RFP incorporated into the virus could affect the FACS analysis channel that detects the emission from the PE-Cy7 Ki67 antibody. Neither pHGG cell line investigated demonstrated a significant change in the percentage of Ki67-positive cells following 24 h of treatment with oncolytic HSV or reovirus (Figure 35D-E and 36D-E). HSV treatment tended to increase proliferation of both SF188 and KNS42 cells but this did not reach statistical significance (mean±SEM SF188 Ki67 positive cells: control 4.5±0.87, HSV 10 pfu/cell 10.5±4.1 p=0.19; KNS42 Ki67 positive cells: control 5.6±3.5, HSV 10 pfu/cell 30.1±22.6 p=0.43) (Figure 35D and 36D).

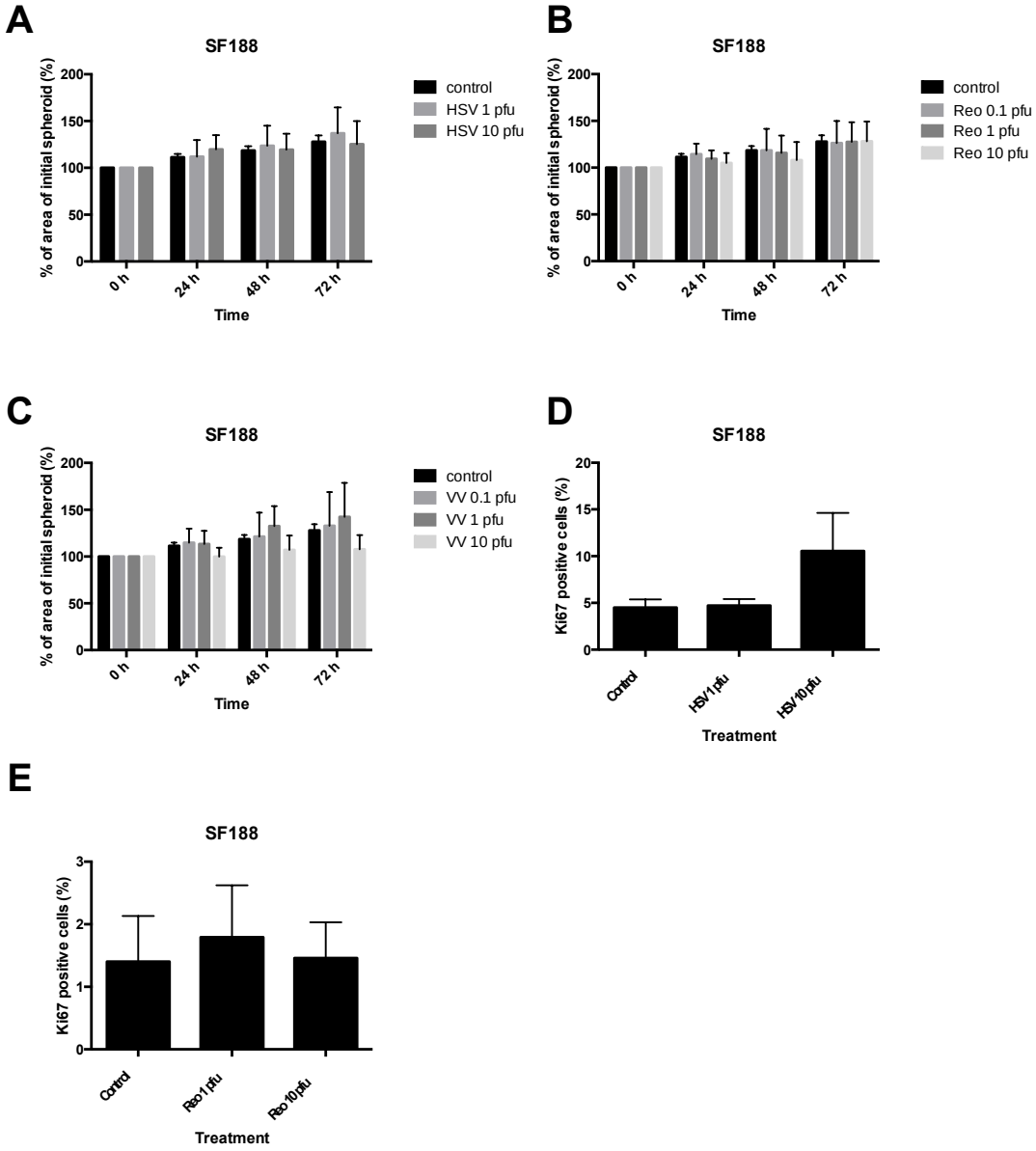

Figure 35: The effects of oncolytic viruses on SF188 tumour spheroid growth and cell proliferation

(A-C) SF188 tumour spheroids were encased in collagen and incubated in culture medium ± OV at nominal 1 and 10 pfu/cell HSV **(A)** and 0.1, 1 and 10 pfu/cell reovirus **(B)** and 0.1, 1 and 10 pfu/cell VV **(C)**. Tumour spheroids were imaged at 0, 24, 48 and 72 h using the EVOS cell imaging system. The area of the tumour spheroid core was measured at each time point using Image J software. Growth over time ((area of spheroid at a given time point ÷ area of spheroid at time 0 h) x100) was calculated. Graphs show mean±SEM of multiple repeats pooled from up to n=3 individual experiments. Results were not statistically significant following evaluation by two-way ANOVA. **(D-E)** $1x10^5$ SF188 cells were seeded into 12 well plates and left to adhere for 4 h. Culture medium ± OV (HSV at 1 and 10 pfu/cell **(D)** or reovirus at 1 and 10 pfu/cell **(E)**) were added to each well. After 24 h treatment, cells were harvested, washed and fixed with 10 % PFA, before re-suspension into 0.3 % saponin followed by incubation with the Ki67 PE-Cy7 mouse anti-human antibody. Ki67 staining was then detected by FACS. Graphs show mean±SEM of at least n=3 individual experiments. Results were not statistically significant following evaluation by one-way ANOVA.

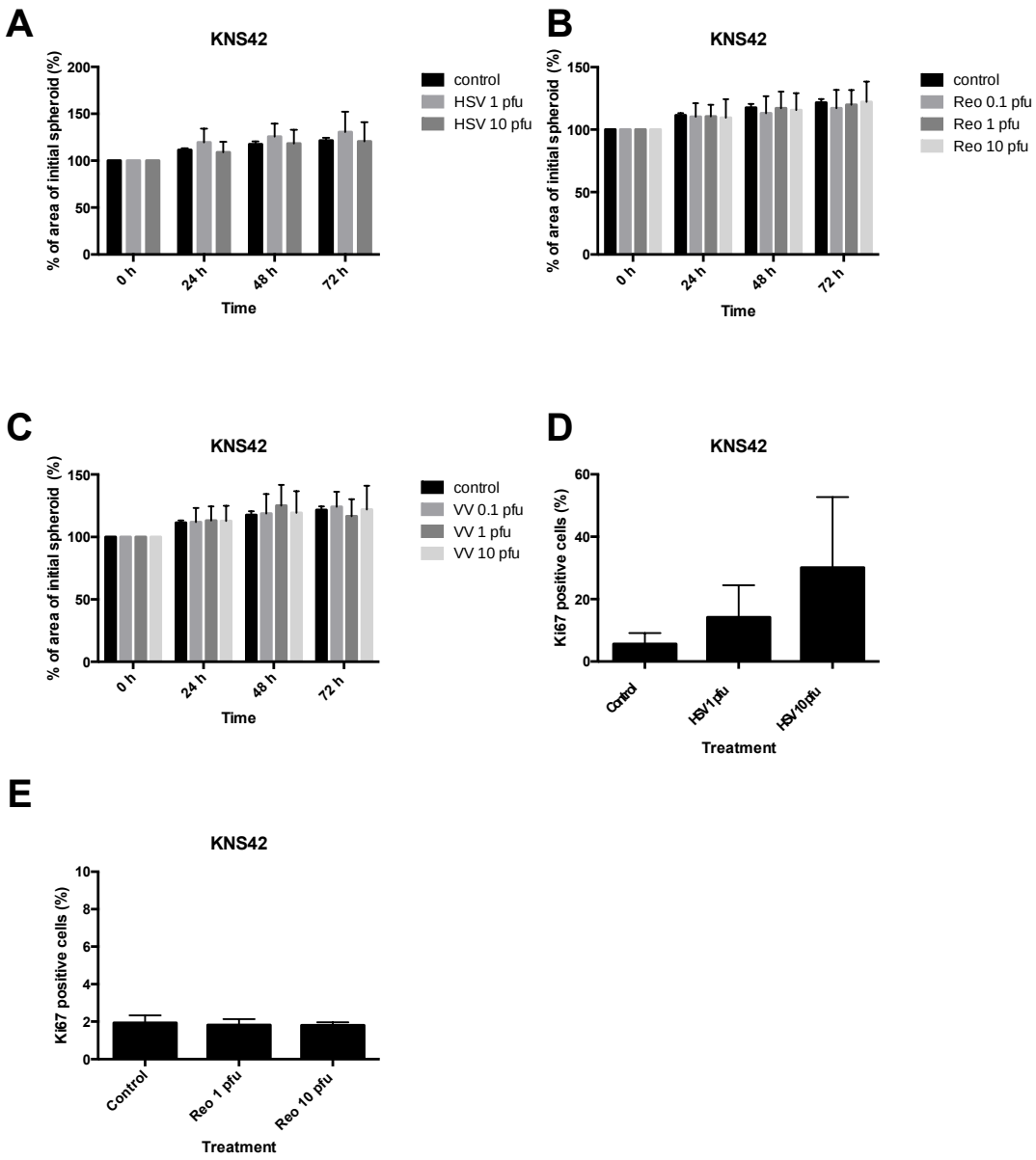

Figure 36: The effects of oncolytic viruses on KNS42 tumour spheroid growth and cell proliferation

(A-C) KNS42 tumour spheroids were encased in collagen and incubated in culture medium ± OV at nominal 1 and 10 pfu/cell HSV **(A)** and 0.1, 1 and 10 pfu/cell reovirus **(B)** and 0.1, 1 and 10 pfu/cell VV **(C)**. Tumour spheroids were imaged at 0, 24, 48 and 72 h using the EVOS cell imaging system. The area of the tumour spheroid core was measured at each time point using Image J software. Growth over time ((area of spheroid at a given time point ÷ area of spheroid at time 0 h) x100) was calculated. Graphs show mean±SEM of multiple repeats pooled from up to n=3 individual experiments. Results were not statistically significant following evaluation by two-way ANOVA. **(D-E)** $1x10^5$ KNS42 cells were seeded into 12 well plates and left to adhere for 4 h. Culture medium ± OV (HSV at 1 and 10 pfu/cell **(D)** or reovirus at 1 and 10 pfu/cell **(E)**) were added to each well. After 24 h treatment, cells were harvested, washed and fixed with 10 % PFA, before re-suspension into 0.3 % saponin followed by incubation with the Ki67 PE-Cy7 mouse anti-human antibody. Ki67 staining was then detected by FACS. Graphs show mean±SEM of at least n=3 individual experiments. Results were not statistically significant following evaluation by one-way ANOVA.

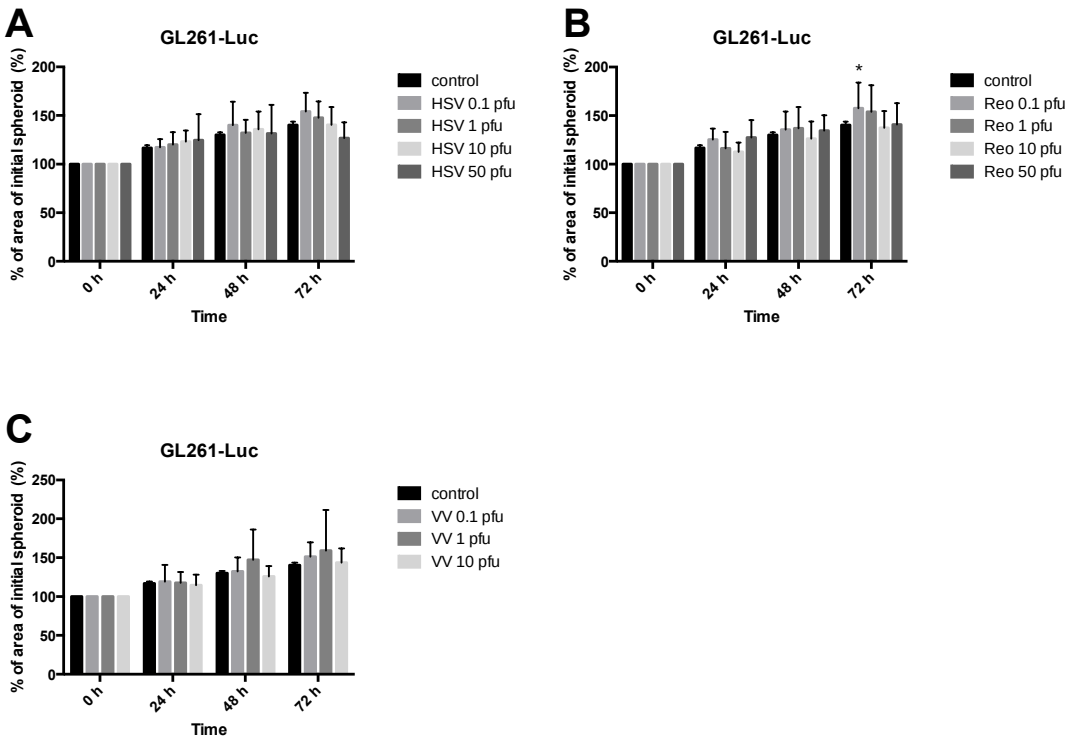

Figure 37: The effects of oncolytic viruses on GL261-Luc tumour spheroid growth

GL261-Luc tumour spheroids were encased in collagen and incubated in culture medium ± OV at nominal 0.1, 1, 10 and 50 pfu/cell HSV **(A),** 0.1, 1, 10 and 50 pfu/cell reovirus **(B)** and 0.1, 1 and 10 pfu/cell VV **(C)**. Tumour spheroids were imaged at 0, 24, 48 and 72 h using the EVOS cell imaging system. The area of the tumour spheroid core was measured at each time point using Image J software. Growth over time ((area of spheroid at a given time point ÷ area of spheroid at time 0 h) x100) was calculated. Graphs show mean±SEM of multiple repeats pooled from up to n=3 individual experiments. * $p<0.05$ by two-way ANOVA.

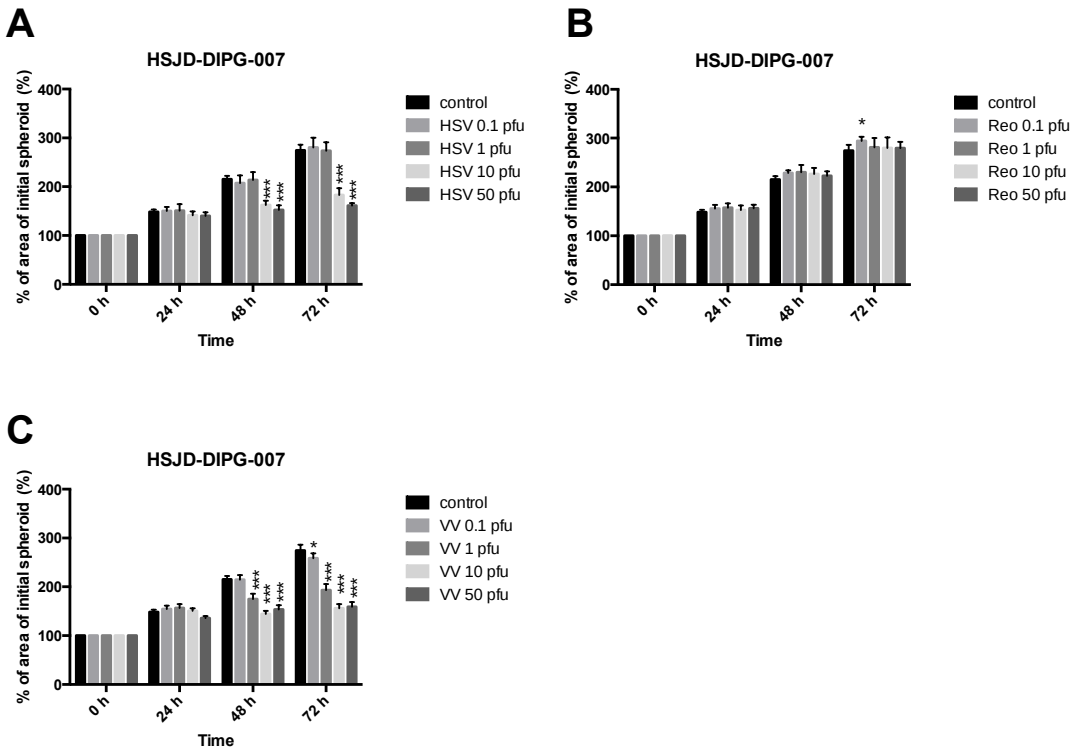

Figure 38: The effects of oncolytic viruses on HSJD-DIPG-007 tumour spheroid growth

.

1x10^3 cells per well of HSJD-DIPG-007 were seeded in an ultra-low attachment round bottom 96 well plate to form spheroid aggregates. Following 72 h incubation, cells were treated with culture medium ± nominal 0.1, 1, 10 and 50 pfu/cell HSV **(A),** reovirus **(B)** or VV **(C)**. Tumour spheroids were imaged at time 0, 24, 48 and 72 h following drug treatment. Growth over time ((area of spheroid at a given time point ÷ area of spheroid at time 0 h) x100) was calculated. Graphs show mean±SEM of one experiment performed with multiple repeats (n=6). * p<0.05, ** p<0.01, *** p<0.001 by two-way ANOVA.

4.7 Evaluation of the effects of oncolytic viruses on cytokine production

OVs are known to be capable of altering the balance of cytokine production within tumours (253). Cytokines are small molecules which have a diverse range of effects on tumour growth, proliferation, inflammation and immune response (374). The glioblastoma microenvironment contains a multitude of cytokines, contributing to tumour pathogenicity. IL-8 is a pro-inflammatory cytokine, expressed at high levels in glioblastoma and plays a role in promoting tumour invasion and angiogenesis (374,375). VEGF is critical for new vessel formation and is also overexpressed in glioblastoma (374,376). Additionally, VEGF has been shown to promote an EMT phenotype, which is associated with increased migration and invasion of tumour cells (377). Thus, the effects of OVs on pHGG IL-8 and VEGF production were evaluated to determine whether changes in cytokine expression may contribute to the anti-migratory effects observed.

The expression of IL-8 from pHGG cell lines (SF188 and KNS42) following OV treatment over 72 h, was evaluated by ELISA. Oncolytic HSV treatment of SF188 at 10 pfu/cell resulted in a statistically significant reduction in IL-8 at 48, 72 and 96 h (mean±SEM: IL-8 48 h: control 2732±874 pg/ml, HSV 10 pfu/cell 416±584 pg/ml p= 0.012; IL-8 72 h: control 3065±148 pg/ml, HSV 10 pfu/cell 128±189 pg/ml p=0.0014; IL-8 96 h: control 3170±318 pg/ml, HSV 1 pfu/cell 1108±141 pg/ml p=0.0272, HSV 10 pfu/cell 411±446 pg/ml p=0.0026) (Figure 39A). Although this trend was observed in KNS42, statistical significance was not reached following analysis (Figure 40A). Conversely, reovirus treatment resulted in a statistically significant increase in SF188 IL-8 expression at: 10 pfu/cell at 24 h (mean±SEM IL-8: control 1201±219 pg/ml, reovirus 10 pfu/cell 12171±3235 pg/ml p=0.0079) 0.1, 1 and 10 pfu/cell at 48 and 72 h (mean±SEM: IL-8 48 h: control 2732±874 pg/ml, reovirus 0.1 pfu/cell 12456±2215 pg/ml p=0.0196, reovirus 1 pfu/cell 13771±2052 pg/ml p=0.0074, reovirus 10 pfu/cell 14358±1941 pg/ml p=0.0047; IL-8 72 h: control 3065±145 pg/ml, reovirus 0.1 pfu/cell 15211±4099 pg/ml p=0.0031, reovirus 1 pfu/cell 14345±3938 pg/ml p=0.0062, reovirus 10 pfu/cell 12934±4552 pg/ml p=0.0177) and 0.1 and 10

pfu/cell at 96 h (mean±SEM IL-8 96 h: control 3170±318 pg/ml, reovirus 0.1 pfu/cell 12292±1885 pg/ml p=0.03, reovirus 10 pfu/cell 12155±1829 pg/ml p=0.033) (Figure 39B). Again, this trend was observed from 48 h in KNS42 cells; however it did not reach statistical significance (Figure 40B). 10 pfu/cell VV treatment resulted in a significant reduction of SF188 IL-8 expression at 72 and 96 h (mean±SEM: IL-8 72 h: control 3065±148 pg/ml, reovirus 10 pfu/cell 154±270 pg/ml p=0.0057; IL-8 96 h: control 3170±318 pg/ml, reovirus 10 pfu/cell 688±540 pg/ml p=0.0199) (Figure 39C); however, this was not observed for KNS42 (Figure 40C).

Treatment of KNS42 cells with 0.1, 1 and 10 pfu/cell HSV at 96 h resulted in a significant reduction in VEGF (mean±SEM VEGF: control 322±239 pg/ml, HSV 0.1 pfu/cell 91.1±27.5 pg/ml p=0.492, HSV 1 pfu/cell 50.5±11.4 pg/ml p=0.178, HSV 10 pfu/cell 60±33.5 pg/ml p=0.0226) (Figure 42A). No significant changes were noted for HSV treatment of SF188 cells (Figure 41A). Reovirus and VV treatment of both SF188 and KNS42 did not significantly alter VEGF expression (Figure 41B-C and 42B-C).

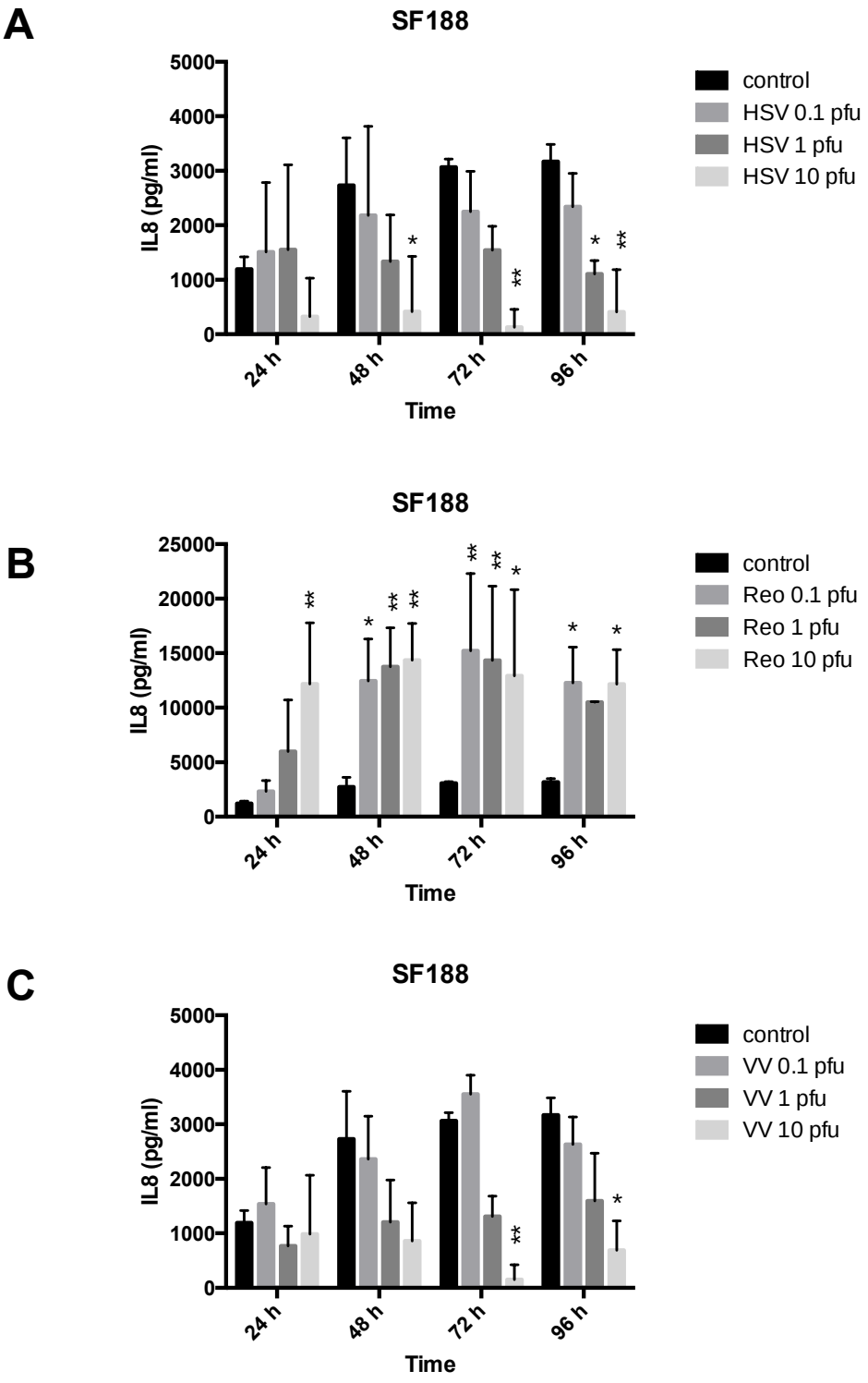

Figure 39: The effects of oncolytic viruses on SF188 IL-8 expression
SF188 cells were seeded at 1x10^5 cells/well in a 12 well plate and left for 4 h to adhere. Cells were then incubated ± 0.1, 1 or 10 pfu/cell OV (HSV **(A)**, reovirus (Reo) **(B)** or VV **(C)**). At 24, 48, 72 or 96 h supernatants were collected and assayed for IL-8 by ELISA. Graphs show mean±SEM of n=3 individual experiments, each performed in triplicate. * p<0.05, ** p<0.01, *** p<0.001 by two-way ANOVA.

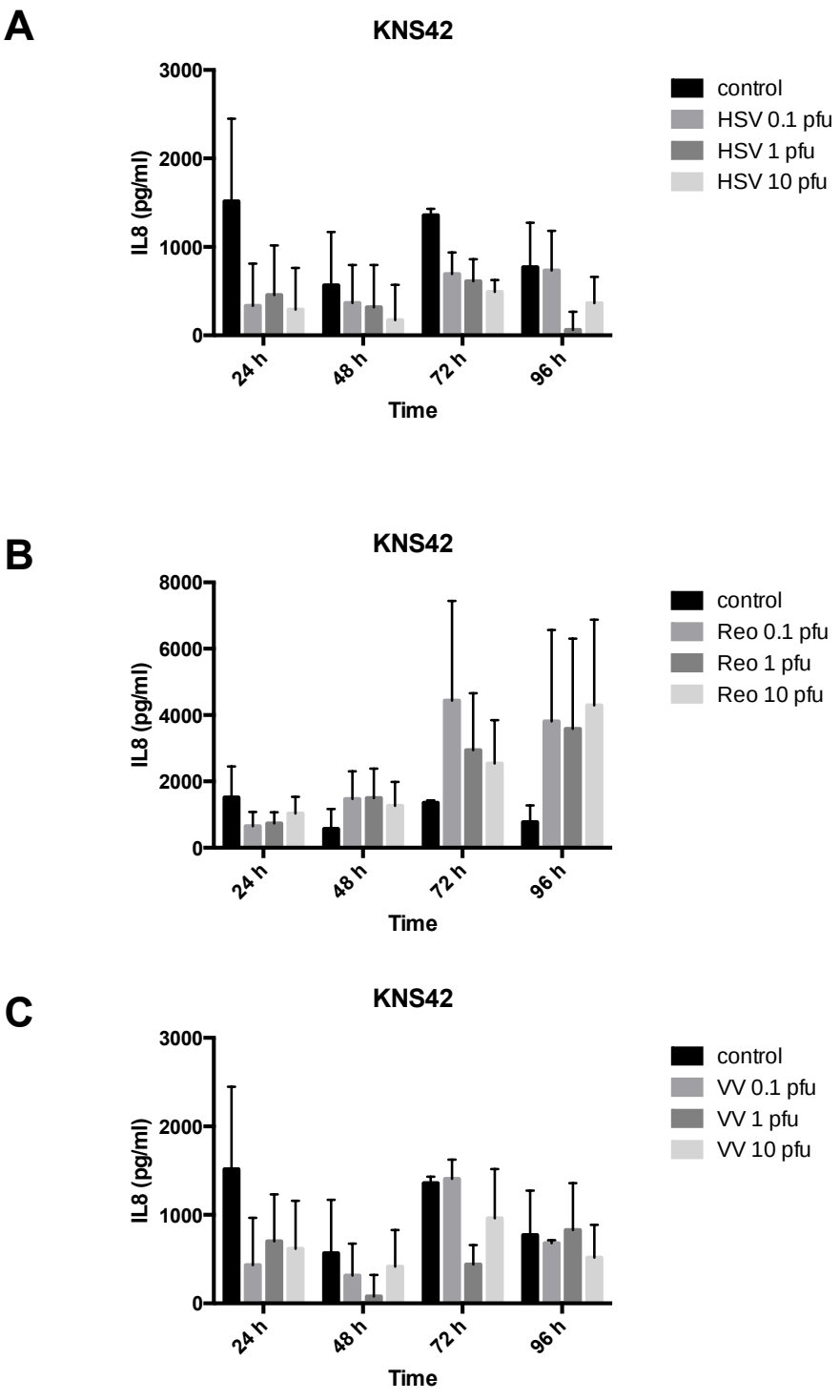

Figure 40: The effects of oncolytic viruses on KNS42 IL-8 expression
KNS42 cells were seeded at $1x10^5$ cells/well in a 12 well plate and left for 4 h to adhere. Cells were then incubated ± 0.1, 1 or 10 pfu/cell OV (HSV **(A)**, reovirus (Reo) **(B)** or VV **(C)**). At 24, 48, 72 or 96 h supernatants were collected and assayed for IL-8 by ELISA. Graphs show mean±SEM of n=3 individual experiments, each performed in triplicate. * $p<0.05$, ** $p<0.01$, *** $p<0.001$ by two-way ANOVA.

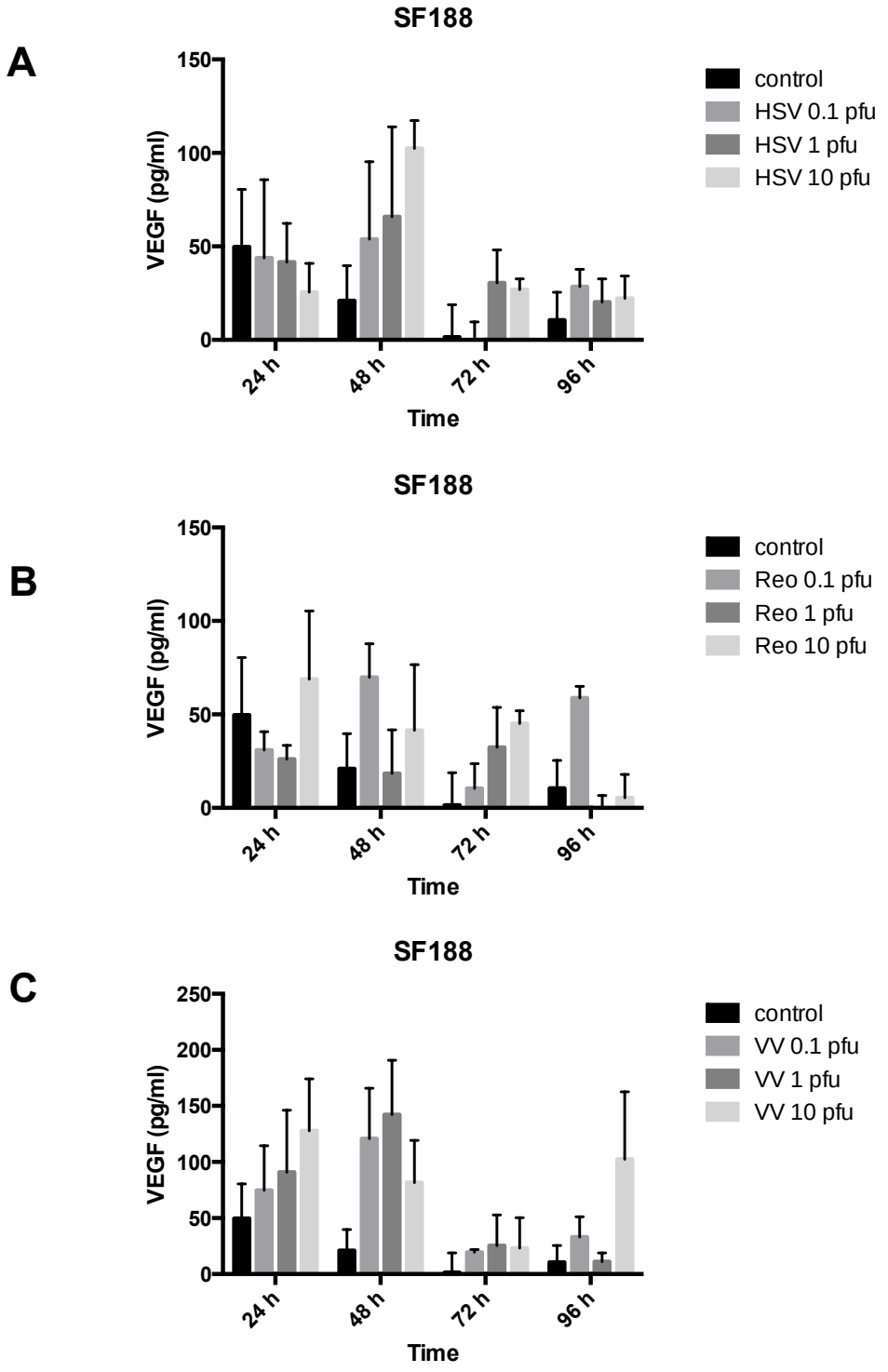

Figure 41: The effects of oncolytic viruses on SF188 VEGF expression
SF188 cells were seeded at $1x10^5$ cells/well in a 12 well plate and left for 4 h to adhere. Cells were then incubated ± 0.1, 1 or 10 pfu/cell OV (HSV **(A)**, reovirus (Reo) **(B)** or VV **(C)**). At 24, 48, 72 or 96 h supernatants were collected and assayed for VEGF by ELISA. Graphs show mean±SEM of n=3 individual experiments, each performed in triplicate. * $p<0.05$, ** $p<0.01$, *** $p<0.001$ by two-way ANOVA.

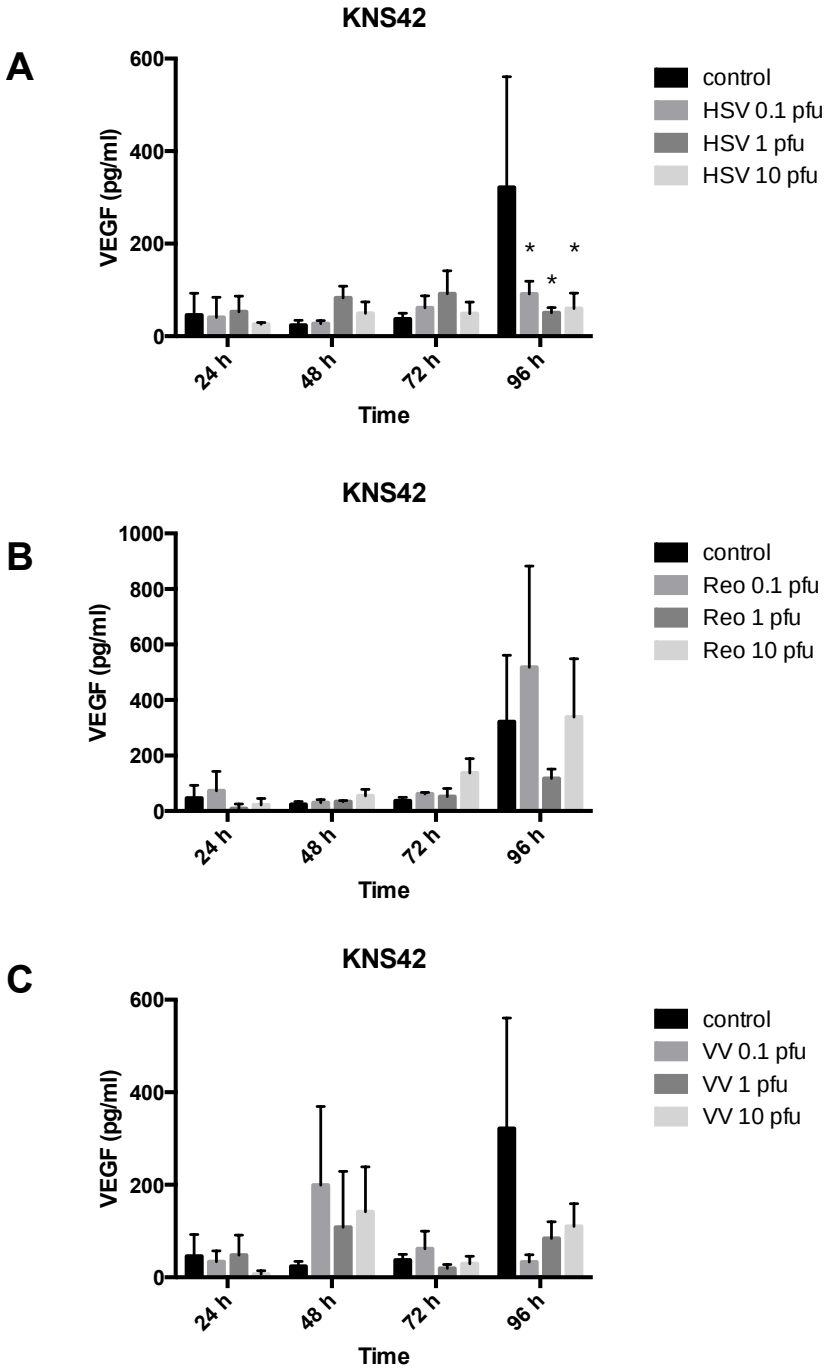

Figure 42: The effects of oncolytic viruses on KNS42 VEGF expression
KNS42 cells were seeded at $1x10^5$ cells/well in a 12 well plate and left for 4 h to adhere. Cells were then incubated ± 0.1, 1 or 10 pfu/cell OV (HSV **(A)**, reovirus (Reo) **(B)** or VV **(C)**). At 24, 48, 72 or 96 h supernatants were collected and assayed for VEGF by ELISA. Graphs show mean±SEM of n=3 individual experiments, each performed in triplicate. * $p<0.05$, ** $p<0.01$, *** $p<0.001$ by two-way ANOVA.

4.8 Discussion

OVs are anti-cancer agents that are capable of promoting toxicity through both selective tumour cell killing and the induction of systemic anti-tumour immune response (254). However, very little is known about the effects of OVs on cancer cell migration and invasion. In this chapter, the anti-migratory and anti-invasive properties of a range of OVs on pHGG, DIPG and mouse glioma cell lines have been demonstrated using both 2D (scratch assay) and 3D (spheroid invasion in collagen) *in vitro* models.

Oncolytic HSV significantly inhibited the migration and invasion of pHGG, DIPG and mouse glioma cell lines. This was not as a result of cytotoxicity when the cell lines were cultured as monolayers at a corresponding 24 h time point, although pHGG monolayers did display a significant reduction in viability as measured by MTT assay 24 h following oncolytic HSV treatment. However, there was no marked loss of viability when cell lines were cultured as multicellular spheroids over 72 h, the time point corresponding with the invasion assay. Reovirus also significantly reduced invasion (but not 2D migration) of pHGG, DIPG and mouse glioma cell lines in a 3D assay. Again, this anti-invasive effect was not associated with a marked reduction in tumour spheroid viability. Furthermore, VV treatment was also capable of significantly reducing both migration and invasion of pHGG, DIPG and mouse glioma cell lines; however, all four cell lines appeared to be the most sensitive to early cytotoxic effects of this virus treatment. In addition, oncolytic HSV and reovirus did not cause a statistically significant change in pHGG proliferation when evaluated by Ki67 intracellular FACS assay, providing further evidence that the anti-migratory and anti-invasive effects observed were specific and not a consequence of anti-proliferative effects.

Finally, the results from this chapter show that OVs can alter pHGG cytokine production. Oncolytic HSV and VV treatment of pHGG cells resulted in an overall reduction of IL-8, a cytokine known to be associated with tumour invasion (374,375). Interestingly, reovirus treatment (which failed to inhibit migration of pHGG monolayers) resulted in increased IL-8 production.

Taken together, these observations suggest, for the first time, that OVs possess anti-migratory and anti-invasive activity against pHGG, DIPG and mouse glioma cells. Of the three viruses investigated, oncolytic HSV represents the most promising candidate to take forward for further investigation, as both its anti-migratory and anti-invasive effects do not appear to be a consequence of cytotoxicity, reduced proliferation or changes in tumour spheroid growth. Overall, these results are highly novel and suggest that OVs may have therapeutic benefits for pHGG and DIPG as an anti-invasive agent, potentially improving outcomes for this patient group.

Unlike its adult counterpart, only a small amount of research has focused on the effects of oncolytic virotherapy for pHGG (378) and there are currently no published studies reporting the effects of OVs on DIPG. Freidman *et al*. have reported that the paediatric cerebellar glioblastoma xenograft, DM456, containing both tumour and cancer stem cells, is sensitive to killing by a range of modified HSVs (323,379). No published studies to date have evaluated the effects of oncolytic VV or reovirus on pHGG viability or cytotoxicity. In addition, there are no reported studies in the literature evaluating the effects of OVs on pHGG or DIPG migration and invasion, suggesting that the results described in this chapter are highly novel.

In this study, oncolytic HSV appeared to be the most promising candidate to take forward for further investigation as a clinical anti-migratory and anti-invasive agent, in addition to its potential cytotoxic activity over time. There was clear evidence to suggest that the anti-migratory and anti-invasive effects of oncolytic HSV on pHGG and DIPG were not a consequence of cytotoxicity. At 24 h, which corresponds to the time point at which migration was analysed by scratch assay in monolayers, over 94 % of cells were still alive following 10 pfu/cell HSV treatment when evaluated by LIVE/DEAD® assay. In this assay, ethidium homodimer is taken up by dead cells with damaged plasma membranes to produce a bright fluorescence upon binding with nucleic acid, which can be quantified by FACS analysis (371). However, at the same corresponding 24 h time point, oncolytic HSV treatment at 0.156 to 10 pfu/cell resulted in approximately 50% reduction in pHGG monolayer

viability when measured by MTT assay. In the MTT assay, tetrazolium MTT is reduced to water insoluble formazan crystals by active mitochondrial dehydrogenase enzymes resulting in a colour change and this assay therefore measures the metabolic activity of live cells (380). The above results illustrate the differences that may be seen when using an assay of viability compared to cytotoxicity. One possible explanation for the discrepancy between the results of the LIVE/DEAD® assay and the MTT assay following 24 h of oncolytic HSV infection of pHGG monolayers is, that the results of the MTT assay may be reflecting a change in the metabolic activity of the cells following virus infection. Overall, these discrepancies highlight a potential limitation in our study when using viability assays such as MTT and WST-1 as a proxy measurement for cytotoxicity. Unfortunately the cytotoxic effects of OV treatment could not be evaluated for tumour spheroids by LIVE/DEAD® assay as a single cell solution is required for FACS analysis, so the WST-1 assay of viability was used as proxy measurement despite its limitations. Spheroids of SF188 cells demonstrated a reduction in viability of no more than 18 % following all HSV treatments by 72 h. Both KNS42 and HSJD-DIPG-007 cell lines were slightly more sensitive, demonstrating a reduction in viability of 32 % and 37 %, respectively, following 10 pfu/cell treatment over 72 h. Oncolytic HSV treatment did not significantly alter proliferation of pHGG cells or tumour spheroid growth. The next chapter will evaluate the potential mechanisms by which oncolytic HSV can inhibit pHGG cell migration and invasion, in particular focusing on the effects of oncolytic HSV on the cell cytoskeleton. HSV at 10 pfu/cell was chosen as the dose to use in further studies, as it was the dose associated with a significant reduction of migration and invasion for both SF188 and KNS42 cell lines.

Paediatric HGG cell lines were overall more sensitive to VV treatment with marked and significant changes in cytotoxicity observed by 96 h. Given the sensitivity of the cell lines to this virus, it is hard to distinguish whether the anti-migratory effects observed were in fact attributable to cytotoxicity. However, these results do highlight the potential clinical benefit of developing oncolytic VV as a cytotoxic therapeutic agent for pHGG. Over

time, all three OVs began to exert significant cytotoxic effects on the pHGG cell lines. This highlights a potential dual mechanism of action for therapy. Early infusion of OV may initially prevent migration and invasion of the tumour; however, over time the cytotoxic effects of the virus may predominate, resulting in tumour cell death. Future work involves testing this hypothesis in an *in vivo* model of pHGG and evaluating potential therapeutic effects.

Oncolytic HSV and VV treatment of pHGG cells resulted in an overall reduction of IL-8 expression. IL-8 is best characterised for its role as a chemotactic agent involved in the inflammatory response and is capable of promoting neutrophil, basophil, and T lymphocyte migration (374). Additionally, IL-8 plays a role in tumour metastasis, and is associated with the invasion of several tumour types including glioblastoma (381-384). IL-8 is highly prevalent in glioblastoma (374,375) and has been shown to be necessary for glioma cell invasion (381). Raychaudhuri *et al*. published that both silencing of the IL-8 gene by use of siRNA or treatment with an IL-8 neutralising antibody, can decrease the invasion of glioblastoma cell lines (381). Furthermore, addition of IL-8 to stem cell medium has been shown to increase transwell migration of patient-derived glioblastoma cancer stem cells (385). Given that IL-8 appears to play an important role in glioblastoma migration, the reduction of IL-8 following oncolytic HSV and VV treatment may, in part, contribute to the anti-migratory effects observed following treatment of pHGG cell lines. In keeping with this hypothesis is the observation that reovirus treatment, which failed to inhibit migration of pHGG monolayers, resulted in increased IL-8 detection. Reovirus has previously been shown to increase secretion of IL-8 in other tumour models (253,386).

Oncolytic HSV treatment significantly reduced the expression of VEGF at 96 h in KNS42 cells. VEGF stimulation of normal epithelial cells and differentiated carcinoma cells has been shown to induce EMT, promoting a more invasive cell phenotype (66,377). VEGF can enhance Snail expression, which acts to repress E-Cadherin transcription, in turn promoting EMT and cell migration (387). The reduction in VEGF following oncolytic

HSV treatment of KNS42 may in part contribute to the anti-migratory and anti-invasive effects observed. Additionally, this observation highlights heterogeneity between pHGG cell lines SF188 and KNS42 in response to OV treatment, as oncolytic HSV treatment of SF188 did not alter VEGF expression at 96 h.

In this study, a scratch assay was used to evaluate the ability of OVs to block pHGG and mouse glioma migration. Although this assay offers the advantage that it requires no specialist equipment and easily allows cell movement and morphology to be imaged in real time, it has several disadvantages (76,388). One major drawback is that using a pipette tip to create a scratch can result in intra- and inter-experimental variation in the size and shape of the scratch (76). Additionally, the process of scratching the cell monolayer itself can damage cells, and result in the release of factors that may influence subsequent cell migration (76).

Growth of tumour spheroids was evaluated by taking into account the change in the area of the tumour spheroid core, which was embedded in collagen over time following virus treatment. It was not possible to count changes in the number of cells contained within tumour spheroid aggregates over time in our system to allow an evaluation of proliferation. Using this method, the OVs investigated in this study did not significantly affect pHGG tumour spheroid growth over time. Proliferation was however evaluated in monolayers of pHGG cells following oncolytic HSV and reovirus treatment using a Ki67 intracellular FACS assay. Ki67 is a nuclear marker used to demonstrate the proliferative phase of the cell cycle as it is expressed in all phases of the cell cycle apart from G0. Ki67 has been reported to be a more specific marker of proliferation than proliferating cell nuclear antigen (PCNA) (389).

In conclusion, the results described in this chapter demonstrate that OVs can inhibit the migration and invasion of pHGG, DIPG and mouse glioma cells. Oncolytic HSV represents the most promising candidate to take forward for further investigation in this regard, as both its anti-migratory and

anti-invasive effects do not, overall, appear to be a consequence of cytotoxicity,reduced proliferation or changes in tumour spheroid growth. The following chapter will evaluate a potential mechanism employed by oncolytic HSV to inhibit pHGG cell migration and invasion and will focus on the effects of viral infection on the cancer cell cytoskeleton.

Chapter 5: Potential mechanism underlying the observed anti-migratory and anti-invasive effects of oncolytic HSV

The results described in the previous chapter show that oncolytic HSV can specifically inhibit the migration and invasion of pHGG and DIPG cells *in vitro*. In this chapter, one potential mechanism underlying this phenomenon is explored.

Cell movement is made possible by the presence of the cell cytoskeleton, which is composed of actin microfilaments, microtubules and intermediate filaments (86). Microtubules play a key role in regulating cell migration through their ability to influence cell mechanics, intracellular trafficking and cell signalling (93). Alongside their ability to orchestrate cell movement, microtubules are also critical for viral replication, forming networks allowing transport of viruses within a host cell (308-310). The results contained in this chapter explore the hypothesis that oncolytic HSV may be able to influence paediatric glioma migration and cancer cell movement through its ability to alter microtubule dynamics.

GSK-3 has a multi-faceted role in controlling cell migration and can influence microtubule remodelling, cell polarity and cell adhesion (213). The results described in chapter three highlight the importance of GSK-3 in glioma migration and demonstrate that GSK-3 inhibition can disrupt the migration and invasion of pHGG and DIPG cell lines. Wild type HSV has previously been shown capable of altering normal human fibroblast microtubule dynamics through inactivation of GSK-3 (311); however, the effects of oncolytic HSV on human cell GSK-3 are unknown. In this chapter, the effects of oncolytic HSV on pHGG GSK-3 activity are evaluated *in vitro,* exploring the potential interaction of oncolytic HSV with molecular pathways critical for cell migration.

5.1 Oncolytic HSV can alter pHGG cell morphology, velocity and polarity

The effects of oncolytic HSV on pHGG cell morphology, velocity and polarity were investigated by live cell imaging of random cell migration. SF188 and KNS42 were incubated with or without 10 pfu/cell oncolytic HSV and time-lapse imaging was performed over 48 h (Movies 7-10). Image J MTrack software was used to track the individual movement of pHGG cells and to evaluate their velocity and polarity.

Over 48 h, oncolytic HSV treatment markedly changed pHGG cell morphology (Movies 7-10) (Figure 43A and B). SF188 cells cultured in normal medium were highly motile and polarised, with a distinct front-rear axis defining a leading protrusive front and a trailing edge. The cell leading edge clearly protruded as filopodia and lamellipodia and the trailing edge tail visibly retracted, progressing the cell forward (Movie 7) (Figure 43A). When treated with oncolytic HSV, SF188 cells were notably less motile and demonstrated a pronounced loss of polarity. Cells exhibited a loss of their distinct leading and trailing edges when compared to cells in culture medium only. SF188 HSV-treated cells became elongated and developed protrusive tails that appeared unable to retract (Movie 8). Overall, following HSV treatment, the SF188 cells appeared anchored to the surface and unable to generate the contractive or retractile forces required to propel the cell forward (Movie 8) (Figure 43A).

As previously demonstrated in chapter three (Figure 15), KNS42 cells were observed to be overall much less motile than SF188 (Movie 9). KNS42 cells cultured in normal medium appeared to have diffuse, extended and well-defined lamellipodia which, unlike SF188, appear to be orientated in opposite directions with no clear front-rear definition. Oncolytic HSV treatment of KNS42 cells resulted in cells rounding up with no discernable lamellipodia (Movie 9 and 10). Oncolytic HSV-treated KNS42 cells also developed multiple thin-branching protrusions over time (Movie 10) (Figure 43B).

Tracking analysis of individual cell movement highlighted that pHGG cells (SF188 and KNS42) treated with oncolytic HSV are much less motile than corresponding controls (Figure 43C) however, when velocity was quantified, a statistically significant reduction was seen only for SF188 cells; (oncolytic HSV treatment of SF188 cells significantly reduced velocity (mean±SEM velocity: control 0.33±0.041 µm/min, HSV 0.078±0.007 µm/min $p<0.001$) (Figure 43D); however, no significant change in velocity was observed following HSV treatment of KNS42 cells (mean±SEM velocity: control 0.13±0.014 µm/min, HSV 0.15±0.022 µm/min $p=0.506$) (Figure 43F)). Treatment with oncolytic HSV significantly reduced polarity of SF188 cells as demonstrated by a reduction in displacement (mean±SEM displacement: control 193±31 µm, HSV 50.5±11.2 µm $p<0.001$) (Figure 43E); however, given that KNS42 cells fail to polarise under normal conditions, it is unsurprising that there are no significant differences in displacement observed following HSV treatment of KNS42 (mean±SEM displacement: control 104±23.6 µm, HSV 71.4±20.1 µm $p=0.305$) (Figure 43G).

Taken together, the observations documented above may start to explain why pHGG cells incubated with oncolytic HSV demonstrated a reduction in migration. The effects of oncolytic HSV on velocity and polarity were only seen for SF188, which may reflect the fact that overall SF188 is a much more migratory and motile cell line than KNS42.

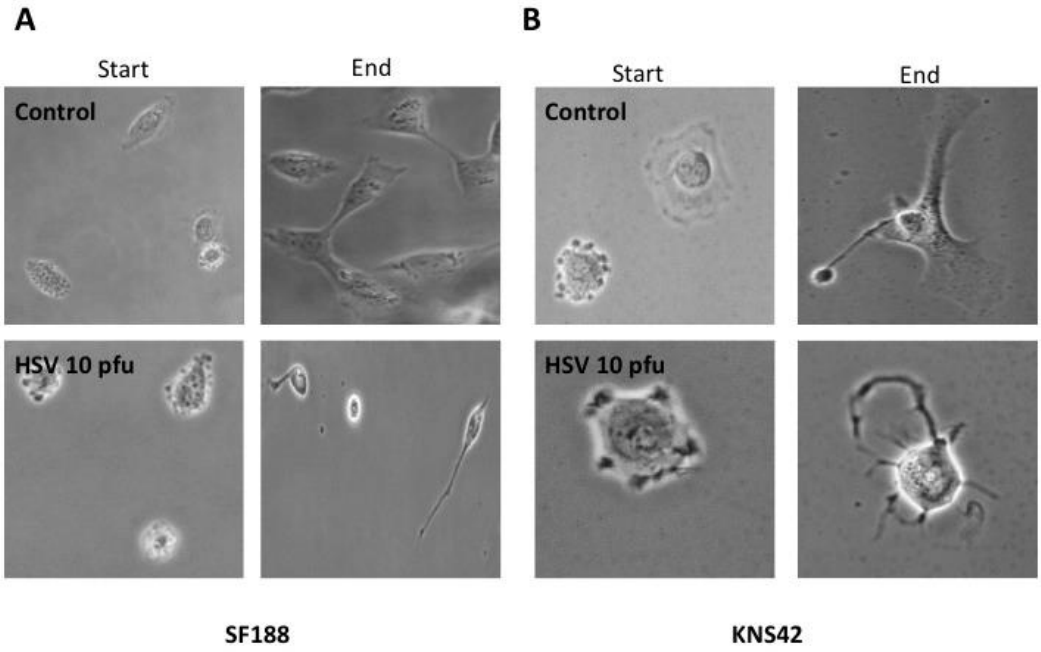
A
Start
End
Control
HSV 10 pfu
B
Start
End
Control
HSV 10 pfu
SF188
KNS42

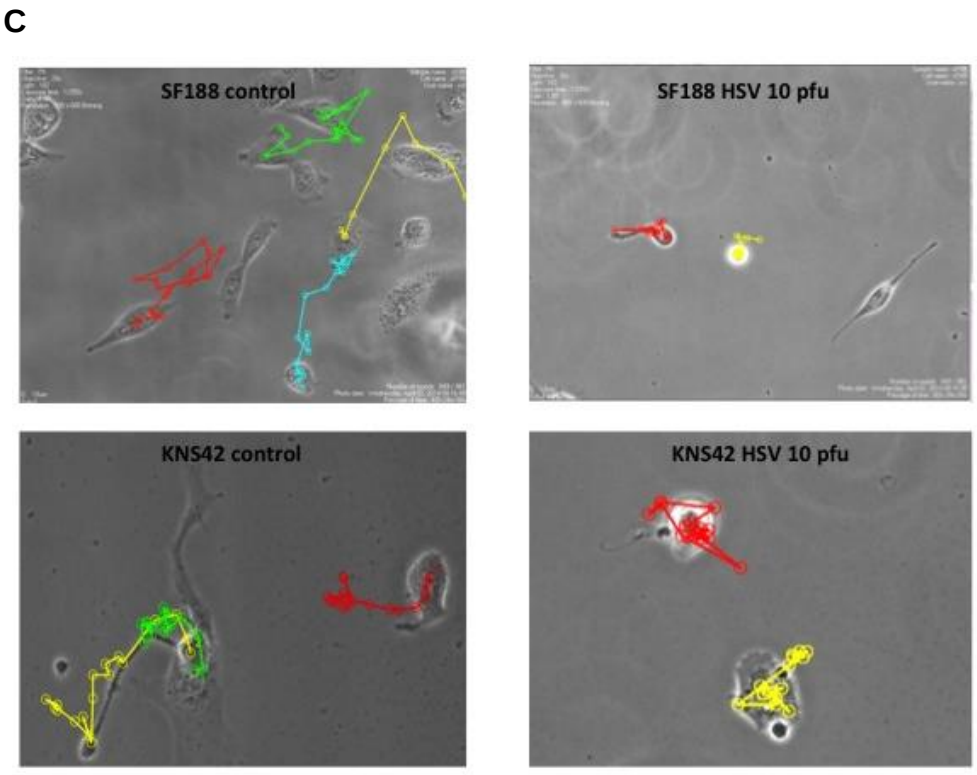
C
SF188 control
SF188 HSV 10 pfu
KNS42 control
KNS42 HSV 10 pfu

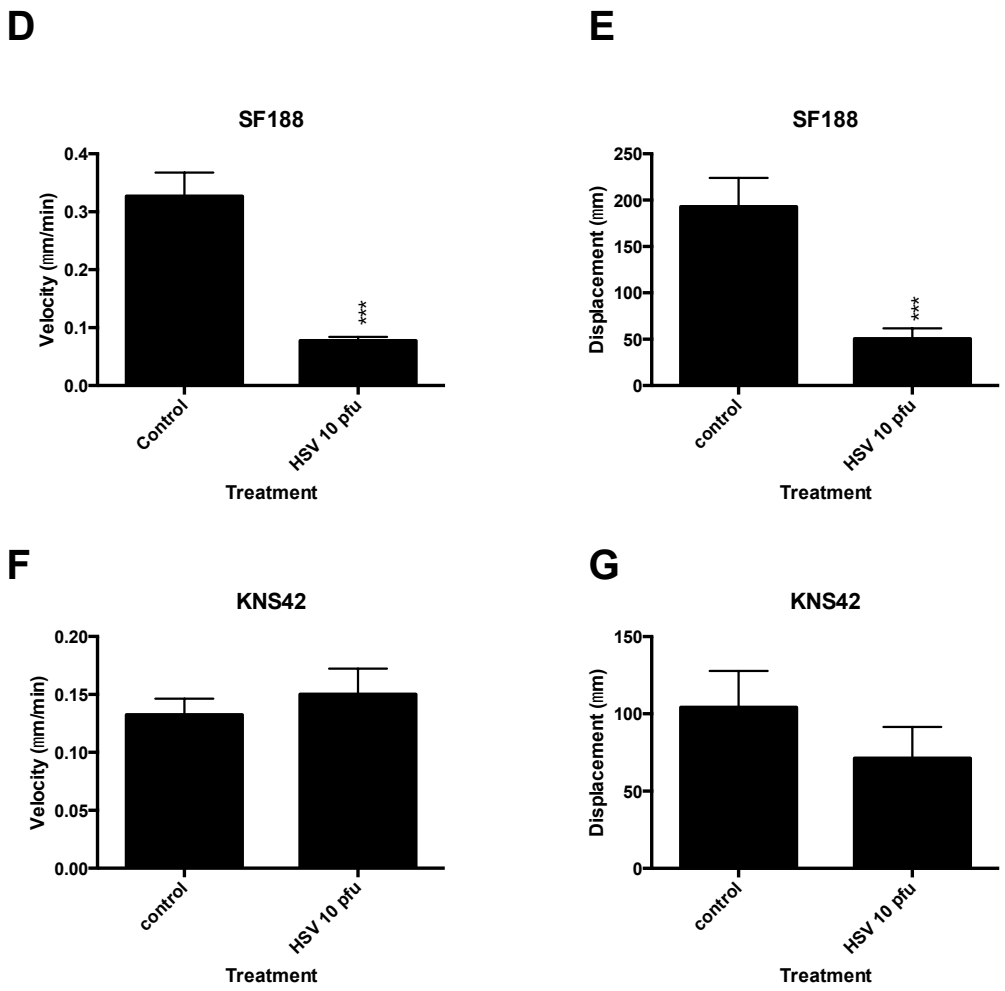

Figure 43: Analysis of the effects of oncolytic HSV treatment on pHGG cell morphology, velocity and polarity

Paediatric glioma cell lines SF188 and KNS42 were incubated ± nominal 10 pfu/cell oncolytic HSV in an Ibidi imaging dish. Live cell imaging was performed for 48 h using the Nikon Biostation IM live cell imaging system. Magnification x40. Stills were taken at time 0 h (start) and 48 h (end) from movies of SF188 **(A)** and KNS42 **(B)** treated ± 10 pfu/cell oncolytic HSV. Tracking analysis of the individual cell movements over 48 h of SF188 and KNS42 were performed from live cell imaging movies using Image J with MTrack software following treatment ± oncolytic HSV **(C)**. Quantification analysis of velocity (distance/time) (**D** and **F**) and displacement (**E** and **G**) was obtained from live cell imaging using Image J with MTrack software of both cell lines (SF188 **D** and **E**, KNS42 **F** and **G**) following treatment ± oncolytic HSV. Graphs show the mean±SEM obtained from five different fields of view. ***p<0.001 by Student's two-tailed t-test.

5.2 Evaluation of the effects of oncolytic HSV on acetylated and detyrosinated tubulin

Microtubules are polymers of α- and β- tubulin dimers that bind to form stiff cylindrical hollow tubes that play a critical role in cell migration (93). Microtubules are dynamic and can undergo polymerisation (growth) and depolymerisation (shrinkage) during a process known as dynamic instability, in order to search, explore and interact with cellular organelles and target sites (93,95,99,100). Whilst the majority of microtubules undergo dynamic instability with relatively short half-life, a subgroup of more 'stable' microtubules demonstrate longer half-lives, secondary to the accumulation of post-translational tubulin modifications, including acetylation and detyrosination (93,100,111). These more 'stable' microtubules are more resistant to disassembly and can facilitate directional trafficking and preferential transportation of organelles, vesicles or proteins within the cell (93,100,112-114). The ability of oncolytic HSV to stabilise pHGG microtubules through the accumulation of post-translational tubulin modifications was evaluated by Western blotting and IF.

The expression of acetylated tubulin from pHGG cell lysates treated ± 10 pfu/cell oncolytic HSV was evaluated by Western blot (Figure 44). Oncolytic HSV treatment of SF188 increased the expression of acetylated tubulin at 24 and 48 h; however, this failed to reach statistical significance (mean±SEM intensity of band, normalised to actin: 24 h: control 0.376±0.177, HSV 0.863±0.263 p=0.209; 48 h: control 0.289±0.115, HSV 1.13±0.356 p=0.133) (Figure 44A and B). Oncolytic HSV treatment of KNS42 also revealed a trend towards increased acetylated tubulin expression by 48 h (mean±SEM intensity of band, normalised to actin: 24 h: control 0.77±0.484, HSV 0.73±0.242 p=0.946; 48 h: control 0.271±0.061, HSV 1.17±0.398 p=0.160) (Figure 44A and C).

Acetylated and detyrosinated tubulin expression from pHGG cells treated ± 10 pfu/cell oncolytic HSV was quantified by IF following 24 and 48 h treatment. Taxol was used as an internal control as it is a known microtubule

stabilising agent (175). SF188 cells treated with 10 pfu/cell oncolytic HSV resulted in a statistically significant increase in both acetylated and detyrosinated tubulin at 24 and 48 h compared to control treated cells (mean±SEM intensity normalised to control: Acetylated tubulin: 24 h: control 1±0.785, HSV 513±135 p=0.00427; 48 h: control 1±0.523, HSV 246±60.8 p<0.001; Detyrosinated tubulin: 24 h: control 1±0.983, HSV 62.4±22.2 p=0.0186; 48 h: control 1±0.397, HSV 4.5±0.594 p<0.001)(Figure 45 and 46). Expression of both acetylated and detyrosinated tubulin appeared to be increased at the 24 h time point. The effects of HSV treatment on SF188 acetylated and detyrosinated tubulin expression were more marked than the effects of 100nM taxol.

For KNS42, oncolytic HSV treatment resulted in a statistically significant increase in acetylated tubulin by 48 h when evaluated by IF (mean±SEM intensity normalised to control: Acetylated tubulin: 24 h: control 1±0.997, HSV 11.5±5.02 p=0.0672; 48 h: control 1±0.804, HSV 6038±2272 p=0.0289) (Figure 47). KNS42 appeared to be more sensitive to the effects of taxol than SF188, with statistically significant increases in both acetylated and detyrosinated tubulin noted following 24 and 48 h of treatment (mean±SEM intensity normalised to control: Acetylated tubulin: 24 h: control 1±0.997, taxol 24.8±5.8 p=0.00258; 48 h: control 1±0.804, taxol 5727±709 p=<0.001; Detyrosinated tubulin: 24 h: control 1±0.099, taxol 1.35±0.12 p=0.04; 48 h: control 1±0.084, taxol 1.81±0.34 p=0.0475) (Figure 47 and 48). Oncolytic HSV did not significantly increase KNS42 expression of detyrosinated tubulin, although a trend towards this was observed (mean±SEM intensity normalised to control: detyrosinated tubulin: 24 h: control 1±0.099, HSV 1.17±0.304 p=0.603; 48 h: control 1±0.084, HSV 96.3±90 p=0.317) (Figure 48).

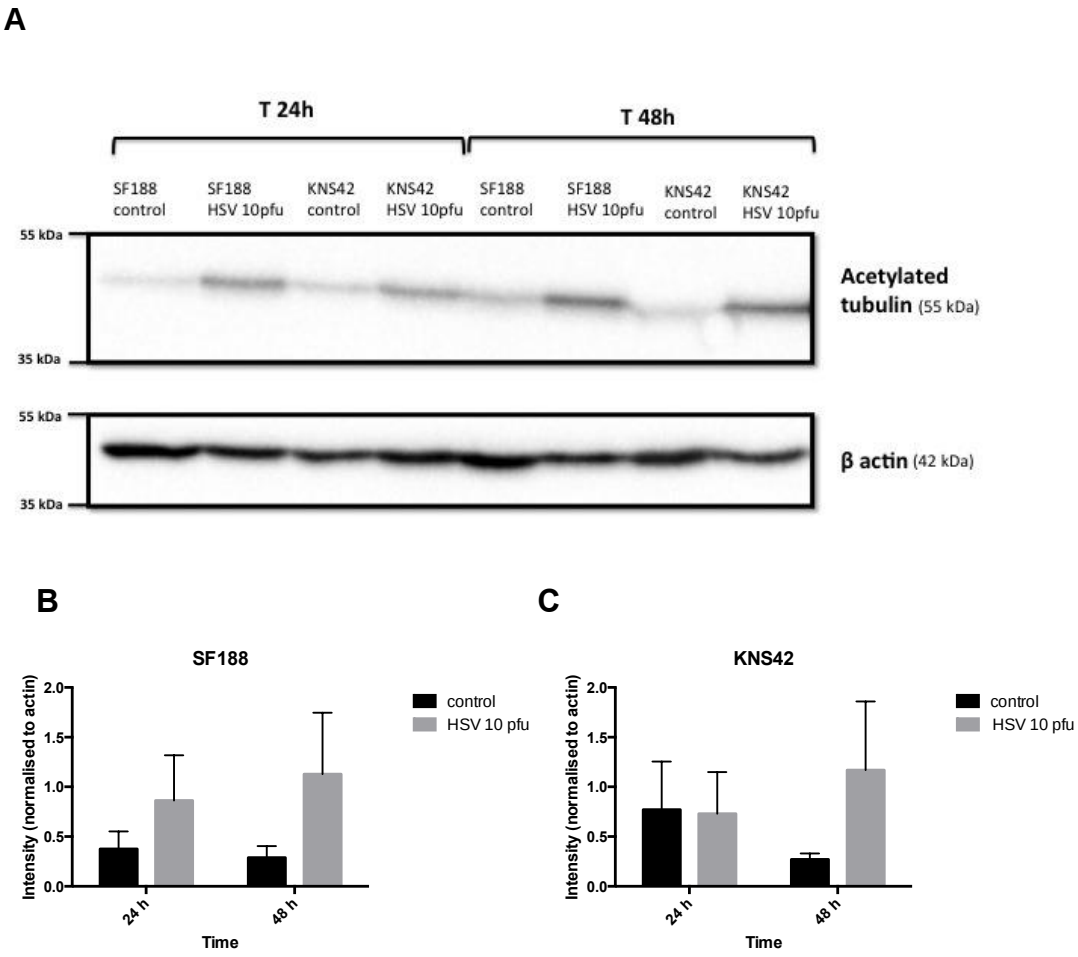

Figure 44: Western blot analysis of the effects of oncolytic HSV on pHGG acetylated tubulin expression

pHGG cell lines SF188 and KNS42 were treated ± 10 pfu/cell oncolytic HSV. Following either 24 or 48 h incubation, cell lysates were obtained. Expression of acetylated tubulin was determined by Western blotting **(A)**. Beta-actin control was included to evaluate protein loading and transfer. Intensity of the acetylated tubulin band was quantified and normalised to the β-actin control using Image J software. **(B)** Quantification of SF188 acetylated tubulin expression following 24 and 48 h treatment ± 10 pfu/cell oncolytic HSV. **(C)** Quantification of KNS42 acetylated tubulin expression following 24 and 48 h treatment ± 10 pfu/cell oncolytic HSV. Graphs show mean ± SEM of n=3 individual experiments.

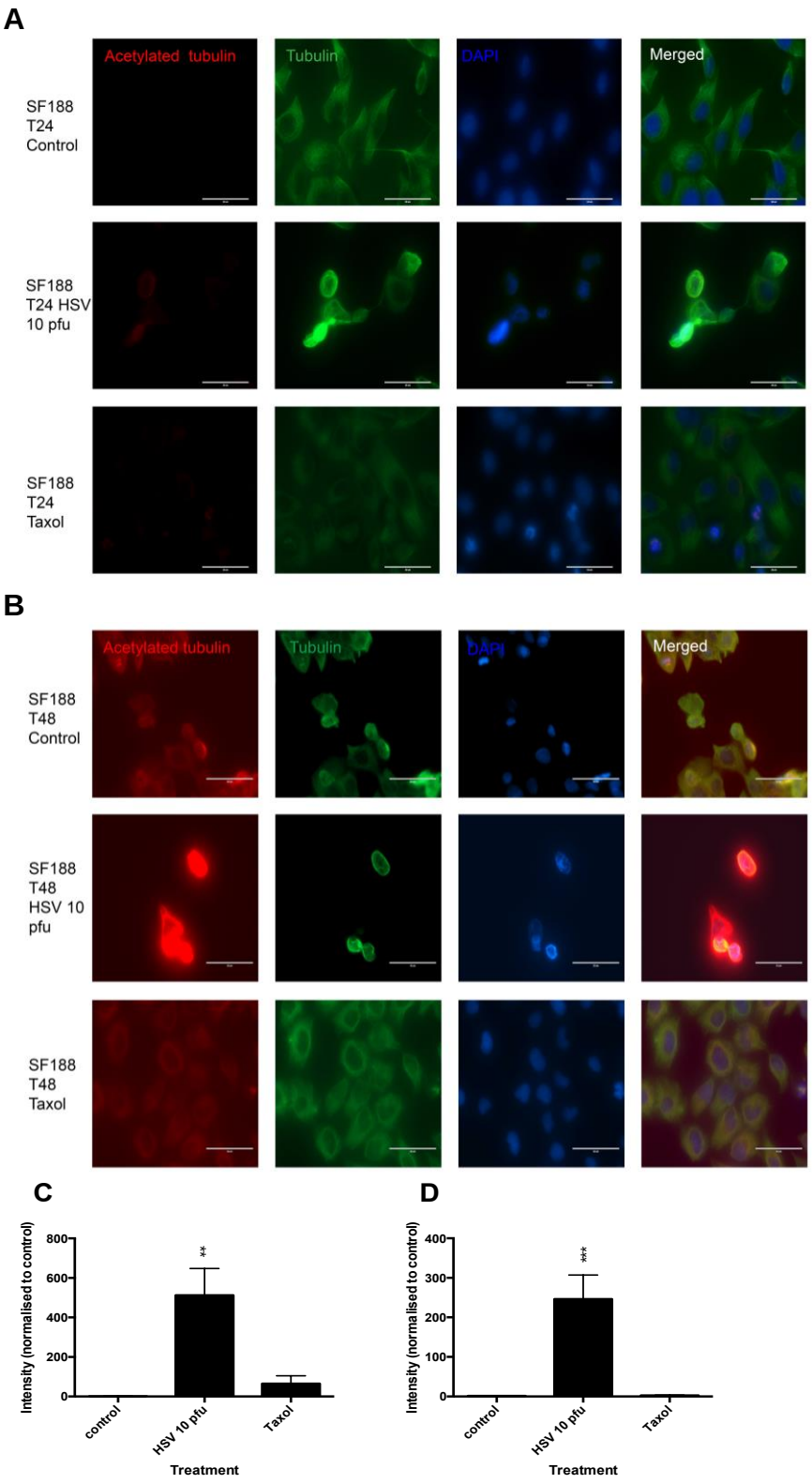

Figure 45: Evaluation of the effects of oncolytic HSV on SF188 acetylated tubulin expression by immunofluorescent labelling

$2x10^5$ cells (SF188) were grown on sterile cover slips and treated ± 10 pfu/cell oncolytic HSV or 100 nM taxol for 24 or 48 h. The effects of treatment at 24 **(A)** or 48 h **(B)** on acetylated tubulin expression were evaluated by IF labelling. Red labelling: acetylated tubulin, green labelling: tubulin, blue labelling: DAPI staining. Magnification x63. White scale bar represents 50 µm. At least 75 cells from each treatment condition were evaluated to determine the intensity of acetylated tubulin labelling normalised to the control at 24 **(C)** and 48 h **(D)**. Error bars are expressed as ±SEM. **p<0.01, ***p<0.001 by Student's two-tailed t-test.

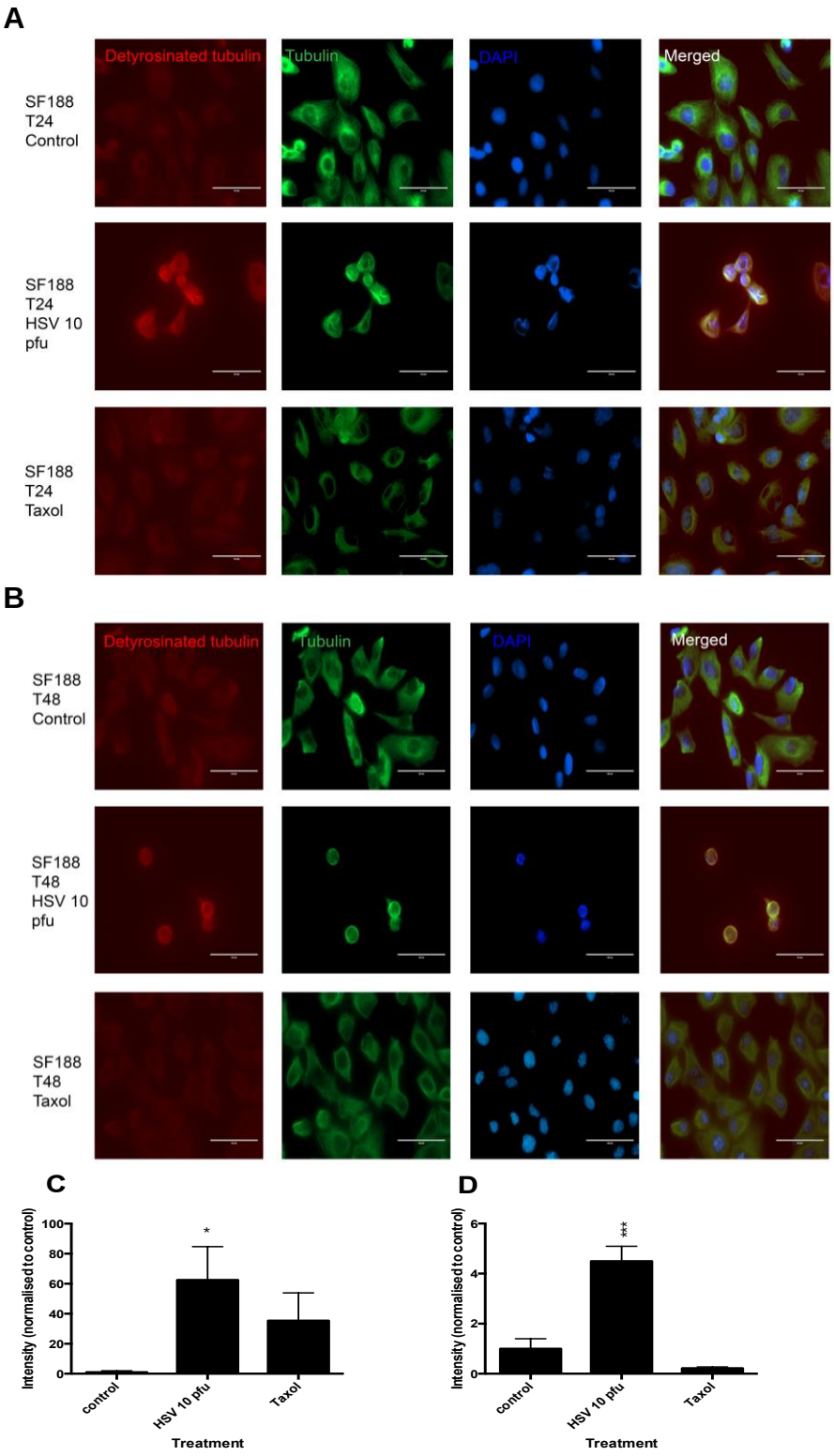

Figure 46: Evaluation of the effects of oncolytic HSV on SF188 detyrosinated tubulin expression by immunofluorescent labelling

$2x10^5$ cells (SF188) were grown on sterile cover slips and treated ± 10 pfu/cell oncolytic HSV or 100 nM taxol for 24 or 48 h. The effects of treatment at 24 **(A)** or 48 h **(B)** on detyrosinated tubulin expression were evaluated by IF labelling. Red labelling: detyrosinated tubulin, green labelling: tubulin, blue labelling: DAPI staining. Magnification x63. White scale bar represents 50 µm. At least 40 cells from each treatment condition were evaluated to determine the intensity of acetylated tubulin labelling normalised to the control at 24 **(C)** and 48 h **(D)**. Error bars are expressed as ±SEM. **p<0.01, ***p<0.001 by Student's two-tailed t-test.

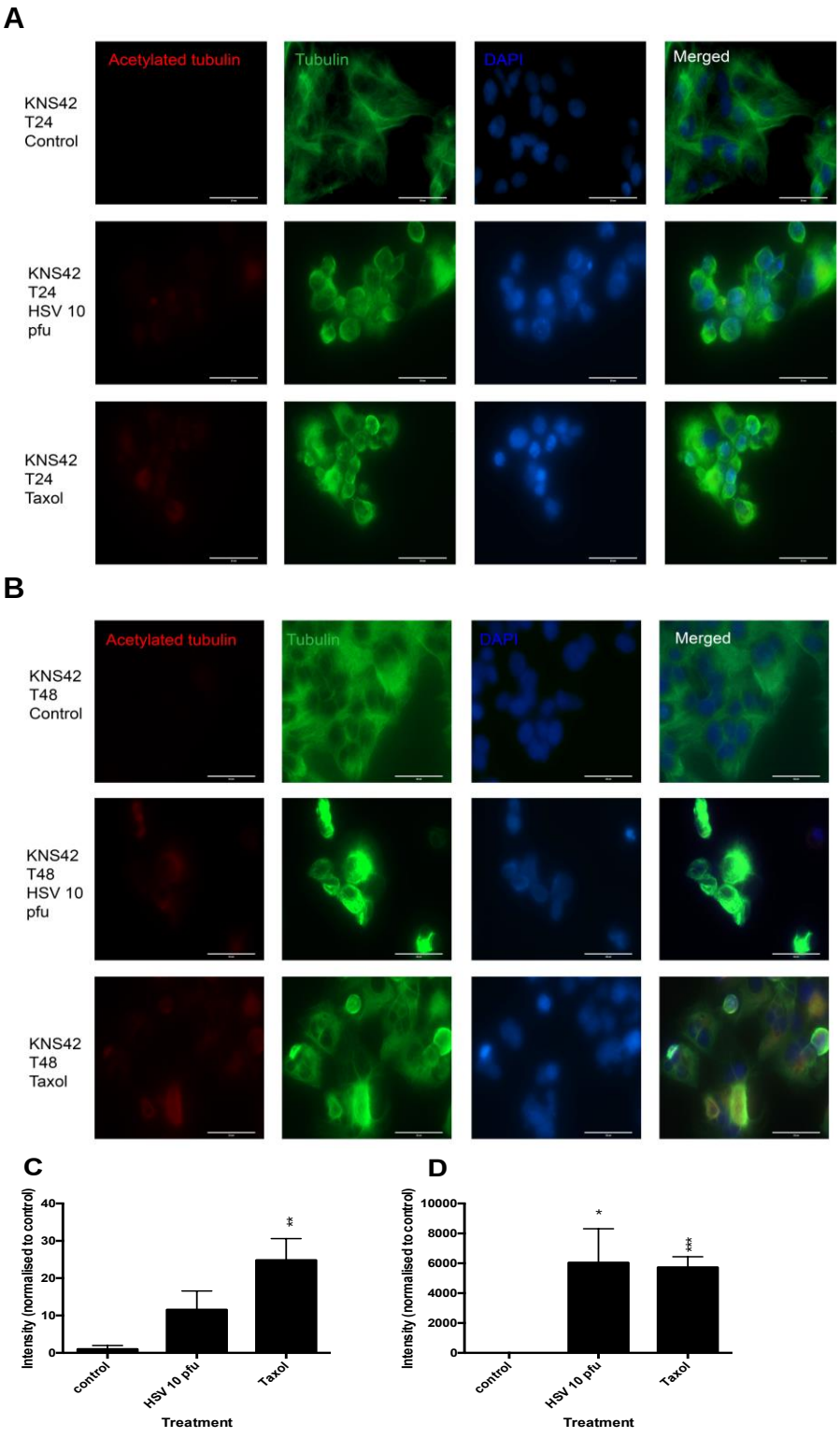

Figure 47: Evaluation of the effects of oncolytic HSV on KNS42 acetylated tubulin expression by immunofluorescent labelling

$2x10^5$ cells (KNS42) were grown on sterile cover slips and treated ± 10 pfu/cell oncolytic HSV or 100 nM taxol for 24 or 48 h. The effects of treatment at 24 **(A)** or 48 h **(B)** on acetylated tubulin expression were evaluated by IF labelling. Red labeling: acetylated tubulin, green labeling: tubulin, blue labeling: DAPI staining. Magnification x63. White scale bar represents 50 µm. At least 80 cells from each treatment condition were evaluated to determine the intensity of acetylated tubulin labelling normalised to the control at 24 **(C)** and 48 h **(D)**. Error bars are expressed as ±SEM. **p<0.01, ***p<0.001 by Student's 2-tailed t-test.

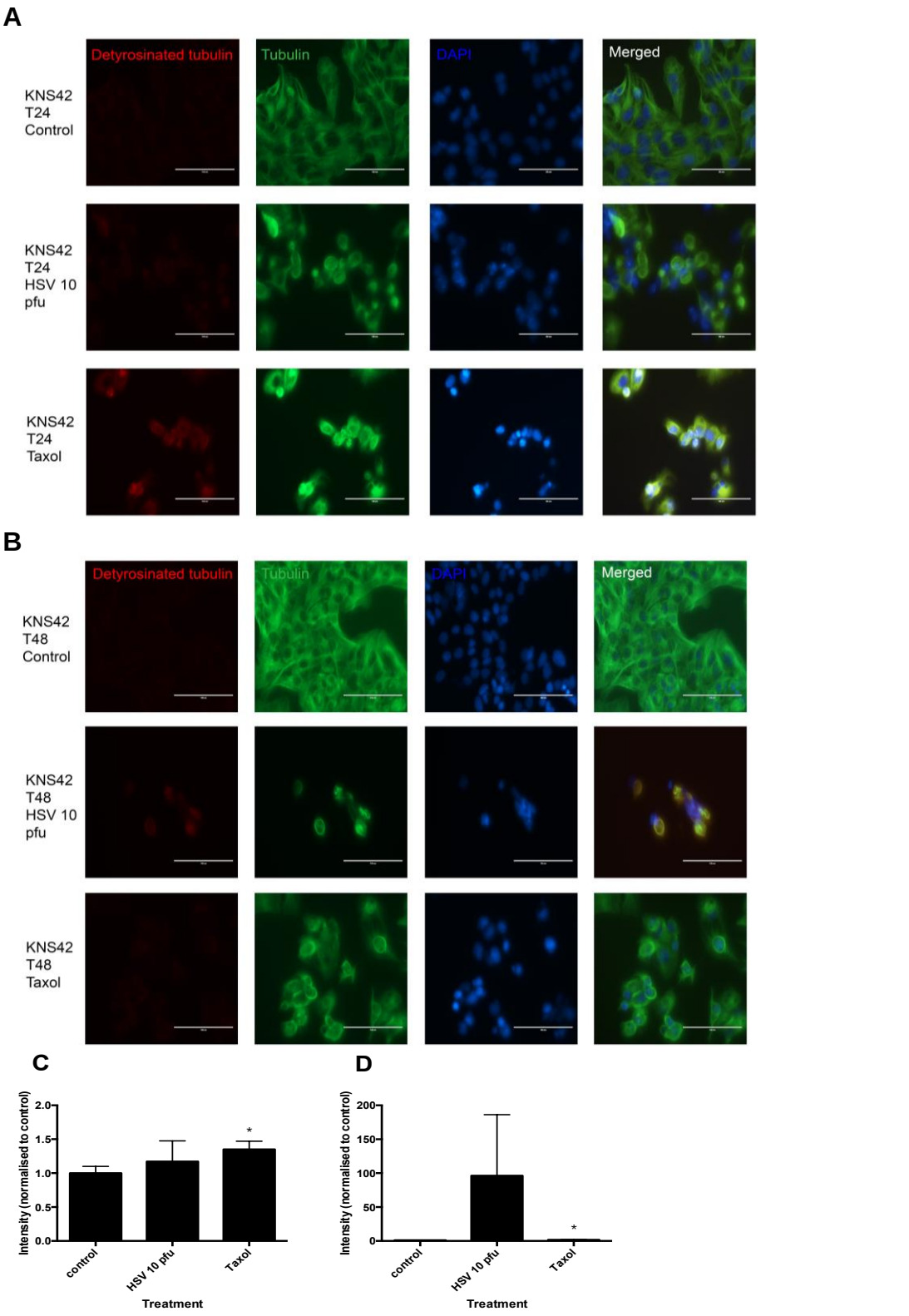

Figure 48: Evaluation of the effects of oncolytic HSV on KNS42 detyrosinated tubulin expression by immunofluorescent labelling

2x10^5 cells (KNS42) were grown on sterile cover slips and treated ± 10 pfu/cell oncolytic HSV or 100 nM taxol for 24 or 48 h. The effects of treatment at 24 **(A)** or 48 h **(B)** on detyrosinated tubulin expression were evaluated by IF labelling. Red labelling: detyrosinated tubulin, green labelling: tubulin, blue labelling: DAPI staining. Magnification x40. White scale bar represents 100 µm. At least 80 cells from each treatment condition were evaluated to determine the intensity of acetylated tubulin labelling normalised to the control at 24 **(C)** and 48 h **(D)**. Error bars are expressed as ±SEM. **P<0.01, ***P<0.001 by Student's two-tailed t-test.

5.3 Evaluation of the effects of oncolytic HSV on pHGG GSK-3 expression

GSK is a serine/threonine protein kinase that plays a key role in orchestrating cell migration through regulation of cell structure, motility, adhesion and cytoskeleton dynamics (195,202,213). The results described in chapter three highlight the importance of GSK-3 in pHGG cell migration and invasion. In a study designed to investigate the mechanism of wild-type HSV spread, HSV was shown to induce the formation of stable microtubule subsets through inactivation of GSK-3β in normal human dermal fibroblasts (311). The effects of oncolytic HSV on human cell GSK-3 expression are currently unknown. Here, for the first time, the effects of oncolytic HSV on pHGG GSK-3 expression are evaluated. Western blotting was employed to analyse the total, activated and inactivated forms of GSK-3 protein isoforms following oncolytic HSV treatment of pHGG cell lines.

Oncolytic HSV treatment of SF188 significantly increased Ser9 phosphorylated GSK-3β (inactivated form) at 24 h (mean±SEM intensity of band, normalised to actin: control 0.391±0.197, HSV 1.49±0.214 p=0.0199) (Figure 49A and B). This effect was much less marked at 48 h (mean±SEM intensity of band, normalised to actin: control 0.621±0.092, HSV 0.736±0.239 p=0.688). For KNS42, oncolytic HSV treatment resulted in a trend towards increased Ser9 phosphorylated GSK-3β at both 24 and 48 h (mean±SEM intensity of band, normalised to actin: 24 h: control 0.956±0.446, HSV 1.93±0.078 p=0.156; 48 h: control 0.457±0.12, HSV 1.2±0.495 p=0.270) (Figure 49A and C). Conversely, oncolytic HSV treatment resulted in a trend towards decreased expression of the activating tyrosine of GSK-3αβ for both pHGG cell lines at 24 and 48 h (mean±SEM SF188 intensity of band, normalised to actin: 24 h: control 1.47±0.591, HSV 0.999±0.481 p=0.574; 48 h: control 0.586±0.227, HSV 0.201±0.086 p=0.226; KNS42 intensity of band, normalised to actin: 24 h: control 2.061±0.92, HSV 1.11±0.624 p=0.446; 48 h: control 1.17±0.321, HSV 0.364±0.028 p=0.126) (Figure 50). Overall, oncolytic HSV treatment resulted in a trend towards decreased total GSK-3β expression at 24 and 48 h for both pHGG cell lines (mean±SEM SF188 intensity of band, normalised to

actin: 24 h: control 1.28±0.382, HSV 0.995±0.287 p=0.586; 48 h: control 1.23±0.167, HSV 0.636±0.273 p=0.153; KNS42 intensity of band, normalised to actin: 24 h: control 1.32±0.515, HSV 1.1±0.281 p=0.735; 48 h: control 1.61±0.508, HSV 0.992±0.368 p=0.388) (Figure 51).

Although the majority of the results described above do not reach statistical significance, they do represent a consistent trend that fits with the biological hypothesis and small differences in kinase activity may have large biological consequences. In conclusion, the trend demonstrated by the results support the hypothesis that oncolytic HSV can decrease GSK-3β activity of pHGG cells, increasing the inactive GSK-3 isoform and reducing the activating tyrosine of GSK-3αβ.

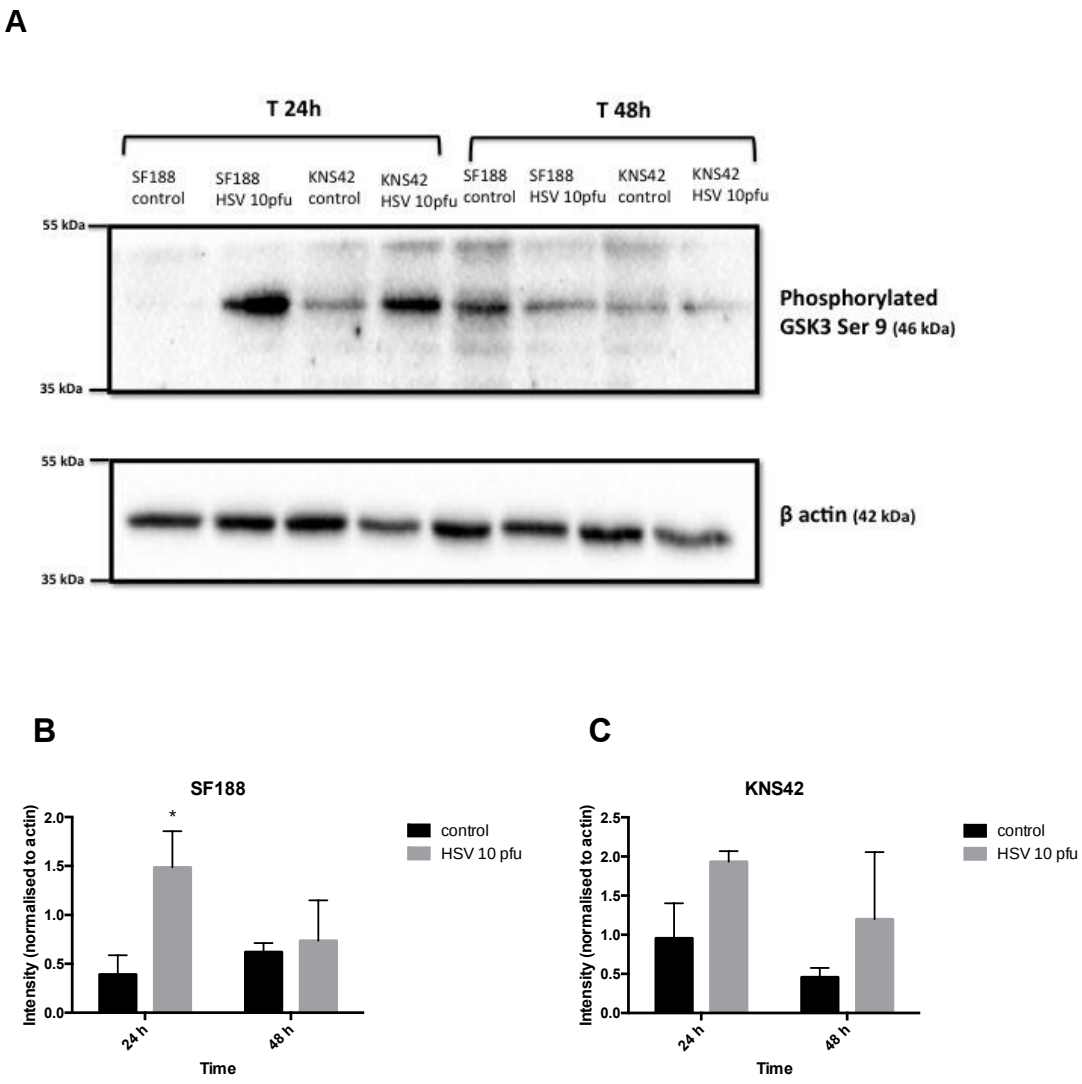

Figure 49: Western blot analysis of the effects of oncolytic HSV on pHGG phosphorylated GSK-3β Ser9

pHGG cell lines SF188 and KNS42 were treated ± 10 pfu/cell oncolytic HSV. Following either 24 or 48 h incubation, cell lysates were obtained. Expression of phosphorylated GSK-3β Ser9 (inactivated form) was determined by Western blotting **(A)**. Beta-actin control was included to evaluate protein loading and transfer. Intensity of the phosphorylated GSK-3β Ser9 band was quantified and normalised to the β-actin control using Image J software. **(B)** Quantification of SF188 phosphorylated GSK-3β Ser9 expression following 24 and 48 h treatment ± 10 pfu/cell oncolytic HSV. **(C)** Quantification of KNS42 phosphorylated GSK-3β Ser9 expression following 24 and 48 h treatment ± 10 pfu/cell oncolytic HSV. Graphs show mean ± SEM of n=3 individual experiments. *p<0.05 by Student's two-tailed t-test.

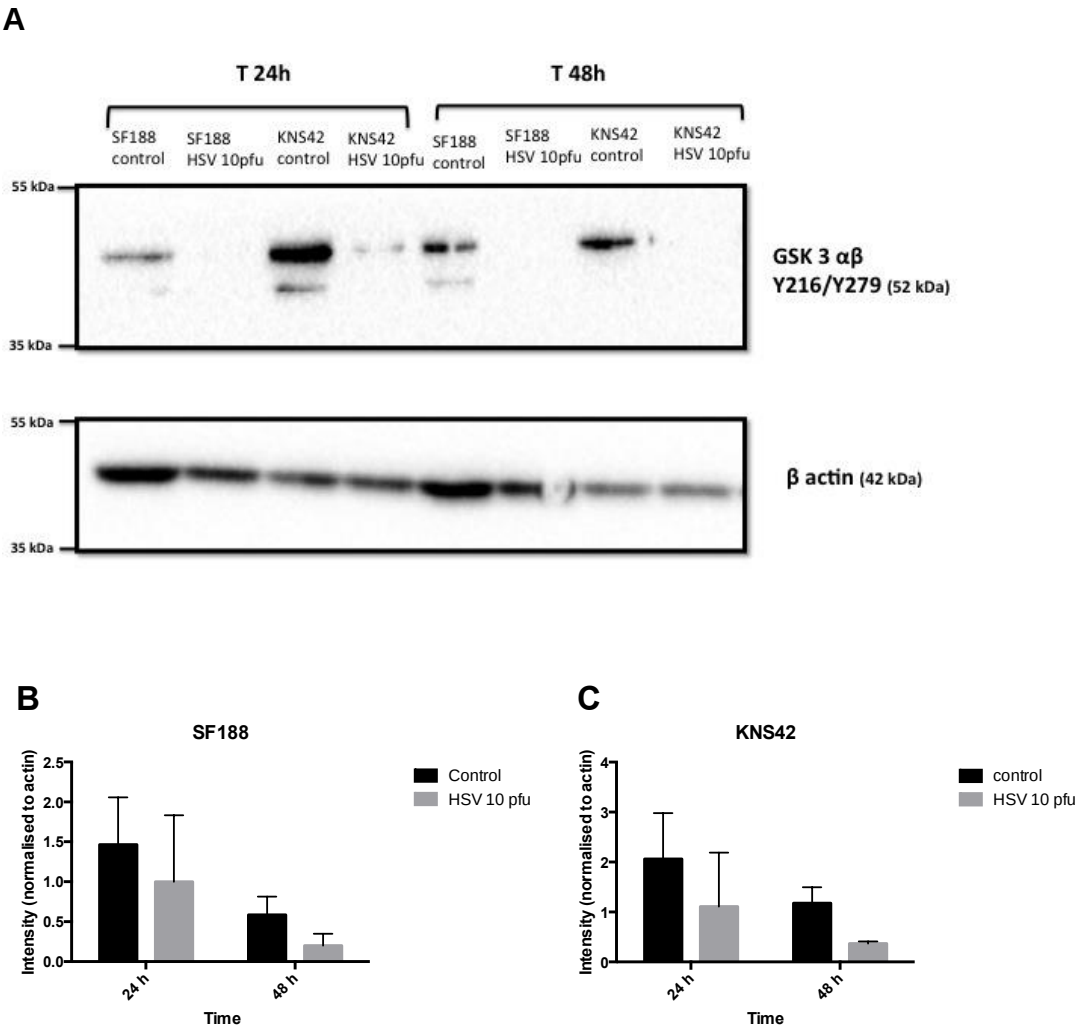

Figure 50: Western blot analysis of the effects of oncolytic HSV on pHGG Tyr216/279 phosphorylated GSK3αβ

pHGG cell lines SF188 and KNS42 were treated ± 10 pfu/cell oncolytic HSV. Following either 24 or 48 h incubation, cell lysates were obtained. Expression of Tyr216/279 phosphorylated GSK3αβ (active form) was determined by Western blotting **(A)**. β-actin control was included to evaluate protein loading and transfer. Intensity of the Tyr216/279 phosphorylated GSK3αβ band was quantified and normalised to the β-actin control using Image J software. **(B)** Quantification of SF188 Tyr216/279 phosphorylated GSK3αβ expression following 24 and 48 h treatment ± 10 pfu/cell oncolytic HSV. **(C)** Quantification of KNS42 Tyr216/279 phosphorylated GSK3αβ expression following 24 and 48 h treatment ± 10 pfu/cell oncolytic HSV. Graphs show mean ± SEM of n=3 individual experiments.

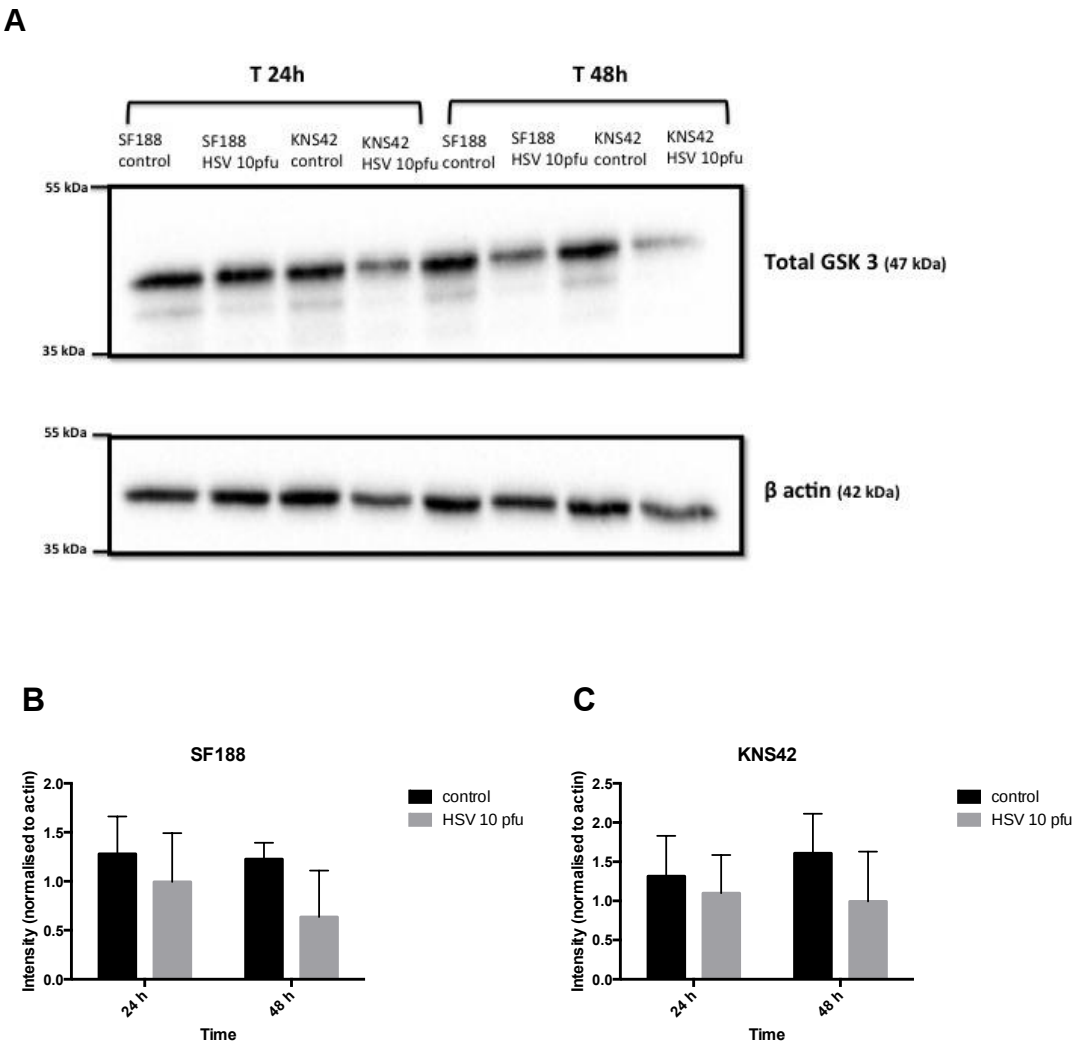

Figure 51: Western blot analysis of the effects of oncolytic HSV on pHGG total GSK3β

pHGG cell lines SF188 and KNS42 were treated ± 10 pfu/cell oncolytic HSV. Following either 24 or 48 h incubation, cell lysates were obtained. Expression of total GSK3β was determined by Western blotting **(A)**. β-actin control was included to evaluate protein loading and transfer. Intensity of the total GSK3β band was quantified and normalised to the β-actin control using Image J software. **(B)** Quantification of SF188 total GSK3β expression following 24 and 48 h treatment ± 10 pfu/cell oncolytic HSV. **(C)** Quantification of KNS42 total GSK3β expression following 24 and 48 h treatment ± 10 pfu/cell oncolytic HSV. Graphs show mean ± SEM of n=3 individual experiments.

5.4 Evaluation of the effects of oncolytic HSV on APC localisation

GSK-3 plays an important role in regulating the polarity of migrating cells (93,213). Polarity cues result in the localised inhibition of GSK-3, which promotes APC to cluster at microtubule plus ends at the leading edge of cells, controlling the direction of movement (93,110). Given that the results in section 5.3 suggest that oncolytic HSV decreases GSK-3β activity in pHGG cells, the effects of virus treatment on APC distribution were evaluated by IF.

SF188 cells cultured in normal medium demonstrated a clear localisation of APC to the leading edge of cells (Figure 52A). This effect was not notable for KNS42; however, this may be a reflection of the fact that this cell line was much less motile than SF188 (Figure 52B). Following treatment with oncolytic HSV, SF188 cells demonstrated diffuse staining of APC throughout the cytoplasm, with a clear loss of APC clustering to a leading edge (Figure 52A). A similar diffuse distribution of APC was seen in SF188 cells treated with the GSK-3 inhibitor BIO.

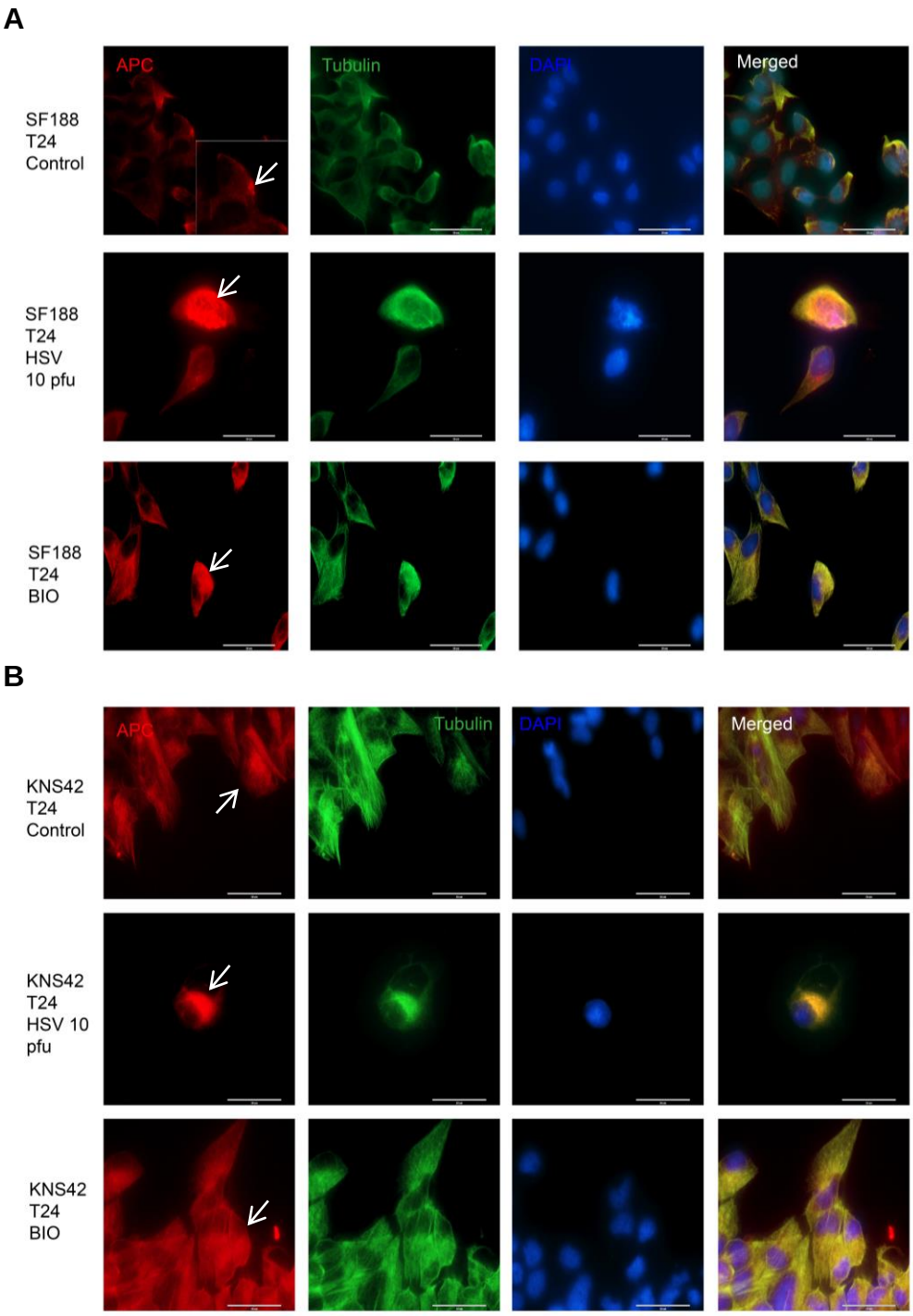

Figure 52: The effects of oncolytic HSV on pHGG APC localisation
$2x10^5$ cells (SF188 **(A)** or KNS42 **(B)**) were grown on sterile cover slips and treated ± 10 pfu/cell oncolytic HSV or 5 μM BIO for 24 h. The effects of treatment at 24 h on APC localisation (white arrows) were evaluated by IF labelling. Red labeling: APC, green labeling: tubulin, blue labeling: DAPI staining. Magnification x63. White scale bar represents 50 μm.

5.5 Evaluation of the effects of oncolytic HSV on DOCK3

DOCK3 is a protein predominantly expressed in the CNS (390) that can drive mesenchymal cancer cell migration and movement (80,391,392). DOCK3 has also been shown to be able to bind and inactivate GSK-3β, by inducing GSK-3 phosphorylation at Ser9 (393). Given that the results in section 5.3 suggest that oncolytic HSV can decrease GSK-3β activity of pHGG cells by increasing the inactive GSK-3 isoform (GSK-3β Ser9), the effects of virus treatment on DOCK3 expression were evaluated.

DOCK3 protein expression was initially investigated by Western blotting of pHGG cell lysates treated ± oncolytic HSV. DOCK3 protein was undetectable in pHGG cell lines using this technique. Further investigation of DOCK3 expression in pHGG cells treated ± oncolytic HSV was carried out by IF. IF labelling revealed increased detection of DOCK3 in virus-treated cells when compared to controls (Figure 53).

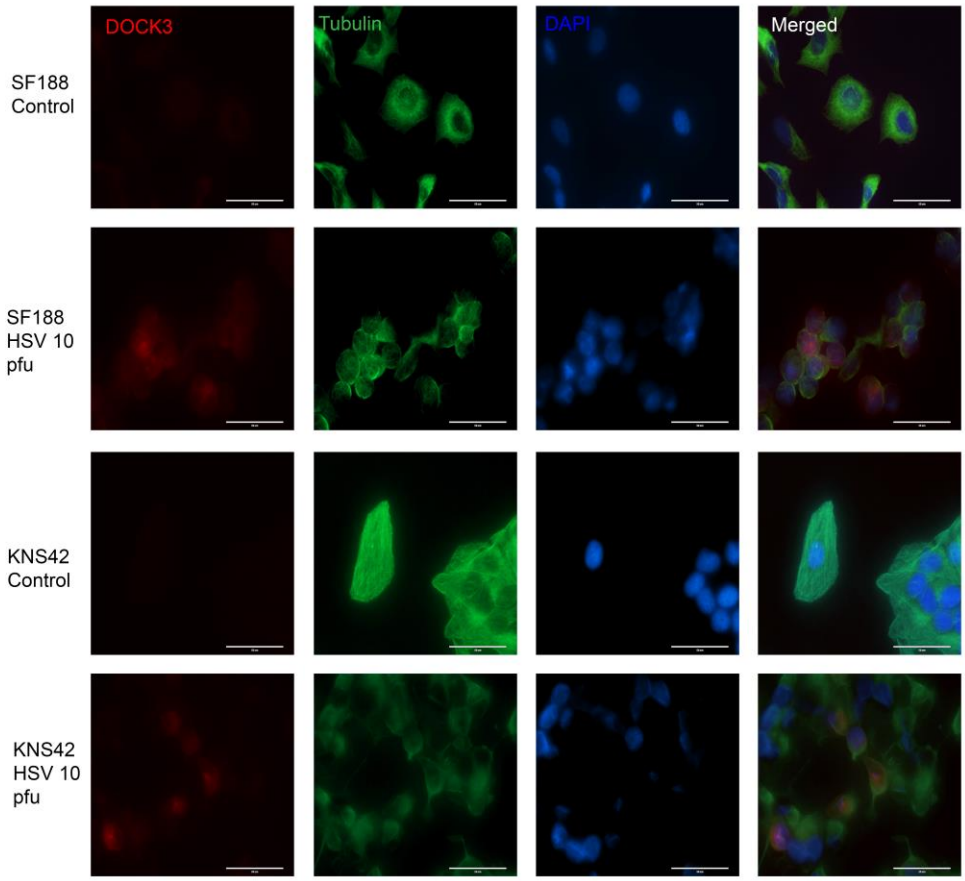

Figure 53: Evaluation of the effects of oncolytic HSV on pHGG DOCK3 by immunofluorescent labelling

$2x10^5$ cells (SF188 or KNS42) were grown on sterile cover slips and treated ± 10 pfu/cell oncolytic HSV. The effects of treatment at 24 h on DOCK3 expression were evaluated by IF labelling. Red labelling: DOCK3, green labelling: tubulin, blue labelling: DAPI staining. Magnification x63. White scale bar represents 50 µm.

5.6 Discussion

The results contained within this thesis demonstrate that oncolytic HSV can inhibit both the *in vitro* migration and invasion of pHGG and DIPG cells. In this chapter, live cell imaging confirmed that oncolytic HSV can alter the movement of individual pHGG cells, resulting in reduced motility and a loss of cell polarity. Both cell lines investigated altered their morphology following oncolytic HSV treatment. SF188 cells exhibited the loss of distinct leading and trailing edges and developed protrusive tails that were unable to fully retract. KNS42 cells generally adopted a rounded morphology and developed multiple thin-branching protrusions following virus treatment. These observations were much more marked for SF188 than KNS42, reflecting the fact that SF188 is a more migratory and motile cell line. These results are highly novel and demonstrate the ability of an OV to alter pHGG movement and morphology.

Oncolytic HSV treatment stabilised pHGG microtubules, as demonstrated by the accumulation of post-translational tubulin modifications. Over 48 h, oncolytic HSV treatment led to increased acetylated and detyrosinated tubulin expression in pHGG cell lines when compared to controls. Again, these observations were generally more marked for the highly migratory cell line SF188, compared to KNS42.

In addition, oncolytic HSV resulted in a trend towards decreased GSK-3β activity in pHGG cells following treatment. GSK-3β is a protein kinase that plays a critical role in regulating cell motility, adhesion and cytoskeleton dynamics. Treatment with oncolytic HSV resulted in a tendancy towards increased Ser9 phosphorylated GSK-3β (inactive form) and a trend towards a reduction in the activating tyrosine of GSK-3αβ. Furthermore, oncolytic HSV treatment of SF188 resulted in a clear loss of APC clustering to the leading edge of the cell. Instead, virus treatment resulted in the diffuse redistribution of APC throughout the cytoplasm. Given that APC localisation plays a critical role in controlling the direction of cell movement, this diffuse

redistribution following oncolytic HSV treatment may explain why the virus-treated cells lost their polarity.

Finally, a tendancy towards increased DOCK3 expression was observed in virus-treated pHGG cells compared to controls when evaluated by IF labelling. Given that DOCK3 is able to bind and inactivate GSK-3β, inducing GSK-3 phosphorylation at Ser9 (393), this observation again demonstrates the potential of oncolytic HSV to alter molecular pathways critical for cell migration and movement. In summary, the results obtained here begin to outline the mechanisms underlying the ability of oncolytic HSV to prevent pHGG cell migration and invasion.

The cell cytoskeleton is composed of highly dynamic adaptable structures that allow a cell to: modulate its shape; migrate; divide; organise intracellular transportation and exert mechanical strength (86,309,394). Viruses have evolved the ability to hijack components of the cytoskeleton in order to facilitate their replication cycle and spread. In doing so, virus infection of a cell can result in the rearrangement of cytoskeletal filaments and influence overall cytoskeletal dynamics (308,309,395). The interaction of HSV with the host cytoskeleton has been well studied (309). HSV replicates and assembles nucleocapsids within the nuclei of infected host cells and, thus, successful replication utilises an effective strategy to transport the virus to and away from the nucleus through the cytoplasm (309). In order to achieve this, HSV makes use of microtubules to provide intracellular tracks for efficient bidirectional transportation of virion particles to and from the nucleus (308,309,396). Microtubules are polarised structures, with highly dynamic plus ends, capable of polymerising (growing) and depolymerising (shrinking) during the process of dynamic instability and relatively stable minus ends, which are associated with the MTOC (93,95,309). Molecular motors associated with microtubules allow the bidirectional trafficking of virus cargo, with plus end directed motors called kinesins directing transport to the cell periphery and minus end motors known as dyneins facilitating movements towards the cell centre (308,309,396-398).

The dynamics and distribution of the microtubules are governed by multiple factors including: post-translational modification of tubulin; MAPs; and GTP hydrolysis (309,399). Herpes simplex family viruses are capable of inducing the acetylation of tubulin, a known marker of microtubule stabilisation, early during the infection of host cells (394,400). Microtubule acetylation is also associated with kinesin binding and may enhance microtubule motor-dependent trafficking (114,395). Viruses such as HSV may have evolved to rely upon such post-translational modifications to identify particular subsets of microtubules that lead to specific cellular destinations (114). Given that the rate of growth of microtubules *in vivo* is slower than the rate of vesicle transport (approximately 0.2 μm/s versus 2 μm/s), viruses may preferentially rely upon stable, ready-formed microtubule tracks for transportation and these stable microtubule networks may be identifiable to virus through the accumulation of specific post-translational modifications (114,401-403).

It is postulated that dynamic microtubules are required for cell migration (404-406). The accumulation of post-translational modifications such as acetylated tubulin, that mark microtubules as stable, have been shown to reduce focal adhesion turnover and subsequent cell migration (407). Additionally, suppression of microtubule dynamics by drugs such as paclitaxel, appears to inhibit cell locomotion by interfering with the ability of the migrating cell to retract its tail (406). As oncolytic HSV appears capable of stabilising microtubules, through accumulation of post-translational modifications such as acetylated and detyrosinated tubulin in pHGG cells, this may explain the reduction in pHGG motility, migration and invasion observed. Furthermore, microtubule stabilisation may also account for the inability of SF188 cells to fully retract their tails following treatment with oncolytic HSV, again contributing to the overall reduction in cell motility.

Work by Naghavi *et al.* has explored the mechanism by which wild-type HSV-1 can manipulate microtubule networks in primary human cell lines (311). The authors demonstrate that HSV-1 infection induces microtubule stabilisation through accumulation of acetylated tubulin and that this involves GSK-3β inactivation by the viral serine/threonine kinase, Us3 (311). Us3

appears to be central for HSV spread and coordinates microtubule regulation of the host cell (311,408,409). In keeping with the work of Naghavi *et al*., the results contained within this chapter suggest that oncolytic HSV is capable of decreasing GSK-3β activity in pHGG cell lines, through increasing the inactive form of GSK-3β (Ser9 phosphorylated GSK-3β). Although the exact mechanism by which this is achieved by the OV remains unclear, this GSK-3 inactivation may facilitate microtubule stabilisation of pHGG cell lines. Further experiments are required to prove this hypothesis and to fully determine the mechanism by which oncolytic HSV inhibits GSK-3β activity.

One potential mechanism by which oncolytic HSV may inhibit GSK-3β activity in pHGG cells involves DOCK3. DOCK3 is one of 11 members of the DOCK family of proteins that, alongside multiple cellular functions, regulate the actin cytoskeleton, cell adhesions and migration (80). DOCK3 has been shown to promote membrane recruitment of GSK-3β, binding and inactivating it through Ser9 GSK-3β phosphorylation (393). Given that oncolytic HSV treatment appears to be associated with an increase in DOCK3 expression within pHGG cells, it is possible that elevated DOCK3 may be able to influence the activity of GSK-3β. One potential hypothesis, which remains the subject of future work, is that elevated levels of DOCK3 may contribute towards the increase in Ser9 phosphorylation of GSK-3β seen in pHGG cells following oncolytic HSV treatment.

Work by Etienne-Manneville and Hall has highlighted the importance of GSK-3β in the determination of cell polarity (110). Cell polarity is essential in migration and is required to generate a front-rear axis (87). The authors demonstrated that phosphorylation of GSK-3β at the leading edge of a migrating cell results in the interaction of APC with microtubule plus ends, promoting directional cell protrusion (110). This localisation of inactive GSK-3β and consequent APC clustering appears to be critical to cell polarity (110). SF188 cells treated with normal medium demonstrated clear localisation of APC to the leading edge; however, following treatment with oncolytic HSV, APC was diffusely distributed throughout the cytoplasm. This

observation highlights the importance of functionally active GSK-3β within pHGG cells, as global inhibition of GSK-3β by oncolytic HSV appears to prevent localised GSK-3β inactivation and APC clustering. Subsequent loss of cell polarity may explain why this cell line demonstrated a marked and significant reduction in both migration and invasion following oncolytic HSV infection.

It is well established that GSK-3β regulates cell migration, influencing dynamics of the cytoskeleton, microtubule remodelling, cell polarity and cell-ECM adhesions (213). The results within this thesis suggest that GSK-3β plays a key role in pHGG cell migration and invasion. Chapter three highlights that pharmacological inhibition of GSK-3β with the known inhibitors LiCl and BIO, significantly reduces pHGG migration and invasion. Furthermore, it appears that oncolytic HSV, also capable of significantly inhibiting pHGG migration and invasion, inactivates GSK-3β. Global GSK-3β inactivation may facilitate microtubule stabilisation of pHGG cell lines and may account for the diffuse redistribution of APC, preventing the formation of a polarised cell axis.

In conclusion, oncolytic HSV treatment resulted in changes in pHGG cell morphology, motility, polarity and microtubule dynamics and this may, in part, be governed by inhibition of GSK-3β. The results documented within this chapter are highly novel and have not previously been reported: they begin to document the molecular mechanisms by which OV such as HSV1716 can inhibit pHGG cell migration and invasion.

Chapter 6: Development of an *in vivo* model of glioma invasion

6.1 Introduction

pHGG and DIPG are highly invasive tumours associated with poor survival outcomes and new treatments that effectively target brain tumour invasion are very much needed. Unfortunately, compared to adult HGG, there is a paucity of robust *in vivo* models of pHGG and DIPG available for drug testing. Orthotopic xenotransplantation of pHGG or DIPG cells into mice has been successfully used as a pre-clinical tool (29,61-63).

Within this thesis, the anti-migratory and anti-invasive effects of two GSK-3 inhibitors, LiCl and BIO, and oncolytic HSV have been demonstrated using 2D and 3D *in vitro* models. Within this chapter, the ability of oncolytic HSV to block glioma invasion and infiltration *in vivo* is explored in two separate mouse models. First, the ability of oncolytic HSV to inhibit the invasion and infiltration of GL261-Luc intracranial tumours is evaluated in a syngeneic orthotopic mouse model of glioma. Second, the ability of oncolytic HSV to improve survival and reduce invasion and infiltration of HSJD-DIPG-007 cells in an orthotopic xenograft model of DIPG is investigated. These experiments form part of ongoing efforts to develop an effective *in vivo* model of glioma invasion, in order to effectively screen novel anti-invasive therapies for paediatric brain tumours.

6.2 Evaluation of the anti-invasive effects of oncolytic HSV in an *in vivo* high grade glioma tumour model

The ability of the pHGG cell line SF188 to establish orthotopic xenografts in Balb/c nude mice was evaluated. The SF188 cell line was transfected with luciferase to allow for bioluminescence imaging of established intracranial tumours. $2.5x10^5$ cells were intracranially injected; however, unfortunately tumours failed to establish, as confirmed by minimal luminescence signal detection at 40 days-post tumour implantation.

In the absence of an orthotopic xenograft model of pHGG, the well-established GL261 mouse model of glioma was considered as a suitable alternative. GL261 cells contain several molecular biological alterations seen in human glioma (410). The GL261 model has a high tumour-take rate with survival time proportionate to the number of cells injected: following intracranial injection of $1x10^5$ GL261 cells, median survival is reported to be approximately 32.5±5.3 days (410,411). The results in chapter four confirm that oncolytic HSV is capable of significantly reducing GL261-Luc migration (Figure 20) and invasion (Figure 26) and GL261-Luc cells appear to be resistant to the cytotoxic effects of oncolytic HSV when investigated over 48 h *in vitro* (Figure 29).

One major drawback of the GL261 mouse model of glioma is that GL261 tumours have limited, if any, infiltration *in vivo*. Pellegatta *et al.* state that intracranial tumours of adherent cell GL261 in C57BL/6 mice form 'non-infiltrating tumours bearing little resemblance to primary mouse glioma' (411). The authors demonstrate that intracranial tumours of GL261 neurospheres however can form tumours that display increased infiltration *in vivo* (411). On the other hand, Szatmári *et al*. charachterised the GL261 tumour model for experimental glioblastoma therapy and showed that 'intracranial tumours had a rapid growth rate with slightly invasive growth pattern' (410). Within this thesis, the GL261 cells used correspond to adherent cell GL261, and therefore this is identified as a potential limitation of the mouse model.

GL261-Luc tumours were established in the brains of two groups (n=8 per group) of C57BL/6 mice. For one group of mice, GL261-Luc cells were premixed with oncolytic HSV at 10 pfu/cell prior to intracranial injection. Four mice per group were sacrificed on day 15 and the remainders on day 25 in order to evaluate the invasion and infiltration of the established tumours into the surrounding brain at different time points.

Analysis of the brains harvested from the control group of mice, injected with untreated GL261-Luc cells, revealed a moderate degree of infiltrative tumour growth at day 15 and 25 by H&E staining (Figure 54-56). By day 15, single cells were seen starting to migrate and invade away from the tumour edge and lymphocyte infiltration was noted at the tumour migrating front (Figure 54). By day 25, tumours again were noted to demonstrate a moderate degree of infiltration into the normal surrounding brain tissue (Figure 55). Heterogeneity was noted within the tumours, with one tumour sample clearly displaying a non-infiltrative border, despite some tumour infiltration and single cell migration and invasion away from all the other tumour edges (Figure 55). Tumour cells were seen to migrate and invade in the proximity of white matter tracts (Figure 56), a well-defined characteristic pattern of HGG migration (24,72,73), however, this may also represent the tumour expending towards the myelin tracts during growth.

Unexpectantly, tumours were not detected by day 25 in brains harvested from mice that received intracranial GL261-Luc premixed with oncolytic HSV (Figure 57 and 58). Consequently, the effects of oncolytic HSV on glioma invasion could not be evaluated within this experiment. Examination of the H&E stained sections of mouse brains injected with tumour cells plus HSV identified multiple sites of inflammation, with perivascular clustering of lymphocytes. Interestingly, these localised inflammatory changes were also noted within the brains of control group mice treated with GL261-Luc cells alone (Figure 57). These changes were not noted within normal mouse brains. Finally, one section obtained from a mouse brain injected with GL261-Luc cells premixed with oncolytic HSV revealed evidence of a local inflammatory reaction along the potential injection tract (Figure 58).

Unfortunately, tumour growth was not evaluated by bioluminescent imaging throughout this experiment. As a result, no conclusions can be drawn as to whether GL261-Luc cells premixed with oncolytic HSV formed tumours which were cleared as a result of virus treatment or whether this group of mice failed to grow tumours in the first instance, due to premixing of the virus with the GL261-Luc cells.

A

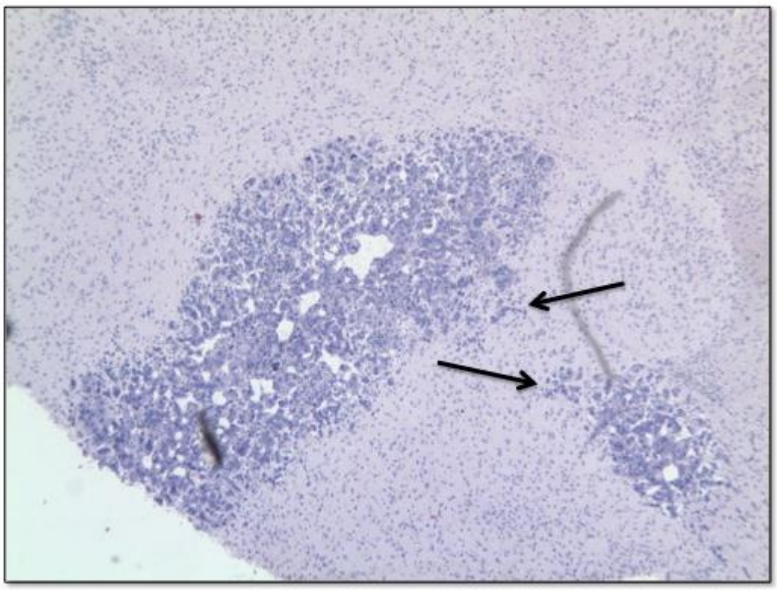

B

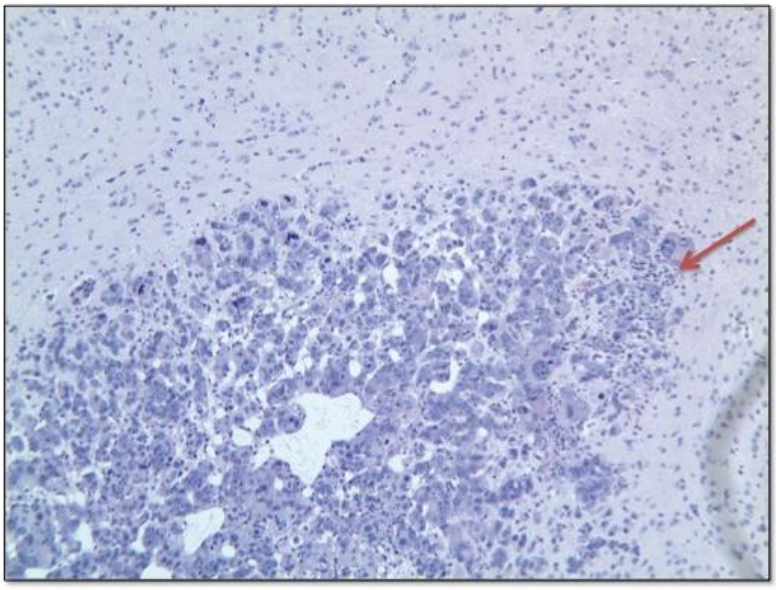

Figure 54: Evaluation of the *in vivo* invasive behavior of GL261-Luc tumours on day 15

$5x10^4$ GL261-Luc cells in 2 µl PBS were stereotactically injected into the brains of 6-8-week-old C57BL/6 mice. Mice were sacrificed on day 15-post injection and brains were immediately harvested into 4 % PFA. Brains were then sliced into coronal sections, embedded in paraffin and sectioned to 4 microns thick. Tissue sections were stained with H&E. **(A)** Black arrows point to the sites of single tumour cells demonstrating migration and invasion away from day 15- established GL261-Luc tumours. Image taken at x5 magnification using the SPOT Insight camera and Leitz DMRB microscope. **(B)** Red arrow points to a site of lymphocyte infiltration at the invading edge of a day 15-established GL261-Luc tumour. Image taken at x10 magnification using the SPOT Insight camera and Leitz DMRB microscope.

A

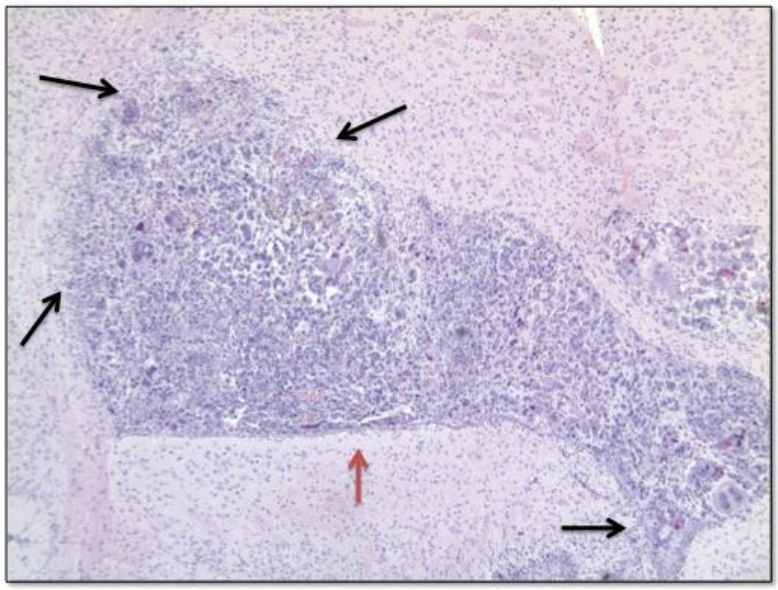

B

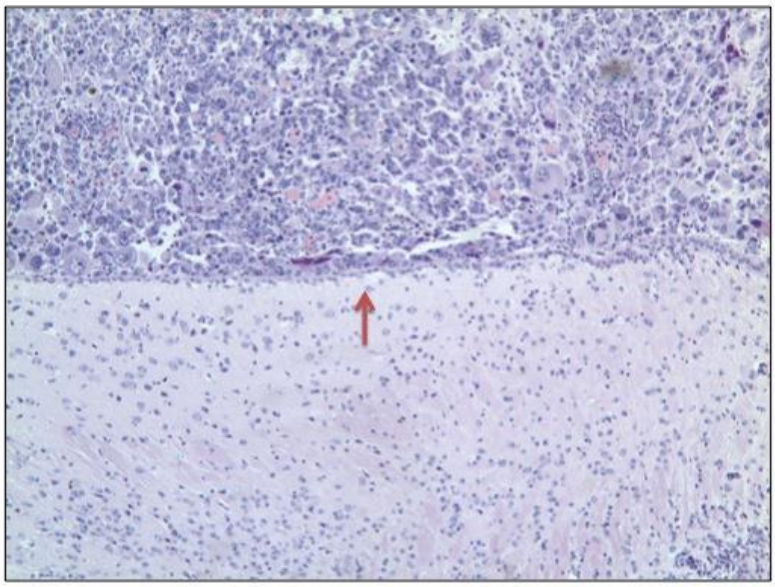

Figure 55: Evaluation of the *in vivo* invasive behavior of GL261-Luc tumours on day 25

$5x10^4$ GL261-Luc cells in 2 µl PBS were stereotactically injected into the brains of 6-8-week-old C57BL/6 mice. Mice were sacrificed on day 25-post injection and brains were immediately harvested into 4 % PFA. Brains were then sliced into coronal sections, embedded in paraffin and sectioned to 4 microns thick. Tissue sections were stained with H&E. **(A)** Black arrows point to the sites of tumour cell infiltration into the normal surrounding mouse brain in day 25-established GL261-Luc tumours. Image taken at x5 magnification using the SPOT Insight camera and Leitz DMRB microscope. (**A** and **B**) Red arrow points to the edge of the same day 25 established GL261-Luc tumour that appears to be non-infiltrative and has a distinct well defined border. Image taken at x10 magnification using the SPOT Insight camera and Leitz DMRB microscope.

A

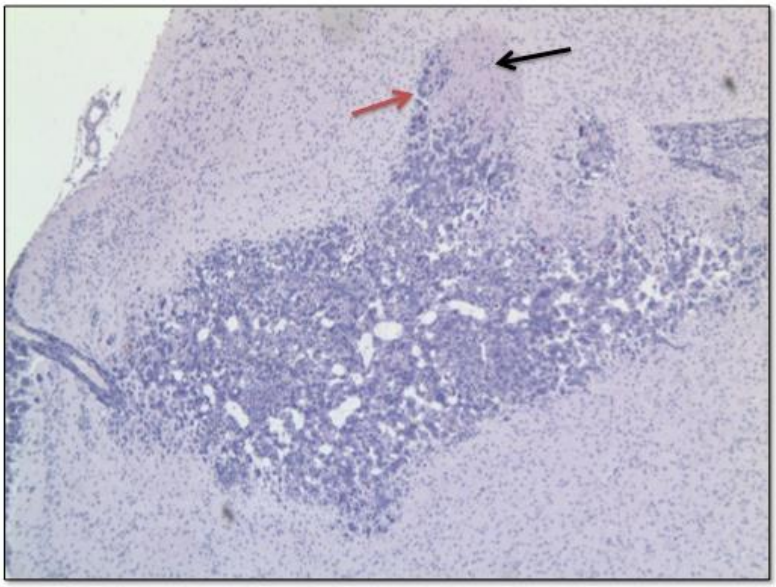

B

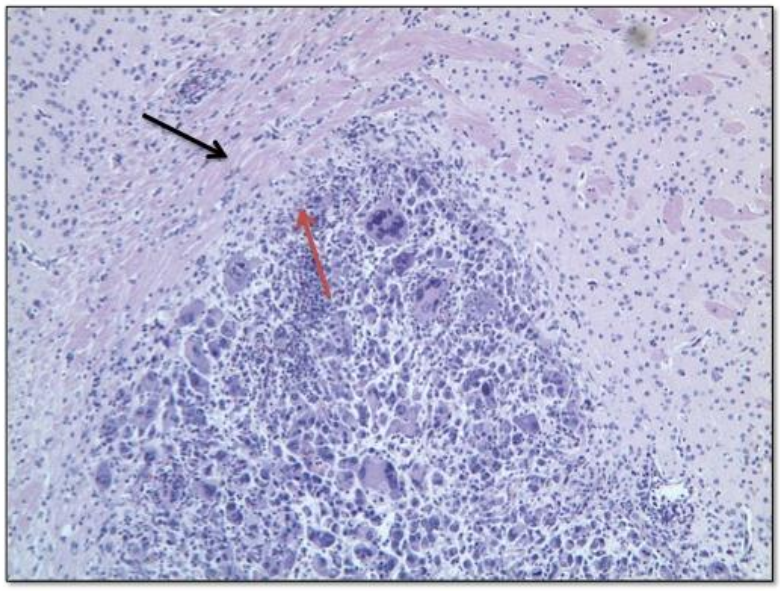

Figure 56: GL261-Luc tumour cells can be seen migrating and invading along white matter tracts.
$5x10^4$ GL261-Luc cells in 2 µl PBS were stereotactically injected into the brains of 6-8-week-old C57BL/6 mice. Mice were sacrificed on day 15- (A) or day 25- (B) post injection and brains were immediately harvested into 4 % PFA. Brains were sliced into coronal sections, embedded in paraffin and sectioned to 4 microns thick. Tissue sections were stained with H&E. **(A)** Black arrow indicates white matter tracts within mouse brain. Red arrow highlights tumour cells from day 15-established GL261-Luc tumours migrating and invading in the proximity of the white matter tract. Image taken at x5 magnification using the SPOT Insight camera and Leitz DMRB microscope. **(B)** Black arrow indicates white matter tracts within mouse brain. Red arrow highlights tumour cells from day 25-established GL261-Luc tumours migrating and invading in the proximity of white matter tracts. Image taken at x10 magnification using the SPOT Insight camera and Leitz DMRB microscope.

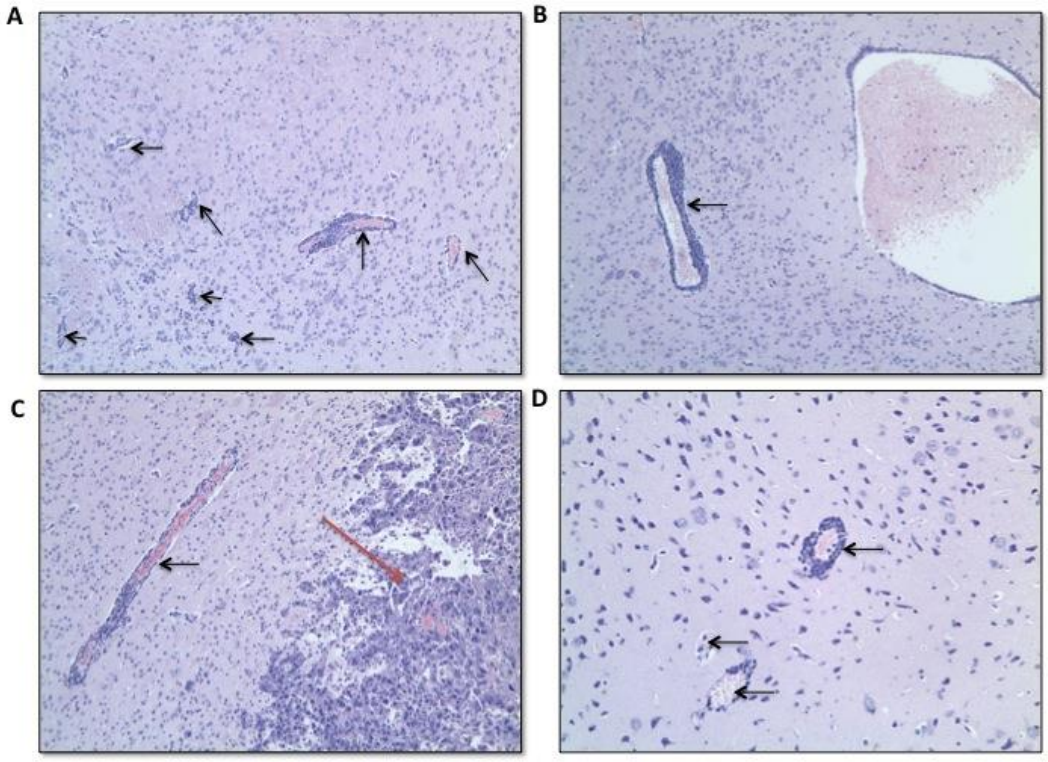

Figure 57: Brain slices of GL261-Luc tumours treated ± oncolytic HSV demonstrate localised sites of inflammation and perivascular clustering of lymphocytes
$5x10^4$ GL261-Luc cells in 2 µl PBS were stereotactically injected into the brains of two groups of 6-8-week-old C57BL/6 mice. For one group of mice, GL261-Luc cells were premixed with oncolytic HSV at 10 pfu/cell prior to intracranial injection. Mice were sacrificed on day 15-post injection and brains were immediately harvested into 4 % PFA. Brains were then sliced into coronal sections, embedded in paraffin and sectioned to 4 microns thick. Tissue sections were stained with H&E. (**A** and **B**) H&E stained brain slices from mouse brains injected with GL261-Luc cells premixed with oncolytic HSV. Black arrows indicate sites of inflammation, with perivascular clustering of lymphocytes noted. Images taken at x10 magnification using the SPOT Insight camera and Leitz DMRB microscope. (**C** and **D**) H&E stained brain slices from mouse brains injected with GL261-Luc cells only. Black arrows indicate sites of inflammation, with perivascular clustering of lymphocytes. Red arrow indicates the presence of an infiltrative GL261-Luc day 15-established tumour. Image C taken at x10 magnification and image D taken at x20 magnification using the SPOT Insight camera and Leitz DMRB microscope.

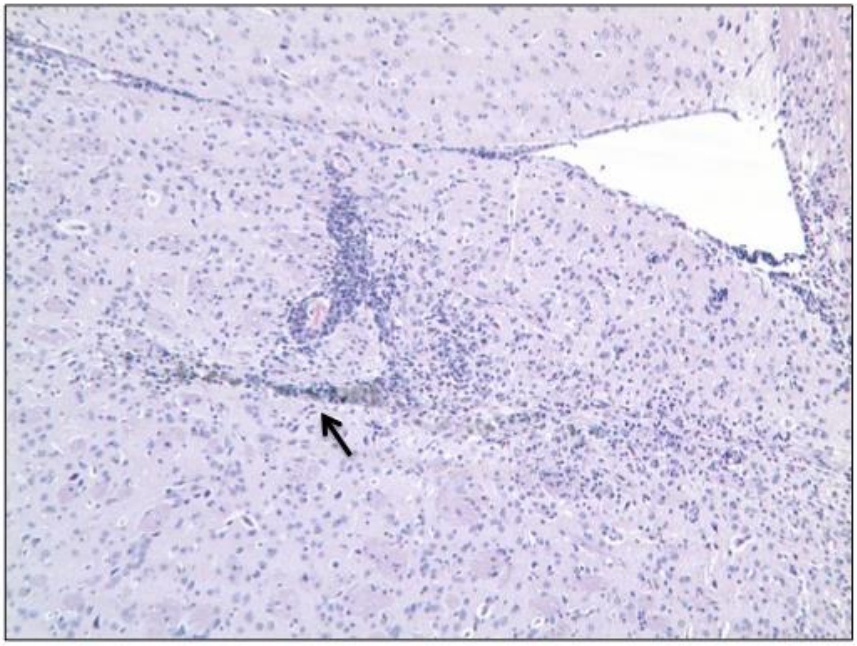

Figure 58: GL261-Luc tumour treated with oncolytic HSV demonstrates localised inflammatory reaction along the potential injection tract

$5x10^4$ GL261-Luc premixed with oncolytic HSV at 10 pfu/cell were stereotactically injected into the brains of 6-8-week-old C57BL/6 mice. Mice were sacrificed on day 15 post injection and brains were immediately harvested into 4 % PFA. Brains were then sliced into coronal sections, embedded in paraffin and sectioned to 4 microns thick. Tissue sections were stained with H&E. Black arrow highlights a localised inflammatory reaction along the potential injection tract. Images taken at x10 magnification using the SPOT Insight camera and Leitz DMRB microscope.

6.3 Evaluation of the effects of oncolytic HSV as an anti-invasive therapy for DIPG

An orthotopic xenograft model of DIPG was established by injecting HSJD-DIPG-007 cells into the fourth ventricle of NOD.SCID mice, allowing tumour cells to grow and invade into the brainstem. In order to evaluate the effects of oncolytic HSV therapy in this model, mice were either injected with HSJD-DIPG-007 cells premixed with PBS (n=6) or HSJD-DIPG-007 cells premixed with oncolytic HSV at 10 pfu/cell (n=6).

Analysis of sections obtained from the brains of mice in the control group, injected with untreated HSJD-DIPG-007 cells, showed a moderate increase in cellularity within the brainstem, adjacent cortex and cerebellum by diffusely infiltrating sheets of atypical glial cells (Figure 59A). These cells had hyperchromatic and moderately pleomorphic nuclei and fine fibrillary cytoplasm (Figure 59B). Mitotic activity was high; however, there was no evidence of necrosis or vascular proliferation. These HSJD-DIPG-007 tumour cells did not form a solid mass as seen within mouse brain following GL261-Luc intracranial injection but appeared to diffusely migrate, invade and infiltrate evenly throughout the midbrain, medulla and cerebellum following their injection into the brainstem (Figure 60A). Invasion also continued until cells reached the subpial surface where they then continued to spread horizontally in clusters (Figure 60B).

Conversely, the brain sections obtained from mice that received intracranial injection of HSJD-DIPG-007 premixed with oncolytic HSV demonstrated well-contained collections of increased cellularity within the brainstem, with very limited infiltration into the surrounding structures (Figure 61A). These well-contained collections consisted of abnormal looking cells where the nucleus was elongated and mixed with apoptotic bodies, indicative of tumour cells (Figure 61B and 62). One section showed a blood vessel surrounded by a cuff of slightly pleomorphic cells, with oval and elongated misshapen nuclei and frequent apoptotic bodies, again likely to be tumour cells (Figure 63). The tumour injection site was noted within the pons, characterised by small areas of cholesterol clefts and microcalcifications and there was a

raised possibility of tumour cells at the site of injection indicated by hyperchromatic misshapen nucleic and a slight focal increase in cellularity (Figure 64).

Finally, the therapeutic efficacy of oncolytic HSV treatment was evaluated in an orthotopic xenograft model of DIPG (Figure 65). Oncolytic HSV treatment prolonged survival (median survival: control PBS treated: 71 days, HSV treated: 109.5 days) although this failed to reach statistical significance ($p=0.123$).

A

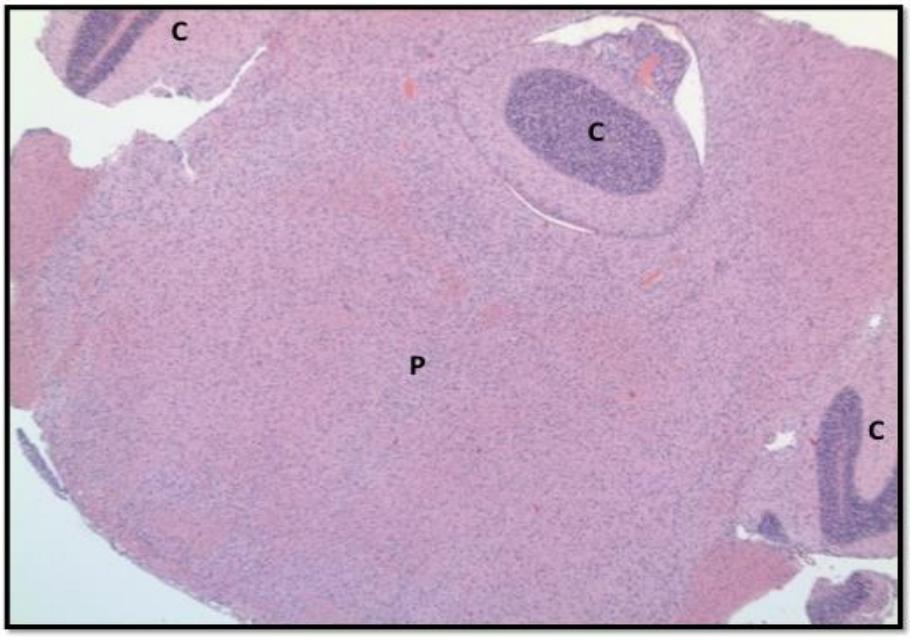

B

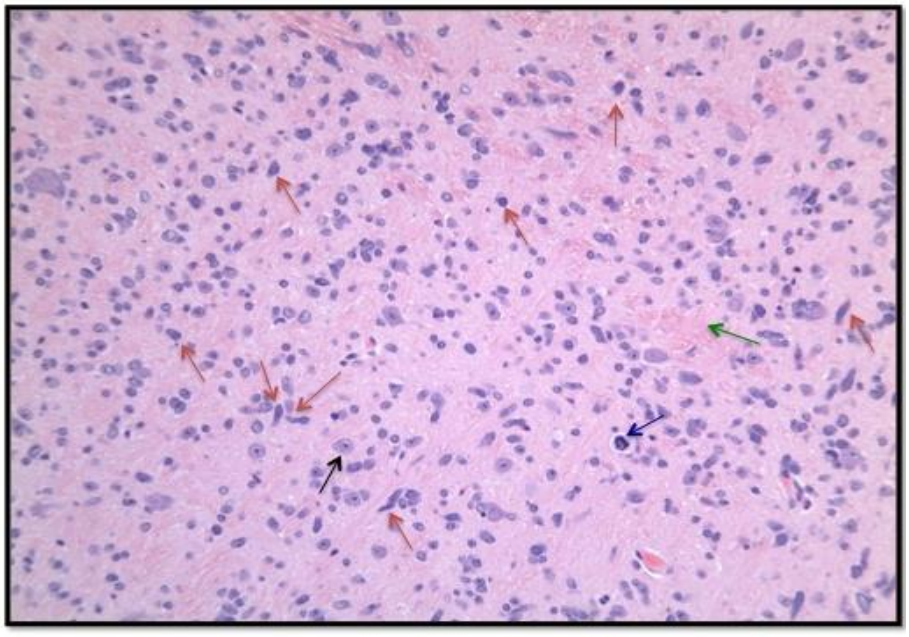

Figure 59: HSJD-DIPG-007 cells diffusely infiltrate mouse brains following intracranial injection

$5x10^5$ disaggregated HSJD-DIPG-007 cells premixed with PBS were stereotactically injected into the brains of 4-5-week-old NOD.SCID mice. Tumours were left to establish and mice were sacrificed when showing signs of disease (i.e. severe ataxia or >15 % weight loss). Images from mouse brain obtained on day 62-post surgery. Brains were harvested into 4 % PFA, sliced into coronal sections, embedded in paraffin and sectioned to 4 microns thick. Tissue sections were stained with H&E. **(A)** Brainstem section showing diffuse infiltration of tumour cells into the pons (**P**) and adjacent cerebellum (**C**). There is moderate increase in cellularity with even distribution of cells in a diffuse pattern. Image taken at x2.5 magnification using the SPOT Insight camera and Leitz DMRB microscope. **(B)** Brainstem section of pons at x20 magnification showing the diffuse distribution of tumour cells. Black arrow indicates normal neuron with prominent nucleolus. Green arrow indicates a white matter tract. Blue arrow indicates mitotic activity. Red arrow shows representative examples of atypical cells with pleomorphic hyperchromatic nuceli indicative of tumour cells. Image taken at x20 magnification using the SPOT Insight camera and Leitz DMRB microscope.

A

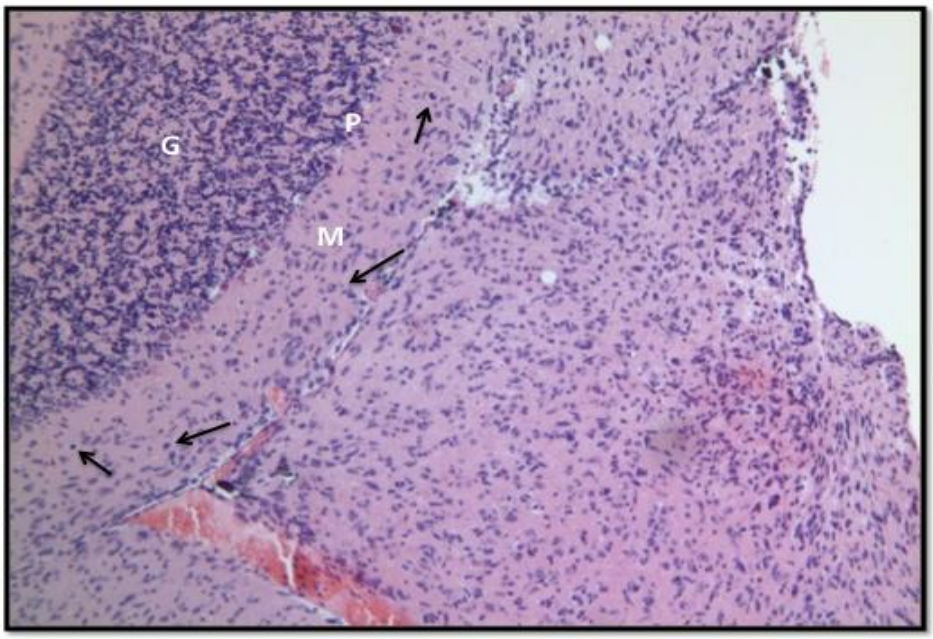

B

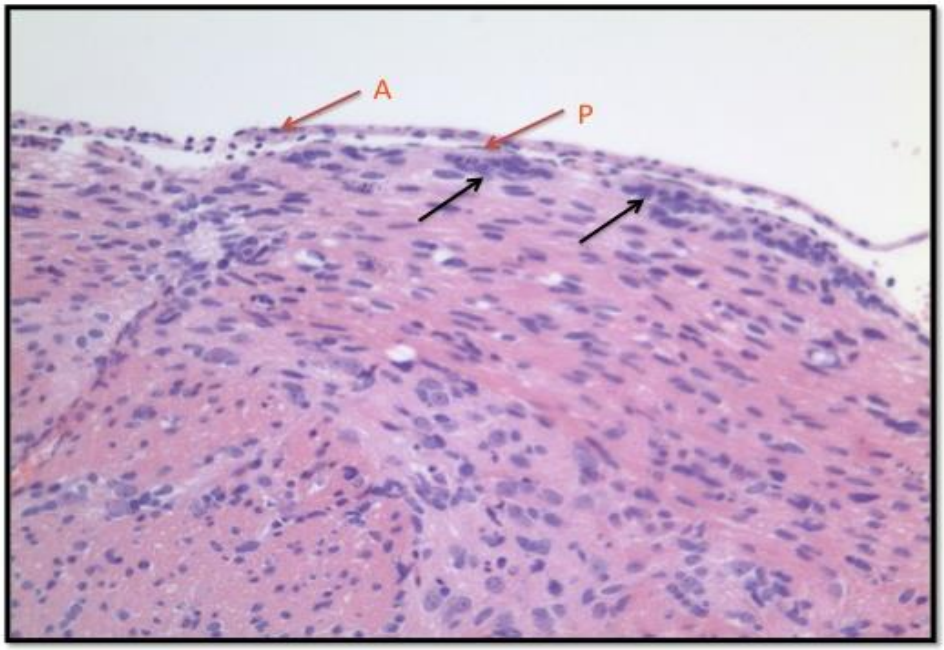

Figure 60: HSJD-DIPG-007 cells are highly infiltrative within mouse brains following intracranial injection.

$5x10^5$ disaggregated HSJD-DIPG-007 cells premixed with PBS were stereotactically injected into the brains of 4-5-week-old NOD.SCID mice. Tumours were left to establish and mice were sacrificed when showing signs of disease (i.e. severe ataxia or >15 % weight loss). Images from mouse brain obtained on day 62-post surgery. Brains were harvested into 4 % PFA, sliced into coronal sections, embedded in paraffin and sectioned to 4 microns thick. Tissue sections were stained with H&E. **(A)** Brain section through the cerebellum shows defined granular (**G**), purkinje (**P**) and molecular (**M**) layers. There is moderate to high increase in cellularity by atypical glial cells within the molecular layer indicating diffuse tumour infiltration (black arrows show representative examples). Image taken at x10 magnification using the SPOT Insight camera and Leitz DMRB microscope. **(B)** Brain section showing clusters of tumour cells (black arrows) accumulating within the subpial region and starting to migrate and invade horizontally. **A** is arachnoid, **P** is pia. Image taken at x20 magnification using the SPOT Insight camera and Leitz DMRB microscope.

A

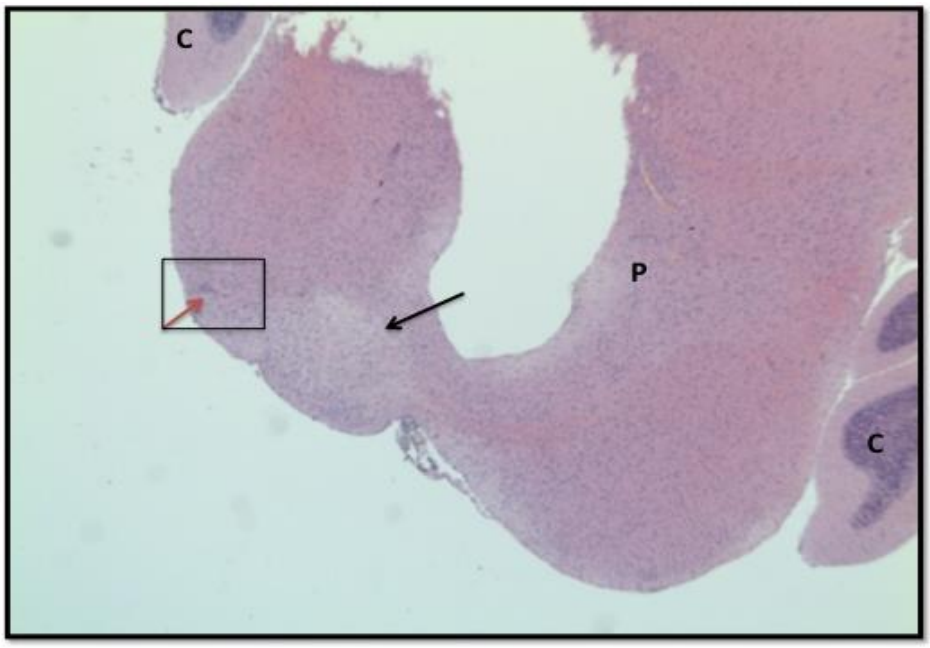

B

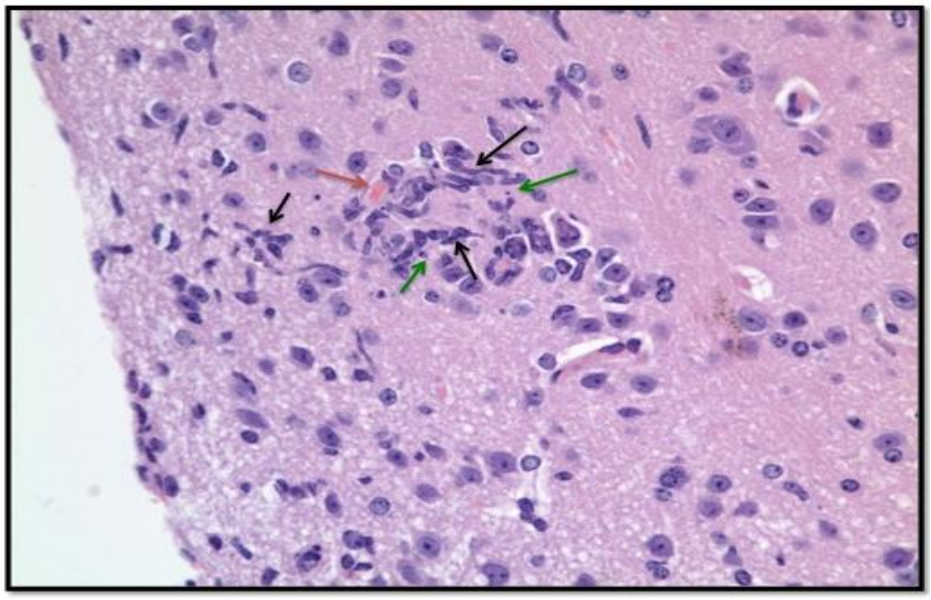

Figure 61: HSJD-DIPG-007 cells treated with oncolytic HSV are well contained within the brainstem following intracranial injection

$5x10^5$ disaggregated HSJD-DIPG-007 cells premixed with oncolytic HSV at 10 pfu/cell were stereotactically injected into the brains of 4-5-week-old NOD.SCID mice. Tumours were left to establish and mice were sacrificed when showing signs of disease (i.e. severe ataxia or >15 % weight loss). Images from a mouse brain obtained on day 123-post surgery. Brains were harvested into 4 % PFA, sliced into coronal sections, embedded in paraffin and sectioned to 4 microns thick. Tissue sections were stained with H&E. **(A)** Cross section of the pons (**P**) and cerebellum (**C**). There is an attenuated area of low cellularity possibly representing the injection site (Black arrow) and a well-contained collection of abnormal looking cells (red arrow). There is no overall increase in cellularity within this section. Image taken at x2.5 magnification using the SPOT Insight camera and Leitz DMRB microscope. **(B)** x40 magnification of the boxed area in figure A, showing the collection of abnormal cells within the pons. There are clusters of small cells with elongated and misshapen hyperchromatic nuclei (black arrow) and apoptotic bodies (green arrow) indicative of tumour cells around blood vessels (red arrow). Image taken at x40 magnification using the SPOT Insight camera and Leitz DMRB microscope.

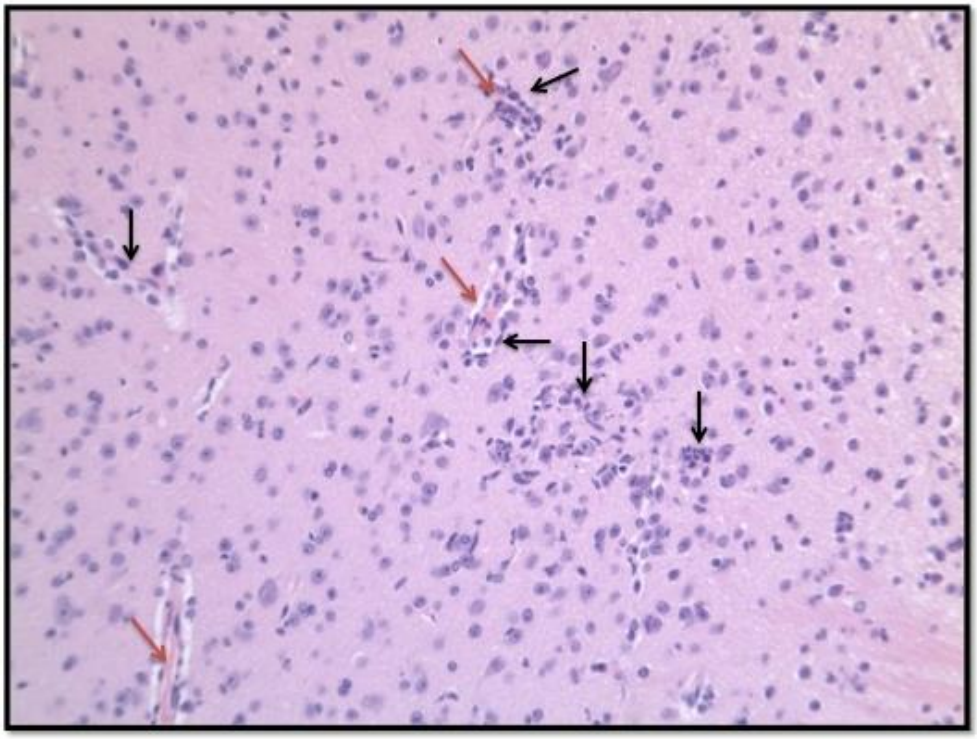

Figure 62: HSJD-DIPG-007 cells treated with oncolytic HSV display well-contained collections of abnormal cells within the pons

$5x10^5$ disaggregated HSJD-DIPG-007 cells premixed with oncolytic HSV at 10 pfu/cell were stereotactically injected into the brains of 4-5-week-old NOD.SCID mice. Tumours were left to establish and mice were sacrificed when showing signs of disease (i.e. severe ataxia or >15 % weight loss). Images from mouse brain obtained on day 78-post surgery. Brains were harvested into 4 % PFA, sliced into coronal sections, embedded in paraffin and sectioned to 4 microns thick. Tissue sections were stained with H&E. Brainstem section showing an area of increased cellularity within the pons. There are small nests of tumour cells (black arrow) seen close to blood vessels (red arrow) which are well-contained. Image taken at x20 magnification using the SPOT Insight camera and Leitz DMRB microscope.

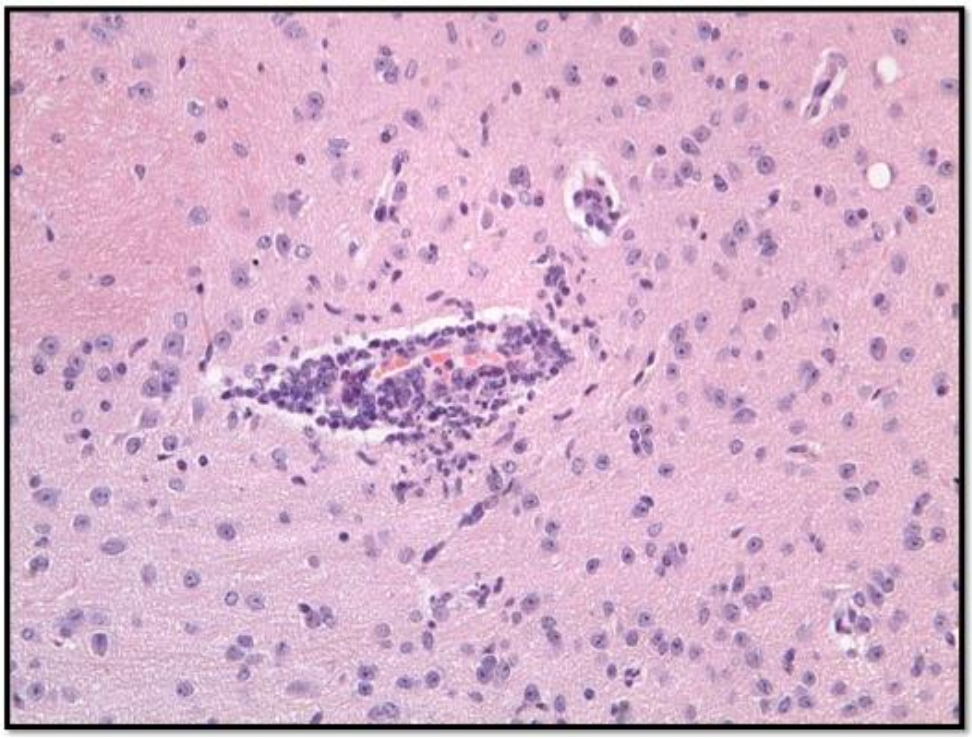

Figure 63: HSJD-DIPG-007 cells treated with oncolytic HSV form localised clusters around blood vessels within the pons
$5x10^5$ disaggregated HSJD-DIPG-007 cells premixed with oncolytic HSV at 10 pfu/cell were stereotactically injected into the brains of 4-5-week-old NOD.SCID mice. Tumours were left to establish and mice were sacrificed when showing signs of disease (i.e. severe ataxia or >15 % weight loss). Images from mouse brain obtained on day 78-post surgery. Brains were harvested into 4 % PFA, sliced into coronal sections, embedded in paraffin and sectioned to 4 microns thick. Tissue sections were stained with H&E. Brainstem section through the pons showing blood vessel surrounded by a cuff of mildly atypical cells with frequent apoptotic bodies indicative of tumour cells. Image taken at x20 magnification using the SPOT Insight camera and Leitz DMRB microscope.

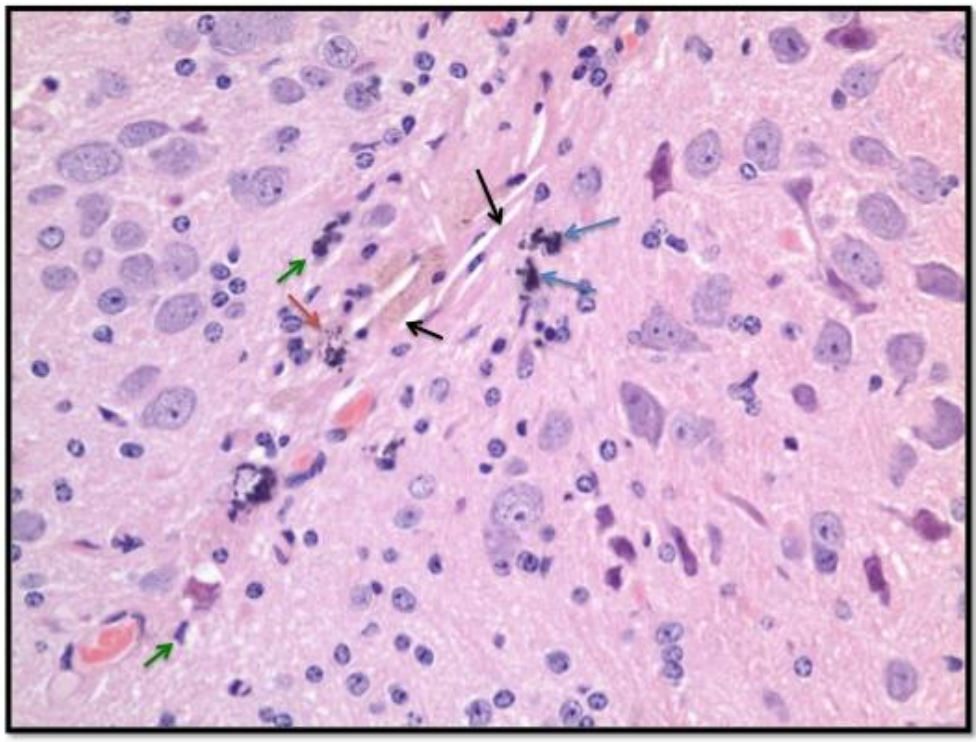

Figure 64: HSJD-DIPG-007 cells treated with oncolytic HSV accumulate around intracranial injection site

$5x10^5$ disaggregated HSJD-DIPG-007 cells premixed with oncolytic HSV at 10 pfu/cell were stereotactically injected into the brains of 4-5-week-old NOD.SCID mice. Tumours were left to establish and mice were sacrificed when showing signs of disease (i.e. severe ataxia or >15 % weight loss). Images from mouse brain obtained on day 137-post surgery. Brains were harvested into 4 % PFA, sliced into coronal sections, embedded in paraffin and sectioned to 4 microns thick. Tissue sections were stained with H&E. Brainstem section through the pons showing needle like clefts (black arrow) probably consisting of cholesterol, surrounded by microcalcifications (blue arrow), possible atypical cells (green arrow) and evidence of possible apoptotic bodies (red arrow) at the potential site of tumour injection. Image taken at x40 magnification using the SPOT Insight camera and Leitz DMRB microscope.

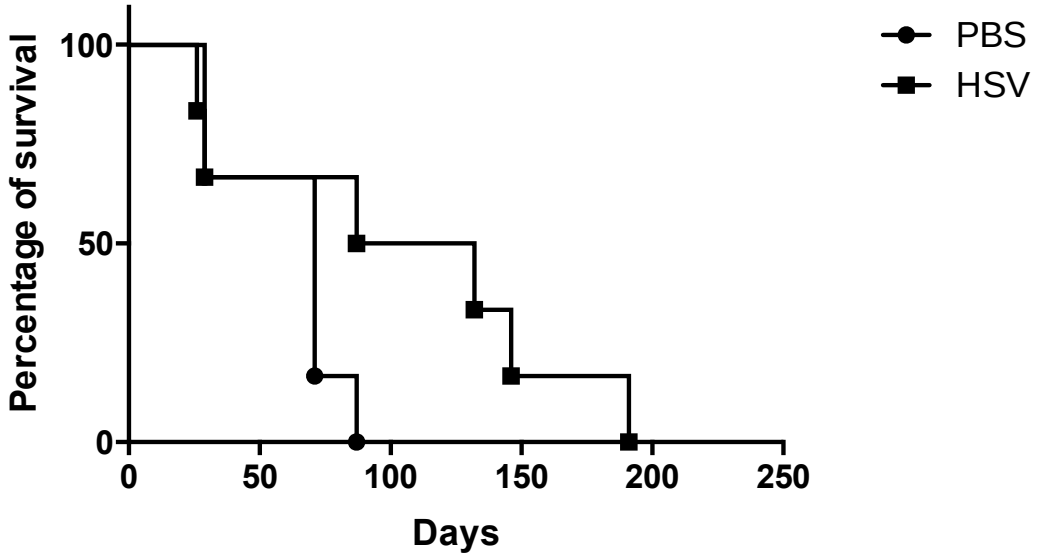

Figure 65: Oncolytic HSV therapy in an orthotopic xenograft model of DIPG

$5x10^5$ disaggregated HSJD-DIPG-007 cells premixed with PBS or oncolytic HSV at 10 pfu/cell were stereotactically injected into the brains of two groups of 4-5-week-old NOD.SCID mice (control and treatment group n=6). Tumours were left to establish and mice were sacrificed when showing signs of disease (i.e. severe ataxia or >15 % weight loss). Survival over time is shown.

6.4 Discussion

The results contained within this chapter highlight the challenges involved in trying to establish an *in vivo* model of paediatric glioma invasion. The orthotopic xenograft model of the pHGG cell line SF188 failed to establish. Although GL261-Luc formed tumours which demonstrated a moderate degree of infiltration into the normal surrounding brain tissue *in vivo*, tumours were not detected in mice when oncolytic HSV was premixed with GL261-Luc cells prior to intracranial injection. Consequently, the effects of oncolytic HSV on glioma invasion could not be evaluated within this experiment. Although it is possible that oncolytic HSV was capable of clearing GL261-Luc tumours, no firm conclusion can be drawn as tumour establishment following premixing of virus with GL261-Luc cells was not determined by bioluminescent imaging.

Following intracranial injection into the brainstem, HSJD-DIPG-007 cells diffusely infiltrated into the cerebellum, pons, midbrain and medulla. However, when mice received intracranial injection of HSJD-DIPG-007 premixed with oncolytic HSV, brainstem sections no longer revealed a diffuse and even pattern of tumour cell infiltration. Instead, oncolytic HSV-treated mice had well-contained collections of abnormal cells within the brainstem, indicative of tumour cells and there was very limited infiltration into the surrounding structures. Thus, in keeping with *in vitro* findings, oncolytic HSV treatment appeared to reduce tumour infiltration in a mouse orthotopic xenograft model of DIPG. Furthermore, oncolytic HSV treatment may also prolong survival in this model (though confirmation of this is required), highlighting the future clinical potential for use of this OV in patients with DIPG.

One potential drawback with the design of these *in vivo* experiments is that oncolytic HSV was premixed with both GL261-Luc and DIPG cells prior to intracranial injection. An alternative and superior methodology would involve the intracranial injection of early established tumours with oncolytic HSV; however, this was not possible within our facility at the time of study. Premixing of the virus with tumour cells prior to injection was deemed a

reasonable alternative as GL261-Luc monolayers appear resistant to the cytotoxic effects of oncolytic HSV over 48 h and HSJD-DIPG-007 cells appear viable following treatment at this time point. This would allow time for the injected viable cells to establish tumours within the brain environment. It is possible that GL261-Luc cells premixed with oncolytic HSV did form tumours that were then cleared by the cytotoxic and immunogenic effects induced by oncolytic HSV treatment; however, it is also possible that premixing of the virus with tumour cells in the GL261-Luc model prevented their ability to establish intracranial tumours. Future *in vivo* experiments should be designed to include intracranial injection of OV into established tumours and should aim to monitor the establishment and subsequent growth of tumours using appropriate imaging techniques. Imaging of established virus-treated tumours would also help to identify the appropriate time point to harvest brains in order to try and evaluate any changes in tumour invasion following oncolytic HSV treatment.

Another potential drawback of the GL261-Luc mouse model used within this chapter was that adherent GL261 cells, as used in this thesis, have been shown to form non-infiltrating tumours *in vivo* with little resemblance to primary mouse glioma (411). GL261 adherent cells can be cultured as neurospheres by supplementing the culture medium with growth factors required for neural stem cells (411). GL261 neurospheres can form aggressively infiltrating intracranial tumours in C57BL/6 mice (411). Future *in vivo* experiments could be designed evaluating the effects of oncolytic HSV on intracranial tumours of GL261 neurospheres, which represents a superior model of *in vivo* tumour invasion. Alternatively, the syngeneic orthotopic CT-2A mouse astrocytoma model could be evaluated as a potential model of brain tumour invasion (412,413). CT-2A tumours have been demonstrated to infiltrate into mouse brain parenchyma, including satellite lesions, and CT-2A cells and neurospheres have been shown to have *in vitro* invasive characteristics (412).

An additional strategy that can be used to study glioma invasion within brain tissue is the organotypic brain slice culture (236,414,415). In this assay, brain slices are maintained in culture in order to maintain the brain cytoarchitecture and the biochemical and electrophysiological properties of neuronal and supporting cells (414,415). Glioma cell spheroids can then be placed on the brain slice and migration across and invasion into the brain tissue can be imaged (415). Although this model cannot be considered as an equivalent alternative to *in vivo* experimentation, it does provide a relatively simple, reproducible three-dimensional system that allows evaluation of migration and invasion within brain tissue. Evaluation of the invasion of pHGG and DIPG cell line spheroids within this assay ± oncolytic HSV is a focus of our future work.

Although oncolytic HSV treatment was shown to enhance therapy in an orthotopic xenograft model of DIPG, this failed to reach statistical significance. This may be due to the small number of mice per treatment group (n=6). Larger scale studies are required in order to make more powered evaluations of the therapeutic efficacy of oncolytic HSV in a mouse model of DIPG.

pHGG and DIPG remain a treatment challenge due to their diffuse and invasive nature. Novel therapeutic anti-invasive strategies are very much needed. Within this thesis, *in vitro* studies have highlighted the potential of GSK-3 inhibitors and oncolytic HSV as novel candidates for future anti-invasive drug development. Future studies aim to develop pre-clinical testing of these therapies within effective *in vivo* models of pHGG and DIPG invasion. The work within this chapter forms the foundation for future studies to develop an effective and reproducible methodology to test the efficacy of potential anti-invasive therapies *in vivo*.

Chapter 7: Conclusion

pHGG and DIPG are highly aggressive tumours associated with diffuse infiltrative growth patterns. This invasive phenotype contributes towards limited therapeutic response and, as such, there is a clear pressing clinical need to develop novel therapies that effectively target tumour migration and invasion. Within this thesis the migratory and invasive characteristics of pHGG and DIPG cell lines were explored, confirming distinct differences in morphology, velocity, migration and invasion patterns.

In addition, for the first time, the small molecule GSK-3 inhibitors LiCl and BIO, previously shown to block migration and invasion of adult HGG cells, were shown to significantly inhibit the migration and invasion of pHGG and DIPG cell lines. Both migration and invasion were evaluated in 2D (transwell membrane, live cell imaging, IF) and 3D (migration on nanofibre plates and spheroid invasion in collagen) systems. In the presence of GSK-3 inhibitors, pHGG cells displayed overall reduced movement and, in the case of SF188, loss of polarity. Both LiCl and BIO instigated pHGG cytoskeletal rearrangement of actin stress fibres and focal adhesions. Overall, this work has demonstrated that it is possible to pharmacologically target migration and invasion of pHGG and DIPG *in vitro* using the GSK-3 inhibitors LiCl and BIO. In conclusion, these agents and their derivatives warrant further pre-clinical investigation as novel anti-migratory and anti-invasive drugs for poor prognosis infiltrative childhood brain tumours.

The work contained within this thesis also highlights that oncolytic virotherapy has the potential to offer an exciting new treatment paradigm for pHGG and DIPG. This project shows, for the first time, that OVs (HSV, reovirus and VV) can inhibit the migration and invasion of pHGG, DIPG and mouse glioma cells. Oncolytic HSV was considered to represent the most interesting candidate, as both its anti-migratory and anti-invasive effects did not appear to be a consequence of cytotoxicity or overall altered cellular proliferation. In the presence of oncolytic HSV, pHGG cells displayed reduced movement and, in the case of SF188, loss of polarity. Additionally,

oncolytic HSV appeared to alter IL-8 production within pHGG cell lines, a cytokine known to be associated with tumour invasion.

The possible mechanism by which oncolytic HSV may reduce pHGG migration and invasion was also explored. Oncolytic HSV altered pHGG cytoskeletal dynamics, stabilising microtubules through the accumulation of post-translational tubulin modifications. Furthermore, oncolytic HSV altered molecular pathways critical for cell polarity, migration and movement. Oncolytic HSV treatment of pHGG cell lines resulted in a tendancy towards inhibited GSK-3β activity and increased DOCK3 expression and prevented the localised clustering of APC to the leading edge of the cell. These observations are highly novel and begin to document the molecular mechanisms by which oncolytic HSV may inhibit pHGG migration and invasion.

Finally, the ability of oncolytic HSV to inhibit glioma invasion was explored *in vivo*. These experiments indicated that mice receiving intracranial injection of HSJD-DIPG-007 cells premixed with oncolytic HSV could demonstrate reduced tumour infiltration and enhanced therapy, compared to controls, in an orthotopic xenograft model of DIPG. This work forms part of ongoing efforts to develop *in vivo* models of glioma invasion, in order to efficiently screen novel anti-invasive therapies for paediatric brain tumours.

Future work related to this project will mainly focus on the further development of reproducible methodology to test the efficacy of potential anti-invasive therapies *in vivo*. Animal studies will focus on drug and virus delivery to brain tumours, either by intracranial or i.v. injection. Alternative drug delivery techniques, such as convection enhanced delivery catheters or local delivery with polymers, could also be explored as mechanisms to overcome the BBB. Subsequent *in vivo* experiments should also monitor the establishment and growth of tumours using appropriate imaging techniques.

Furthermore, a mouse organotypic brain slice assay for use with pHGG and DIPG tumour spheroids is currently planned. This assay offers a

reproducible three-dimensional system to effectively screen drug and virus candidates, evaluating their ability to alter paediatric glioma cell migration and invasion within human brain tissue.

Additional work is also planned to evaluate the specific effects of GSK-3β inhibition on pHGG microtubule dynamics and post-translational modifications. The direct effects of DOCK3 knockdown and overexpression on pHGG GSK-3β activity and migration also remain to be explored. Finally, screening the effects of a diverse panel of novel GSK-3β inhibitors on pHGG and DIPG migration and invasion remains a major part of ongoing studies in this area.

Although relatively rare, pHGG and DIPG are associated with dismal prognosis. Five-year survival outcome is approximately 15-35 % for patients with pHGG and 90 % of children with DIPG will succumb to their disease within two years of diagnosis (36-38,416). Despite advances in the field of radiotherapy and the onset of novel biologically targeted therapeutics, survival statistics have failed to improve over the past couple of decades (20). The hallmark characteristic of glioma cells to invade and diffusely infiltrate normal brain tissue substantially contributes towards poor prognosis by preventing complete surgical resection and localisation of tumour for radiotherapy. The development of effective anti-invasive strategies, as proposed within this thesis, would be very much welcomed and could considerably improve clinical outcomes in this field.

Both LiCl and BIO have potential for clinical application, although current hurdles for the use of such agents in the paediatric clinical arena include optimisation of drug delivery, determination of effective working dosage and avoidance of toxic systemic accumulation. Pre-clinical *in vivo* drug testing and evaluation of clinical experience from adult dosing regimens could begin to address these issues and are required in order to develop these agents for use in paediatric oncology patients.

Oncolytic virotherapy offers a completely novel treatment approach for poor prognosis children's brain tumours. Although clinical experience for use in children with intracranial tumours is limited to a few case reports (325,328,329), promising results have been demonstrated in adult patients with glioma in terms of safety, tolerability and multiple dose delivery (334,336-338). Excitingly, a phase I trial evaluating the safety of injecting oncolytic HSV1716 into or near the tumour resection cavity of relapsed or refractory HGGs is currently recruiting paediatric patients between 12 and 21 years of age (332). Rationale for this study is based upon the known cytotoxic and immunogenic effects of oncolytic virotherapy as well as clinical experience of delivering oncolytic HSV to paediatric patients with extracranial solid tumours (252,254,279,408,409,417). Importantly, the results within this thesis suggest, for the first time, that oncolytic HSV may also have a role as an anti-invasive therapeutic, potentially reducing tumour migration and infiltration from residual cancer cells. This additional mechanism of action against a principle hallmark of cancer again highlights the clinical potential for oncolytic virotherapy and opens the door to an exciting new era of treatments for paediatric neuro-oncology, with the potential to improve outcomes in this patient population.

In conclusion, the studies contained within this thesis provide compelling evidence that pHGG and DIPG migration and invasion can be effectively targeted and highlight the exciting clinical potential of two novel anti-invasive therapeutic strategies for these devastating diseases of childhood.

Appendices

8.1 Appendix 1 - List of Suppliers

Abcam	330 Cambridge Science Park, Milton Road, Milton, Cambridge, CB4 0FL, UK
AbD Serotec	Endeavour House, The Langford Business Park, Langford Lane, Kidlington, Oxfordshire, OX5 1GE, UK
Atom Scientific	Arrow Trading Estate, Corporation Road, Audenshaw, Manchester, M34 5LR, UK
BD Biosciences	The Danby Building, Edmund Halley Road, Oxford, OX4 4DQ, UK
BDH	100 Matsonford Road, Radnor, PA 19087-6880, USA
Bio-Rad Laboratories Ltd.	Bio-Rad House, Maxted Road, Hemel Hempstead, Hertfordshire, HP2 7DX, UK
Biotium	3159 Corporate Place, Hayward, CA 94545, USA
Calbiochem	10394 Pacific Center, San Diego, CA 92121, USA
Cell Signaling Technology	3 Trask Lane, Danvers, MA 01923, USA
Corning Ltd.	Elwy House, Lakeside Business Village, St. David's Park, CH5 3XD, UK
Dako Ltd.	Cambridge House, St Thomas Place, Ely, Cambridgeshire, CB7 4EX, UK
Essen BioScience	300 West Morgan Road, Ann Arbor, MI 48108, USA
Genelux Corporation	3030 Bunker Hill Street, 310 San Diego, California 92109, USA

Genetex Inc.	2456 Alton Parkway, Irvine, CA 92606, USA
Graph Pad Software Inc.	7825 Fay Avenue, Suite 230, La Jolla, CA 92037,USA
Greiner Bio-One	Unit 5, Brunel Way, Stonehouse, GL10 3SX, UK
IBM United Kingdom Ltd.	PO Box 41, North Harbour, Portsmouth, Hampshire, PO6 3AU, UK
Labtech International Ltd.	2 Birch House, Brambleside, Uckfield, East Sussex, TN22 1QQ, UK
Leica	Larch House, Woodlands Business Park, Breckland, Linford Wood, Milton Keynes, MK14 6FG, UK
Microsoft	Microsoft UK Headquarters, Microsoft Campus, Thames Valley Park Reading, Berkshire, RG6 1WG, UK
Millipore Ltd.	Number One Industrial Estate, Consett, DH8 6SZ, UK
Molecular Devices	1311 Orleans Drive, Sunnyvale, CA 94089, USA
Nanofiber solutions LLC	1275 Kinnear Road, Columbus, OH 43212, USA
Nikon	Shinagawa Intercity Tower C, 2-15-3, Konan, Minato-ku, Tokyo 108-6290
Oncolytics Biotech Inc.	210, 1167 Kensington Crescent, North West Calgary, AB, T2N 1X7, Canada
Peprotech EC Ltd.	29 Margravine Road, London, W6 8LL, UK
Perkin-Elmer Inc.	940 Winter Street, Waltham, Massachusetts, 0245, USA

R&D systems	614 McKinley Place NE, Minneapolis, MN 55413, USA
Roche	Charles Avenue, Burgess Hill, West Sussex, RH15 9RY, UK
Sarstedt Ltd.	68 Boston Road, Leicester, LE4 1AW, UK
Scientific Laboratory Supplies Ltd.	The Square, Hessle, North Humberside, HU13 0AE, UK
Selleckchem	Unit 7, Acorn Business Centre, Oaks Drive, Newmarket, Suffolk, CB8 7SY, UK
Sigma-Aldrich Company Ltd.	The Old Brickyard, New Road, Gillingham, Dorset, SP8 4XT, UK
Solmedia	Unit 2, Battlefield Enterprise Park, Vernon Drive, Shrewsbury, SY1 3TF, UK
SouthernBiotech	160 Oxmoor Boulevard, Number 100, Birmingham, AL 35209, USA
SPOT Imaging	6540 Burrough, Sterling Heights, MI 48314, USA
Starlab UK	4 Tanners Drive, Blakelands, Milton Keynes, MK14 5NA, UK
The Jackson Laboratory	600 Main Street, Bar Harbor, ME 04609, USA
Thermo Fisher Scientific	Stafford House, Boundary Way, Hemel Hempstead, HP2 7GE, UK
Virttu Biologics	2nd, Western Infirmary, McGregor Building, Glasgow, G11 6NT, UK
Weber Scientific International Ltd.	40 Udney Park Road, Teddington, Middlesex, TW11 9BG, UK
Zeiss	509 Coldhams Lane, Cambridge, CB1 3JS, UK

8.2 Appendix 2 – Media, Buffers and Reagents

General chemicals were 'AnalaR' or molecular biology grade and were purchased from BDH or Sigma-Aldrich unless otherwise stated.

Tumour stem medium (TSM) base

Reagent	Vendor	Volume (ml)
Neurobasal-A medium (1x) liquid	Thermo Fisher Scientific	250
DMEM/F-12 (1x) liquid 1:1	Thermo Fisher Scientific	250
HEPES buffer solution (1 M)	Thermo Fisher Scientific	5
Sodium Pyruvate 100 mM liquid	Thermo Fisher Scientific	5
MEM Non-essential amino acids (100x)	Thermo Fisher Scientific	5
GlutaMAX-1 supplement	Thermo Fisher Scientific	5
Antibiotic-Antimycotic (100x) liquid	Thermo Fisher Scientific	5

Table 9: Constituents of tumour stem medium (TSM) base for HSJD-DIPG-007 culture.

FACS buffer

In PBS: 0.1 % sodium azide
0.01 % FCS

RIPA buffer

In PBS: 1 % Nonidet P40
0.1 % SDS
0.5 % sodium deoxycholate
0.025 % sodium azide

Loading Buffer (2x)

100 mM Tris pH 6.8

4 % (w/v) SDS

0.2 % (w/v) bromophenol blue

20 % (v/v) glycerol

Made with ddH_2O

Before use add 200 mM dithiothreitol (DTT)

Tris-glycine SDS polyacrylamide gel

Solution components	**Component volumes (ml) per 10 ml gel volume**	
	6 % Gel	**10 % Gel**
H_2O	5.3	4
30 % acrylamide mix	2	3.3
1.5M Tris (pH 8.8)	2.5	2.5
10 % SDS	0.1	0.1
10 % ammonium persulfate	0.1	0.1
TEMED	0.008	0.004

Table 10: Solutions for preparing 5 and 10 % gels for tris-glycine SDS polyacrylamide gel electrophoresis

Running buffer (1x)

25 mM Tris

250 mM glycine

0.1 % SDS

Made with ddH_2O

Novex Tris Glycine Transfer Buffer (1x)

12 mM Tris

96 mM glycine

Made with ddH_2O

TBS buffer (10x)

200 mM Tris

5 M NaCl

Made with ddH_2O

pH to7.5 with concentrated HCl

Coating buffer (10x)

1 M $NaHCO_3$ pH 8.2

then dilute 1:10 with ddH_2O

8.3 Supplementary material included on CD

Movie 1: Live cell imaging of SF188 in culture medium

Movie 2: Live cell imaging of SF188 treated with LiCl

Movie 3: Live cell imaging of SF188 treated with BIO

Movie 4: Live cell imaging of KNS42 in culture medium

Movie 5: Live cell imaging of KNS42 treated with LiCl

Movie 6: Live cell imaging of KNS42 treated with BIO

Movie 7: Live cell imaging of SF188 in culture medium

Movie 8: Live cell imaging of SF188 treated with oncolytic HSV

Movie 9: Live cell imaging of KNS42 in culture medium

Movie 10: Live cell imaging of KNS42 treated with oncolytic HSV

References

1. Dolecek TA, Propp JM, Stroup NE, Kruchko C. CBTRUS statistical report: primary brain and central nervous system tumors diagnosed in the United States in 2005-2009. Neuro Oncol 2012;14 Suppl 5:v1-49.

2. Pollack IF. Multidisciplinary management of childhood brain tumors: a review of outcomes, recent advances, and challenges. J Neurosurg Pediatr 2011;8(2):135-48.

3. Gottardo NG, Gajjar A. Chemotherapy for malignant brain tumors of childhood. J Child Neurol 2008;23(10):1149-59.

4. Pollack IF, Jakacki RI. Childhood brain tumors: epidemiology, current management and future directions. Nat Rev Neurol 2011;7(9):495-506.

5. Karajannis M, Allen JC, Newcomb EW. Treatment of pediatric brain tumors. J Cell Physiol 2008;217(3):584-9.

6. Bouffet E, Tabori U, Huang A, Bartels U. Possibilities of new therapeutic strategies in brain tumors. Cancer Treat Rev 2010;36(4):335-41.

7. Pollack IF. Brain tumors in children. N Engl J Med 1994;331(22):1500-7.

8. Friedman GK, Pressey JG, Reddy AT, Markert JM, Gillespie GY. Herpes simplex virus oncolytic therapy for pediatric malignancies. Mol Ther 2009;17(7):1125-35.

9. Sievert AJ, Fisher MJ. Pediatric low-grade gliomas. J Child Neurol 2009;24(11):1397-408.

10. Ginn KF, Gajjar A. Atypical teratoid rhabdoid tumor: current therapy and future directions. Front Oncol 2012;2:114.

11. Echevarria ME, Fangusaro J, Goldman S. Pediatric central nervous system germ cell tumors: a review. Oncologist 2008;13(6):690-9.

12. Van Meir EG, Hadjipanayis CG, Norden AD, Shu HK, Wen PY, Olson JJ. Exciting new advances in neuro-oncology: the avenue to a cure for malignant glioma. CA Cancer J Clin 2010;60(3):166-93.

13. Hadziahmetovic M, Shirai K, Chakravarti A. Recent advancements in multimodality treatment of gliomas. Future Oncol 2011;7(10):1169-83.

14. Merchant TE, Farr JB. Proton beam therapy: a fad or a new standard of care. Curr Opin Pediatr 2014;26(1):3-8.

15. Dasgupta T, Haas-Kogan DA. The combination of novel targeted molecular agents and radiation in the treatment of pediatric gliomas. Front Oncol 2013;3:110.

16. Nageswara Rao AA, Scafidi J, Wells EM, Packer RJ. Biologically targeted therapeutics in pediatric brain tumors. Pediatr Neurol 2012;46(4):203-11.

17. Wells EM, Nageswara Rao AA, Scafidi J, Packer RJ. Neurotoxicity of biologically targeted agents in pediatric cancer trials. Pediatr Neurol 2012;46(4):212-21.

18. Northcott PA, Pfister SM, Jones DT. Next-generation (epi)genetic drivers of childhood brain tumours and the outlook for targeted therapies. Lancet Oncol 2015;16(6):e293-302.

19. Hargrave D. Paediatric high and low grade glioma: the impact of tumour biology on current and future therapy. Br J Neurosurg 2009;23(4):351-63.

20. National Cancer Intelligence Network National Registry of Childhood Tumour. 2010. <http://www.google.co.uk/url?sa=t&rct=j&q=&esrc=s&source=web&cd=1&ved=0CDsQFjAA&url=http%3A%2F%2Fwww.ncin.org.uk%2Fview%3Frid%3D492&ei=JxUJUv-4M8Kq0QWWuoDQBw&usg=AFQjCNG6IY_fcBKzHqZpZN-3JcbhvlfaQQ&bvm=bv.50500085,d.d2k%3E. Accessed 2015 12th September.

21. Gajjar A, Pfister SM, Taylor MD, Gilbertson RJ. Molecular insights into pediatric brain tumors have the potential to transform therapy. Clin Cancer Res 2014;20(22):5630-40.

22. Network Glia. Netzwerk Glia e.V. 2011. <http://www.networkglia.eu/en/home%3E. Accessed 2015 3rd September.

23. Louis DN, Ohgaki H, Wiestler OD, Cavenee WK, Burger PC, Jouvet A*, et al.* The 2007 WHO classification of tumours of the central nervous system. Acta Neuropathol 2007;114(2):97-109.

24. Louis DN. Molecular pathology of malignant gliomas. Annu Rev Pathol 2006;1:97-117.

25. Schumacher M, Schulte-Monting J, Stoeter P, Warmuth-Metz M, Solymosi L. Magnetic resonance imaging compared with biopsy in the diagnosis of brainstem diseases of childhood: a multicenter review. J Neurosurg 2007;106(2 Suppl):111-9.

26. Warren KE. Diffuse intrinsic pontine glioma: poised for progress. Front Oncol 2012;2:205.

27. Rineer J, Schreiber D, Choi K, Rotman M. Characterization and outcomes of infratentorial malignant glioma: a population-based study using the Surveillance Epidemiology and End-Results database. Radiother Oncol 2010;95(3):321-6.

28. Qaddoumi I, Sultan I, Gajjar A. Outcome and prognostic features in pediatric gliomas: a review of 6212 cases from the Surveillance, Epidemiology, and End Results database. Cancer 2009;115(24):5761-70.

29. Jones C, Perryman L, Hargrave D. Paediatric and adult malignant glioma: close relatives or distant cousins? Nat Rev Clin Oncol 2012;9(7):400-13.

30. Fangusaro J. Pediatric high grade glioma: a review and update on tumor clinical characteristics and biology. Front Oncol 2012;2:105.

31. Broniscer A, Baker SJ, West AN, Fraser MM, Proko E, Kocak M*, et al.* Clinical and molecular characteristics of malignant transformation of low-grade glioma in children. J Clin Oncol 2007;25(6):682-9.

32. Soffietti R, Baumert BG, Bello L, von Deimling A, Duffau H, Frenay M*, et al.* Guidelines on management of low-grade gliomas: report of an EFNS-EANO Task Force. Eur J Neurol 2010;17(9):1124-33.

33. Sposto R, Ertel IJ, Jenkin RD, Boesel CP, Venes JL, Ortega JA*, et al.* The effectiveness of chemotherapy for treatment of high grade astrocytoma in children: results of a randomized trial. A report from the Childrens Cancer Study Group. J Neurooncol 1989;7(2):165-77.

34. Finlay JL, Boyett JM, Yates AJ, Wisoff JH, Milstein JM, Geyer JR*, et al.* Randomized phase III trial in childhood high-grade astrocytoma comparing vincristine, lomustine, and prednisone with the eight-drugs-in-1-day regimen. Childrens Cancer Group. J Clin Oncol 1995;13(1):112-23.

35. Cohen KJ, Pollack IF, Zhou T, Buxton A, Holmes EJ, Burger PC*, et al.* Temozolomide in the treatment of high-grade gliomas in children: a report from the Children's Oncology Group. Neuro Oncol 2011;13(3):317-23.

36. Schroeder KM, Hoeman CM, Becher OJ. Children are not just little adults: recent advances in understanding of diffuse intrinsic pontine glioma biology. Pediatr Res 2014;75(1-2):205-9.

37. Hargrave D, Bartels U, Bouffet E. Diffuse brainstem glioma in children: critical review of clinical trials. Lancet Oncol 2006;7(3):241-8.

38. Khatua S, Moore KR, Vats TS, Kestle JR. Diffuse intrinsic pontine glioma-current status and future strategies. Childs Nerv Syst 2011;27(9):1391-7.

39. Gajjar A, Bowers DC, Karajannis MA, Leary S, Witt H, Gottardo NG. Pediatric Brain Tumors: Innovative Genomic Information Is Transforming the Diagnostic and Clinical Landscape. J Clin Oncol 2015.

40. Yan H, Parsons DW, Jin G, McLendon R, Rasheed BA, Yuan W*, et al.* IDH1 and IDH2 mutations in gliomas. N Engl J Med 2009;360(8):765-73.

41. Paugh BS, Qu C, Jones C, Liu Z, Adamowicz-Brice M, Zhang J*, et al.* Integrated molecular genetic profiling of pediatric high-grade gliomas reveals key differences with the adult disease. J Clin Oncol 2010;28(18):3061-8.

42. Brennan CW, Verhaak RG, McKenna A, Campos B, Noushmehr H, Salama SR*, et al.* The somatic genomic landscape of glioblastoma. Cell 2013;155(2):462-77.

43. Sturm D, Bender S, Jones DT, Lichter P, Grill J, Becher O*, et al.* Paediatric and adult glioblastoma: multiform (epi)genomic culprits emerge. Nat Rev Cancer 2014;14(2):92-107.

44. Sturm D, Witt H, Hovestadt V, Khuong-Quang DA, Jones DT, Konermann C*, et al.* Hotspot mutations in H3F3A and IDH1 define distinct epigenetic and biological subgroups of glioblastoma. Cancer Cell 2012;22(4):425-37.

45. Buczkowicz P, Hoeman C, Rakopoulos P, Pajovic S, Letourneau L, Dzamba M*, et al.* Genomic analysis of diffuse intrinsic pontine gliomas identifies three molecular subgroups and recurrent activating ACVR1 mutations. Nat Genet 2014;46(5):451-6.

46. Khuong-Quang DA, Buczkowicz P, Rakopoulos P, Liu XY, Fontebasso AM, Bouffet E*, et al.* K27M mutation in histone H3.3 defines clinically and biologically distinct subgroups of pediatric diffuse intrinsic pontine gliomas. Acta Neuropathol 2012;124(3):439-47.

47. Bjerke L, Mackay A, Nandhabalan M, Burford A, Jury A, Popov S*, et al.* Histone H3.3. mutations drive pediatric glioblastoma through upregulation of MYCN. Cancer Discov 2013;3(5):512-9.

48. Verhaak RG, Hoadley KA, Purdom E, Wang V, Qi Y, Wilkerson MD*, et al.* Integrated genomic analysis identifies clinically relevant subtypes of glioblastoma characterized by abnormalities in PDGFRA, IDH1, EGFR, and NF1. Cancer Cell 2010;17(1):98-110.

49. Phillips HS, Kharbanda S, Chen R, Forrest WF, Soriano RH, Wu TD*, et al.* Molecular subclasses of high-grade glioma predict prognosis, delineate a pattern of disease progression, and resemble stages in neurogenesis. Cancer Cell 2006;9(3):157-73.

50. Marusyk A, Polyak K. Tumor heterogeneity: causes and consequences. Biochim Biophys Acta 2010;1805(1):105-17.

51. Rodriguez A, Tatter SB, Debinski W. Neurosurgical Techniques for Disruption of the Blood-Brain Barrier for Glioblastoma Treatment. Pharmaceutics 2015;7(3):175-87.

52. Zhang RD, Price JE, Fujimaki T, Bucana CD, Fidler IJ. Differential permeability of the blood-brain barrier in experimental brain metastases produced by human neoplasms implanted into nude mice. Am J Pathol 1992;141(5):1115-24.

53. Bidros DS, Vogelbaum MA. Novel drug delivery strategies in neuro-oncology. Neurotherapeutics 2009;6(3):539-46.

54. van Tellingen O, Yetkin-Arik B, de Gooijer MC, Wesseling P, Wurdinger T, de Vries HE. Overcoming the blood-brain tumor barrier for effective glioblastoma treatment. Drug Resist Updat 2015;19:1-12.

55. Aparicio-Blanco J, Torres-Suarez AI. Glioblastoma Multiforme and Lipid Nanocapsules: A Review. J Biomed Nanotechnol 2015;11(8):1283-311.

56. Ung TH, Malone H, Canoll P, Bruce JN. Convection-enhanced delivery for glioblastoma: targeted delivery of antitumor therapeutics. CNS Oncol 2015;4(4):225-34.

57. Walker DA, Liu J, Kieran M, Jabado N, Picton S, Packer R*, et al.* A multi-disciplinary consensus statement concerning surgical approaches to low-grade, high-grade astrocytomas and diffuse intrinsic pontine gliomas in childhood (CPN Paris 2011) using the Delphi method. Neuro Oncol 2013;15(4):462-8.

58. Puget S, Blauwblomme T, Grill J. Is biopsy safe in children with newly diagnosed diffuse intrinsic pontine glioma? Am Soc Clin Oncol Educ Book 2012:629-33.

59. Wang ZJ, Rao L, Bhambhani K, Miller K, Poulik J, Altinok D*, et al.* Diffuse intrinsic pontine glioma biopsy: a single institution experience. Pediatr Blood Cancer 2015;62(1):163-5.

60. Cage TA, Samagh SP, Mueller S, Nicolaides T, Haas-Kogan D, Prados M*, et al.* Feasibility, safety, and indications for surgical biopsy of intrinsic brainstem tumors in children. Childs Nerv Syst 2013;29(8):1313-9.

61. Misuraca KL, Cordero FJ, Becher OJ. Pre-Clinical Models of Diffuse Intrinsic Pontine Glioma. Front Oncol 2015;5:172.

62. Caretti V, Sewing AC, Lagerweij T, Schellen P, Bugiani M, Jansen MH*, et al.* Human pontine glioma cells can induce murine tumors. Acta Neuropathol 2014;127(6):897-909.

63. Grasso CS, Tang Y, Truffaux N, Berlow NE, Liu L, Debily MA*, et al.* Functionally defined therapeutic targets in diffuse intrinsic pontine glioma. Nat Med 2015;21(6):555-9.

64. Becher OJ, Hambardzumyan D, Walker TR, Helmy K, Nazarian J, Albrecht S*, et al.* Preclinical evaluation of radiation and perifosine in a genetically and histologically accurate model of brainstem glioma. Cancer Res 2010;70(6):2548-57.

65. Demuth T, Berens ME. Molecular mechanisms of glioma cell migration and invasion. J Neurooncol 2004;70(2):217-28.

66. Hanahan D, Weinberg RA. Hallmarks of cancer: the next generation. Cell 2011;144(5):646-74.

67. Giese A, Bjerkvig R, Berens ME, Westphal M. Cost of migration: invasion of malignant gliomas and implications for treatment. J Clin Oncol 2003;21(8):1624-36.

68. Gaspar LE, Fisher BJ, Macdonald DR, LeBer DV, Halperin EC, Schold SC, Jr.*, et al.* Supratentorial malignant glioma: patterns of recurrence and implications for external beam local treatment. Int J Radiat Oncol Biol Phys 1992;24(1):55-7.

69. Burger PC, Dubois PJ, Schold SC, Jr., Smith KR, Jr., Odom GL, Crafts DC*, et al.* Computerized tomographic and pathologic studies of the untreated, quiescent, and recurrent glioblastoma multiforme. J Neurosurg 1983;58(2):159-69.

70. Giese A, Westphal M. Treatment of malignant glioma: a problem beyond the margins of resection. J Cancer Res Clin Oncol 2001;127(4):217-25.

71. Zhong J, Paul A, Kellie SJ, O'Neill GM. Mesenchymal migration as a therapeutic target in glioblastoma. J Oncol 2010;2010:430142.

72. Agudelo-Garcia PA, De Jesus JK, Williams SP, Nowicki MO, Chiocca EA, Liyanarachchi S*, et al.* Glioma cell migration on three-dimensional nanofiber scaffolds is regulated by substrate topography and abolished by inhibition of STAT3 signaling. Neoplasia 2011;13(9):831-40.

73. Cayre M, Canoll P, Goldman JE. Cell migration in the normal and pathological postnatal mammalian brain. Prog Neurobiol 2009;88(1):41-63.

74. Kakita A, Goldman JE. Patterns and dynamics of SVZ cell migration in the postnatal forebrain: monitoring living progenitors in slice preparations. Neuron 1999;23(3):461-72.

75. Kramer N, Walzl A, Unger C, Rosner M, Krupitza G, Hengstschlager M*, et al.* In vitro cell migration and invasion assays. Mutat Res 2013;752(1):10-24.

76. Hulkower KI, RL H. Cell migration and invasion assays as tools for drug discovery. Pharmaceutics 2011;3:107-24.

77. Roussos ET, Condeelis JS, Patsialou A. Chemotaxis in cancer. Nat Rev Cancer 2011;11(8):573-87.

78. Saito K, Ozawa Y, Hibino K, Ohta Y. FilGAP, a Rho/Rho-associated protein kinase-regulated GTPase-activating protein for Rac, controls tumor cell migration. Mol Biol Cell 2012;23(24):4739-50.

79. Pankova K, Rosel D, Novotny M, Brabek J. The molecular mechanisms of transition between mesenchymal and amoeboid invasiveness in tumor cells. Cell Mol Life Sci 2010;67(1):63-71.

80. Gadea G, Blangy A. Dock-family exchange factors in cell migration and disease. Eur J Cell Biol 2014;93(10-12):466-77.

81. Alexander S, Friedl P. Cancer invasion and resistance: interconnected processes of disease progression and therapy failure. Trends Mol Med 2012;18(1):13-26.

82. Vehlow A, Cordes N. Invasion as target for therapy of glioblastoma multiforme. Biochim Biophys Acta 2013;1836(2):236-44.

83. Rorth P. Collective guidance of collective cell migration. Trends Cell Biol 2007;17(12):575-9.

84. Yilmaz M, Christofori G. Mechanisms of motility in metastasizing cells. Mol Cancer Res 2010;8(5):629-42.

85. Roussos ET, Balsamo M, Alford SK, Wyckoff JB, Gligorijevic B, Wang Y*, et al.* Mena invasive (MenaINV) promotes multicellular streaming motility and transendothelial migration in a mouse model of breast cancer. J Cell Sci 2011;124(Pt 13):2120-31.

86. Huber F, Boire A, Lopez MP, Koenderink GH. Cytoskeletal crosstalk: when three different personalities team up. Curr Opin Cell Biol 2015;32:39-47.

87. Etienne-Manneville S. Polarity proteins in migration and invasion. Oncogene 2008;27(55):6970-80.

88. Etienne-Manneville S. Polarity proteins in glial cell functions. Curr Opin Neurobiol 2008;18(5):488-94.

89. Charest PG, Firtel RA. Big roles for small GTPases in the control of directed cell movement. Biochem J 2007;401(2):377-90.

90. Parsons JT, Horwitz AR, Schwartz MA. Cell adhesion: integrating cytoskeletal dynamics and cellular tension. Nat Rev Mol Cell Biol 2010;11(9):633-43.

91. Wehrle-Haller B, Imhof BA. Actin, microtubules and focal adhesion dynamics during cell migration. Int J Biochem Cell Biol 2003;35(1):39-50.

92. Etienne-Manneville S. Actin and microtubules in cell motility: which one is in control? Traffic 2004;5(7):470-7.

93. Etienne-Manneville S. Microtubules in cell migration. Annu Rev Cell Dev Biol 2013;29:471-99.

94. Vicente-Manzanares M, Horwitz AR. Adhesion dynamics at a glance. J Cell Sci 2011;124(Pt 23):3923-7.

95. Etienne-Manneville S. From signaling pathways to microtubule dynamics: the key players. Curr Opin Cell Biol 2010;22(1):104-11.

96. Bartolini F, Gundersen GG. Generation of noncentrosomal microtubule arrays. J Cell Sci 2006;119(Pt 20):4155-63.

97. Luxton GW, Gundersen GG. Orientation and function of the nuclear-centrosomal axis during cell migration. Curr Opin Cell Biol 2011;23(5):579-88.

98. Manneville JB, Etienne-Manneville S. Positioning centrosomes and spindle poles: looking at the periphery to find the centre. Biol Cell 2006;98(9):557-65.

99. Kirschner M, Mitchison T. Beyond self-assembly: from microtubules to morphogenesis. Cell 1986;45(3):329-42.

100. Bartolini F, Gundersen GG. Formins and microtubules. Biochim Biophys Acta 2010;1803(2):164-73.

101. Schuyler SC, Pellman D. Microtubule "plus-end-tracking proteins": The end is just the beginning. Cell 2001;105(4):421-4.

102. Galjart N, Perez F. A plus-end raft to control microtubule dynamics and function. Curr Opin Cell Biol 2003;15(1):48-53.

103. Ferreira JG, Pereira AL, Maiato H. Microtubule plus-end tracking proteins and their roles in cell division. Int Rev Cell Mol Biol 2014;309:59-140.

104. Kumar P, Wittmann T. +TIPs: SxIPping along microtubule ends. Trends Cell Biol 2012;22(8):418-28.

105. Komarova Y, De Groot CO, Grigoriev I, Gouveia SM, Munteanu EL, Schober JM*, et al.* Mammalian end binding proteins control persistent microtubule growth. J Cell Biol 2009;184(5):691-706.

106. Nelson S, Nathke IS. Interactions and functions of the adenomatous polyposis coli (APC) protein at a glance. J Cell Sci 2013;126(Pt 4):873-7.

107. Zumbrunn J, Kinoshita K, Hyman AA, Nathke IS. Binding of the adenomatous polyposis coli protein to microtubules increases microtubule stability and is regulated by GSK3 beta phosphorylation. Curr Biol 2001;11(1):44-9.

108. Nathke I. APC at a glance. J Cell Sci 2004;117(Pt 21):4873-5.

109. Nathke I. Cytoskeleton out of the cupboard: colon cancer and cytoskeletal changes induced by loss of APC. Nat Rev Cancer 2006;6(12):967-74.

110. Etienne-Manneville S, Hall A. Cdc42 regulates GSK-3beta and adenomatous polyposis coli to control cell polarity. Nature 2003;421(6924):753-6.

111. Schulze E, Kirschner M. Dynamic and stable populations of microtubules in cells. J Cell Biol 1987;104(2):277-88.

112. Peris L, Wagenbach M, Lafanechere L, Brocard J, Moore AT, Kozielski F*, et al.* Motor-dependent microtubule disassembly driven by tubulin tyrosination. J Cell Biol 2009;185(7):1159-66.

113. Hammond JW, Huang CF, Kaech S, Jacobson C, Banker G, Verhey KJ. Posttranslational modifications of tubulin and the polarized transport of kinesin-1 in neurons. Mol Biol Cell 2010;21(4):572-83.

114. Reed NA, Cai D, Blasius TL, Jih GT, Meyhofer E, Gaertig J*, et al.* Microtubule acetylation promotes kinesin-1 binding and transport. Curr Biol 2006;16(21):2166-72.

115. Rao JS. Molecular mechanisms of glioma invasiveness: the role of proteases. Nat Rev Cancer 2003;3(7):489-501.

116. Hynes RO. The extracellular matrix: not just pretty fibrils. Science 2009;326(5957):1216-9.

117. Mohanam S, Gladson CL, Rao CN, Rao JS. Biological significance of the expression of urokinase-type plasminogen activator receptors (uPARs) in brain tumors. Front Biosci 1999;4:D178-87.

118. Levicar N, Strojnik T, Kos J, Dewey RA, Pilkington GJ, Lah TT. Lysosomal enzymes, cathepsins in brain tumour invasion. J Neurooncol 2002;58(1):21-32.

119. Hagemann C, Anacker J, Ernestus RI, Vince GH. A complete compilation of matrix metalloproteinase expression in human malignant gliomas. World J Clin Oncol 2012;3(5):67-79.

120. Scaringi C, Minniti G, Caporello P, Enrici RM. Integrin inhibitor cilengitide for the treatment of glioblastoma: a brief overview of current clinical results. Anticancer Res 2012;32(10):4213-23.

121. Schnell O, Krebs B, Wagner E, Romagna A, Beer AJ, Grau SJ*, et al.* Expression of integrin alphavbeta3 in gliomas correlates with tumor grade and is not restricted to tumor vasculature. Brain Pathol 2008;18(3):378-86

122. Bello L, Francolini M, Marthyn P, Zhang J, Carroll RS, Nikas DC*, et al.* Alpha(v)beta3 and alpha(v)beta5 integrin expression in glioma periphery. Neurosurgery 2001;49(2):380-9; discussion 90.

123. Rooprai HK, Vanmeter T, Panou C, Schnull S, Trillo-Pazos G, Davies D*, et al.* The role of integrin receptors in aspects of glioma invasion in vitro. Int J Dev Neurosci 1999;17(5-6):613-23.

124. Paulus W, Tonn JC. Basement membrane invasion of glioma cells mediated by integrin receptors. J Neurosurg 1994;80(3):515-9.

125. Gumbiner BM. Regulation of cadherin-mediated adhesion in morphogenesis. Nat Rev Mol Cell Biol 2005;6(8):622-34.

126. Friedl P, Wolf K. Tumour-cell invasion and migration: diversity and escape mechanisms. Nat Rev Cancer 2003;3(5):362-74.

127. Satelli A, Li S. Vimentin in cancer and its potential as a molecular target for cancer therapy. Cell Mol Life Sci 2011;68(18):3033-46.

128. Hugo H, Ackland ML, Blick T, Lawrence MG, Clements JA, Williams ED*, et al.* Epithelial--mesenchymal and mesenchymal--epithelial transitions in carcinoma progression. J Cell Physiol 2007;213(2):374-83.

129. Bremnes RM, Donnem T, Al-Saad S, Al-Shibli K, Andersen S, Sirera R*, et al.* The role of tumor stroma in cancer progression and prognosis: emphasis on carcinoma-associated fibroblasts and non-small cell lung cancer. J Thorac Oncol 2011;6(1):209-17.

130. Hanahan D, Coussens LM. Accessories to the crime: functions of cells recruited to the tumor microenvironment. Cancer Cell 2012;21(3):309-22.

131. Chaffer CL, Weinberg RA. A perspective on cancer cell metastasis. Science 2011;331(6024):1559-64.

132. Elliott BE, Hung WL, Boag AH, Tuck AB. The role of hepatocyte growth factor (scatter factor) in epithelial-mesenchymal transition and breast cancer. Can J Physiol Pharmacol 2002;80(2):91-102.

133. Ma Y, Liu H, Zhang H, Shao RG. [The TGF-beta signaling pathway induced EMT in breast cancer]. Yao Xue Xue Bao 2015;50(4):385-92.

134. Moustakas A, Heldin P. TGFbeta and matrix-regulated epithelial to mesenchymal transition. Biochim Biophys Acta 2014;1840(8):2621-34.

135. Karnoub AE, Dash AB, Vo AP, Sullivan A, Brooks MW, Bell GW*, et al.* Mesenchymal stem cells within tumour stroma promote breast cancer metastasis. Nature 2007;449(7162):557-63.

136. Joyce JA, Pollard JW. Microenvironmental regulation of metastasis. Nat Rev Cancer 2009;9(4):239-52.

137. Wyckoff J, Wang W, Lin EY, Wang Y, Pixley F, Stanley ER*, et al.* A paracrine loop between tumor cells and macrophages is required for tumor cell migration in mammary tumors. Cancer Res 2004;64(19):7022-9.

138. Abraham S, Zhang W, Greenberg N, Zhang M. Maspin functions as tumor suppressor by increasing cell adhesion to extracellular matrix in prostate tumor cells. J Urol 2003;169(3):1157-61.

139. Sager R, Sheng S, Pemberton P, Hendrix MJ. Maspin. A tumor suppressing serpin. Adv Exp Med Biol 1997;425:77-88.

140. Chen EI, Yates JR. Maspin and tumor metastasis. IUBMB Life 2006;58(1):25-9.

141. Reardon DA, Neyns B, Weller M, Tonn JC, Nabors LB, Stupp R. Cilengitide: an RGD pentapeptide alphanubeta3 and alphanubeta5 integrin inhibitor in development for glioblastoma and other malignancies. Future Oncol 2011;7(3):339-54.

142. Reardon DA, Cheresh D. Cilengitide: a prototypic integrin inhibitor for the treatment of glioblastoma and other malignancies. Genes Cancer 2011;2(12):1159-65.

143. Leblond P, Dewitte A, Le Tinier F, Bal-Mahieu C, Baroncini M, Sarrazin T*, et al.* Cilengitide targets pediatric glioma and

neuroblastoma cells through cell detachment and anoikis induction. Anticancer Drugs 2013;24(8):818-25.

144. Lomonaco SL, Finniss S, Xiang C, Lee HK, Jiang W, Lemke N*, et al.* Cilengitide induces autophagy-mediated cell death in glioma cells. Neuro Oncol 2011;13(8):857-65.

145. Maurer GD, Tritschler I, Adams B, Tabatabai G, Wick W, Stupp R*, et al.* Cilengitide modulates attachment and viability of human glioma cells, but not sensitivity to irradiation or temozolomide in vitro. Neuro Oncol 2009;11(6):747-56.

146. Mikkelsen T, Brodie C, Finniss S, Berens ME, Rennert JL, Nelson K*, et al.* Radiation sensitization of glioblastoma by cilengitide has unanticipated schedule-dependency. Int J Cancer 2009;124(11):2719-27.

147. Stupp R, Dietrich PY, Ostermann Kraljevic S, Pica A, Maillard I, Maeder P*, et al.* Promising survival for patients with newly diagnosed glioblastoma multiforme treated with concomitant radiation plus temozolomide followed by adjuvant temozolomide. J Clin Oncol 2002;20(5):1375-82.

148. Stupp R, Mason WP, van den Bent MJ, Weller M, Fisher B, Taphoorn MJ*, et al.* Radiotherapy plus concomitant and adjuvant temozolomide for glioblastoma. N Engl J Med 2005;352(10):987-96.

149. Stupp R, Hegi ME, Neyns B, Goldbrunner R, Schlegel U, Clement PM*, et al.* Phase I/IIa study of cilengitide and temozolomide with concomitant radiotherapy followed by cilengitide and temozolomide maintenance therapy in patients with newly diagnosed glioblastoma. J Clin Oncol 2010;28(16):2712-8.

150. Reardon DA, Fink KL, Mikkelsen T, Cloughesy TF, O'Neill A, Plotkin S*, et al.* Randomized phase II study of cilengitide, an integrin-targeting arginine-glycine-aspartic acid peptide, in recurrent glioblastoma multiforme. J Clin Oncol 2008;26(34):5610-7.

151. de Groot JF, Lamborn KR, Chang SM, Gilbert MR, Cloughesy TF, Aldape K*, et al.* Phase II study of aflibercept in recurrent malignant glioma: a North American Brain Tumor Consortium study. J Clin Oncol 2011;29(19):2689-95.

152. Eskens FA, Dumez H, Hoekstra R, Perschl A, Brindley C, Bottcher S*, et al.* Phase I and pharmacokinetic study of continuous twice weekly intravenous administration of Cilengitide (EMD 121974), a novel inhibitor of the integrins alphavbeta3 and alphavbeta5 in patients with advanced solid tumours. Eur J Cancer 2003;39(7):917-26.

153. Hariharan S, Gustafson D, Holden S, McConkey D, Davis D, Morrow M*, et al.* Assessment of the biological and pharmacological effects of

the alpha nu beta3 and alpha nu beta5 integrin receptor antagonist, cilengitide (EMD 121974), in patients with advanced solid tumors. Ann Oncol 2007;18(8):1400-7.

154. Stupp R, Hegi ME, Gorlia T, Erridge SC, Perry J, Hong YK*, et al.* Cilengitide combined with standard treatment for patients with newly diagnosed glioblastoma with methylated MGMT promoter (CENTRIC EORTC 26071-22072 study): a multicentre, randomised, open-label, phase 3 trial. Lancet Oncol 2014;15(10):1100-8.

155. Zagzag D, Friedlander DR, Margolis B, Grumet M, Semenza GL, Zhong H*, et al.* Molecular events implicated in brain tumor angiogenesis and invasion. Pediatr Neurosurg 2000;33(1):49-55.

156. Natarajan M, Hecker TP, Gladson CL. FAK signaling in anaplastic astrocytoma and glioblastoma tumors. Cancer J 2003;9(2):126-33.

157. Liu TJ, LaFortune T, Honda T, Ohmori O, Hatakeyama S, Meyer T*, et al.* Inhibition of both focal adhesion kinase and insulin-like growth factor-I receptor kinase suppresses glioma proliferation in vitro and in vivo. Mol Cancer Ther 2007;6(4):1357-67.

158. Angers-Loustau A, Hering R, Werbowetski TE, Kaplan DR, Del Maestro RF. SRC regulates actin dynamics and invasion of malignant glial cells in three dimensions. Mol Cancer Res 2004;2(11):595-605.

159. Araujo J, Logothetis C. Dasatinib: a potent SRC inhibitor in clinical development for the treatment of solid tumors. Cancer Treat Rev 2010;36(6):492-500.

160. Franceschi E, Stupp R, van den Bent MJ, van Herpen C, Laigle Donadey F, Gorlia T*, et al.* EORTC 26083 phase I/II trial of dasatinib in combination with CCNU in patients with recurrent glioblastoma. Neuro Oncol 2012;14(12):1503-10.

161. Reardon DA, Vredenburgh JJ, Desjardins A, Peters KB, Sathornsumetee S, Threatt S*, et al.* Phase 1 trial of dasatinib plus erlotinib in adults with recurrent malignant glioma. J Neurooncol 2012;108(3):499-506.

162. Broniscer A, Baker SD, Wetmore C, Pai Panandiker AS, Huang J, Davidoff AM*, et al.* Phase I trial, pharmacokinetics, and pharmacodynamics of vandetanib and dasatinib in children with newly diagnosed diffuse intrinsic pontine glioma. Clin Cancer Res 2013;19(11):3050-8.

163. Biological Medicine for Diffuse Intrinsic Pontine Glioma (DIPG) Eradication (BIOMEDE). U.S. National Institutes of Health <https://clinicaltrials.gov/ct2/show/NCT02233049>. Accessed 2015 14th September.

164. Truffaux N, Philippe C, Paulsson J, Andreiuolo F, Guerrini-Rousseau L, Cornilleau G*, et al.* Preclinical evaluation of dasatinib alone and in combination with cabozantinib for the treatment of diffuse intrinsic pontine glioma. Neuro Oncol 2015;17(7):953-64.

165. Huveldt D, Lewis-Tuffin LJ, Carlson BL, Schroeder MA, Rodriguez F, Giannini C*, et al.* Targeting Src family kinases inhibits bevacizumab-induced glioma cell invasion. PLoS One 2013;8(2):e56505.

166. Tonn JC, Kerkau S, Hanke A, Bouterfa H, Mueller JG, Wagner S*, et al.* Effect of synthetic matrix-metalloproteinase inhibitors on invasive capacity and proliferation of human malignant gliomas in vitro. Int J Cancer 1999;80(5):764-72.

167. Price A, Shi Q, Morris D, Wilcox ME, Brasher PM, Rewcastle NB*, et al.* Marked inhibition of tumor growth in a malignant glioma tumor model by a novel synthetic matrix metalloproteinase inhibitor AG3340. Clin Cancer Res 1999;5(4):845-54.

168. Coussens LM, Fingleton B, Matrisian LM. Matrix metalloproteinase inhibitors and cancer: trials and tribulations. Science 2002;295(5564):2387-92.

169. Groves MD, Puduvalli VK, Conrad CA, Gilbert MR, Yung WK, Jaeckle K*, et al.* Phase II trial of temozolomide plus marimastat for recurrent anaplastic gliomas: a relationship among efficacy, joint toxicity and anticonvulsant status. J Neurooncol 2006;80(1):83-90.

170. Levin VA, Phuphanich S, Yung WK, Forsyth PA, Maestro RD, Perry JR*, et al.* Randomized, double-blind, placebo-controlled trial of marimastat in glioblastoma multiforme patients following surgery and irradiation. J Neurooncol 2006;78(3):295-302.

171. Rao Malla R, Gopinath S, Alapati K, Gorantla B, Gondi CS, Rao JS. Knockdown of cathepsin B and uPAR inhibits CD151 and alpha3beta1 integrin-mediated cell adhesion and invasion in glioma. Mol Carcinog 2013;52(10):777-90.

172. Engelhard HH, Homer RJ, Duncan HA, Rozental J. Inhibitory effects of phenylbutyrate on the proliferation, morphology, migration and invasiveness of malignant glioma cells. J Neurooncol 1998;37(2):97-108.

173. Mohanam S, Jasti SL, Kondraganti SR, Chandrasekar N, Kin Y, Fuller GN*, et al.* Stable transfection of urokinase-type plasminogen activator antisense construct modulates invasion of human glioblastoma cells. Clin Cancer Res 2001;7(8):2519-26.

174. Demchik LL, Sameni M, Nelson K, Mikkelsen T, Sloane BF. Cathepsin B and glioma invasion. Int J Dev Neurosci 1999;17(5-6):483-94.

175. Dumontet C, Jordan MA. Microtubule-binding agents: a dynamic field of cancer therapeutics. Nat Rev Drug Discov 2010;9(10):790-803.

176. Tonn JC, Haugland HK, Saraste J, Roosen K, Laerum OD. Differential effects of vincristine and phenytoin on the proliferation, migration, and invasion of human glioma cell lines. J Neurosurg 1995;82(6):1035-43.

177. Terzis AJ, Thorsen F, Heese O, Visted T, Bjerkvig R, Dahl O*, et al.* Proliferation, migration and invasion of human glioma cells exposed to paclitaxel (Taxol) in vitro. Br J Cancer 1997;75(12):1744-52.

178. Gerecitano JF, Stephenson JJ, Lewis NL, Osmukhina A, Li J, Wu K*, et al.* A Phase I trial of the kinesin spindle protein (Eg5) inhibitor AZD4877 in patients with solid and lymphoid malignancies. Invest New Drugs 2013;31(2):355-62.

179. Jones R, Vuky J, Elliott T, Mead G, Arranz JA, Chester J*, et al.* Phase II study to assess the efficacy, safety and tolerability of the mitotic spindle kinesin inhibitor AZD4877 in patients with recurrent advanced urothelial cancer. Invest New Drugs 2013;31(4):1001-7.

180. Infante JR, Kurzrock R, Spratlin J, Burris HA, Eckhardt SG, Li J*, et al.* A Phase I study to assess the safety, tolerability, and pharmacokinetics of AZD4877, an intravenous Eg5 inhibitor in patients with advanced solid tumors. Cancer Chemother Pharmacol 2012;69(1):165-72.

181. Pusztai L, Jeong JH, Gong Y, Ross JS, Kim C, Paik S*, et al.* Evaluation of microtubule-associated protein-Tau expression as a prognostic and predictive marker in the NSABP-B 28 randomized clinical trial. J Clin Oncol 2009;27(26):4287-92.

182. Cooper JR, Wagenbach M, Asbury CL, Wordeman L. Catalysis of the microtubule on-rate is the major parameter regulating the depolymerase activity of MCAK. Nat Struct Mol Biol 2010;17(1):77-82.

183. Ohnishi T, Arita N, Hayakawa T, Izumoto S, Taki T, Yamamoto H. Motility factor produced by malignant glioma cells: role in tumor invasion. J Neurosurg 1990;73(6):881-8.

184. Munson J, Bonner M, Fried L, Hofmekler J, Arbiser J, Bellamkonda R. Identifying new small molecule anti-invasive compounds for glioma treatment. Cell Cycle 2013;12(14):2200-9.

185. Fenteany G, Zhu S. Small-molecule inhibitors of actin dynamics and cell motility. Curr Top Med Chem 2003;3(6):593-616.

186. Ivkovic S, Beadle C, Noticewala S, Massey SC, Swanson KR, Toro LN*, et al.* Direct inhibition of myosin II effectively blocks glioma

invasion in the presence of multiple motogens. Mol Biol Cell 2012;23(4):533-42.

187. Kwiatkowska A, Didier S, Fortin S, Chuang Y, White T, Berens ME*, et al.* The small GTPase RhoG mediates glioblastoma cell invasion. Mol Cancer 2012;11:65.

188. Vigorito E, Bell S, Hebeis BJ, Reynolds H, McAdam S, Emson PC*, et al.* Immunological function in mice lacking the Rac-related GTPase RhoG. Mol Cell Biol 2004;24(2):719-29.

189. Davis FM, Stewart TA, Thompson EW, Monteith GR. Targeting EMT in cancer: opportunities for pharmacological intervention. Trends Pharmacol Sci 2014;35(9):479-88.

190. Tanaka H, Kono E, Tran CP, Miyazaki H, Yamashiro J, Shimomura T*, et al.* Monoclonal antibody targeting of N-cadherin inhibits prostate cancer growth, metastasis and castration resistance. Nat Med 2010;16(12):1414-20.

191. Lahat G, Zhu QS, Huang KL, Wang S, Bolshakov S, Liu J*, et al.* Vimentin is a novel anti-cancer therapeutic target; insights from in vitro and in vivo mice xenograft studies. PLoS One 2010;5(4):e10105.

192. Chaffer CL, Brennan JP, Slavin JL, Blick T, Thompson EW, Williams ED. Mesenchymal-to-epithelial transition facilitates bladder cancer metastasis: role of fibroblast growth factor receptor-2. Cancer Res 2006;66(23):11271-8.

193. Jope RS, Johnson GV. The glamour and gloom of glycogen synthase kinase-3. Trends Biochem Sci 2004;29(2):95-102.

194. Mukai F, Ishiguro K, Sano Y, Fujita SC. Alternative splicing isoform of tau protein kinase I/glycogen synthase kinase 3beta. J Neurochem 2002;81(5):1073-83.

195. Luo J. Glycogen synthase kinase 3beta (GSK3beta) in tumorigenesis and cancer chemotherapy. Cancer Lett 2009;273(2):194-200.

196. Meijer L, Flajolet M, Greengard P. Pharmacological inhibitors of glycogen synthase kinase 3. Trends Pharmacol Sci 2004;25(9):471-80.

197. Hoeflich KP, Luo J, Rubie EA, Tsao MS, Jin O, Woodgett JR. Requirement for glycogen synthase kinase-3beta in cell survival and NF-kappaB activation. Nature 2000;406(6791):86-90.

198. MacAulay K, Doble BW, Patel S, Hansotia T, Sinclair EM, Drucker DJ*, et al.* Glycogen synthase kinase 3alpha-specific regulation of murine hepatic glycogen metabolism. Cell Metab 2007;6(4):329-37.

199. Kaidanovich-Beilin O, Lipina TV, Takao K, van Eede M, Hattori S, Laliberte C*, et al.* Abnormalities in brain structure and behavior in GSK-3alpha mutant mice. Mol Brain 2009;2:35.

200. Medina M, Wandosell F. Deconstructing GSK-3: The Fine Regulation of Its Activity. Int J Alzheimers Dis 2011;2011:479249.

201. McCubrey JA, Steelman LS, Bertrand FE, Davis NM, Sokolosky M, Abrams SL*, et al.* GSK-3 as potential target for therapeutic intervention in cancer. Oncotarget 2014;5(10):2881-911.

202. Grimes CA, Jope RS. The multifaceted roles of glycogen synthase kinase 3beta in cellular signaling. Prog Neurobiol 2001;65(4):391-426.

203. Farago M, Dominguez I, Landesman-Bollag E, Xu X, Rosner A, Cardiff RD*, et al.* Kinase-inactive glycogen synthase kinase 3beta promotes Wnt signaling and mammary tumorigenesis. Cancer Res 2005;65(13):5792-801.

204. Leis H, Segrelles C, Ruiz S, Santos M, Paramio JM. Expression, localization, and activity of glycogen synthase kinase 3beta during mouse skin tumorigenesis. Mol Carcinog 2002;35(4):180-5.

205. Ma C, Wang J, Gao Y, Gao TW, Chen G, Bower KA*, et al.* The role of glycogen synthase kinase 3beta in the transformation of epidermal cells. Cancer Res 2007;67(16):7756-64.

206. Ougolkov AV, Billadeau DD. Targeting GSK-3: a promising approach for cancer therapy? Future Oncol 2006;2(1):91-100.

207. Miyashita K, Kawakami K, Nakada M, Mai W, Shakoori A, Fujisawa H*, et al.* Potential therapeutic effect of glycogen synthase kinase 3beta inhibition against human glioblastoma. Clin Cancer Res 2009;15(3):887-97.

208. Watcharasit P, Bijur GN, Zmijewski JW, Song L, Zmijewska A, Chen X*, et al.* Direct, activating interaction between glycogen synthase kinase-3beta and p53 after DNA damage. Proc Natl Acad Sci U S A 2002;99(12):7951-5.

209. Beurel E, Jope RS. The paradoxical pro- and anti-apoptotic actions of GSK3 in the intrinsic and extrinsic apoptosis signaling pathways. Prog Neurobiol 2006;79(4):173-89.

210. Doble BW, Woodgett JR. Role of glycogen synthase kinase-3 in cell fate and epithelial-mesenchymal transitions. Cells Tissues Organs 2007;185(1-3):73-84.

211. Zhou W, Wang L, Gou SM, Wang TL, Zhang M, Liu T*, et al.* ShRNA silencing glycogen synthase kinase-3 beta inhibits tumor growth and angiogenesis in pancreatic cancer. Cancer Lett 2012;316(2):178-86.

212. Cao Q, Lu X, Feng YJ. Glycogen synthase kinase-3beta positively regulates the proliferation of human ovarian cancer cells. Cell Res 2006;16(7):671-7.

213. Sun T, Rodriguez M, Kim L. Glycogen synthase kinase 3 in the world of cell migration. Dev Growth Differ 2009;51(9):735-42.

214. Rath N, Olson MF. Rho-associated kinases in tumorigenesis: re-considering ROCK inhibition for cancer therapy. EMBO Rep 2012;13(10):900-8.

215. Jiang W, Betson M, Mulloy R, Foster R, Levay M, Ligeti E*, et al.* p190A RhoGAP is a glycogen synthase kinase-3-beta substrate required for polarized cell migration. J Biol Chem 2008;283(30):20978-88.

216. Koivisto L, Hakkinen L, Matsumoto K, McCulloch CA, Yamada KM, Larjava H. Glycogen synthase kinase-3 regulates cytoskeleton and translocation of Rac1 in long cellular extensions of human keratinocytes. Exp Cell Res 2004;293(1):68-80.

217. Farooqui R, Zhu S, Fenteany G. Glycogen synthase kinase-3 acts upstream of ADP-ribosylation factor 6 and Rac1 to regulate epithelial cell migration. Exp Cell Res 2006;312(9):1514-25.

218. Morfini G, Szebenyi G, Elluru R, Ratner N, Brady ST. Glycogen synthase kinase 3 phosphorylates kinesin light chains and negatively regulates kinesin-based motility. EMBO J 2002;21(3):281-93.

219. Lansbergen G, Grigoriev I, Mimori-Kiyosue Y, Ohtsuka T, Higa S, Kitajima I*, et al.* CLASPs attach microtubule plus ends to the cell cortex through a complex with LL5beta. Dev Cell 2006;11(1):21-32.

220. Wittmann T, Waterman-Storer CM. Spatial regulation of CLASP affinity for microtubules by Rac1 and GSK3beta in migrating epithelial cells. J Cell Biol 2005;169(6):929-39.

221. Schaller MD. Paxillin: a focal adhesion-associated adaptor protein. Oncogene 2001;20(44):6459-72.

222. Cai X, Li M, Vrana J, Schaller MD. Glycogen synthase kinase 3- and extracellular signal-regulated kinase-dependent phosphorylation of paxillin regulates cytoskeletal rearrangement. Mol Cell Biol 2006;26(7):2857-68.

223. Bianchi M, De Lucchini S, Marin O, Turner DL, Hanks SK, Villa-Moruzzi E. Regulation of FAK Ser-722 phosphorylation and kinase activity by GSK3 and PP1 during cell spreading and migration. Biochem J 2005;391(Pt 2):359-70.

224. Jope RS. Lithium and GSK-3: one inhibitor, two inhibitory actions, multiple outcomes. Trends Pharmacol Sci 2003;24(9):441-3.

225. O'Brien WT, Klein PS. Validating GSK3 as an in vivo target of lithium action. Biochem Soc Trans 2009;37(Pt 5):1133-8.

226. Eldar-Finkelman H, Martinez A. GSK-3 Inhibitors: Preclinical and Clinical Focus on CNS. Front Mol Neurosci 2011;4:32.

227. Stambolic V, Ruel L, Woodgett JR. Lithium inhibits glycogen synthase kinase-3 activity and mimics wingless signalling in intact cells. Curr Biol 1996;6(12):1664-8.

228. Cheng K, Creacy S, Larner J. 'Insulin-like' effects of lithium ion on isolated rat adipocytes. II. Specific activation of glycogen synthase. Mol Cell Biochem 1983;56(2):183-9.

229. Nunes MA, Viel TA, Buck HS. Microdose lithium treatment stabilized cognitive impairment in patients with Alzheimer's disease. Curr Alzheimer Res 2013;10(1):104-7.

230. Forlenza OV, Diniz BS, Radanovic M, Santos FS, Talib LL, Gattaz WF. Disease-modifying properties of long-term lithium treatment for amnestic mild cognitive impairment: randomised controlled trial. Br J Psychiatry 2011;198(5):351-6.

231. Fornai F, Longone P, Cafaro L, Kastsiuchenka O, Ferrucci M, Manca ML*, et al.* Lithium delays progression of amyotrophic lateral sclerosis. Proc Natl Acad Sci U S A 2008;105(6):2052-7.

232. Lubner SJ, Kunnimalaiyaan M, Holen KD, Ning L, Ndiaye M, Loconte NK*, et al.* A preclinical and clinical study of lithium in low-grade neuroendocrine tumors. Oncologist 2011;16(4):452-7.

233. Effect of Lithium Carbonate on Low-Dose Radioiodine Therapy in Early Thyroid Cancer. 2013. U.S. National Institutes of Health <https://clinicaltrials.gov/ct2/show/NCT00251316?term=Effect+of+Lithium+Carbonate+on+Low-Dose+Radioiodine+Therapy+in+Early+Thyroid+Cancer&rank=1>. Accessed 2015 18th September.

234. Evaluation of Lithium and It's Effect on Clinically Localized Prostate Cancer. 2014. U.S National Institutes of Health <https://clinicaltrials.gov/ct2/show/study/NCT02198859?term=lithium+cancer&rank=4>. Accessed 2015 18th September.

235. Levine S, Saltzman A, Katof B, Meister A, Cooper TB. Prevention of lithium nephrotoxicity in a novel one-hour model in rats. Psychopharmacology (Berl) 1998;138(1):34-9.

236. Nowicki MO, Dmitrieva N, Stein AM, Cutter JL, Godlewski J, Saeki Y*, et al.* Lithium inhibits invasion of glioma cells; possible involvement of glycogen synthase kinase-3. Neuro Oncol 2008;10(5):690-9.

237. Meijer L, Shearer J, Bettayeb K, Ferandin Y. Diversity of the intracellular mechanisms underlying the anti-tumor properties of indirubins. International Congress Series 2007;1304:60-74.

238. Hoessel R, Leclerc S, Endicott JA, Nobel ME, Lawrie A, Tunnah P*, et al.* Indirubin, the active constituent of a Chinese antileukaemia medicine, inhibits cyclin-dependent kinases. Nat Cell Biol 1999;1(1):60-7.

239. Gan WJ YT, Wen S, Liu Y, Tan Z, Deng C, Wu J, Liu M Studies on the mechanism of indirubin action in the treatment of chronic myelocytic leukemia (CML). II. 5'-Nucleotidase in the peripheral white blood cells of CML. China Academy of Medical Sciences 1985;6:611-13.

240. Eisenbrand G, Hippe F, Jakobs S, Muehlbeyer S. Molecular mechanisms of indirubin and its derivatives: novel anticancer molecules with their origin in traditional Chinese phytomedicine. J Cancer Res Clin Oncol 2004;130(11):627-35.

241. Leclerc S, Garnier M, Hoessel R, Marko D, Bibb JA, Snyder GL*, et al.* Indirubins inhibit glycogen synthase kinase-3 beta and CDK5/p25, two protein kinases involved in abnormal tau phosphorylation in Alzheimer's disease. A property common to most cyclin-dependent kinase inhibitors? J Biol Chem 2001;276(1):251-60.

242. Park EJ, Choi SJ, Kim YC, Lee SH, Park SW, Lee SK. Novel small molecule activators of beta-catenin-mediated signaling pathway: structure-activity relationships of indirubins. Bioorg Med Chem Lett 2009;19(8):2282-4.

243. Meijer L, Skaltsounis AL, Magiatis P, Polychronopoulos P, Knockaert M, Leost M*, et al.* GSK-3-selective inhibitors derived from Tyrian purple indirubins. Chem Biol 2003;10(12):1255-66.

244. Hooper C, Killick R, Lovestone S. The GSK3 hypothesis of Alzheimer's disease. J Neurochem 2008;104(6):1433-9.

245. Perabo FG, Frossler C, Landwehrs G, Schmidt DH, von Rucker A, Wirger A*, et al.* Indirubin-3'-monoxime, a CDK inhibitor induces growth inhibition and apoptosis-independent up-regulation of survivin in transitional cell cancer. Anticancer Res 2006;26(3A):2129-35.

246. Williams SP, Nowicki MO, Liu F, Press R, Godlewski J, Abdel-Rasoul M*, et al.* Indirubins decrease glioma invasion by blocking migratory phenotypes in both the tumor and stromal endothelial cell compartments. Cancer Res 2011;71(16):5374-80.

247. Georgievska B, Sandin J, Doherty J, Mortberg A, Neelissen J, Andersson A*, et al.* AZD1080, a novel GSK3 inhibitor, rescues synaptic plasticity deficits in rodent brain and exhibits peripheral target engagement in humans. J Neurochem 2013;125(3):446-56.

248. Cohen Y, Chetrit A, Cohen Y, Sirota P, Modan B. Cancer morbidity in psychiatric patients: influence of lithium carbonate treatment. Med Oncol 1998;15(1):32-6.

249. Gould TD, Gray NA, Manji HK. Effects of a glycogen synthase kinase-3 inhibitor, lithium, in adenomatous polyposis coli mutant mice. Pharmacol Res 2003;48(1):49-53.

250. Aguilar-Morante D, Morales-Garcia JA, Sanz-SanCristobal M, Garcia-Cabezas MA, Santos A, Perez-Castillo A. Inhibition of glioblastoma growth by the thiadiazolidinone compound TDZD-8. PLoS One 2010;5(11):e13879.

251. Kotliarova S, Pastorino S, Kovell LC, Kotliarov Y, Song H, Zhang W*, et al.* Glycogen synthase kinase-3 inhibition induces glioma cell death through c-MYC, nuclear factor-kappaB, and glucose regulation. Cancer Res 2008;68(16):6643-51.

252. Russell SJ, Peng KW, Bell JC. Oncolytic virotherapy. Nat Biotechnol 2012;30(7):658-70.

253. Prestwich RJ, Harrington KJ, Pandha HS, Vile RG, Melcher AA, Errington F. Oncolytic viruses: a novel form of immunotherapy. Expert Rev Anticancer Ther 2008;8(10):1581-8.

254. Kaufman HL, Kohlhapp FJ, Zloza A. Oncolytic viruses: a new class of immunotherapy drugs. Nat Rev Drug Discov 2015;14(9):642-62.

255. Meurs E, Chong K, Galabru J, Thomas NS, Kerr IM, Williams BR*, et al.* Molecular cloning and characterization of the human double-stranded RNA-activated protein kinase induced by interferon. Cell 1990;62(2):379-90.

256. Elde NC, Child SJ, Geballe AP, Malik HS. Protein kinase R reveals an evolutionary model for defeating viral mimicry. Nature 2009;457(7228):485-9.

257. Koks CA, De Vleeschouwer S, Graf N, Van Gool SW. Immune Suppression during Oncolytic Virotherapy for High-Grade Glioma; Yes or No? J Cancer 2015;6(3):203-17.

258. Lichty BD, Breitbach CJ, Stojdl DF, Bell JC. Going viral with cancer immunotherapy. Nat Rev Cancer 2014;14(8):559-67.

259. Motz GT, Coukos G. Deciphering and reversing tumor immune suppression. Immunity 2013;39(1):61-73.

260. Steinbrink K, Jonuleit H, Muller G, Schuler G, Knop J, Enk AH. Interleukin-10-treated human dendritic cells induce a melanoma-antigen-specific anergy in CD8(+) T cells resulting in a failure to lyse tumor cells. Blood 1999;93(5):1634-42.

261. Curiel TJ, Wei S, Dong H, Alvarez X, Cheng P, Mottram P*, et al.* Blockade of B7-H1 improves myeloid dendritic cell-mediated antitumor immunity. Nat Med 2003;9(5):562-7.

262. Elia AR, Cappello P, Puppo M, Fraone T, Vanni C, Eva A*, et al.* Human dendritic cells differentiated in hypoxia down-modulate antigen uptake and change their chemokine expression profile. J Leukoc Biol 2008;84(6):1472-82.

263. Gabrilovich DI, Ostrand-Rosenberg S, Bronte V. Coordinated regulation of myeloid cells by tumours. Nat Rev Immunol 2012;12(4):253-68.

264. Gottfried E, Kunz-Schughart LA, Ebner S, Mueller-Klieser W, Hoves S, Andreesen R*, et al.* Tumor-derived lactic acid modulates dendritic cell activation and antigen expression. Blood 2006;107(5):2013-21.

265. Harlin H, Meng Y, Peterson AC, Zha Y, Tretiakova M, Slingluff C*, et al.* Chemokine expression in melanoma metastases associated with CD8+ T-cell recruitment. Cancer Res 2009;69(7):3077-85.

266. Proost P, Mortier A, Loos T, Vandercappellen J, Gouwy M, Ronsse I*, et al.* Proteolytic processing of CXCL11 by CD13/aminopeptidase N impairs CXCR3 and CXCR7 binding and signaling and reduces lymphocyte and endothelial cell migration. Blood 2007;110(1):37-44.

267. Facciabene A, Motz GT, Coukos G. T-regulatory cells: key players in tumor immune escape and angiogenesis. Cancer Res 2012;72(9):2162-71.

268. Gabrilovich DI, Nagaraj S. Myeloid-derived suppressor cells as regulators of the immune system. Nat Rev Immunol 2009;9(3):162-74.

269. Whiteside TL. Tumor-induced death of immune cells: its mechanisms and consequences. Semin Cancer Biol 2002;12(1):43-50.

270. Hamanishi J, Mandai M, Iwasaki M, Okazaki T, Tanaka Y, Yamaguchi K*, et al.* Programmed cell death 1 ligand 1 and tumor-infiltrating CD8+ T lymphocytes are prognostic factors of human ovarian cancer. Proc Natl Acad Sci U S A 2007;104(9):3360-5.

271. Schroder K, Hertzog PJ, Ravasi T, Hume DA. Interferon-gamma: an overview of signals, mechanisms and functions. J Leukoc Biol 2004;75(2):163-89.

272. Chesler DA, Reiss CS. The role of IFN-gamma in immune responses to viral infections of the central nervous system. Cytokine Growth Factor Rev 2002;13(6):441-54.

273. Russell SJ, Peng KW. Viruses as anticancer drugs. Trends Pharmacol Sci 2007;28(7):326-33.

274. Gelderblom HR. Medical Microbiology In: Baron S, editor. Structure and Classification of Viruses. 4th edition ed. University of Texas Medical Branch at Galveston;1996.

275. Hennig T, O'Hare P. Viruses and the nuclear envelope. Curr Opin Cell Biol 2015;34:113-21.

276. Karasneh GA, Shukla D. Herpes simplex virus infects most cell types in vitro: clues to its success. Virol J 2011;8:481.

277. McGeoch DJ, Rixon FJ, Davison AJ. Topics in herpesvirus genomics and evolution. Virus Res 2006;117(1):90-104.

278. Kukhanova MK, Korovina AN, Kochetkov SN. Human herpes simplex virus: life cycle and development of inhibitors. Biochemistry (Mosc) 2014;79(13):1635-52.

279. Friedman GK, Raborn J, Kelly VM, Cassady KA, Markert JM, Gillespie GY. Pediatric glioma stem cells: biologic strategies for oncolytic HSV virotherapy. Front Oncol 2013;3:28.

280. Andtbacka RH, Kaufman HL, Collichio F, Amatruda T, Senzer N, Chesney J*, et al.* Talimogene Laherparepvec Improves Durable Response Rate in Patients With Advanced Melanoma. J Clin Oncol 2015;33(25):2780-8.

281. Markert JM, Medlock MD, Rabkin SD, Gillespie GY, Todo T, Hunter WD*, et al.* Conditionally replicating herpes simplex virus mutant, G207 for the treatment of malignant glioma: results of a phase I trial. Gene Ther 2000;7(10):867-74.

282. Pyles RB, Warnick RE, Chalk CL, Szanti BE, Parysek LM. A novel multiply-mutated HSV-1 strain for the treatment of human brain tumors. Hum Gene Ther 1997;8(5):533-44.

283. Kasuya H, Kodera Y, Nakao A, Yamamura K, Gewen T, Zhiwen W*, et al.* Phase I Dose-escalation Clinical Trial of HF10 Oncolytic Herpes Virus in 17 Japanese Patients with Advanced Cancer. Hepatogastroenterology 2014;61(131):599-605.

284. Todo T. Oncolytic virus therapy using genetically engineered herpes simplex viruses. Front Biosci 2008;13:2060-4.

285. NFDA approves first-of-its-kind product for the treatment of melanoma. U.S. Department of Health and Human Services <http://www.fda.gov/NewsEvents/Newsroom/PressAnnouncements/ucm469571.htm%3E. Accessed 2015 24th November.

286. Roberts KL, Smith GL. Vaccinia virus morphogenesis and dissemination. Trends Microbiol 2008;16(10):472-9.

287. Eager RM, Nemunaitis J. Clinical development directions in oncolytic viral therapy. Cancer Gene Ther 2011;18(5):305-17.

288. Swanson JA, Watts C. Macropinocytosis. Trends Cell Biol 1995;5(11):424-8.

289. Parato KA, Breitbach CJ, Le Boeuf F, Wang J, Storbeck C, Ilkow C*, et al.* The oncolytic poxvirus JX-594 selectively replicates in and destroys cancer cells driven by genetic pathways commonly activated in cancers. Mol Ther 2012;20(4):749-58.

290. Ady JW, Heffner J, Mojica K, Johnsen C, Belin LJ, Love D*, et al.* Oncolytic immunotherapy using recombinant vaccinia virus GLV-1h68 kills sorafenib-resistant hepatocellular carcinoma efficiently. Surgery 2014;156(2):263-9.

291. Ehrig K, Kilinc MO, Chen NG, Stritzker J, Buckel L, Zhang Q*, et al.* Growth inhibition of different human colorectal cancer xenografts after a single intravenous injection of oncolytic vaccinia virus GLV-1h68. J Transl Med 2013;11:79.

292. Zhang Q, Yu YA, Wang E, Chen N, Danner RL, Munson PJ*, et al.* Eradication of solid human breast tumors in nude mice with an intravenously injected light-emitting oncolytic vaccinia virus. Cancer Res 2007;67(20):10038-46.

293. Wagner R, Matrosovich M, Klenk HD. Functional balance between haemagglutinin and neuraminidase in influenza virus infections. Rev Med Virol 2002;12(3):159-66.

294. Izmailyan R, Chang W. Vaccinia virus WR53.5/F14.5 protein is a new component of intracellular mature virus and is important for calcium-independent cell adhesion and vaccinia virus virulence in mice. J Virol 2008;82(20):10079-87.

295. Coombs KM. Reovirus structure and morphogenesis. Curr Top Microbiol Immunol 2006;309:117-67.

296. Mainou BA, Zamora PF, Ashbrook AW, Dorset DC, Kim KS, Dermody TS. Reovirus cell entry requires functional microtubules. MBio 2013;4(4).

297. Campbell JA, Schelling P, Wetzel JD, Johnson EM, Forrest JC, Wilson GA*, et al.* Junctional adhesion molecule a serves as a

receptor for prototype and field-isolate strains of mammalian reovirus. J Virol 2005;79(13):7967-78.

298. Maginnis MS, Forrest JC, Kopecky-Bromberg SA, Dickeson SK, Santoro SA, Zutter MM*, et al.* Beta1 integrin mediates internalization of mammalian reovirus. J Virol 2006;80(6):2760-70.

299. Mainou BA, Dermody TS. Src kinase mediates productive endocytic sorting of reovirus during cell entry. J Virol 2011;85(7):3203-13.

300. Strong JE, Coffey MC, Tang D, Sabinin P, Lee PW. The molecular basis of viral oncolysis: usurpation of the Ras signaling pathway by reovirus. EMBO J 1998;17(12):3351-62.

301. Rosen L, Evans HE, Spickard A. Reovirus infections in human volunteers. Am J Hyg 1963;77:29-37.

302. Hammill AM, Conner J, Cripe TP. Oncolytic virotherapy reaches adolescence. Pediatr Blood Cancer 2010;55(7):1253-63.

303. Kolb EA, Sampson V, Stabley D, Walter A, Sol-Church K, Cripe T*, et al.* A phase I trial and viral clearance study of reovirus (Reolysin) in children with relapsed or refractory extra-cranial solid tumors: a Children's Oncology Group Phase I Consortium report. Pediatr Blood Cancer 2015;62(5):751-8.

304. Black AJ, Morris DG. Clinical trials involving the oncolytic virus, reovirus: ready for prime time? Expert Rev Clin Pharmacol 2012;5(5):517-20.

305. Morris DG, Feng X, DiFrancesco LM, Fonseca K, Forsyth PA, Paterson AH*, et al.* REO-001: A phase I trial of percutaneous intralesional administration of reovirus type 3 dearing (Reolysin(R)) in patients with advanced solid tumors. Invest New Drugs 2013;31(3):696-706.

306. Galanis E, Markovic SN, Suman VJ, Nuovo GJ, Vile RG, Kottke TJ*, et al.* Phase II trial of intravenous administration of Reolysin((R)) (Reovirus Serotype-3-dearing Strain) in patients with metastatic melanoma. Mol Ther 2012;20(10):1998-2003.

307. Adair RA, Roulstone V, Scott KJ, Morgan R, Nuovo GJ, Fuller M*, et al.* Cell carriage, delivery, and selective replication of an oncolytic virus in tumor in patients. Sci Transl Med 2012;4(138):138ra77.

308. Radtke K, Dohner K, Sodeik B. Viral interactions with the cytoskeleton: a hitchhiker's guide to the cell. Cell Microbiol 2006;8(3):387-400.

309. Lyman MG, Enquist LW. Herpesvirus interactions with the host cytoskeleton. J Virol 2009;83(5):2058-66.

310. Taylor MP, Koyuncu OO, Enquist LW. Subversion of the actin cytoskeleton during viral infection. Nat Rev Microbiol 2011;9(6):427-39.

311. Naghavi MH, Gundersen GG, Walsh D. Plus-end tracking proteins, CLASPs, and a viral Akt mimic regulate herpesvirus-induced stable microtubule formation and virus spread. Proc Natl Acad Sci U S A 2013;110(45):18268-73.

312. Abdullah JM, Mustafa Z, Ideris A. Newcastle disease virus interaction in targeted therapy against proliferation and invasion pathways of glioblastoma multiforme. Biomed Res Int 2014;2014:386470.

313. Prechtel AT, Turza NM, Kobelt DJ, Eisemann JI, Coffin RS, McGrath Y*, et al.* Infection of mature dendritic cells with herpes simplex virus type 1 dramatically reduces lymphoid chemokine-mediated migration. J Gen Virol 2005;86(Pt 6):1645-57.

314. Theodoridis AA, Eich C, Figdor CG, Steinkasserer A. Infection of dendritic cells with herpes simplex virus type 1 induces rapid degradation of CYTIP, thereby modulating adhesion and migration. Blood 2011;118(1):107-15.

315. Leary SE, Olson JM. The molecular classification of medulloblastoma: driving the next generation clinical trials. Curr Opin Pediatr 2012;24(1):33-9.

316. Lasner TM, Kesari S, Brown SM, Lee VM, Fraser NW, Trojanowski JQ. Therapy of a murine model of pediatric brain tumors using a herpes simplex virus type-1 ICP34.5 mutant and demonstration of viral replication within the CNS. J Neuropathol Exp Neurol 1996;55(12):1259-69.

317. Friedman GK, Moore BP, Nan L, Kelly VM, Etminan T, Langford CP*, et al.* Pediatric medulloblastoma xenografts including molecular subgroup 3 and CD133+ and CD15+ cells are sensitive to killing by oncolytic herpes simplex viruses. Neuro Oncol 2015.

318. Yang WQ, Senger D, Muzik H, Shi ZQ, Johnson D, Brasher PM*, et al.* Reovirus prolongs survival and reduces the frequency of spinal and leptomeningeal metastases from medulloblastoma. Cancer Res 2003;63(12):3162-72.

319. Studebaker AW, Kreofsky CR, Pierson CR, Russell SJ, Galanis E, Raffel C. Treatment of medulloblastoma with a modified measles virus. Neuro Oncol 2010;12(10):1034-42.

320. Studebaker AW, Hutzen B, Pierson CR, Russell SJ, Galanis E, Raffel C. Oncolytic measles virus prolongs survival in a murine model of cerebral spinal fluid-disseminated medulloblastoma. Neuro Oncol 2012;14(4):459-70.

321. Lun XQ, Zhou H, Alain T, Sun B, Wang L, Barrett JW*, et al.* Targeting human medulloblastoma: oncolytic virotherapy with myxoma virus is enhanced by rapamycin. Cancer Res 2007;67(18):8818-27.

322. Yu L, Baxter PA, Zhao X, Liu Z, Wadhwa L, Zhang Y*, et al.* A single intravenous injection of oncolytic picornavirus SVV-001 eliminates medulloblastomas in primary tumor-based orthotopic xenograft mouse models.

323. Friedman GK, Langford CP, Coleman JM, Cassady KA, Parker JN, Markert JM*, et al.* Engineered herpes simplex viruses efficiently infect and kill CD133+ human glioma xenograft cells that express CD111. J Neurooncol 2009;95(2):199-209.

324. Morton CL, Houghton PJ, Kolb EA, Gorlick R, Reynolds CP, Kang MH*, et al.* Initial testing of the replication competent Seneca Valley virus (NTX-010) by the pediatric preclinical testing program. Pediatr Blood Cancer 2010;55(2):295-303.

325. Csatary LK, Gosztonyi G, Szeberenyi J, Fabian Z, Liszka V, Bodey B*, et al.* MTH-68/H oncolytic viral treatment in human high-grade gliomas. J Neurooncol 2004;67(1-2):83-93.

326. Wolff JE, Classen CF, Wagner S, Kortmann RD, Palla SL, Pietsch T*, et al.* Subpopulations of malignant gliomas in pediatric patients: analysis of the HIT-GBM database. J Neurooncol 2008;87(2):155-64.

327. Meeting report on the paediatric high-grade glioma medicines expert workshop. 2011. European Medicines Agency <http://www.ema.europa.eu/docs/en_GB/document_library/Report/2011/07/WC500108351.pdf%3E. Accessed 2015 24th November.

328. Wagner S, Csatary CM, Gosztonyi G, Koch HC, Hartmann C, Peters O*, et al.* Combined treatment of pediatric high-grade glioma with the oncolytic viral strain MTH-68/H and oral valproic acid. APMIS 2006;114(10):731-43.

329. Freeman AI, Zakay-Rones Z, Gomori JM, Linetsky E, Rasooly L, Greenbaum E*, et al.* Phase I/II trial of intravenous NDV-HUJ oncolytic virus in recurrent glioblastoma multiforme. Mol Ther 2006;13(1):221-8.

330. Cripe TP, Ngo MC, Geller JI, Louis CU, Currier MA, Racadio JM*, et al.* Phase 1 study of intratumoral Pexa-Vec (JX-594), an oncolytic and immunotherapeutic vaccinia virus, in pediatric cancer patients. Mol Ther 2015;23(3):602-8.

331. Burke MJ, Ahern C, Weigel BJ, Poirier JT, Rudin CM, Chen Y*, et al.* Phase I trial of Seneca Valley Virus (NTX-010) in children with

relapsed/refractory solid tumors: a report of the Children's Oncology Group. Pediatr Blood Cancer 2015;62(5):743-50.

332. Oncolytic HSV-1716 in Treating Younger Patients With Refractory or Recurrent High Grade Glioma That Can Be Removed By Surgery. U.S. National Institutes of Health <https://clinicaltrials.gov/ct2/show/study/NCT02031965?term=HSV+1716+pediatric&rank=1>. Accessed 2015 September 24th.

333. Wild-Type Reovirus in Combination With Sargramostim in Treating Younger Patients With High-Grade Recurrent or Refractory Brain Tumors. <https://clinicaltrials.gov/ct2/show/study/NCT02444546?term=reovirus+pediatric&rank=1>. Accessed 2015 12th December.

334. Wollmann G, Ozduman K, van den Pol AN. Oncolytic virus therapy for glioblastoma multiforme: concepts and candidates. Cancer J 2012;18(1):69-81.

335. Martuza RL, Malick A, Markert JM, Ruffner KL, Coen DM. Experimental therapy of human glioma by means of a genetically engineered virus mutant. Science 1991;252(5007):854-6.

336. Parker JN, Bauer DF, Cody JJ, Markert JM. Oncolytic viral therapy of malignant glioma. Neurotherapeutics 2009;6(3):558-69.

337. Forsyth P, Roldan G, George D, Wallace C, Palmer CA, Morris D*, et al.* A phase I trial of intratumoral administration of reovirus in patients with histologically confirmed recurrent malignant gliomas. Mol Ther 2008;16(3):627-32.

338. Harrow S, Papanastassiou V, Harland J, Mabbs R, Petty R, Fraser M*, et al.* HSV1716 injection into the brain adjacent to tumour following surgical resection of high-grade glioma: safety data and long-term survival. Gene Ther 2004;11(22):1648-58.

339. Kottke T, Errington F, Pulido J, Galivo F, Thompson J, Wongthida P*, et al.* Broad antigenic coverage induced by vaccination with virus-based cDNA libraries cures established tumors. Nat Med 2011;17(7):854-9.

340. Alonso-Camino V, Rajani K, Kottke T, Rommelfanger-Konkol D, Zaidi S, Thompson J*, et al.* The profile of tumor antigens which can be targeted by immunotherapy depends upon the tumor's anatomical site. Mol Ther 2014;22(11):1936-48.

341. Cockle JV, Rajani K, Zaidi S, Kottke T, Thompson J, Diaz RM*, et al.* Combination viroimmunotherapy with checkpoint inhibition to treat glioma, based on location-specific tumor profiling. Neuro Oncol 2015.

342. Markert JM, Liechty PG, Wang W, Gaston S, Braz E, Karrasch M*, et al.* Phase Ib trial of mutant herpes simplex virus G207 inoculated pre- and post-tumor resection for recurrent GBM. Mol Ther 2009;17(1):199-207.

343. Markert JM, Razdan SN, Kuo HC, Cantor A, Knoll A, Karrasch M*, et al.* A phase 1 trial of oncolytic HSV-1, G207, given in combination with radiation for recurrent GBM demonstrates safety and radiographic responses. Mol Ther 2014;22(5):1048-55.

344. Rampling R, Cruickshank G, Papanastassiou V, Nicoll J, Hadley D, Brennan D*, et al.* Toxicity evaluation of replication-competent herpes simplex virus (ICP 34.5 null mutant 1716) in patients with recurrent malignant glioma. Gene Ther 2000;7(10):859-66.

345. Papanastassiou V, Rampling R, Fraser M, Petty R, Hadley D, Nicoll J*, et al.* The potential for efficacy of the modified (ICP 34.5(-)) herpes simplex virus HSV1716 following intratumoural injection into human malignant glioma: a proof of principle study. Gene Ther 2002;9(6):398-406.

346. Kicielinski KP, Chiocca EA, Yu JS, Gill GM, Coffey M, Markert JM. Phase 1 clinical trial of intratumoral reovirus infusion for the treatment of recurrent malignant gliomas in adults. Mol Ther 2014;22(5):1056-62.

347. Chiocca EA, Abbed KM, Tatter S, Louis DN, Hochberg FH, Barker F*, et al.* A phase I open-label, dose-escalation, multi-institutional trial of injection with an E1B-Attenuated adenovirus, ONYX-015, into the peritumoral region of recurrent malignant gliomas, in the adjuvant setting. Mol Ther 2004;10(5):958-66.

348. Bax DA, Little SE, Gaspar N, Perryman L, Marshall L, Viana-Pereira M*, et al.* Molecular and phenotypic characterisation of paediatric glioma cell lines as models for preclinical drug development. PLoS One 2009;4(4):e5209.

349. Ma XH, Piao S, Wang D, McAfee QW, Nathanson KL, Lum JJ*, et al.* Measurements of tumor cell autophagy predict invasiveness, resistance to chemotherapy, and survival in melanoma. Clin Cancer Res 2011;17(10):3478-89.

350. Del Duca D, Werbowetski T, Del Maestro RF. Spheroid preparation from hanging drops: characterization of a model of brain tumor invasion. J Neurooncol 2004;67(3):295-303.

351. Johnson J, Nowicki MO, Lee CH, Chiocca EA, Viapiano MS, Lawler SE*, et al.* Quantitative analysis of complex glioma cell migration on electrospun polycaprolactone using time-lapse microscopy. Tissue Eng Part C Methods 2009;15(4):531-40.

352. AMSBIO. Cultrex® 3-D Spheroid Colorimetric Proliferation/Viability Assay. <http://www.amsbio.com/datasheets/3511-096-K.pdf%3E. Accessed 2015 12th December.

353. Caretti V, Zondervan I, Meijer DH, Idema S, Vos W, Hamans B*, et al.* Monitoring of tumor growth and post-irradiation recurrence in a diffuse intrinsic pontine glioma mouse model. Brain Pathol 2011;21(4):441-51.

354. Vinci M, Gowan S, Boxall F, Patterson L, Zimmermann M, Court W*, et al.* Advances in establishment and analysis of three-dimensional tumor spheroid-based functional assays for target validation and drug evaluation. BMC Biol 2012;10:29.

355. van Beusechem VW, Mastenbroek DC, van den Doel PB, Lamfers ML, Grill J, Wurdinger T*, et al.* Conditionally replicative adenovirus expressing a targeting adapter molecule exhibits enhanced oncolytic potency on CAR-deficient tumors. Gene Ther 2003;10(23):1982-91.

356. Mehta G, Hsiao AY, Ingram M, Luker GD, Takayama S. Opportunities and challenges for use of tumor spheroids as models to test drug delivery and efficacy. J Control Release 2012;164(2):192-204.

357. Smith SJ, Wilson M, Ward JH, Rahman CV, Peet AC, Macarthur DC*, et al.* Recapitulation of tumor heterogeneity and molecular signatures in a 3D brain cancer model with decreased sensitivity to histone deacetylase inhibition. PLoS One 2012;7(12):e52335.

358. Petrie RJ, Doyle AD, Yamada KM. Random versus directionally persistent cell migration. Nat Rev Mol Cell Biol 2009;10(8):538-49.

359. Fackler OT, Grosse R. Cell motility through plasma membrane blebbing. J Cell Biol 2008;181(6):879-84.

360. Ma Q, Yang Y, Feng D, Zheng S, Meng R, Fa P*, et al.* MAGI3 negatively regulates Wnt/beta-catenin signaling and suppresses malignant phenotypes of glioma cells. Oncotarget 2015;6(34):35851-65.

361. Zhang FY, Hu Y, Que ZY, Wang P, Liu YH, Wang ZH*, et al.* Shikonin Inhibits the Migration and Invasion of Human Glioblastoma Cells by Targeting Phosphorylated beta-Catenin and Phosphorylated PI3K/Akt: A Potential Mechanism for the Anti-Glioma Efficacy of a Traditional Chinese Herbal Medicine. Int J Mol Sci 2015;16(10):23823-48.

362. Nie E, Zhang X, Xie S, Shi Q, Hu J, Meng Q*, et al.* Beta-catenin is involved in Bex2 down-regulation induced glioma cell invasion/migration inhibition. Biochem Biophys Res Commun 2015;456(1):494-9.

363. Williams SP. The role of glycogen synthase kinase in glioblastoma multiforme migration and invasion: The Ohio State University; 2011.

364. Simon D, Benitez MJ, Gimenez-Cassina A, Garrido JJ, Bhat RV, Diaz-Nido J*, et al.* Pharmacological inhibition of GSK-3 is not strictly correlated with a decrease in tyrosine phosphorylation of residues 216/279. J Neurosci Res 2008;86(3):668-74.

365. Mitchell PB. On the 50th anniversary of John Cade's discovery of the anti-manic effect of lithium. Aust N Z J Psychiatry 1999;33(5):623-8.

366. Siegal T. Which drug or drug delivery system can change clinical practice for brain tumor therapy? Neuro Oncol 2013;15(6):656-69.

367. Kunz-Schughart LA, Kreutz M, Knuechel R. Multicellular spheroids: a three-dimensional in vitro culture system to study tumour biology. Int J Exp Pathol 1998;79(1):1-23.

368. Cheng V, Esteves F, Chakrabarty A, Cockle J, Short S, Bruning-Richardson A. High-content analysis of tumour cell invasion in three-dimensional spheroid assays. Oncoscience 2015;2(6):596-606.

369. Artym VV, Matsumoto K. Imaging cells in three-dimensional collagen matrix. Curr Protoc Cell Biol 2010;Chapter 10:Unit 10 18 1-20.

370. Huijbers IJ, Iravani M, Popov S, Robertson D, Al-Sarraj S, Jones C*, et al.* A role for fibrillar collagen deposition and the collagen internalization receptor endo180 in glioma invasion. PLoS One 2010;5(3):e9808.

371. MolecularProbes. 2005. LIVE/DEAD® viability/cytotoxicity kit for mamalian cells. In Product information. <https://tools.thermofisher.com/content/sfs/manuals/mp03224.pdf>. Accessed 2015 2nd December.

372. Scholzen T, Gerdes J. The Ki-67 protein: from the known and the unknown. J Cell Physiol 2000;182(3):311-22.

373. Louis DN, Edgerton S, Thor AD, Hedley-Whyte ET. Proliferating cell nuclear antigen and Ki-67 immunohistochemistry in brain tumors: a comparative study. Acta Neuropathol 1991;81(6):675-9.

374. Zhu VF, Yang J, Lebrun DG, Li M. Understanding the role of cytokines in Glioblastoma Multiforme pathogenesis. Cancer Lett 2012;316(2):139-50.

375. Brat DJ, Bellail AC, Van Meir EG. The role of interleukin-8 and its receptors in gliomagenesis and tumoral angiogenesis. Neuro Oncol 2005;7(2):122-33.

376. Reynes G, Vila V, Martin M, Parada A, Fleitas T, Reganon E*, et al.* Circulating markers of angiogenesis, inflammation, and coagulation in patients with glioblastoma. J Neurooncol 2011;102(1):35-41.

377. Goel HL, Mercurio AM. VEGF targets the tumour cell. Nat Rev Cancer 2013;13(12):871-82.

378. Cockle JV, Picton SV, Melcher A. Future clinical potential of oncolytic virotherapy for pediatric CNS tumors. CNS Oncol 2013;2(4):307-10.

379. Friedman GK, Nan L, Haas MC, Kelly VM, Moore BP, Langford CP*, et al.* gamma(1)34.5-deleted HSV-1-expressing human cytomegalovirus IRS1 gene kills human glioblastoma cells as efficiently as wild-type HSV-1 in normoxia or hypoxia. Gene Ther 2015;22(4):348-55.

380. van Tonder A, Joubert AM, Cromarty AD. Limitations of the 3-(4,5-dimethylthiazol-2-yl)-2,5-diphenyl-2H-tetrazolium bromide (MTT) assay when compared to three commonly used cell enumeration assays. BMC Res Notes 2015;8:47.

381. Raychaudhuri B, Vogelbaum MA. IL-8 is a mediator of NF-kappaB induced invasion by gliomas. J Neurooncol 2011;101(2):227-35.

382. Kubo F, Ueno S, Hiwatashi K, Sakoda M, Kawaida K, Nuruki K*, et al.* Interleukin 8 in human hepatocellular carcinoma correlates with cancer cell invasion of vessels but not with tumor angiogenesis. Ann Surg Oncol 2005;12(10):800-7.

383. Inoue K, Slaton JW, Eve BY, Kim SJ, Perrotte P, Balbay MD*, et al.* Interleukin 8 expression regulates tumorigenicity and metastases in androgen-independent prostate cancer. Clin Cancer Res 2000;6(5):2104-19.

384. Bates RC, DeLeo MJ, 3rd, Mercurio AM. The epithelial-mesenchymal transition of colon carcinoma involves expression of IL-8 and CXCR-1-mediated chemotaxis. Exp Cell Res 2004;299(2):315-24.

385. Infanger DW, Cho Y, Lopez BS, Mohanan S, Liu SC, Gursel D*, et al.* Glioblastoma stem cells are regulated by interleukin-8 signaling in a tumoral perivascular niche. Cancer Res 2013;73(23):7079-89.

386. Steele L, Errington F, Prestwich R, Ilett E, Harrington K, Pandha H*, et al.* Pro-inflammatory cytokine/chemokine production by reovirus treated melanoma cells is PKR/NF-kappaB mediated and supports innate and adaptive anti-tumour immune priming. Mol Cancer 2011;10:20.

387. Yang AD, Camp ER, Fan F, Shen L, Gray MJ, Liu W*, et al.* Vascular endothelial growth factor receptor-1 activation mediates epithelial to mesenchymal transition in human pancreatic carcinoma cells. Cancer Res 2006;66(1):46-51.

388. Liang CC, Park AY, Guan JL. In vitro scratch assay: a convenient and inexpensive method for analysis of cell migration in vitro. Nat Protoc 2007;2(2):329-33.

389. Kayaselcuk F, Zorludemir S, Gumurduhu D, Zeren H, Erman T. PCNA and Ki-67 in central nervous system tumors: correlation with the histological type and grade. J Neurooncol 2002;57(2):115-21.

390. Namekata K, Kimura A, Kawamura K, Harada C, Harada T. Dock GEFs and their therapeutic potential: neuroprotection and axon regeneration. Prog Retin Eye Res 2014;43:1-16.

391. Zhu X, Gao G, Chu K, Yang X, Ren S, Li Y*, et al.* Inhibition of RAC1-GEF DOCK3 by miR-512-3p contributes to suppression of metastasis in non-small cell lung cancer. Int J Biochem Cell Biol 2015;61:103-14.

392. Sanz-Moreno V. Tumour invasion: a new twist on Rac-driven mesenchymal migration. Curr Biol 2012;22(11):R449-51.

393. Namekata K, Harada C, Guo X, Kimura A, Kittaka D, Watanabe H*, et al.* Dock3 stimulates axonal outgrowth via GSK-3beta-mediated microtubule assembly. J Neurosci 2012;32(1):264-74.

394. Naranatt PP, Krishnan HH, Smith MS, Chandran B. Kaposi's sarcoma-associated herpesvirus modulates microtubule dynamics via RhoA-GTP-diaphanous 2 signaling and utilizes the dynein motors to deliver its DNA to the nucleus. J Virol 2005;79(2):1191-206.

395. Van den Broeke C, Favoreel HW. Actin' up: herpesvirus interactions with Rho GTPase signaling. Viruses 2011;3(4):278-92.

396. Sodeik B, Ebersold MW, Helenius A. Microtubule-mediated transport of incoming herpes simplex virus 1 capsids to the nucleus. J Cell Biol 1997;136(5):1007-21.

397. Miki H, Okada Y, Hirokawa N. Analysis of the kinesin superfamily: insights into structure and function. Trends Cell Biol 2005;15(9):467-76.

398. Pfister KK, Shah PR, Hummerich H, Russ A, Cotton J, Annuar AA*, et al.* Genetic analysis of the cytoplasmic dynein subunit families. PLoS Genet 2006;2(1):e1.

399. Howard J, Hyman AA. Dynamics and mechanics of the microtubule plus end. Nature 2003;422(6933):753-8.

400. Frampton AR, Jr., Uchida H, von Einem J, Goins WF, Grandi P, Cohen JB*, et al.* Equine herpesvirus type 1 (EHV-1) utilizes microtubules, dynein, and ROCK1 to productively infect cells. Vet Microbiol 2010;141(1-2):12-21.

401. Rusan NM, Tulu US, Fagerstrom C, Wadsworth P. Reorganization of the microtubule array in prophase/prometaphase requires cytoplasmic dynein-dependent microtubule transport. J Cell Biol 2002;158(6):997-1003.

402. Salaycik KJ, Fagerstrom CJ, Murthy K, Tulu US, Wadsworth P. Quantification of microtubule nucleation, growth and dynamics in wound-edge cells. J Cell Sci 2005;118(Pt 18):4113-22.

403. Hill DB, Plaza MJ, Bonin K, Holzwarth G. Fast vesicle transport in PC12 neurites: velocities and forces. Eur Biophys J 2004;33(7):623-32.

404. Liao G, Nagasaki T, Gundersen GG. Low concentrations of nocodazole interfere with fibroblast locomotion without significantly affecting microtubule level: implications for the role of dynamic microtubules in cell locomotion. J Cell Sci 1995;108 (Pt 11):3473-83.

405. Waterman-Storer CM, Salmon WC, Salmon ED. Feedback interactions between cell-cell adherens junctions and cytoskeletal dynamics in newt lung epithelial cells. Mol Biol Cell 2000;11(7):2471-83.

406. Ganguly A, Yang H, Sharma R, Patel KD, Cabral F. The role of microtubules and their dynamics in cell migration. J Biol Chem 2012;287(52):43359-69.

407. Tran AD, Marmo TP, Salam AA, Che S, Finkelstein E, Kabarriti R*, et al.* HDAC6 deacetylation of tubulin modulates dynamics of cellular adhesions. J Cell Sci 2007;120(Pt 8):1469-79.

408. Friedman GK, Cassady KA, Beierle EA, Markert JM, Gillespie GY. Targeting pediatric cancer stem cells with oncolytic virotherapy. Pediatr Res 2012;71(4 Pt 2):500-10.

409. Markert JM, Parker JN, Gillespie GY, Whitley RJ. Genetically engineered human herpes simplex virus in the treatment of brain tumours. Herpes 2001;8(1):17-22.

410. Szatmari T, Lumniczky K, Desaknai S, Trajcevski S, Hidvegi EJ, Hamada H*, et al.* Detailed characterization of the mouse glioma 261 tumor model for experimental glioblastoma therapy. Cancer Sci 2006;97(6):546-53.

411. Pellegatta S, Poliani PL, Corno D, Menghi F, Ghielmetti F, Suarez-Merino B*, et al.* Neurospheres enriched in cancer stem-like cells are highly effective in eliciting a dendritic cell-mediated immune response against malignant gliomas. Cancer Res 2006;66(21):10247-52.

412. Binello E, Qadeer ZA, Kothari HP, Emdad L, Germano IM. Stemness of the CT-2A Immunocompetent Mouse Brain Tumor Model: Characterization In Vitro. J Cancer 2012;3:166-74.

413. Martinez-Murillo R, Martinez A. Standardization of an orthotopic mouse brain tumor model following transplantation of CT-2A astrocytoma cells. Histol Histopathol 2007;22(12):1309-26.

414. De Simoni A, Yu LM. Preparation of organotypic hippocampal slice cultures: interface method. Nat Protoc 2006;1(3):1439-45.

415. Ohnishi T, Matsumura H, Izumoto S, Hiraga S, Hayakawa T. A novel model of glioma cell invasion using organotypic brain slice culture. Cancer Res 1998;58(14):2935-40.

416. Broniscer A, Gajjar A. Supratentorial high-grade astrocytoma and diffuse brainstem glioma: two challenges for the pediatric oncologist. Oncologist 2004;9(2):197-206.

417. Children's Hospital Medical Center, Cincinnati. HSV1716 in patients with non-central nervous system (Non-CNS) solid tumors. U.S. National Institutes of Health <http://clinicaltrials.gov/ct2/show/record/NCT00931931?term=hsv1716+non+cns+solid+tumor&rank=1%3E. Accessed 2013 12th August.